METHANATION OF CARBON MONOXIDE AND CARBON DIOXIDE ON RANEY NICKEL, AND COMPUTER SIMULATION OF CHAIN GROWTH IN THE FISCHER-TROPSCH SYNTHESIS

By

© CHUNG BOON LEE, B. ENG.

A Thesis

Submitted to the Faculty of Graduate Studies

in Partial Fulfilment of the Requirements

for the Degree

Doctor of Philosophy

McMaster University

November, 1982

METHANATION OF CARBON OXIDES ON RANEY NICKEL AND SIMULATION OF CHAIN GROWTH IN FISCHER-TROPSCH SYNTHESIS

DOCTOR OF PHILOSOPHY (1982)
(Chemical Engineering)

McMASTER UNIVERSITY
Hamilton, Ontario

TITLE: Methanation of Carbon Monoxide and Carbon Dioxide on Raney Nickel, and Computer Simulation of Chain Growth in the Fischer-Tropsch Synthesis

AUTHOR: Chung Boon Lee, B. Eng. (McMaster University)

SUPERVISOR: Professor R. B. Anderson

NUMBER OF PAGES: 381, xv

To Marilyn

and

To my Parents

ABSTRACT

The methanation of carbon monoxide and carbon dioxide was studied over Raney nickel. The catalyst was characterized by chemisorption techniques. A differential plug-flow reactor was used to obtain kinetic data. The reaction rates were investigated as a function of temperature, reactants and products concentrations. The power rate law was found inadequate in representing the kinetic data of carbon dioxide methanation. The orders of reaction for hydrogen and carbon monoxide were obtained. Carbonaceous species were found on the catalyst surface after methanation reaction, which could react with hydrogen to give methane. Multilayers of carbon species were deposited on the catalyst surface during CO methanation; less than a monolayer was found when carbon dioxide was used as feed. The effects of reaction conditions on the amount of residual carbon was also investigated.

The data in general agrees with a mechanism involving the hydrogenation of carbonaceous species as the rate determining step. The differences between CO and CO_2 methanations were also discussed.

The carbon chain growth process in the Fischer-Tropsch synthesis was simulated using available data in the literature.

The simulation was done by representing the hydrocarbon chains by numbers stored in vectors. Various chain growth schemes were tested. The results suggested that the carbon chain growth process could involve the stepwise additions of both one-carbon and two-carbon units.

ACKNOWLEDGEMENTS

The author wishes to acknowledge his appreciation to those people who have contributed to this work.

The author is indebted to his research director, Professor R.B. Anderson, for his guidance, support and patience.

The contributions of Dr. M.H.I. Baird, Dr. J. Vlachopoulos and Dr. W.W. Smeltzer, members of the supervisory committee, are also acknowledged.

Special thanks are due to his wife, Marilyn for her encouragement and patience.

Financial assistance provided by the Department of Chemical Engineering and the National Research Council of Canada was also gratefully accepted.

TABLE OF CONTENTS

LIST OF FIGURES

LIST OF TABLES

Chapter 1

INTRODUCTION

1.1 General

The scarcity of fluid forms of fossil fuel has resulted in an ardent search for future energy sources. Various kinds of energies such as nuclear, solar and wind energies have gained popularity as a result. However, with the possible exception of nuclear energy, they are essentially still in their development stage; and are expected to ease the energy crisis to only a small extent. The recent nuclear accident on Three-Mile Island hinders the possible expansion of nuclear energy as an alternative source of energy in the foreseeable future. For these reasons, as well as the traditional reliance of the industry and economy on liquid fuel, the latter will remain the main source of energy in the near future.

Despite the occasional findings of new oil wells, the projected oil supply is still not very encouraging. Exploration for new oil supplies is often restricted by harsh geographic and climatic conditions, and is proving more and more costly. On the other hand, oil import is not only subject to frequent rises in price, but also is to a large extent affected by political events. In view of these, other sources of energy have to be found which are

competitive and can be utilized easily. One of such alternatives is coal which is in abundance in North America.

Coal can be utilized essentially in two ways. It can be burned directly in solid form such as in most power plants. This method, however, presents severe environmental problems such as acid rain etc. The other means is to convert coal into oil and gas. One of the major steps in the conversion of coal into pipeline quality gas is the production of substitute natural gas (SNG) by the gasification of coal. Coal can also be converted into oil by hydrogenation and/or solvent extraction. An alternative means of obtaining synthetic oil is by the Fischer-Tropsch (F-T) process which combines synthesis gas (a mixture of hydrogen (H_2) and carbon monoxide (CO)) from coal gasification to form higher hydrocarbons. This technology is well established; in South Africa the Sasol plant supplies one-third of the country's demand for oil.

One of the final steps in the production of SNG from synthesis gas is hydrogenating the carbon monoxide to augment the heating value. Since methane (CH_4) is obtained as product, the term methanation has been widely used, and is extended to include the hydrogenation of carbon dioxide (CO_2) to methane. Traditionally, methanation

has been used to remove traces of CO and CO_2 from hydrogen-rich gases such as in ammonia synthesis.

$$3H_2 + CO \longrightarrow CH_4 + H_2O \qquad (1\text{-}1)$$

$$4H_2 + CO_2 \longrightarrow CH_4 + 2H_2O \qquad (1\text{-}2)$$

Methanation can be carried out on nickel catalysts at 200 to 400°C at pressures up to 10 MPa. The reaction is almost irreversible under these conditions. However, the large heat of reaction ($-\Delta H^\circ$ = 210 kJ/mol at 200°C) presents a major problem in the design of commercial methanator. One method is to recycle a portion of the partially cooled product gas through the catalyst bed; this hot gas recycle reactor system has been successfully tested in the Bureau of Mines.

In spite of the large amount of work done on methanation reaction using H_2/CO feed, the picture is still far from clear, and there is still no general agreement regarding the kinetics or mechanism. This stems from the fact that different catalysts were used and that the reaction conditions were very much different with respect to temperature, pressure and the relative concentration of the reactants. The large heat of reaction also complicates kinetics studies. The order of reaction with

respect to CO has been found to vary from -0.9 to 0.7 (1-3), while values of 0.8 to 1.4 have been reported for H_2 (1,2,4). For the hydrogenation of CO_2 the general consensus is that the order for CO_2 is 0.5 (5,6) while for H_2, zero order.

The purpose of the present investigation is to learn of the kinetics and mechanism of methanation of carbon oxides. To this end, the ratios of H_2/CO and H_2/CO_2 were varied over a wide range to resolve the pressure effects of the reactants. In addition, the condition of the catalyst surface was also investigated after reaction.

The transitional metals, especially those in Group VIII of the periodic table, have been commonly used as catalysts for methanation, either in supported or unsupported form. The catalyst used in the present study was Raney nickel. Raney nickel is prepared by removing aluminum from a nickel-aluminum alloy by aqueous alkali at elevated temperatures.

A single-pass differential catalytic reactor was used to collect kinetic data. A differential reactor is used because the data are amenable to easy and direct analysis, and do not require integration of rate equations. Perhaps the more important advantage is that the data are free from distortion due to physical transport processes such as diffusion and heat transfer.

1.2 Methanation of Carbon Monoxide

1.2.1 Mechanism of CO Methanation

The hydrogenation of CO to methane is the simplest example of the synthesis of hydrocarbon from synthesis gas. Therefore, it is necessary to involve at least some work done in Fischer-Tropsch (F-T) synthesis. One of the earliest proposed mechanisms for F-T reaction was the carbide theory of Fischer and Tropsch (8), which was later refined by Craxford and Rideal (9,10). Essentially this theory postulates that adsorbed CO is reduced to surface carbide, which is hydrogenated to methylene radicals. These methylene radicals polymerize and desorb as olefinic and paraffinic hydrocarbons. The carbide theory was subsequently found to be inadequate to explain the hydrocarbon synthesis in the presence of the iron group metals (11,12). For methanation in particular, the temperature of hydrogenation of the surface nickel carbide is higher than the temperature of appreciable methane production. In addition, the rate of methanation is much greater than the carbide formation rate (13-15).

Oxygen-containing substances, such as methanol or formaldehyde, have been considered to be the intermediate products in methanation (16). However, attempts to detect these intermediates have not been successful (17). Moreover, the yield of methane is less with methanol as a starting material than when a mixture of hydrogen and carbon monoxide is used (18).

Fischer and Tropsch (19) had also earlier suggested that carbon monoxide reacts with the catalyst to form an intermediate of metal carbonyl which is then reduced to give methane. In the seventies, Pichler (20) also presented a similar explanation for F-T synthesis. This is now known as the CO insertion mechanism by which the carbon chain grows by stepwise insertion of carbon monoxide between the growing carbon chain and the metal surface, and its subsequent hydrogenation.

Instead of intermediate compounds, surface complexes or radicals have also been considered to play a role in methanation. Orlov (21) suggested that methylene radicals are formed in the primary stages of hydrogenation of carbon monoxide. The existence of CH_2 radicals was subsequently proved by Eidus and Zelinskii (22) in the methylation of benzene to toluene. Eidus (23) further suggested that methylene is the result of hydrogenation of carbon monoxide through an unstable oxygen-containing group. A similar mechanism was also proposed by Hamai (24), in which an intermediate oxygenated complex precedes the formation of the $M-CH_2$ species.

Storch et al. (11) proposed that formation of adsorbed oxygenated complex of HCOH forms the basis in F-T synthesis. The formation of hydrocarbons is by a stepwise condensation reaction with the elimination of water. This step bears strong resemblance to the addition polymerization

in polymer chemistry. Nijs and Jacobs (25) also concluded that F-T synthesis involves hydroxyl-condensation mechanism involving HCOH species. This species can be regarded as the 'monomer' unit in F-T synthesis, and is thought to be formed by the reaction:

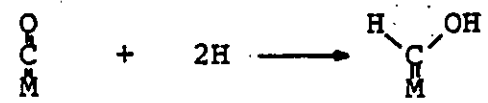

(1-3)

In methanation this species does not add on to any growing carbon chain by condensation but is reduced to methane instead.

Vlasenko and Yuzefovich (26) also invoked a HCOH surface complex which, however, is reduced to methylene radical. They stressed the importance of electronic charge or polarization factor in methanation. It was proposed that the formation of a positively charged HCOH species is the slowest step in methanation.

Blyholder et al. (27) suggested that methane is formed by the hydrogenation of HCO species to a methoxy group which is further hydrogenated to methane. No condensation type reaction is involved. The species HCO was thought to be formed by CO-insertion mechanism.

In contrast to the previous belief that CHOH or other oxygenated complexes are the intermediates, the work on methanation after the 1973 oil embargo has produced evidence that carbonaceous species resulting from the decomposition of

carbon monoxide by the Boudouard reaction on the catalyst surface could be the pertinent surface species.

$$2CO \longrightarrow C + CO_2 \qquad (1\text{-}4)$$

At temperatures above 450 K exposure of nickel surface to CO results in the buildup of carbon on the surface (28). Tøttrup (29) studied the decomposition of CO in a thermogravimetric flow system in temperature range 553 - 673 K, and the data were found to be best correlated by assuming dissociation of adsorbed CO as rate determining step.

Rabo et al. (30) showed that adsorption of CO on nickel at 573 K is dissociative, resulting in disproportionation to CO_2 and a Ni-C species which is very reactive to H_2. Wentrcek et al. (31) reported the detection of carbidic surface species using Auger electron microscope when catalyst surface (Ni/Al_2O_3) was exposed to CO at 550 K. This carbon is very reactive towards H_2. However, this species is unstable at higher temperatures (723 K) and is transformed to unreactive graphite. Araki and Ponec (32) concluded that dissociation of CO is one of the important reaction steps in methanation, the other being hydrogenation of deposited carbon by adsorbed hydrogen. They proposed that the hydrogenation of surface species CH_x (x = 0 - 1) is the limiting step in methanation. Using temperature programmed desorption in the presence of H_2, McCarty and Wise (33) identified four

types of carbon deposited from CO on nickel surface at 550 K and suggested that one of these carbons, the α state is the likely intermediate in methanation. The α carbon was slowly transformed into the less active β carbon with an activation energy of 33.5 kJ/mol. Amenomiya et al. (34) with the aid of infrared and mass spectrometers, detected carbon and CH_x species during methanation and concluded that CH is the most abundant species at the reaction condition.

The application of temperature programmed reaction in recent work by Zagli et al. (35) led to the conclusion that the decomposition of CO is the rate determining step in CO methanation. This conclusion was reached from the observation that both methane and water peaks were produced at the same temperature when adsorbed CO was slowly heated in hydrogen. The same conclusion was also reached by Betta and Shelef (36) who demonstrated that there is no kinetic isotope effect for hydrogen in methanation on nickel catalyst. However, the Boudouard reaction as the slowest step in methanation does not reconcile with the fact that the rate of reaction does depend on the partial pressure of hydrogen. Goodman and coworkers (37), using a specially designed ultra high vacuum system, investigated methanation over a single nickel crystal, and their data are consistent with a mechanism in which an active surface carbon species is the dominant route to methane formation.

The importance of carbidic intermediates is by no means limited to methanation over nickel catalyst. It has also been thought to play an important role in F-T synthesis. Biloen et al. (38) showed that ^{13}C from CO decomposition when hydrogenated will give hydrocarbons containing several ^{13}C atoms within one molecule. They concluded that the intermediate is an oxygen-free species CH_x . Using transient reaction techniques, Matsumoto and Bennett (39) have shown that *-CO or *-C species are the likely intermediates in methanation over iron catalyst. Joyner (40) similarly proposed CH species as the relevant intermediate in F-T synthesis. These results underline the close relationship between F-T synthesis and methanation reaction.

Other catalysts active in methanation or F-T reaction can also deposit carbon on the surface. Ekerdt and Bell (41) found that ruthenium catalyst after hydrogenation of CO contains a reservoir of carbon atoms on the surface. Sexton and Somorjai (42) found a carbonaceous deposit over rhodium surface during methanation. King (43) investigated CO hydrogenation over supported ruthenium and iron catalyst, and concluded that the data are consistent with initial formation of surface carbon. No hydroxy-carbene or formyl species during the reaction were found.

In summary, the mechanism of methanation of CO is still not resolved. Evidence accumulated suggests that the mechanism can be divided essentially into two major categories. One stipulates the formation of a CH_xO complex on the catalyst surface, while the recent evidence suggests the possibility of carbon resulting from dissociation of CO as a relevant intermediate. The choice of the type of intermediate brings out the important question of how the oxygen in CO is removed from the carbon atom. Is it removed as oxygen atom and then hydrogenated to water or is it removed as water from an oxygenated species such as CH_xO ? Before a mechanism can be regarded as established this central issue must be resolved.

1.2.2 Kinetic Studies

While there is still controversy over the mechanism and intermediates in methanation of CO, kinetic data collected in various studies present a more consistent picture. Generally the rate is found to increase with the partial pressure of H_2 and decrease with the partial pressure of CO. The overall reaction order is positive with respect to total pressure of the system. Hence the rate increases with the total pressure. However, different studies result in different orders of reaction.

Many correlations have been proposed for the methanation reaction. They are often based on different methanistic assumptions. Earlier works have been reviewed by Vlasenko and Yuzefovich (26), and by Mills and Steffgen (44).

These data yield various orders of reaction for hydrogen and carbon monoxide under different temperatures and partial pressures. Luyten and Junger (45) found that at 573 K and with H_2/CO ratios from 1 to 6, the rate over nickel on kieselguhr was approximately proportional to hydrogen partial pressure but retarded by carbon monoxide according to:

$$r = k P_{H_2}^{0.9} P_{CO}^{-0.2} \qquad (1\text{-}5)$$

The activation energy was 113 kJ/mol. This value differs considerably from 146 kJ/mol found by Nicolai and coworkers (46) in studies made under identical conditions on similar catalysts.

Using a flow method, Akers and White (47) made an extensive study of the kinetics of methanation at atmospheric pressure on an industrial nickel-kielselguhr catalyst in temperature range 573 to 623 K at H_2/CO ratios from 1.2 to 4. The conclusion was reached that the limiting step is the reaction between an adsorbed CO and three molecules of H_2 according to the equation:

$$r = \frac{k P_{CO} P_{H_2}^{3}}{(a + bP_{CO} + cP_{CO_2} + dP_{CH_4})^4} \qquad (1\text{-}6)$$

However, the result has been criticized because of the large

external and internal gradients in temperature and concentrations.

The retarding influence of CO is apparently due to its strong adsorption on the catalyst surface, leading to a corresponding decrease in the degree of hydrogen coverage. The inhibiting effect of CO has also been observed with other catalysts. Karn, Shultz and Anderson (48) found the following empirical expression for methanation of CO over a ruthenium catalyst:

$$r = k P_{H_2}^{1.33} P_{CO}^{-0.13} \qquad (1\text{-}7)$$

This group also studied methanation on Raney nickel catalyst using pressures from 0.1 to 2.2 MPa and found that the total pressure dependence was to the 0.3 power for CO hydrogenation. The activation energy was 121 - 134 kJ/mol.

The kinetic picture is changed, however, when a low concentration of CO in excess of hydrogen is used. The order of reaction for CO can change from as low as -0.9 as reported by Bousquet et al. (1,2) to positive values. Apparently the reaction undergoes a change in reaction regime as the concentration of CO is decreased. The Russian school reported zero order with respect to CO. In a flow-circulation system with a nickel-chromium catalyst at 402 - 448 K and a feed of 0.3 volume percent

of CO in hydrogen, Vlasenko et al. (50) found the rate to be independent of both CO and H_2. Independence of rate on CO was also reported by Cognion and Marguerin (51) who employed a chromatographic pulse reactor with H_2 as carrier gas for nickel supported on alumina.

That the order of reaction with respect to CO depends on its concentration was shown by Schoubye (18) who found that the order is zero at low concentration of CO, but approaches -0.5 at higher concentration. He proposed a kinetic model with H_2 adsorption as the rate determining step and arrived at the following rate expression:

$$r = \frac{k_1 P_{H_2}^{\ n}}{\left(1 + k_2 \left(P_{CO}/P_{H_2}\right)\right)^{0.5}} \qquad (1\text{-}8)$$

Van Herwijnen et al. (52) studied the reaction on a supported nickel catalyst at partial pressures of CO below 2 kPa and at temperatures between 443 and 483 K. The rate determining step was proposed to be the reaction between an adsorbed enol complex and adsorbed H_2. The data were found to be best correlated by the expression:

$$r = \frac{k_1 P_{CO}}{\left(1 + k_2 P_{CO}\right)^2} \qquad (1\text{-}9)$$

A low activation energy of 42 kJ/mol was obtained.

The involvement of an enol complex in methanation was also proposed by Vannice (4) who studied the kinetics on supported group VIII metals. A model was proposed in which the rate determining step is the rupture of the C-O bond in the enol complex CHOH, the existence of which has yet to be established. For Ni/Al_2O_3 the power rate law was

$$r = k P_{H_2}^{0.8} P_{CO}^{-0.3} \qquad (1\text{-}10)$$

At still lower concentration of CO or at higher temperatures, the rate of reaction often increases with CO partial pressure. Lee et al. (3) found that the rate expression

$$r = \frac{k_1 P_{CO} P_{H_2}^{0.5}}{1 + k_2 P_{H_2} + k_3 P_{CH_4}} \qquad (1\text{-}11)$$

correlates their experimental data best. The activation energy was found to be 29 kJ/mol. It is suspected that diffusional effect might be important under the reaction condition.

Similarly, at temperature of 673 K, Saletore and Thomson (53) found that the rate increases with CO partial pressure in the absence of CO_2. However when CO_2 is present the reaction rate is independent of CO

concentration. The data were subject to significant thermal and concentration gradients since the effectiveness factor was calculated to be 0.25 .

Randhava et al. (54) was interested in the removal of low concentration of CO from H_2 for use in low temperature fuel cells. With CO concentration of 500-900 ppm in H_2 over nickel catalyst at 458-573 K, the reaction rate was given by:

$$r = k P_{CO}^{0.7} \qquad (1\text{-}12)$$

When the reaction was carried out over ruthenium catalyst under similar conditions, the CO dependency was found to be even larger (55):

$$r = k P_{CO} \qquad (1\text{-}13)$$

Under these conditions the rate is undoubtedly governed by diffusional effect.

While the effect of CO on the reaction rate depends on its concentration, temperature has also been found to exert a strong influence on the reaction order. Goodman et al. (37) found that depending on the temperature, the rate could be zero order in the reactant pressures, especially H_2 . At 503 K the rate was zero order in total pressure in the pressure range 0.13 - 13.3 kPa for a

H_2/CO feed gas of ratio 4/1. However at 625 K, the rate increases strongly with the total pressure. The observed result was attributed to saturated H_2 coverage at 0.13 kPa reactant pressure at the lower temperature; an increase in H_2 partial pressure results in no substantial increase in adsorbed H_2. A mechanism was proposed by the authors, which involves the hydrogenation of an active carbon species.

While recent evidence points strongly to the possible involvement of carbidic species in the reaction mechanism, the important role of adsorbed CO has not been completely abandoned. Huang and Richardson (56) investigated the effect of alkali on CO methanation on a series of 8% Ni/SiO_2-Al_2O_3 catalysts and arrived at the equation:

$$r = \frac{k_1 P_{CO} P_{H_2}^{0.5}}{(1 + k_2 P_{CO})^2} \qquad (1\text{-}14)$$

from which it was concluded that the rate determining step is the reaction of an adsorbed hydrogen atom H_a with adsorbed carbon monoxide CO_a on the catalyst surface to give species HCO. Recently Ho and Harriott (57) studied the reaction and concluded the rate is governed by the reaction step:

$$CO_a + 2H_a \longrightarrow C_a + H_2O \qquad (1\text{-}15)$$

and arrived at the following rate equation:

$$r = \frac{k_1 P_{CO} P_{H_2}}{(1 + k_2 P_{CO} + k_3 P_{H_2})^2} \qquad (1\text{-}16)$$

Table 1-1 summarizes the various rate equations reported in the literature. These equations undoubtedly represent the collected data well and reflect the particular kinetics involved at the widely different reaction conditions. Hence, it is not surprising that they do not agree with each other, either in form or order of reaction. The various reported values of CO order of reaction are an illustration of the various kinetic regimes involved. As the partial pressure of CO increases the order of reaction decreases from positive values to negative values at higher concentrations. Various values of activation energy have also been reported, the lower ones apparently associated with lower concentrations of CO and hence possibly with a diffusion process. The order of reaction for H_2 is more consistent; the rate in most reported studies has been found to increase with hydrogen partial pressure.

1.2.3 Infrared Spectra Studies

As methanation involves CO adsorbed on the catalyst surface, information on the modes and strength of adsorption is important. In this respect infrared (IR) spectra studies have provided important information. In addition, an in-situ IR technique has also been used to find surface species relevant in methanation.

Table 1-1

Rate Equations for CO Methanation

Equation	Reference
$k\ P_{H_2}^{0.9}\ P_{CO}^{-0.2}$	45
$k\ P_{H_2}^{1.33}\ P_{CO}^{-0.13}$	48
$k\ P_{H_2}^{0.8}\ P_{CO}^{-0.3}$	4
$k\ P_{CO}^{0.7}$	54
$k\ P_{CO}$	55
$\frac{kP_{CO}P_{H_2}^{3}}{(a+bP_{CO}+cP_{CO_2}+dP_{CH_4})^{4}}$	47
$\frac{k\ P_{H_2}^{n}}{(1 + k_2(P_{CO}/P_{H_2}))^{0.5}}$	18
$\frac{k_1 P_{CO}}{(1 + k_2\ P_{CO})^{2}}$	52

Table 1-1 (continued)

Equation	Reference
$\frac{k_1 P_{CO} P_{H_2}^{0.5}}{(1 + k_2 P_{H_2} + k_3 P_{CH_4})}$	3
$\frac{k_1 P_{CO} P_{H_2}^{0.5}}{(1 + k_2 P_{CO})^2}$	56
$\frac{k_1 P_{CO} P_{H_2}}{(1 + k_2 P_{CO} + k_3 P_{H_2})^2}$	57

Generally CO is adsorbed on nickel in molecular form. Studies of the IR spectra of the adsorbed molecules have shown the existence of at least five types of bonding CO to the nickel surface (58,59). Each mode of bonding is associated with a different structure characterized by different bond strength (table 1-2). The form of bonding which prevails depends on a number of factors, including crystal structure and surface coverage. With crystalline specimens, modes A and C are observed (59), while at higher coverages species corresponding to mode B are favoured (59-61). On disordered crystallites, CO is much less strongly chemisorbed and only in linear structures (modes D and E).

Other surface conditions are also important in deciding the distribution of these 'linear' and 'bridged' CO. Primet et al. (62) found that for completely reduced sample of Ni/SiO_2 catalyst, the ratio of the linearly and bridged bonded species are independent of temperature in the 293 - 373 K range. However, on partially reduced samples, the linearly bonded CO is favoured. Eischens (63) found that the presence of adsorbed and dissolved H_2 in the catalyst also influences the properties of nickel toward the adsorption of CO. Supposedly adsorbed and/or dissolved hydrogen alters the electronic properties of the metal, possibly by transferring electrons to the nickel atoms. The IR spectrum shows changes corresponding to change from linear

Table 1-2

Surface Species for CO Chemisorbed on Nickel Surfaces

Species	Infrared Band	Frequency cm^{-1}
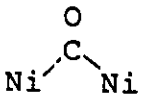	A	1915
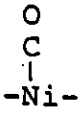	C	2035
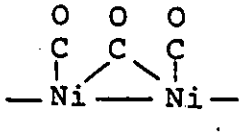	B	1963
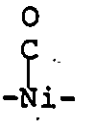	D	2057
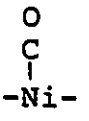	E	2082

structures to bridged structures, depending on the thoroughness with which H_2 has been removed from the metal after reduction. However, Primet et al. (62) showed that the presence of H_2 on nickel surfaces shifts the CO band from 2040 cm^{-1} to 2070 cm^{-1} and suggested that hydrogen is electron-attracting. Mercury and sulphur compounds which are known poisons for methanation reaction are also inhibitors for bridged CO formation on nickel surface (64-67).

It is generally accepted that the linearly or bridged bonded CO (mode A and C respectively) is important in methanation. However, the existence of the bridged structure as such has been questioned. Blyholder (68) has shown that all available data on the IR spectra of chemisorbed CO can be explained by assuming only a linear form of bonding. In addition, by distinguishing between surface sites and surface atoms, the spectra of CO on various nickel catalysts can be described on the assumption that only linearly bonded CO is present (69). Regardless of the actual mode of bonding to the metal surface, each type of adsorption should evidently be characterized by bonds of different strengths between the adsorbate and the catalyst surface, which should determine the thermal stability of the adsorbed CO and hence its stability toward hydrogenation. Heal et al. (70,71) have correlated the linearly bonded species with methane formation over nickel, cobalt and iron. However, Fujimoto et al. (72) have observed that on ruthenium

the bridged form is hydrogenated at lower temperatures than the linearly bonded CO, and suggested that the former is responsible for methane formation. Martin et al. (73) reported that when CO adsorbed on Ni/SiO_2 is heated above 400 K, a new band occurs at 1830 cm^{-1} corresponding to CO bonded to four nickel atoms. This species can be regarded as a precursor to the formation of carbidic species.

It is generally agreed that hydrogen is adsorbed dissociatively on a nickel surface. However, Vlasenko and Yuzefovich (26) concluded that hydrogen is adsorbed in the molecular form under methanation conditions. They argued that due to the influence of the adsorbed CO, the electronic state of the surface changes, resulting in a decrease in the energy of bonding between hydrogen molecules and the metal surface, and dissociation of the molecules does not occur. However, Siddiqui and Tompkins (74) concluded that in the presence of CO, hydrogen is adsorbed dissociatively with a positive charge. Selwood (75) evaluated the chemisorptive bonding of hydrogen on nickel based on published data on chemisorption and magnetic measurements, and concluded that chemisorbed hydrogen on nickel must consist of an atom carrying a negative charge and the stoichiometry is one hydrogen atom to one nickel atom.

Various attempts have also been made to find the intermediate in methanation by IR technique. Blyholder and Neff (76) obtained IR spectra of surface complexes formed

when CO and H_2 are exposed at 453 K to Fe/SiO_2 which they interpreted as having the following structure:

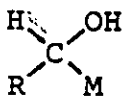

However, on nickel catalyst, they found no surface complexes at temperatures up to 453 K even though methane was readily formed and detected (77). Kölbel and Tillmetz (78) made calculations showing that formation of complex of the type M-C(H)-OH on a nickel surface is not favoured. They also suggested that the reactive species on nickel surface could be a methylene group. Surface methylene as an intermediate species has also been suggested by King (43), while Joyner (40) considered CH species to be important.

IR spectra study has helped to show that CO adsorbs in different forms on nickel surface. Of importance in methanation are the linearly and bridged bonded CO species with stretching frequencies in the region 2040 cm^{-1} and 1940 cm^{-1} respectively. Debates continue as to the actual existence of the bridged bonded CO as such, as well as to which species is responsible for the formation of methane. The attempts to find intermediate species in methanation by IR studies have not been fruitful. Although <u>in-situ</u> investigation revealed the presence of $-CH_2-$ and $-CH_3$ groups (41), their roles in methanation are still not clear.

1.2.4 Poisoning and other Studies

Methanation over nickel catalysts is very susceptible to poisoning by sulphur compounds. Poisoning studies have provided pertinent information in understanding the reaction. Using LEED, flash desorption and work function measurements, Erley and Wagner (79) have shown that inhibition of methanation reaction is due to the suppression of CO adsorption which is complete when surface coverage by sulphur is greater than 0.3 . Klosterman and Hobert (64) studied the reaction behaviour of a series of sulphur compounds on Ni/SiO_2 and concluded that the sulphur atoms from dissociation of these compounds block the sites required for dissociation of CO. A similar conclusion was also reached by Wentrcek et al. (66).

Poisoning and other studies suggest that methanation may require an ensemble of nickel atoms. Rostrup-Nielsen and Pedersen (80) concluded that the poisoning of methanation and Boudouard reactions is due to geometrical effect, and that the methanation reaction requires an ensemble with several nickel atoms. Employing IR spectroscopy and saturation magnetization techniques, Primet et al. (62) investigated CO adsorption on Ni/SiO_2 catalyst, and suggested the existence of a stable chemical form comprising a mixture of linear and multicentered CO, similar to that observed in metal clusters, where the CO is bonded to one, two or three metal atoms in well

defined proportions. Similarly Burton and Pugel (81) employed a flash desorption technique and identified the active site for CO adsorption as a three nickel atoms site. Pannell and coworkers (82) studied chemisorption of O_2, H_2 and CO on unsupported nickel and found that 0.54 CO molecules are irreversibly adsorbed per surface nickel atom. Harberts et al. (83) detected by thermal desorption the existence of strongly bound states of CO, α_1 and α_2 on nickel and nickel-copper alloys. They attributed the α_2 state to the recombination of C and O adsorbed species. A similar explanation was also given by Somorjai et al. (84) in their study of methanation over rhodium catalyst.

Adsorption studies of CO and H_2 have also shown that interaction leads to an enhancement effect. The effect of a chemisorbed layer of one gas on the chemisorption of another was first investigated by Griffin (85) who found that preadsorbed CO on copper and nickel catalysts increases the amount of H_2 adsorbed. Similarly Ghosh et al. (86) reported that on cobalt at constant pressure, chemisorption of H_2 is greater from a $1H_2$+1CO mixture than from a $2H_2$+1CO mixture, and the amount of CO adsorbed is greater from a $1H_2$+1CO mixture than from pure CO. Sastri et al. (87) observed a similar enhancement effect and suggested the existence of the complex HCOH. Wedler et al. (88) found that the heat of adsorption of H_2 on nickel is increased by the presence of preadsorbed CO. The maximum coverage of

CO on nickel at temperatures above 300 K is increased by the presence of preadsorbed H_2 on the surface.

1.3 Methanation of Carbon Dioxide

The hydrogenation of carbon dioxide to methane has received relatively little attention compared to the methanation of carbon monoxide. One reason for this is the historical role of H_2+CO gas in the Fischer-Tropsch synthesis. The renewed interest in substitute natural gas (SNG) and the engineering problem associated with the removal of heat in CO methanation have helped to shift research efforts towards CO_2 hydrogenation.

Carbon dioxide methanation on nickel contrasts that of carbon monoxide in the following respects:

(1) CO_2 is not hydrogenated in the presence of CO even in very low concentrations.

(2) Only methane is formed and no higher hydrocarbons are obtained.

(3) The reaction rate has been reported to be higher than that of CO.

One of the earliest proposed mechanisms for CO_2 methanation was made by Bahr (89), who proposed that reduction of CO_2 to methane occurs through the intermediate formation of CO. This view was questioned on the basis of the difference in methanation behaviours of the two carbon oxides (90-92). Medsford (93) proposed a mechanism not involving the formation of CO on the surface as an intermediate. This

mechanism was further developed by Pichler (94) who suggested that the hydrogenation takes place with atomic hydrogen present on the catalyst surface:

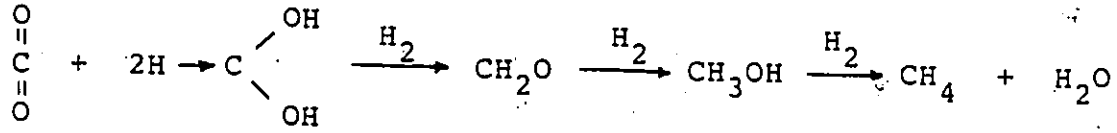

Similarly Vlasenko and Yuzefovich (26) proposed the following reactions to be the rate determining step in the methanation of CO_2:

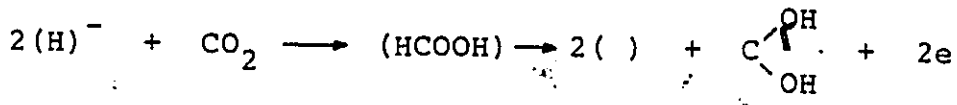

According to this scheme, the slowest step is the formation of an enol complex from adsorbed hydrogen and gaseous CO_2 and the intermediate enol complex reacts with H_2 in the gas phase to give methane. This mechanism is controversial since it proposes that the process is initiated by the activation of only the hydrogen on the catalyst surface, with the subsequent reactions taking place in the gas phase.

Other mechanisms were also proposed from kinetic studies. However, these earlier kinetic data were usually collected under high conversion conditions using pelleted catalysts, so that the intrinsic kinetics were often masked by heat and mass transport limitations. For example, Binder and White (95) studied the kinetics in a flow system at atmospheric pressure in the temperature range 533 -673 K

on a nickel-kielselguhr catalyst and concluded that the rate determining step is between one adsorbed CO_2 molecule and at least two adsorbed H_2 molecules. Similarly Dew and coworkers (96) investigated the kinetics on the same catalyst under pressures of 0.2 - 3.0 MPa and found that the data were correlated well by assuming the rate determining step involves an adsorbed CO_2 molecule and four adsorbed H_2 molecules. The following equation was obtained:

$$r = \frac{k_1 P_{CO_2} P_{H_2}^4}{(1 + k_2 P_{H_2} + k_3 P_{CO_2})^5} \quad (1\text{-}17)$$

At low pressure, about 0.2 MPa, the data could also be correlated by the equation:

$$r = \frac{k_1 P_{CO_2}^{0.5} P_{H_2}^2}{(1 + k_2 P_{H_2})^3} \quad (1\text{-}18)$$

which corresponds to a mechanism in which a dissociated CO_2 molecule reacts with two adsorbed H_2 molecules; the adsorption equilibrium constant for dissociated CO_2 is assumed to be negligible compared to that for H_2 .

Solc (5) investigated the kinetics using an excess of H_2 on a nickel-chromia catalyst and concluded that the order of reaction for CO_2 is 0.5 . This value was also reported by Cognion and Margnerin (51) and Pour (7).

Pour also found that H_2 has a fractional order of reaction at partial pressures below 25 kPa but zero order at higher pressures up to 100 kPa. The following rate equation was obtained:

$$r = \frac{k_1 P_{H_2} P_{CO_2}^{-\frac{1}{2}}}{\left(1 + k_2^{\frac{1}{2}} P_{H_2}^{\frac{1}{2}} \right)^3} \qquad (1\text{-}19)$$

However, Vlasenko et al. (97) found a first order dependency on CO_2 in temperature range 398 - 598 K when an excess of H_2 was used at a total pressure of 100 kPa.

Van Herwijnen et al. (52) studied the reaction at CO_2 pressures below 2 kPa and at temperatures between 473 and 503 K, and concluded that the rate of adsorption of CO_2 is the rate determining step as expressed by the following equation:

$$r = \frac{k_1 P_{CO_2}}{\left(1 + k_2 P_{CO_2} \right)} \qquad (1\text{-}20)$$

Thus, different mechanisms have been proposed for CO_2 methanation, varying from CO intermediate formation to enol complex, as well as chemisorbed CO_2 species. Kinetic studies have not been very fruitful because of the often extreme reaction conditions employed, resulting in the true kinetics being distorted by transport limitations. In addition, the reaction was often carried out in excess

hydrogen and failed to reveal the full kinetic picture. Thus, other studies are needed to furnish more consistent information, as found in the earlier studies of the adsorption of CO_2 . Eischens and Pliskan (98) suggested that CO_2 adsorbed on Ni/SiO_2 at room temperature and at a pressure of 160 Pa has the form of carboxylate $O=\overset{O}{C}-Ni$. Besten et al. (60) proposed that a possible mode of CO_2 adsorption could be $\overset{O=C-O}{Ni\ \ Ni}$. By infrared spectroscopy Blyholder and Neff (99) concluded that at 293 K CO_2 dissociates into chemisorbed CO and oxygen on Fe/SiO_2 catalyst. Hirota (100) by an isotopic desorption method concluded that about 1/3 of the nickel surface chemisorbs CO_2 very strongly at 195, 273 and 292 K, and part of the CO_2 chemisorbed is not desorbed even on evacuation at 573 K. Quinn and Roberts (101) studied the adsorption of CO_2 on nickel films in the temperature range 193 - 373 K and concluded that the surface is about 30% covered with CO_2 and the adsorption is probably dissociative. Similarly Brennan and Hayward (102) concluded from calorimetric measurement that nickel can adsorb CO_2 to only a small extent and can subsequently adsorb H_2 . They also suggested that adsorbed CO_2 could dissociate.

The more recent investigations of CO_2 methanation provide evidence confirming the dissociative adsorption of CO_2, and supporting the original Bahr mechanism. Maatman et al. (103) proposed that the mechanism involves two slow reaction

steps, either of which can be rate determining, the dissociative adsorption of H_2 and CO_2. Falconer and Zagli (104,105) investigated the reaction over ruthenium and nickel by temperature programmed desorption and reaction techniques and concluded that CO_2 dissociates to CO and O on adsorption at elevated temperatures, and that both CO and CO_2 methanation follows the same mechanism after adsorption. Gupta et al. (106) concluded that on ruthenium-molecular sieve catalyst the presence of H_2 is necessary for the dissociation of CO_2; methanation of CO_2 proceeds through the formation of CO and O species on the catalyst surface. Similar results were obtained by Solymosi et al. (107) on supported rhodium. The reaction steps consist of dissociation of CO_2 and the subsequent further dissociation into active surface carbon. Somorjai et al. found that on both iron (108) and rhodium (84) surfaces deposition of carbon occurs as a result of methanation of CO_2 or CO. By infrared studies, Martin et al. (73) concluded that adsorption of CO_2 is dissociative on nickel.

In summary the mechanism of CO_2 methanation is now beginning to receive more attention. From the data currently available, it seems likely that CO_2 hydrogenation proceeds through the intermediate formation of CO. The observed difference between the two carbon oxides in methanation is related to CO being more strongly adsorbed than CO_2.

1.4 Thermodynamics of Methanation

The formation of methane from carbon monoxide and carbon dioxide can be described by the following reactions:

$$3H_2 + CO \longrightarrow CH_4 + H_2O \quad (1\text{-}1)$$

$$4H_2 + CO_2 \longrightarrow CH_4 + 2H_2O \quad (1\text{-}2)$$

Also of importance in methanation is the water-gas shift reaction:

$$CO + H_2O \longrightarrow CO_2 + H_2 \quad (1\text{-}21)$$

The above reactions all have large negative values of Gibb's free energy over a wide range of temperatures, particularly reaction (1-1). Hence, they all have high equilibrium constant values K, and the reactions are very favourable thermodynamically. Because of the magnitudes of the equilibrium constants, the methanation rate will be neither limited nor affected by thermodynamics at moderate conversion of CO or CO_2.

Reactions (1-1) and (1-2) are highly exothermic. The exothermicity is only slightly dependent on temperature as shown in figure 1-1. The high heats of reaction present engineering problems in the design of large reactors. Failure

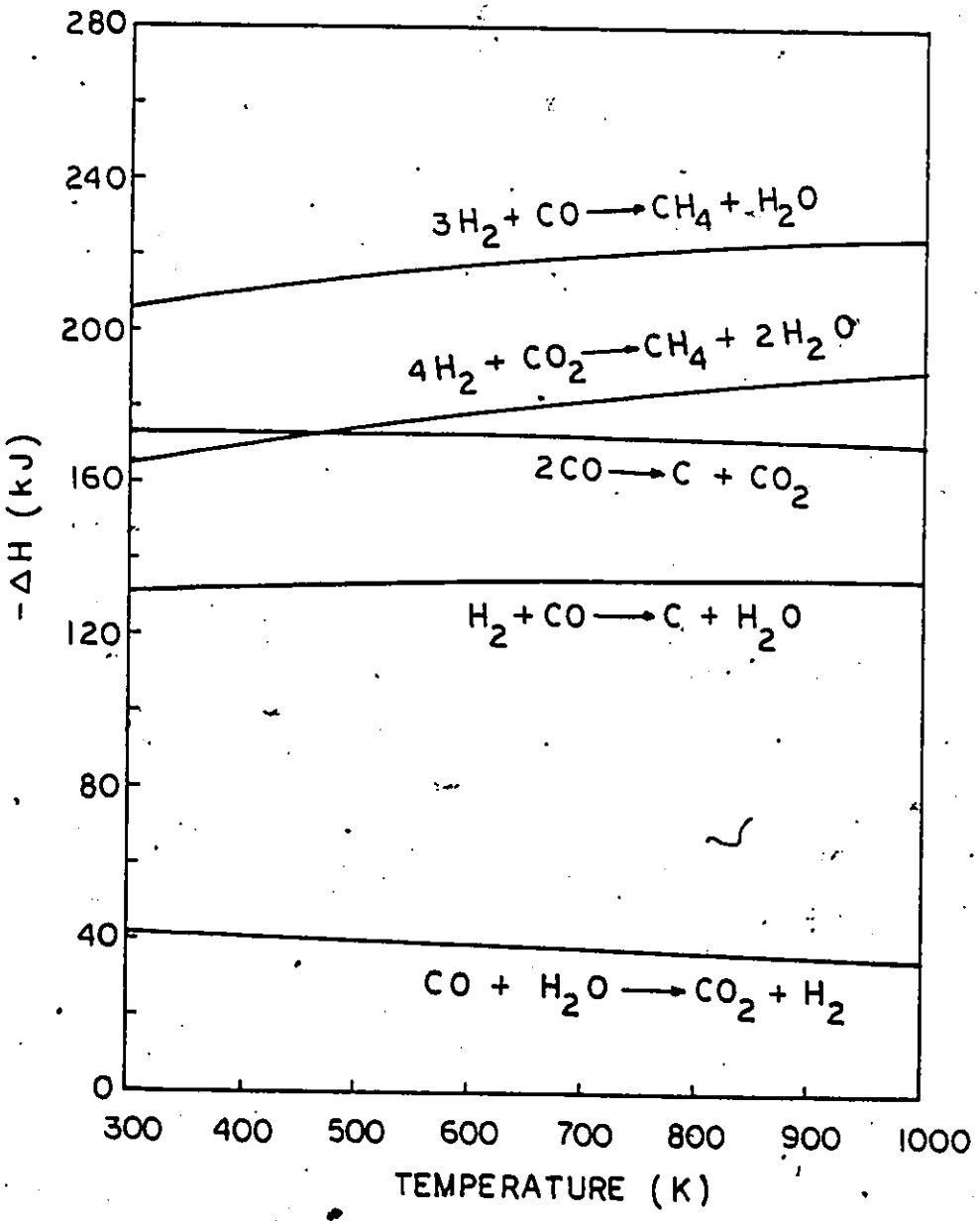

Figure 1-1 Effect of Temperature on the Heats of Reaction

to remove the heat will result in overheating and deactivation of the catalysts.

The equilibrium constants are affected critically by temperature. As the reactions are exothermic, increasing the temperature will decrease the values of the constants, the decrease being larger the greater the heat of reaction. As the latter is only slightly affected by temperature, one can expect almost linear plots of ln K as a function of reciprocal temperature as shown in figure 1-2.

By assuming ideal solution and gas behaviours, it can be shown that the equilibrium constants can be expressed in terms of the partial pressures of the reactants and products (109).

$$K_{CO} = \frac{P_{CH_4} P_{H_2O}}{P_{H_2}^{3} P_{CO}} = K_{p,CO} \qquad (1\text{-}22)$$

$$K_{CO_2} = \frac{P_{CH_4} P_{H_2O}^{2}}{P_{H_2}^{4} P_{CO_2}} = K_{p,CO_2} \qquad (1\text{-}23)$$

It can be seen that the equilibrium yield of methane is strongly affected by the H_2/CO and H_2/CO_2 ratios. Theoretically the methane yields are highest at higher

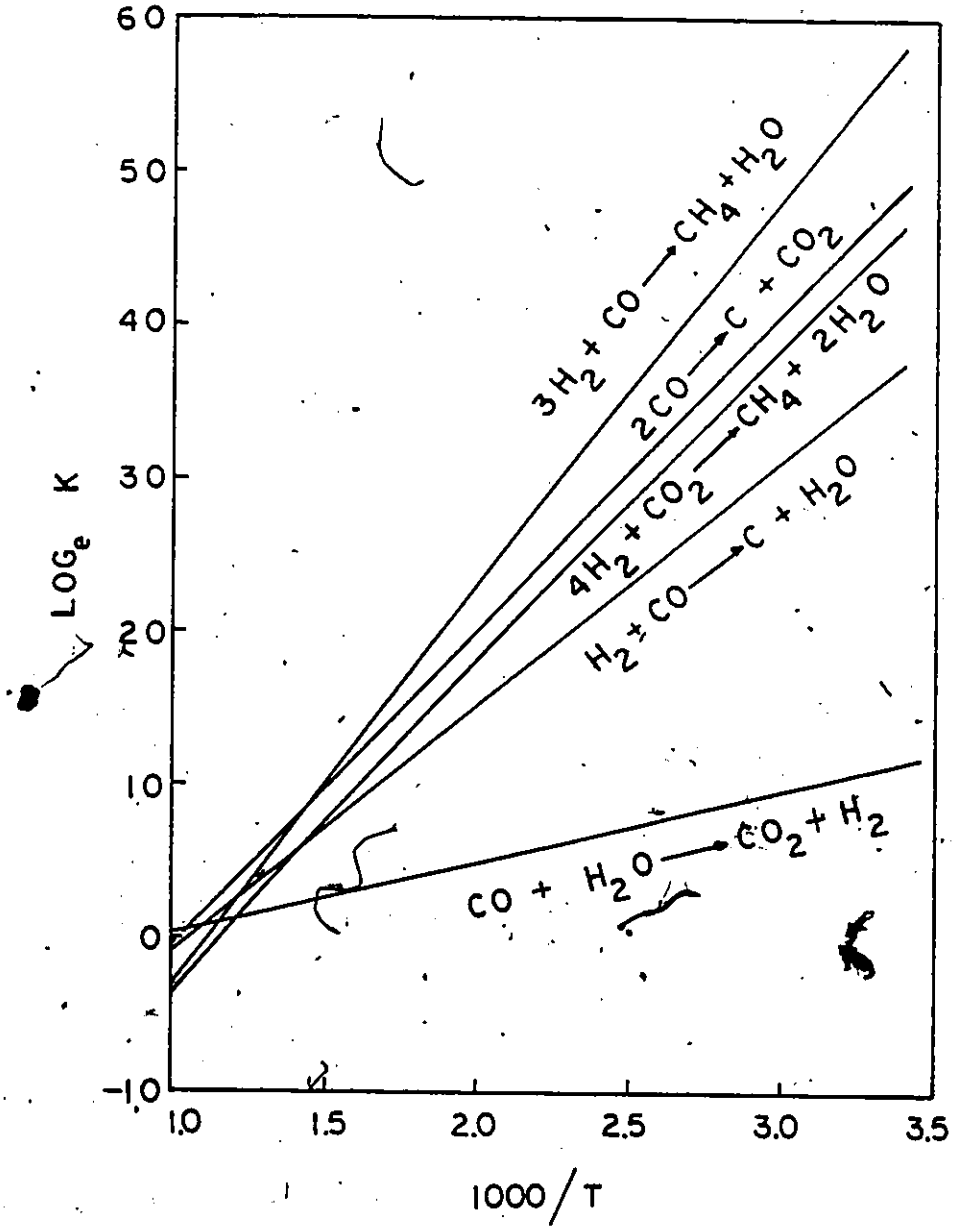

Figure 1-2 Effect of Temperature on the Equilibrium Constants

ratios. Although the water-gas shift reaction does not produce methane, it is of paramount importance in methanation because it alters the H_2/CO and H_2/CO_2 ratios and hence the equilibrium production of methane.

The equilibrium constants K are independent of total operating pressure. However, when expressed in terms of mole fractions, one has, for CO methanation, the following equation:

$$K_{CO} = \frac{y_{CH_4}\, y_{H_2O}}{y_{CO}\, y_{H_2O}^3} P^{-2} = K_{y,CO}\, P^{-2} \quad (1\text{-}23)$$

where K_{CO} = equilibrium constant for CO methanation

y = mole fraction

$K_{y,CO}$ = equilibrium constant in terms of mole fraction

P = total pressure.

Hence increasing the total pressure will increase K_y and the equilibrium yields of methane. This pressure effect on the equilibrium yield is small however when the values of K are large. At higher temperatures where the values of K are about unity, increasing pressure will significantly increase the yield of methane. For the water gas shift equilibrium is independent of pressure.

In methanation carbon may be formed by the following reactions:

$$2CO \longrightarrow C + CO_2 \qquad (1\text{-}25)$$

$$CO + H_2 \longrightarrow C + H_2O \qquad (1\text{-}26)$$

Deposition of carbon may result in a decrease in catalyst activity. Whether carbon deposition occurs or not is mainly governed by the H_2/CO ratio. Increasing pressure tends to decrease the minimum ratio required to inhibit carbon formation. At ratios above two, temperatures above 600 K tend to favour increased carbon deposition. Despite these temperature and pressure effects, carbon deposition is still primarily related to the H_2/CO ratio. In general higher ratios will prevent carbon laydown.

1.5 Reactor

In the study of chemical kinetics or the evaluation of the performance of catalysts, it is important that the data collected reflect the true chemical events occurring at the catalyst surface. As the concentration of reactants and the temperature at the catalyst surface are practically impossible to measure and the usual measurements only reflect the bulk conditions, the interphase and intraparticle transfer of mass and heat should be fast compared with the reaction rate on the surface. Thus, the design of the reactor should aim at the elimination of any concentration and temperature gradients. In this event, the bulk condition can be taken as a good measurement of the surface conditions. Large gas

velocities, small catalyst particles and low reaction rates tend to favour the elimination of complications due to mass and heat transfer limitations (110).

Perhaps the most important criterion in the design of a catalytic reactor is the temperature effect. As reaction rates generally increase with temperature in an exponential manner, attempts to account for possible temperature gradients can lead to large uncertainties and distortion of the kinetic picture. Ideally the catalyst bed should be isothermal. A well characterized flow pattern across the catalyst bed is also imperative in the deduction of kinetics. Ideally flow patterns such as plug flow or perfectly mixed flow lend themselves to easy mathematical treatments (111).

Before a reaction can proceed in a heterogenous catalytic system, the reactants must reach the catalyst surface from the bulk phase. The concentration difference between the bulk phase and the catalyst surface constitutes the driving force for mass transfer. To minimize this concentration gradient, one must have a high mass transfer coefficient; this can be achieved by increasing the flow rate thereby decreasing the thickness of the boundary layer at the catalyst surface. Interphase mass transfer can be correlated in terms of the j-factor (110,112).

Similar reasoning also applies to the elimination or minimization of temperature gradients between the bulk phase and the catalyst surface. This magnitude depends on

the heat transfer coefficient between the fluid and the catalyst surface and hence on the flow rate and the heat of reaction. The heat transfer coefficient can be obtained from the j-factor (110,112).

For reactions on a porous catalyst, intraparticle transfer through the pores is also important because these pores offer resistance to mass and heat transfer. The effects of gradients inside the particles are usually described in terms of the Thiele modulus and an effectiveness factor (110,112,113). Small particle diameters will minimize these gradients.

As a kinetic study is concerned with how the reaction rate is affected by temperature and concentrations of the reactants and products, an ideal reactor should be one where interphase and intraparticle gradients are minimal, and only under this condition can measured data reflect accurately the events at the catalyst surface. In addition, for ease of analysis of data, the bulk phase should be of uniform concentration and temperature, independent of its position in the reactor. This uniformity in concentration and temperature could be achieved by external means such as stirring or by keeping the conversion at a low level. A low conversion, usually between 1 to 4%, helps to maintain the temperatures and concentrations across the catalyst bed practically the same.

In comparison with an integral reactor a differential reactor is superior, because the various gradients cited above are minimized by controlling the conversion. Low conversion enables one to obtain the reaction rate without resorting to integration or differentiation techniques as required with data from an integral reactor. Hougen (114) has provided excellent testimony in favour of the differential reactor systems. However, the low level of conversion obtained in a differential reactor requires precise analysis of product samples to obtain accurate kinetic data. With modern analytical techniques and instruments this poses no great problem.

From the data acquired in a differential reactor, the rate of reaction can be determined easily from the effluent composition and flow rate according to the following equation (115):

$$r = \lim_{X \to 0} \frac{dX}{d\,(W/Q)} = \frac{X\,Q}{W} \qquad (1\text{-}27)$$

No differentiation of the data nor integration of an assumed rate equation are needed to obtain the reaction rate. Once the rate is obtained, empirical or theoretically-derived rate equations can be tested.

Differential reactors have been widely used for various kinetic studies, including sulphur dioxide

oxidation (116), ethylene hydrogenation (117), hydrogen oxidation (118), and carbon monoxide oxidation (119). It has also proved to be a favourite tool for studying methanation kinetics (4,18,56,57,103,107,120-125).

1.6 Analysis of Data

In the investigation of a reaction, one often fits the data to possible kinetic equations which are either empirical or theoretically-derived based on a set of assumptions. These equations are often invaluable in the subsequent design and operation of large scale reactors. They are also important in contributing qualitative insight into a possible reaction mechanism, and can suggest new experiments to elucidate further understandings based on predictions of the equations. In spite of the use of powerful tools such as infrared spectroscopy, isotopic tracer studies, etc., most heterogeneous reactions still elude a complete understanding on the molecular level. On a less sophisticated level, one can turn to an approximate approach which often invokes certain assumptions, established or based on experimental evidence, regarding the possible surface species and the slowest reaction step. This method will result in a rate equation which is to be tested against the data collected.

The rate equation often used in heterogeneous catalyst studies can generally be classified into two

categories. The first one is the power rate law which can be regarded as based on the Freudlich isotherm (112,115):

$$r = k P_A^a P_B^b \qquad (1\text{-}28)$$

where k = constant

P_A, P_B = partial pressures of A and B, respectively

a, b = exponents

The rate is expressed in terms of the partial pressures of the reactants raised to the appropriate power. Despite its empirical nature, the use of the power rate law is very common in the investigation of kinetics. However, as pointed out by Weller (126), power rate law should only be used as a guide for design purpose in real plant operation within the range of operation conditions under which the rate equation is obtained. One should exercise caution when employing the power rate law for the investigation of reaction mechanism. While it does give some definite qualitative information, its mechanistic interpretation is limited. However, it is quite a convenient tool in the preliminary investigation of a reaction, and certainly has its place in reaction kinetic studies.

The second kind of rate equation commonly used is the Langmuir-Hinshelwood equation (112,113):

$$r = \frac{k P_A P_B}{(1 + K_A P_A + K_B P_B)^n} \qquad (1\text{-}29)$$

where k = rate constant

K = adsorption constant

It is usually derived from a postulated reaction path with certain assumptions such as a rate determining step. Although not without its share of criticism (126), the Langmuir-Hinshelwood equation has the merit of conveying a more realistic description of a catalytic reaction than the power rate law. In particular, a properly selected equation furnishes very useful information regarding the effects of reactant partial pressures, total pressure and temperature. More significantly, one can attach a meaningful mechanistic interpretation to the model. Between the Langmuir-Hinshelwood equation and the power rate law, the former is preferable because greater understanding and control of reaction conditions are provided by the more flexible model. In addition, the power rate laws may not have the proper mathematical form for describing the kinetic data collected under vastly different conditions.

In the analysis of data from heterogeneous systems, the use of kinetic expressions more complicated than Langmuir-Hinshelwood type equations are seldom warranted.

While the data should be analysed and represented by as sophisticated and theoretical a model as possible, it is not necessary to go to the extreme to account for every catalytic effect on the metal surface with involved mathematics when these effects and forces are not yet completely understood. This is especially true when kinetic data often have substantial experimental errors. On the other hand, within the objective of adequate data representation, the kinetic model selected should be concise and have the minimum number of parameters. It has been pointed out that any improved fit involving complicated Langmuir-Hinshelwood type equations arises from the greater flexibility of the equations with the abundance of parameters. Despite the fact that the assumptions used in deriving the Langmuir-Hinshelwood equations are not strictly correct, they are often employed in kinetic studies because they convey qualitative understanding as well as a concise and realistic picture of the reaction mechanism (127).

In arriving at the best kinetic model, one often goes through the following procedures:

(1) identification of model

(2) estimation of model parameters.

These two procedures are highly interactive. For a given model one may obtain negative values for some parameters,

e.g. rate constants, which are physically impossible, thus casting doubt on the validity of the proposed model. Model identification involves some types of discrimination techniques while parameter estimation usually involves regression analysis. These statistical methods have been described in the literature (128-130), and the pertinent procedures are discussed in appendix B.

To test a kinetic equation the data are fitted to this equation and evaluated by some criteria such as minimum sum of squares between the predicted and observed rates. The criteria for model rejection may be based on:

(1) lack of fit as evidenced by an excessively large residual sum of squares

(2) unacceptable characteristics of the estimated parameters, such as negative rate constant.

Negative adsorption constants should not necessarily be rejected since they may result from enhanced adsorption (131). Very often more than one equation is found to be an adequate mathematical representation of the data. Since no investigation can be exhaustive in examining all possible reactions, at this stage one can only say that the equation or equations is an adequate representation of the data over the experimental conditions investigated, but by no means is the mechanism identified or proved. A good fit is a necessary but not sufficient condition for proving any mechanism.

The estimation of the best parameter values for a given model is essentially achieved by minimizing some appropriate measure of errors, usually the difference between the observed and predicted rates. In the least-squares approach, the sum of squares of the errors is minimized. Since Langmuir-Hinshelwood equations are highly non-linear, linear regression should not be used. Non-linear regression techniques involving search in the parameter domain to minimize the errors was used in this study.

Chapter 2

CHARACTERIZATION OF CATALYST

2.1 Introduction

The rate and selectivity of a heterogenous reaction depend on the catalyst and the reactants used. Since the activity of a catalyst in a reaction is intimately related to its properties, knowledge of these properties is important.

The catalyst employed in this work was a commercial sample of Raney nickel (W.R. Grace Co.). This catalyst was in the form of powder of a mean diameter of 0.04 mm. The characteristics of Raney nickel have been detailed elsewhere (132-140). Essentially it is obtained by leaching out the aluminum in a nickel-aluminum alloy. Thus, the constituents of Raney nickel are nickel, residual alloy due to incomplete leaching, alumina trihydrate, and sodium as $NaAlO_2$. Details of the chemical compositions can be found in references (132-135).

The Raney nickel sample contained 90% and 3-4% by weight of nickel and aluminum, respectively, the remaining constituents being mainly alumina tridhydrate. The catalyst was stored under distilled water. Samples were weighed by difference in a sample tube after in-situ removal of water by

evacuation at room temperature. The following sections summarize the investigations performed in the characterization of the catalyst.

2.2 Adsorption Studies

2.2.1 General

Since adsorption constitutes an important part in any heterogenous reaction, adsorption studies were performed to obtain information such as surface area, pore radius, metal site density, etc. A glass vacuum system was used to measure adsorption isotherms by standard volumetric techniques (115). A Pyrex sample cell fitted with two stopcocks permitted flowing of hydrogen over the sample during hydrogen treatment. The catalyst was pretreated with hydrogen under the same conditions as were used for the catalyst before kinetic experiments, usually 12 - 14 hours at 623 K. It was then evacuated at the same temperature for one hour and cooled to room temperature. Hydrogen treatment was done to ensure absence of any nickel oxide since the catalyst might be oxidized during long storage.

2.2.2 Nitrogen Adsorption

A nitrogen adsorption isotherm was determined at 77 K over a range of relative pressures from 0.05 to 1 as shown in figure 2-1. The isotherm obtained was of type IV, very similar to that of sample COM I employed by Freel et al. (133,135), except that the pore volume was somewhat lower, possibly due to the high temperature treatment (132).

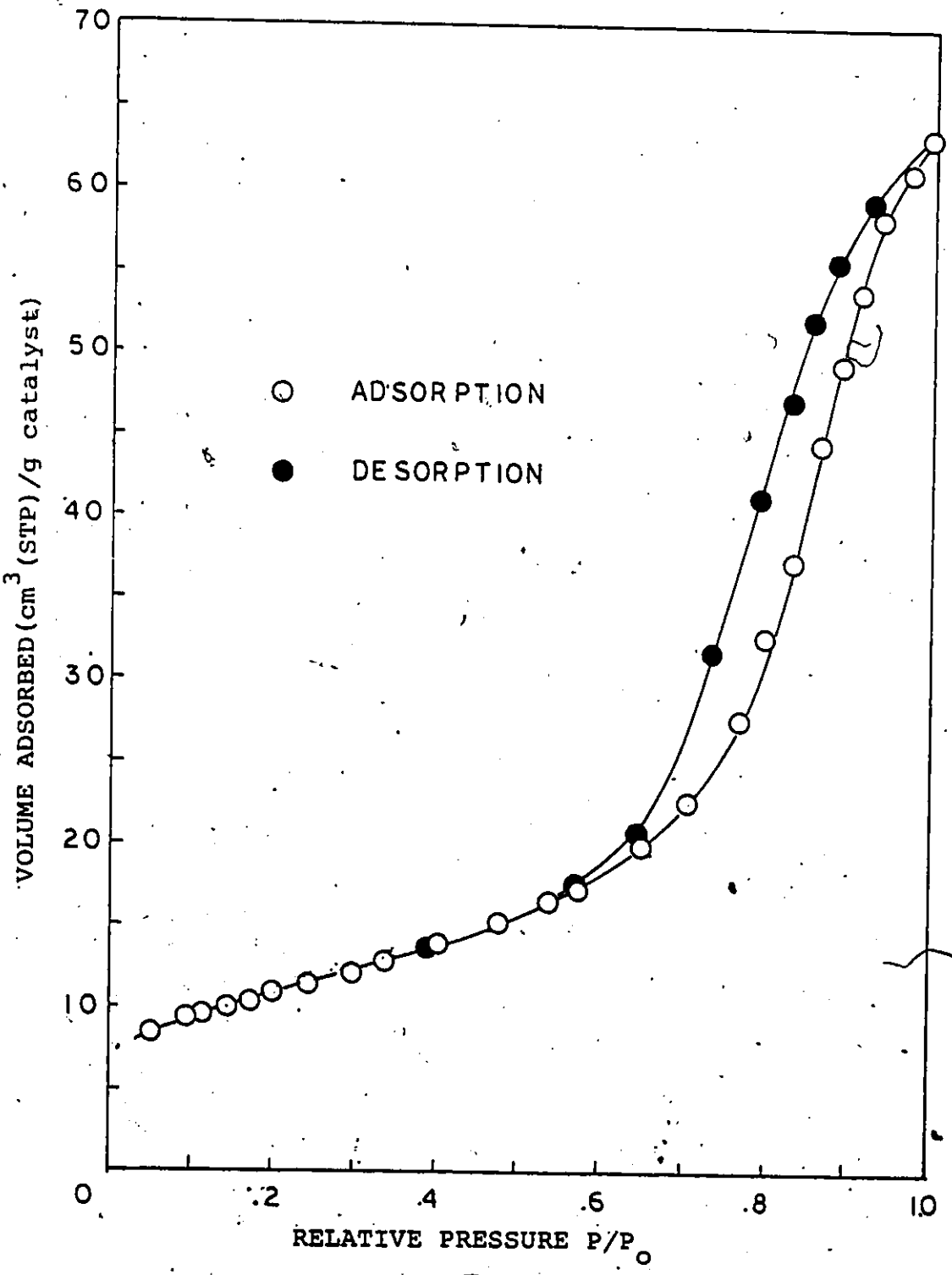

Figure 2-1 Nitrogen Adsorption Isoth[illegible] at 77 K

The surface area was determined by using the linearized form of the BET equation (141):

$$\frac{x}{V(1-x)} = \frac{1}{V_m c} + \frac{x(c-1)}{V_m c} \qquad (2\text{-}1)$$

where x = relative pressure

V = volume adsorbed

V_m = volume corresponding to a monolayer

c = constant

Data in the relative pressure range of 0.05 to 0.35 were plotted as shown in figure 2-2. In the calculation it is assumed that each molecule of physically adsorbed nitrogen occupies 0.163 nm^2, based on the assumption that the adsorbed layer has the same density as the liquid phase. As the intercept which gives a value of $1/V_m c$ is very close to zero and difficult to read accurately, the data were plotted in the following way:

$$\frac{1}{V(1-x)} = \frac{1}{V_m} + \frac{(1-x)}{V_m c x} \qquad (2\text{-}2)$$

The result is shown in figure 2-3. The intercept gives directly the value of $1/V_m$. From either plot, the monolayer volume was estimated to be 8.9 cm^3 (STP) per gram of catalyst.

The surface area of the catalyst is related to

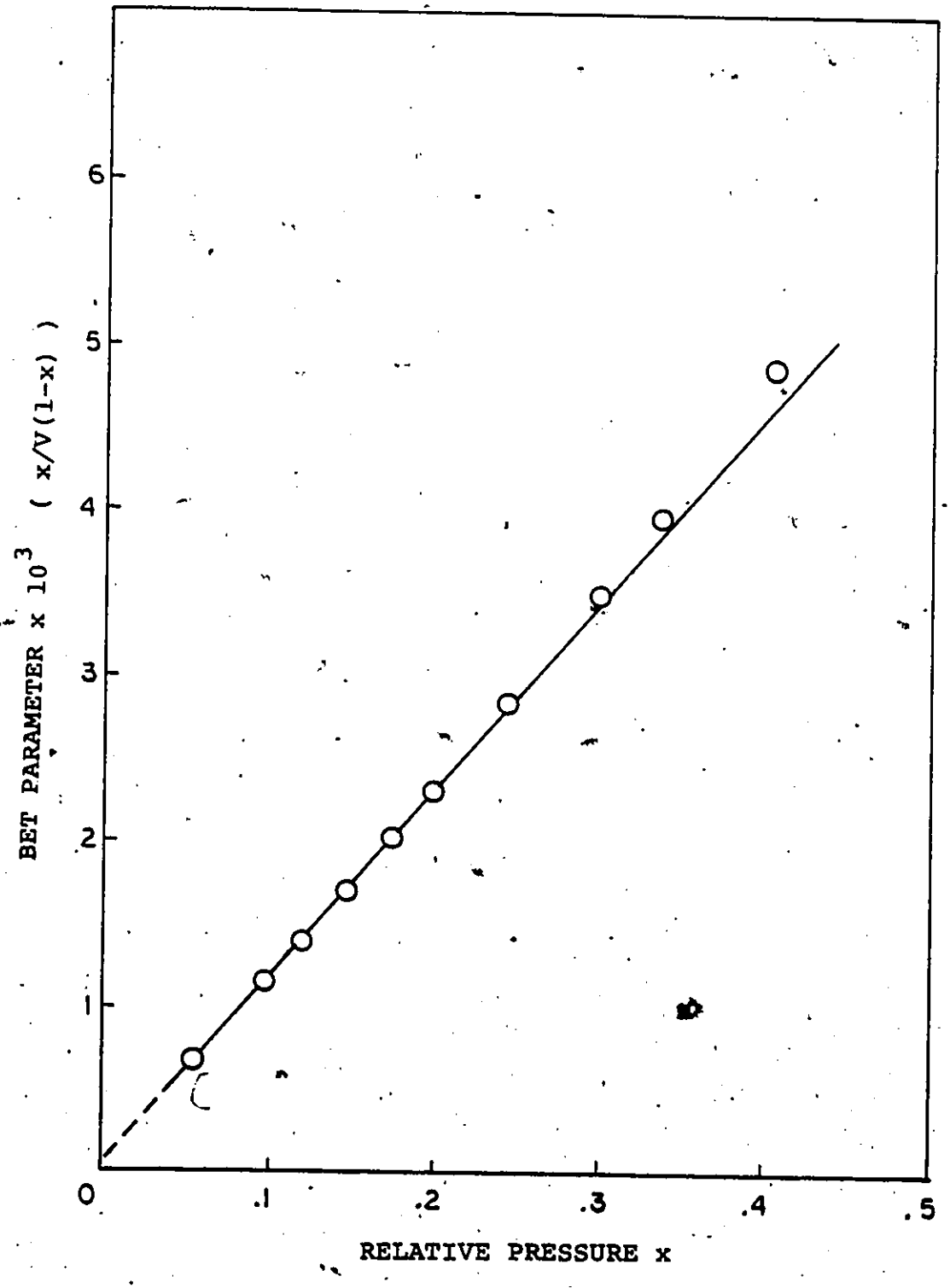

Figure 2-2 B.E.T. Plot for Nitrogen Adsorption Data

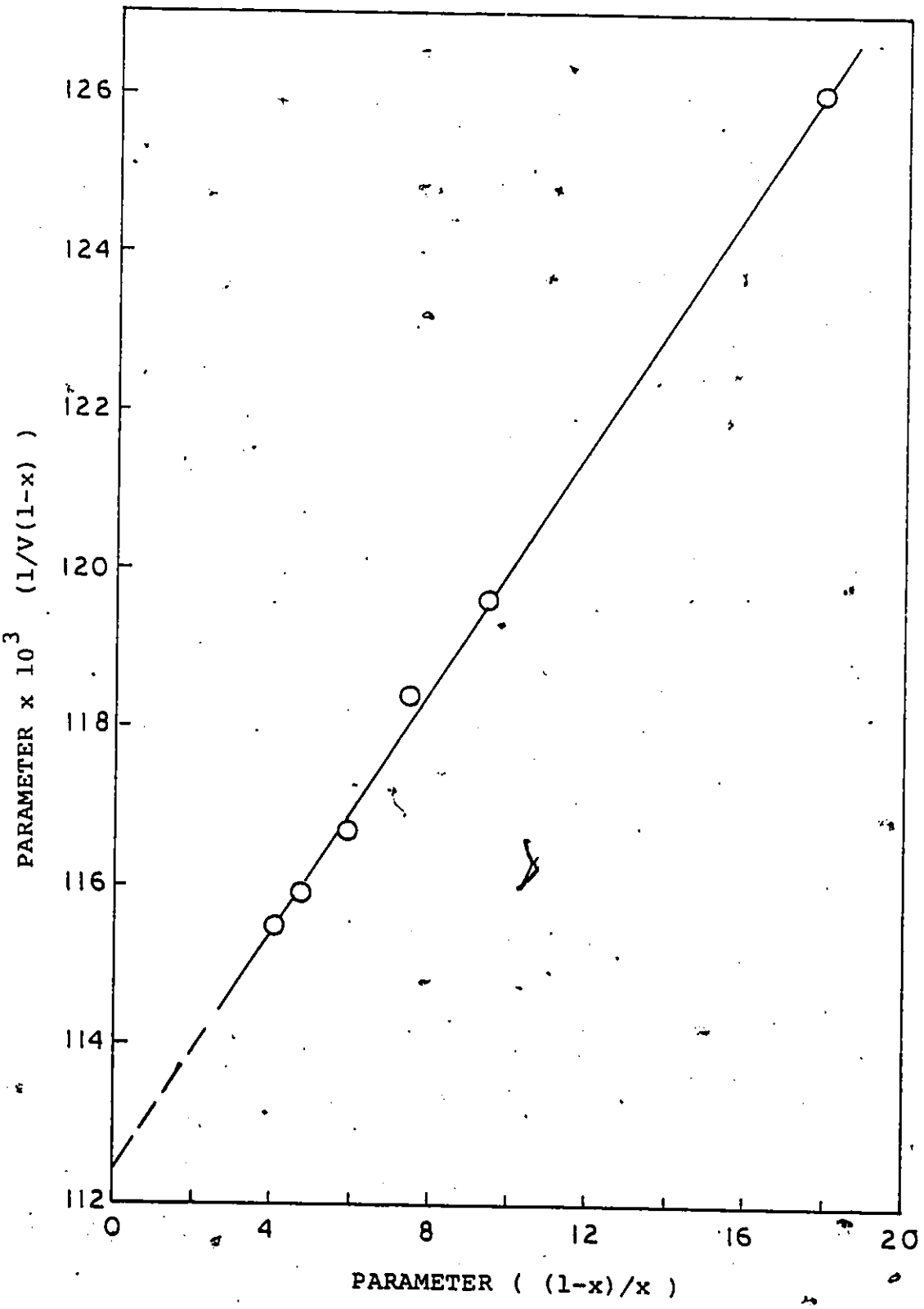

Figure 2-3 B.E.T. Plot for Nitrogen Adsorption Data

the monolayer volume by:

$$S = 4.37\ V_m \qquad (2\text{-}3)$$

where S is the total surface area in m^2 per gram of catalyst. Using the value of V_m obtained above, the total surface area was found to be 38.9 m^2/g, approximately half of the expected value of 80 m^2/g. The low surface area could be due to the high temperature used for hydrogen treatment and evacuation. Nicolau (132) reported that the total surface area decreased from 80.1 m^2/g for evacuation at 379 K to 22.2 m^2/g when evacuated at 865 K.

The total amount of nitrogen adsorbed at saturation (at relative pressure of 1.0) and the average pore radius are related by the following equation (115):

$$\bar{r} = 0.71\ V_s/V_m \qquad (2\text{-}4)$$

where $\bar{r}$ = average pore radius in nm

V_s = amount of nitrogen adsorbed at saturation in cm^3

The equation assumes that the pores are cylindrical and uniform. Using a value of 63.5 cm^3 for V_s from the isotherm, the average pore radius was estimated to be 5.07 nm.

An alternative way of obtaining the total surface area is the use of the universal t-plot of De Boer (142). In this method as long as multilayers are formed freely, the amount of gas adsorbed is proportional to the thickness (t) of the adsorbed layer. The thickness can be related

to the relative pressure by the standard or universal isotherm (143). Thus, through this correlation one can plot the volume of adsorbed nitrogen versus the thickness. The surface area is given by the slope of the V-t plot. Since zero adsorption corresponds to zero thickness, the straight portion of the curve should pass through the origin. At higher relative pressures, deviation from linearity occurs due to capillary condensation and filling. The surface area is given by:

$$S = 1.547\ V/t \qquad (2-5)$$

where V = volume adsorbed in cm^3

t = thickness of adsorbed layer in nm

The value obtained by this method is 37.9 m^2/g which agrees well with the surface area obtained by the BET method. Capillary condensation occurs approximately at the same relative pressure as the hysteresis exhibited by the nitrogen isotherm (i.e. at a relative pressure of about 0.8 or adsorbed layer of thickness 1 nm). Figure 2-4 shows the V-t plot.

2.2.3 Pore Size Distribution

The nitrogen isotherm also yields information regarding the pore size distribution of the catalyst (144,145). The calculation assumes that during desorption the radius of the pore and the relative pressure are related by the Kelvin equation for cylindrical pores (112):

$$r = 0.405/\log(1/x) \qquad (2-6)$$

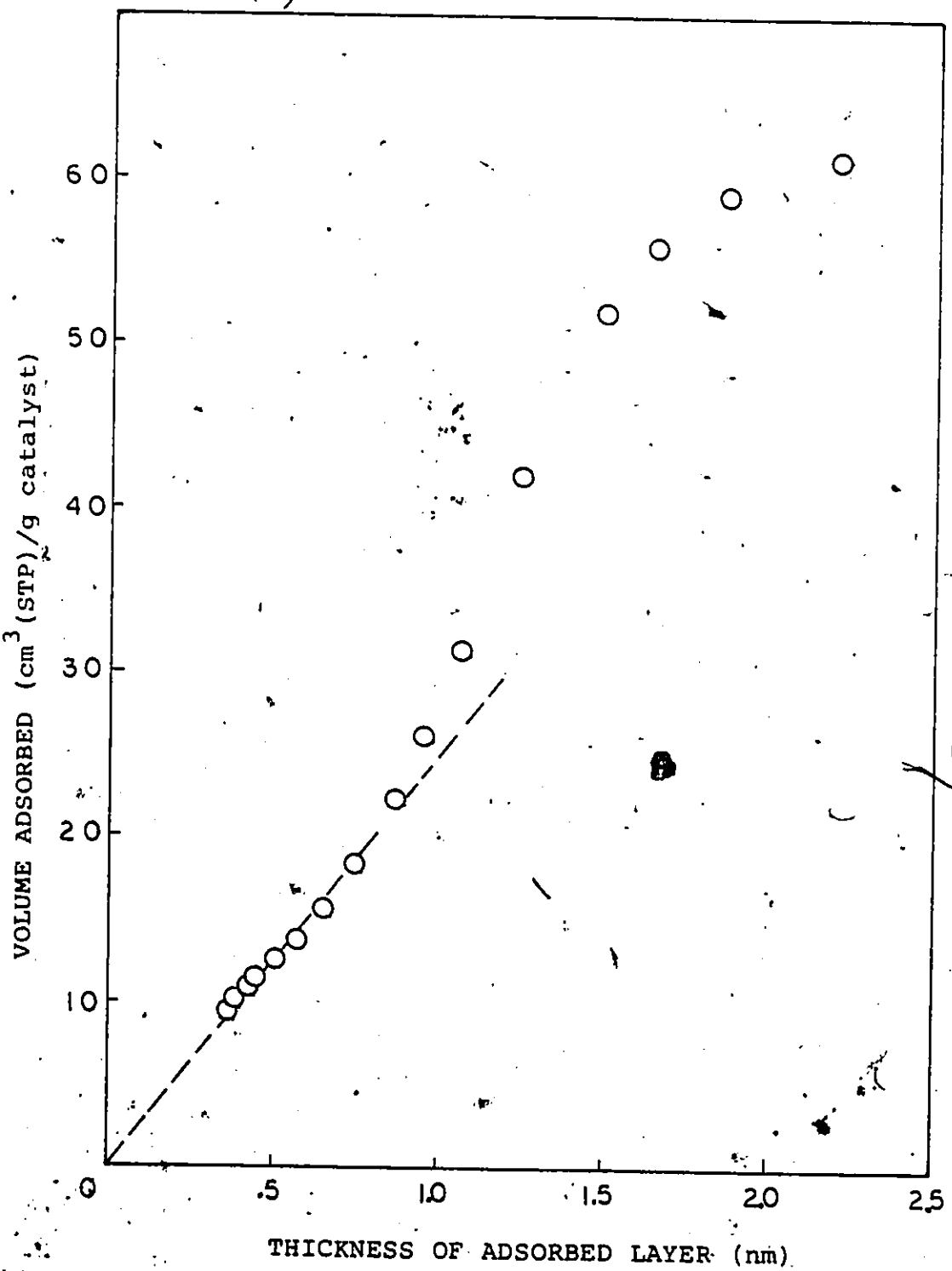

Figure 2-4 Volume Adsorbed versus Thickness of Adsorbed Layer

where r_p = radius of pore in nm

x = relative pressure

while the Cohen equation:

$$r_p = 0.2025/\log(1/x) \qquad (2-7)$$

applies to the adsorption process when capillary condensation takes place. The method developed by Anderson (146,147) was applied to a cylindrical pore model using the adsorbed layer thickness data of De Boer (143). The frequency distribution for pore radius of the catalyst sample appears in figure 2-5. The results from adsorption and desorption data are in good agreement with maxima at pore radius of about 4 nm.

The calculations also yielded cumulative estimates of the surface area and amount adsorbed at saturation (figure 2-6), and these compare favourably with the values previously determined using the other methods.

Table 2-1 summarizes the results obtained from the nitrogen adsorption isotherm for the Raney nickel sample.

2.2.4 Chemisorption

The nitrogen isotherm gives the total surface area which includes the metal surface area. To obtain the latter the technique of chemisorption is used. Ideally a gas which selectively chemisorbs on the metal only should be used. For this purpose hydrogen and carbon monoxide are commonly used (4,120,121,135,148-151). However, to correct for the amount of adsorbate which may be weakly adsorbed,

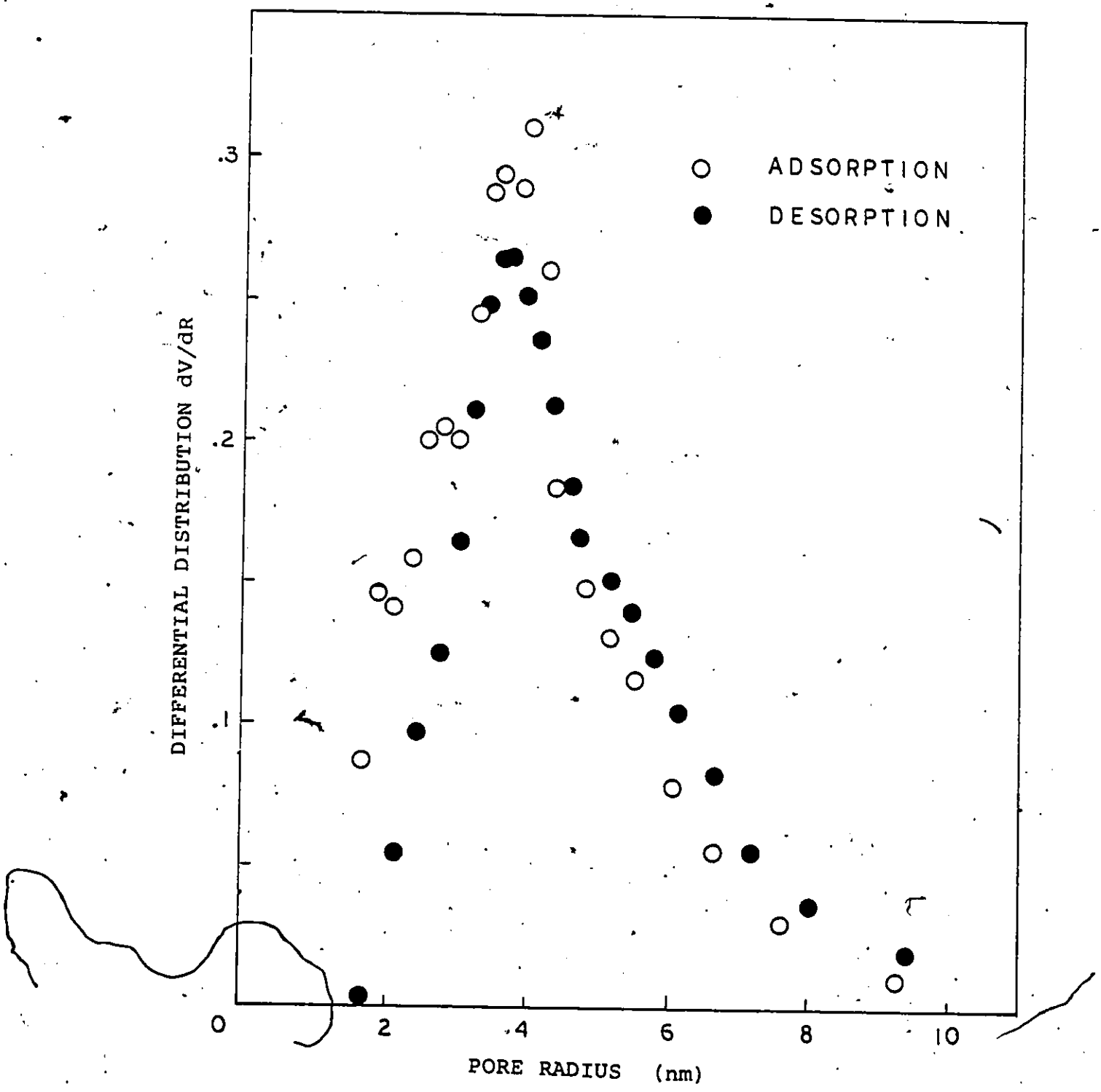

Figure 2-5 Pore Size Distribution

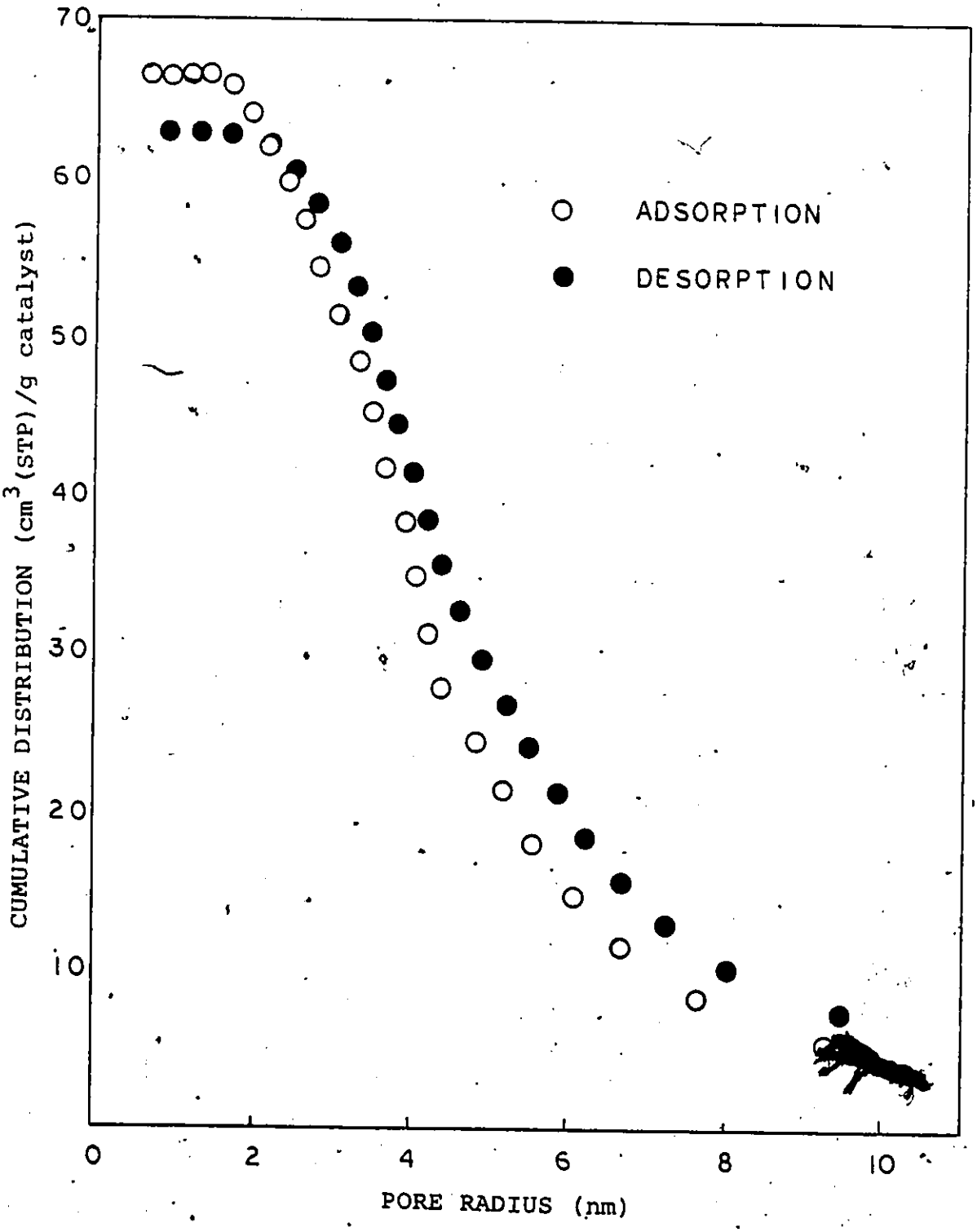

Figure 2-6 Cumulative Distribution of Pore Size

Table 2-1

Summary of Catalyst Properties determined from N_2 Adsorption Isotherm

Method	Surface Area (m^2/g)	Pore Volume (cm^3)	'Average' Pore Radius (nm)
Saturation	-	63.5	-
B.E.T.	38.88	-	-
Equation 2-4	-	-	5.1
De Boer	37.90	-	-
Pore Distribution			
Adsorption	52.94	66.4	4.0
Desorption	42.90	62.7	4.0

the two-isotherms approach is used. After the first isotherm is obtained, the catalyst is evacuated for a brief period to remove the weakly adsorbed adsorbate. Then, a second adsorption isotherm is determined. The difference in amount adsorbed is due to the strongly chemisorbed gas (135).

Hydrogen generally adsorbs on nickel dissociatively with one hydrogen atom adsorbed per surface metal atom (75). From the amount adsorbed at saturation on the nickel surface area can be calculated by using an appropriate value for the area associated with a single metal atom on the surface. The average area for a surface nickel atom is 0.0677 nm^2 (148).

For carbon monoxide as an adsorbate the situation is complicated by the fact that the adsorption mode on nickel is not clear. Both linear and bridge-form adsorptions are known to occur, the latter taking up two nickel atoms per adsorbed CO molecule. Thus one would expect the ratio of adsorbed CO to H_2 to lie between one and two.

Hydrogen was passed through the sample of catalyst at 623 K overnight, after which it was evacuated for three hours and cooled to room temperature. The first hydrogen adsorption isotherm was obtained at 77 K and pressures up to 60 kPa. The time required for equilibration at any one pressure was about 30 - 45 minutes. The sample was then evacuated at 195 K for one hour before readsorption was performed to obtain the second isotherm at 77 K. Similar

procedures were also used for carbon monoxide. The isotherms obtained are shown in figures 2-7 and 2-8.

The amount of hydrogen strongly chemisorbed was 3.2 cm^3 (STP) per gram catalyst, while for carbon monoxide 4.3-cm^3. This corresponds to about 50% of the chemisorbed CO molecules being adsorbed on the metal surface in the bridge form. From the amount of hydrogen chemisorbed and assuming an area of 0.0677 nm^2 per surface nickel atom, the nickel surface area was estimated to be 11.64 m^2 per gram catalyst, corresponding to a surface concentration of 1.72×10^{20} nickel atoms per gram catalyst.

Chemisorption data can also be used to calculate the average crystallite size of nickel in the catalyst. Assuming cubic crystallites of length l with five exposed surfaces, it can be shown that the following equation holds:

$$l = 5w/Sd \qquad (2\text{-}8)$$

where l = length

S = surface area of metal atoms per gram of catalyst

d = density of the metal

w = weight fraction of metal in catalyst

The density of nickel is 8.9 g/cm^3, and the concentration of nickel in the Raney nickel is 90% by weight. The estimated average crystallite length was found to be 43.4 nm, corresponding to a dispersion of 1.86%.

Though the low temperature chemisorption gives a

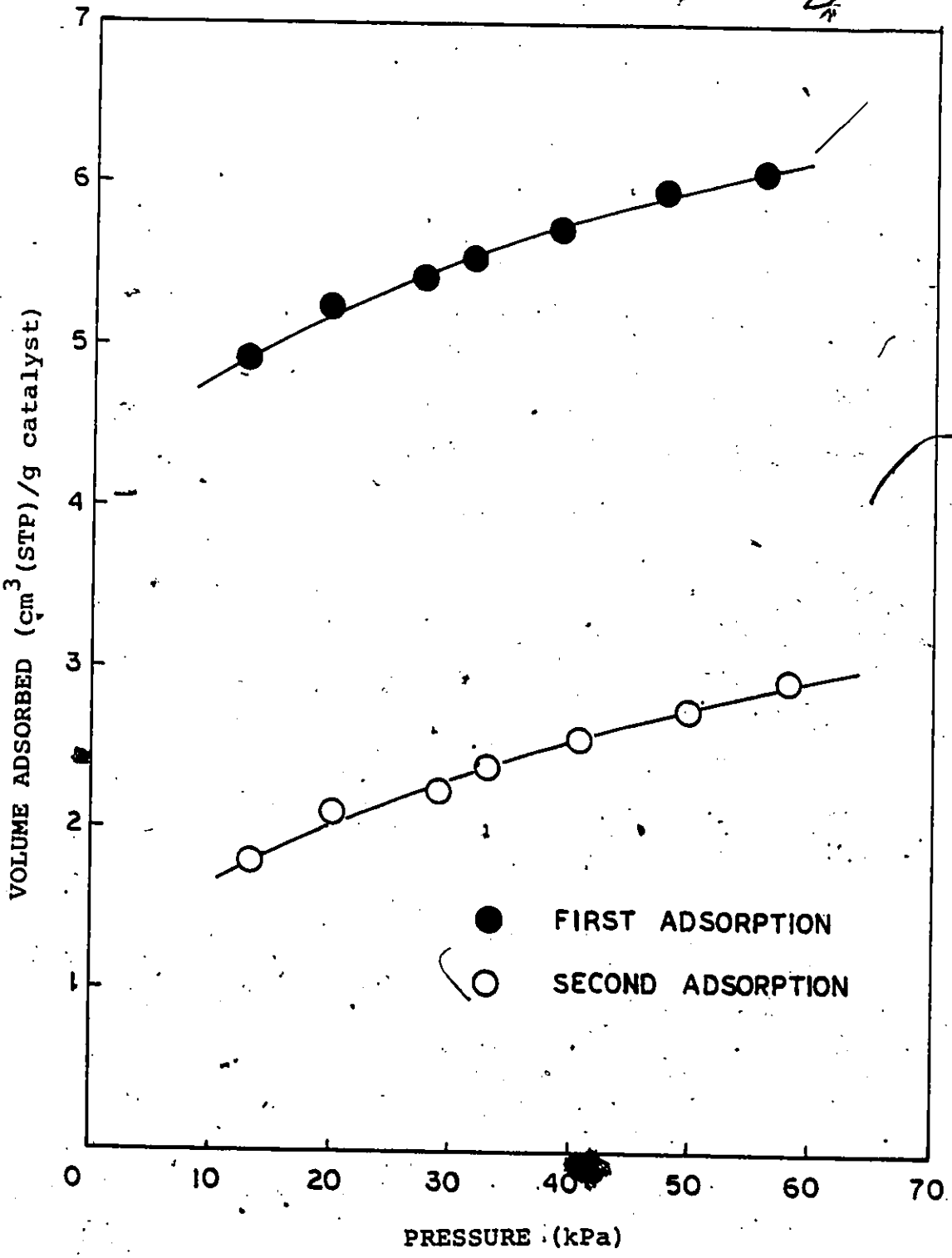

Figure 2-7 Hydrogen Adsorption at 77 K

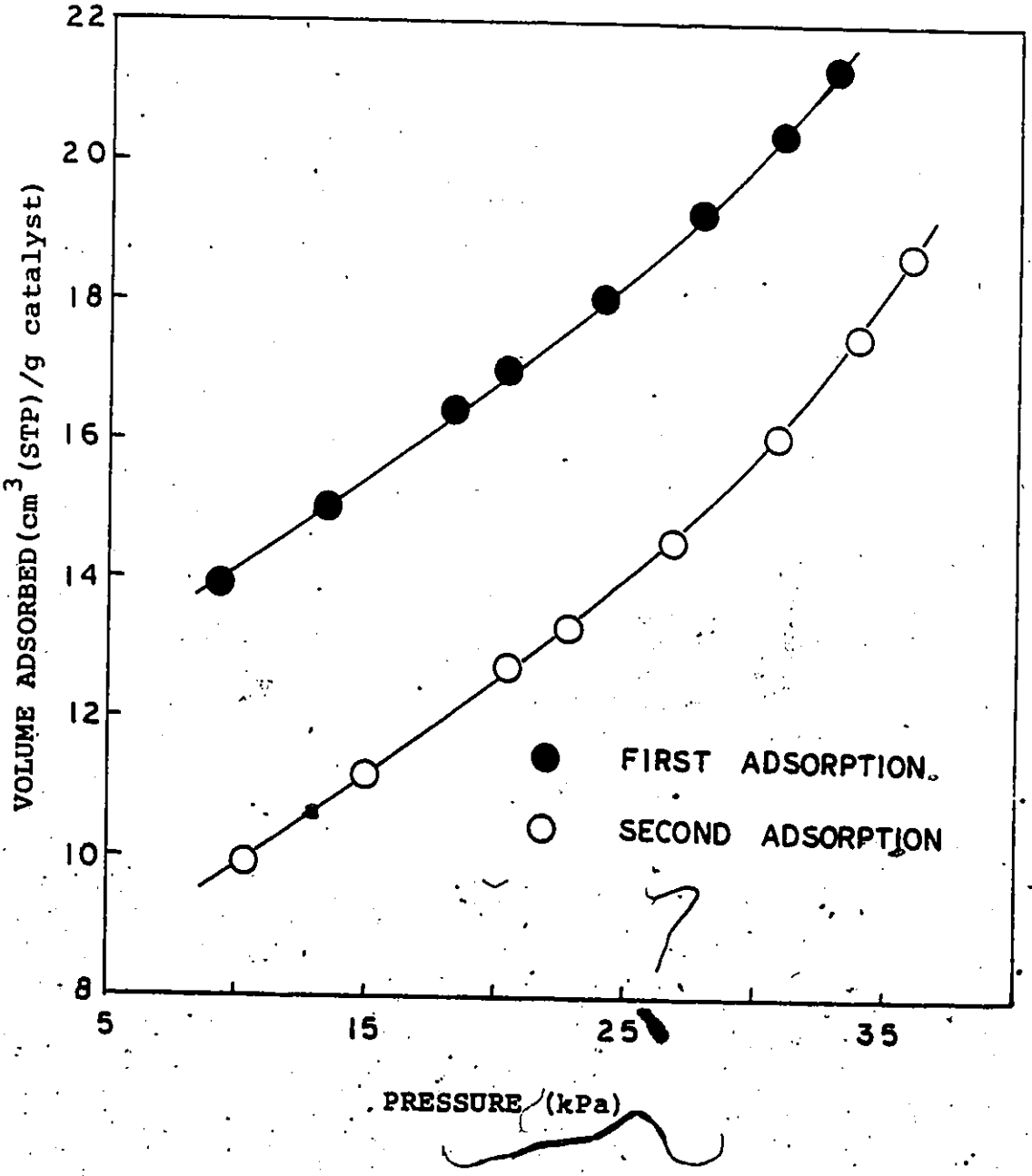

Figure 2-8 Carbon Monoxide Adsorption at 77 K

measure of the active surface area of the nickel, more relevant is the chemisorption of the reactants at temperatures comparable to the actual reaction temperatures. To see if the chemisorptive behavior of the catalyst is different at reaction temperatures, several sets of experiments were performed to determine the extent of adsorption in the temperature range 463 - 523 K. For hydrogen and carbon dioxide chemisorptions under these conditions, the time for equilibration was 10 - 20 minutes. With carbon monoxide as the adsorbate, slow adsorption still persisted after 30 minutes; the data points were taken 40 minutes after the catalyst was exposed to new CO pressures. The isotherms obtained are shown in figures 2-9 to 2-11.

For hydrogen adsorption the amount adsorbed decreased with temperature. For a temperature increase of 60 K, the decrease was only some 0.6 cm^3 . Analysing the isotherms by the Langmuir equation, the amount corresponding to a monolayer was found to be 5.4 cm^3. This value is greater than the 3.5 cm^3/g obtained in the low temperature (77 K) adsorption, and is a measure of the total available adsorption sites in one gram of catalyst. The amount adsorbed at 77 K represents the number of strong adsorption sites only, due to the heterogeneous nature of the catalyst surface. Surface heterogeneity was demonstrated by Keier and Roginii (152) who showed that weak sites are the

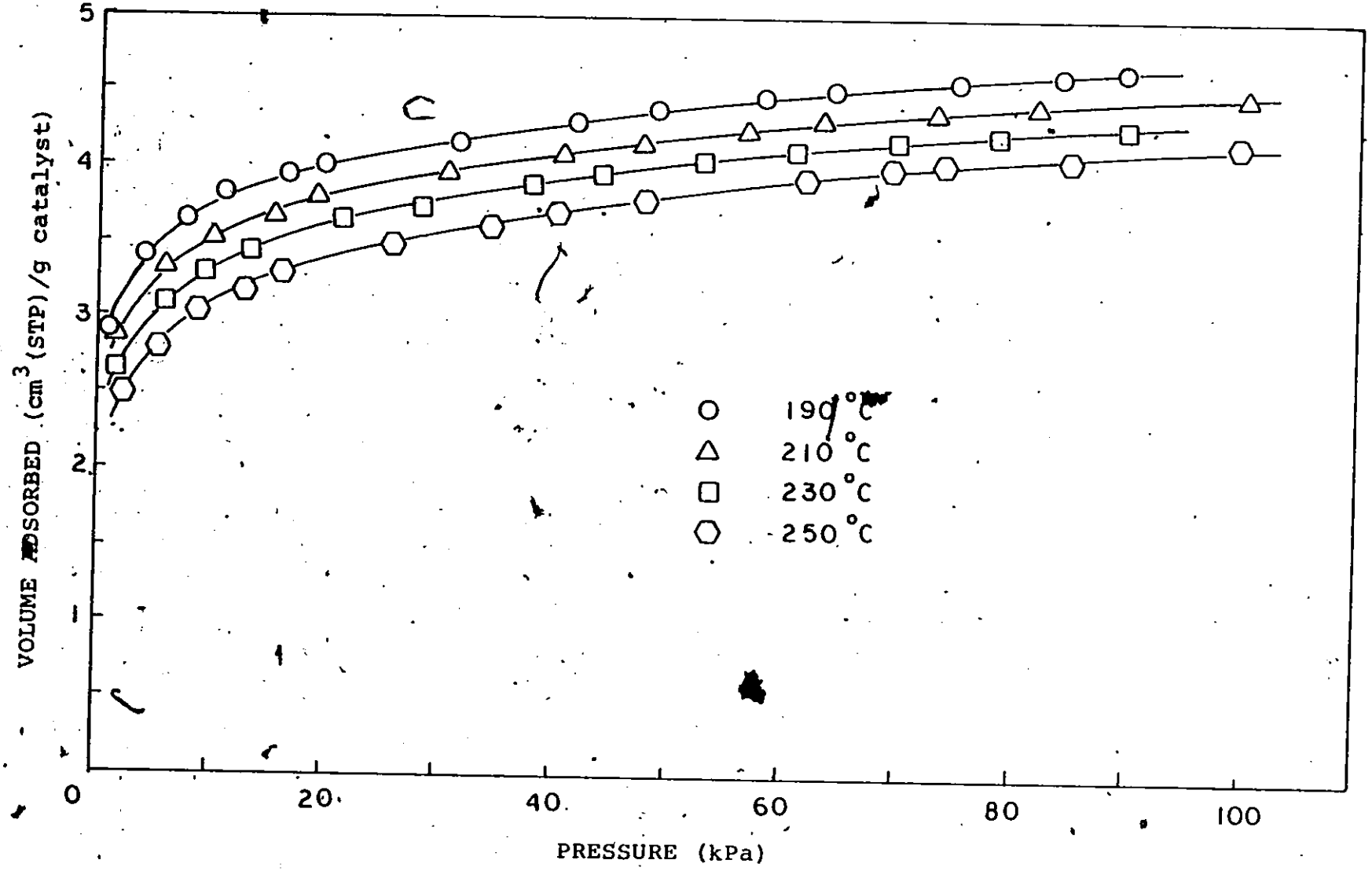

Figure 2-9 Hydrogen Adsorption at High Temperatures

last to adsorb and the first to desorb the adsorbate.

For carbon monoxide adsorption the effect of temperature was similar with a slight decrease (0.5 to 0.7 cm^3) in amount adsorbed as the temperature was raised from 463 to 523 K. However, the amount adsorbed was a much stronger function of pressure. At pressures above 13 kPa, the amount increased linearly with pressure, and over a range of 53 kPa, the increase in adsorbed CO was 3.25 cm^3. The isotherms apparently did not level out. Since CO is known to decompose on nickel surfaces at high temperatures yielding oxygen and carbon species which diffuse into the matrix of the metal, one may not have an equilibration situation. Diffusion of carbon into metal matrix has been reported in the decomposition of CO on nickel (29,153).

In contrast to hydrogen and carbon monoxide adsorptions, the amount of carbon dioxide chemisorbed at the corresponding temperatures and pressures was much less. The isotherms resemble those of CO in that at pressures above 20 kPa the amount adsorbed increased almost linearly with pressure. Falconer (105) has reported that there is little CO_2 adsorption at room temperature on nickel, while at higher temperatures, the amount increases significantly, and concluded that CO_2 adsorption is activated. The maximum amount adsorbed was found to occur at about 438 K. Since the amount adsorbed decreases with temperature starting at least at 463 K in the present

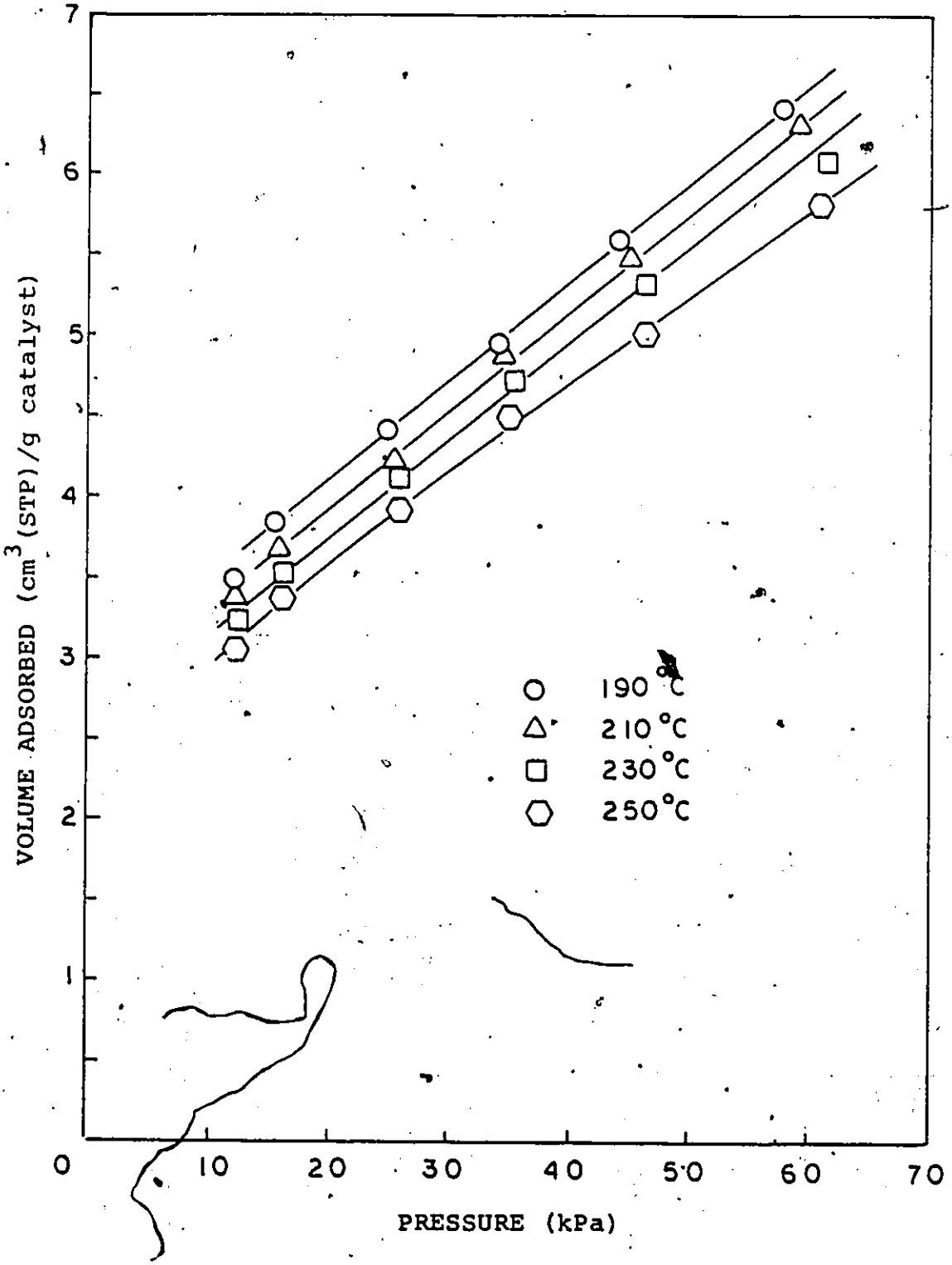

Figure 2-10 Carbon Monoxide Adsorption at High Temperatures

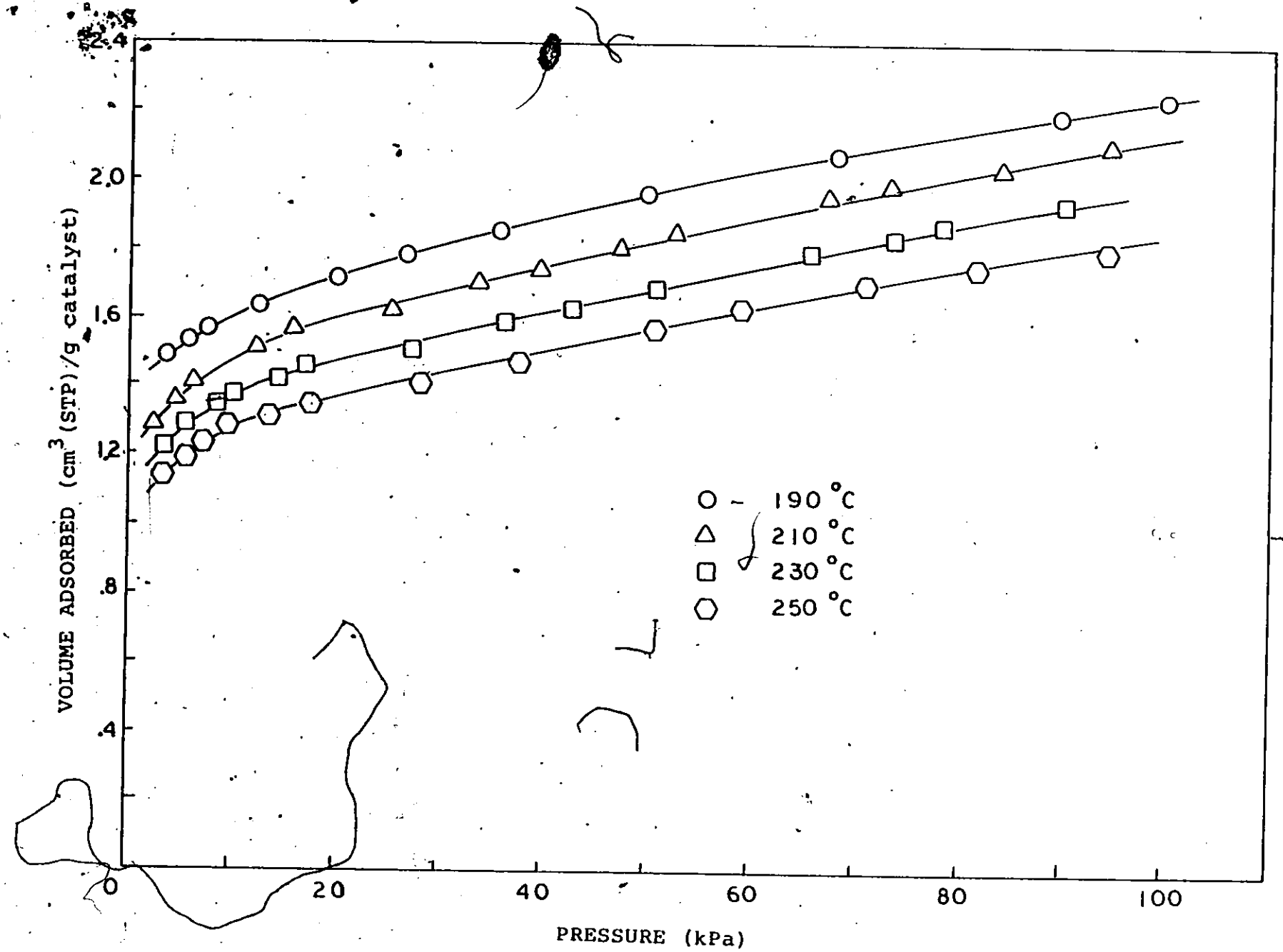

Figure 2-11 Carbon Dioxide Adsorption at High Temperatures

isotherms, these results agree with Falconer's finding. Brennan et al. (102) has reported that the chemisorption of CO_2 on nickel films is small, and a 'saturated' surface can still chemisorb an amount of hydrogen equivalent to one quarter of the capacity of a clean surface.

The chemisorption of the reactant gases on Raney nickel at high temperatures revealed that the gases behave differently. While CO is readily adsorbed and exhibits strong pressure dependence, CO_2 is chemisorbed only to a small extent. The small chemisorption of CO_2 compared to CO will have strong bearings on the activity and selectivity of the catalyst.

Chapter 3

EXPERIMENTAL

3.1 Materials

A commercial Raney nickel (courtesy of W.R. Grace Co.) consisting of 90% nickel was used. It was stored under distilled water and samples were taken when needed. It was in fine particle form with average size of 0.04 mm in diameter. This catalyst has been described in the previous chapter.

The carrier gas for the gas chromatograph system was high purity helium from the Matheson Co., and the hydrogen, ultra high purity grade (99.999% - Matheson Co.), was used without purification. The carbon monoxide, ultra high purity grade from Matheson, was passed through a charcoal trap to remove carbonyl before being used. The carbon dioxide, CP grade from Canadian Liquid Co., was also passed through an activated charcoal trap.

Methane (Matheson, ultra high purity grade) was used without purification, and helium, ultra high purity grade (Matheson Co.), was used as diluent in the kinetic study.

3.2 Flow System

The apparatus for the kinetic experiments was a continuous flow system, consisting of the feed system, the reactor and the effluent system. A schematic diagram of

this flow system is shown in figure 3-1.

The feed system served to mix the reactant gases in desired proportions and to provide a constant flow of this mixed feed gas to the reactor. A Matheson mass flowmeter (Multiflow Controller Model 8249) with four solenoid valves was used. Three of these valves had a range of 0 - 500 cm^3/min. and were used for hydrogen, carbon dioxide and helium diluent streams. Carbon monoxide was connected to the 0 - 200 cm^3/min. range solenoid valve.

The flow of the individual reactant gas could be adjusted conveniently by turning the corresponding knob to the appropriate setting as percentage of the maximum flow as indicated on the digital display. The flow of each gas stream was held constant, independent of the flow of the other gas and pressure.

Prior to the procurement of the Matheson mass flowmeter, the feed gases were mixed by passing them through two capillary flowmeters. With this device the flow rates affected each other and depended on the reactor pressure. To obtain the required feed composition, it was necessary to analyse the gas composition continuously and to make appropriate adjustments in the individual feed rate, a time-consuming procedure. With the Matheson flowmeter, however, feed gas of desired composition could be attained directly. Since the individual reactant gas flows were independent of each other, the desired flow rate and composition could usually

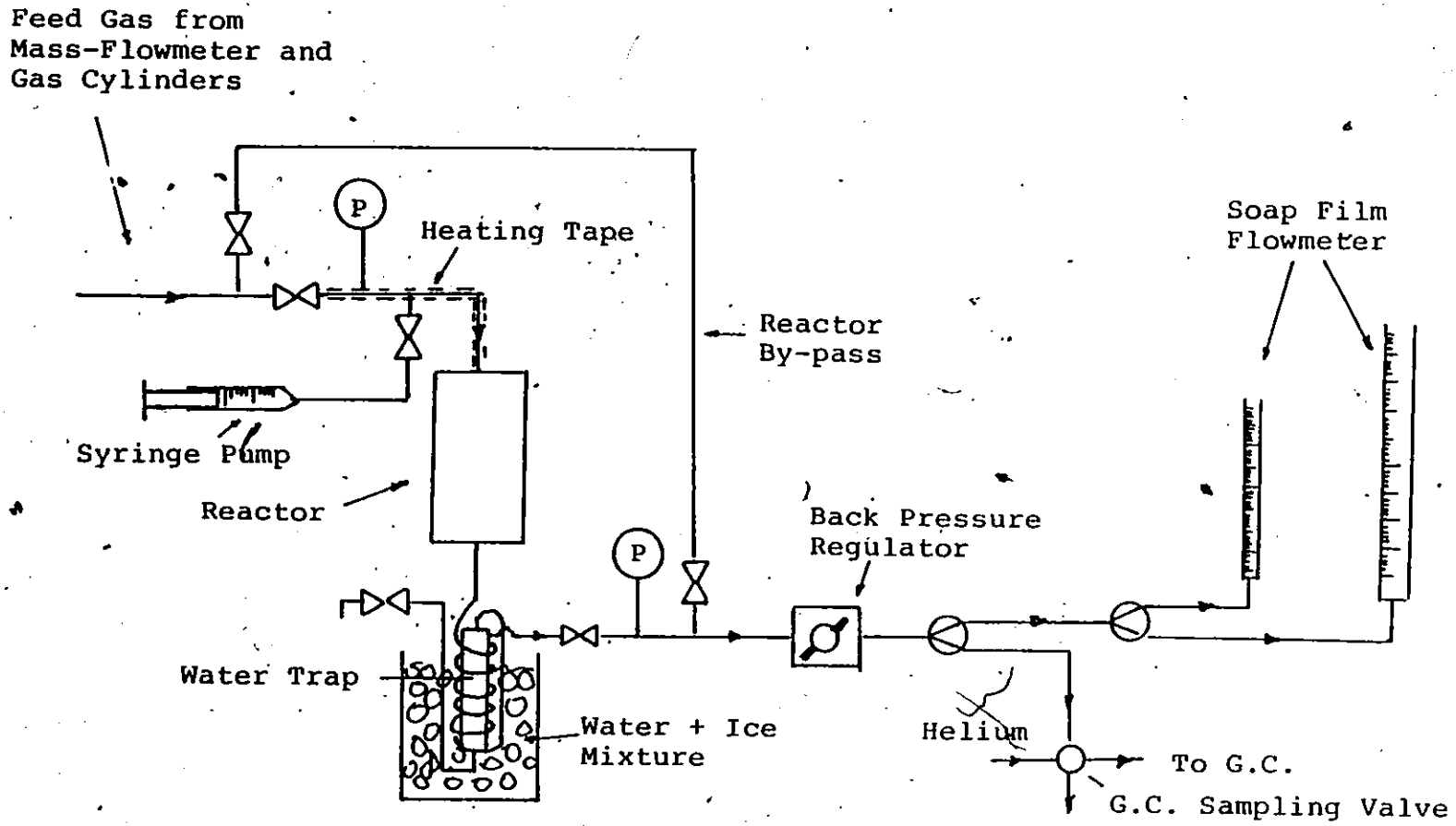

Figure 3-1 Equipment Layout

be obtained after 2 - 3 small adjustments of the flowmeter.

Before being led into the reactor, the feed gas passed through the preheating zone comprising one meter of 0.64 cm OD tubing. This portion of the tubing was wrapped with heating tapes and the temperature was controlled by a variable transformer. To ensure better heat transfer and mixing, the initial portion of the preheating zone was filled with glass beads.

The effluent from the reactor passed into an ice trap consisting of 1.2 m of 0.64 cm OD copper tubing connected to the top of an 2.54 cm diameter steel tube about 20 cm long. The gas then left from the side of this steel tube. Water collected in the tube was drawn from the bottom of the trap. The whole water trap system was surrounded with crushed ice contained in a 16 dm^3 stainless steel bucket.

The gas from the ice trap flowed to the effluent system which regulated the pressure in the reactor, measured the flow rate and analysed the composition of the effluent stream. Downstream (0.6 m) of the ice trap was a variable back-pressure regulator (Fairchild Hiller, Stratos Industrial Products, U.S.A.) which was capable of controlling the reactor pressure in the range 0 - 207 kPa (gauge). The effluent was combined in a glass tee, one arm of which led to the gas chromatography sampling valve and the other to a three-way glass stop-cock which could divert the effluent to two soap-film flowmeters. One had a volume of 50 cm^3 and was made from a calibrated burette. For higher flow rates, a soap-film flowmeter of range 0 - 200 cm^3

was used. It was constructed from a glass tube of 2.54 cm in diameter and calibrated in intervals of 50 cm^3. The effluent from the flowmeters was led via a vent line to the fumehood where it was burned off in a Bunsen burner. The temperature of the effluent was measured by a mercury thermometer near the flowmeters.

The pressure of the reactor was measured by two calibrated pressure gauges (Winter's Thermogauges, Toronto) located 46 cm upstream of the reactor and 30 cm downstream from the ice trap respectively. Both gauges had a range of 0 - 207 kPa (gauge). A by-pass of the reactor was also provided for.

To test the effect of water on the reaction rate, deaerated distilled water was introduced using a [redacted]ti-speed transmission pump (Harvard Apparatus Co., Mass.) which had 12 discrete speed settings and could accommodate syringes of 2 to 50 cm^3 capacity. One 50 cm^3 syringe was used with the lowest three settings of the pump. The latter was calibrated with distilled water pumping against atmospheric pressure. The water was introduced in the preheating zone 15 cm upstream of the reactor. It was evaporated and carried by the feed gas into the reactor. By introducing the water from below to the horizontal section of the preheating zone, a steady vaporization rate could be obtained and sudden surges in pressure were not observed.

3.3 The Reactor

Reactions were carried out in a single pass, fixed bed differential reactor. The reactor consisted of a 0.95 cm stainless steel tube surrounded by a 10.16 cm diameter aluminum cylindrical block. The length of the aluminum block was 17.78 cm. Six holes were drilled in the top of the block, symmetrically located midway between the reactor tube and the outside of the block. These holes accommodated 250 watt Hotwatt cartridge heaters (15.24 cm x 0.95 cm), which were connected in parallel to a temperature controller (Electronic Control System). The aluminum block was enclosed by 2 cm of fibre glass insulation. Figure 3-2 shows the details of the reactor.

The temperature in the reactor was measured by a 1.59 mm Ceramo stainless steel-clad chromel-alumel thermocouple. It was located in the reactor at the top of the catalyst bed, and was soldered into a 2.54 cm x 0.95 cm steel cylinder which was kept in position with a 0.95 cm Swagelok fitting.

The catalyst was supported in the reactor by a stainless steel mesh gauze which was spot-welded to a "hair-pin" shaped device of steel wire long enough to extend from the bottom of the reactor tube to the tip of the thermocouple. The tightness of the gauze against the inside wall of the reactor tube was sufficient to hold in position the catalyst bed which rested on a layer of glass wool (1.6 mm when wet) on top of the gauze. The "hair-pin" kept the gauze in a

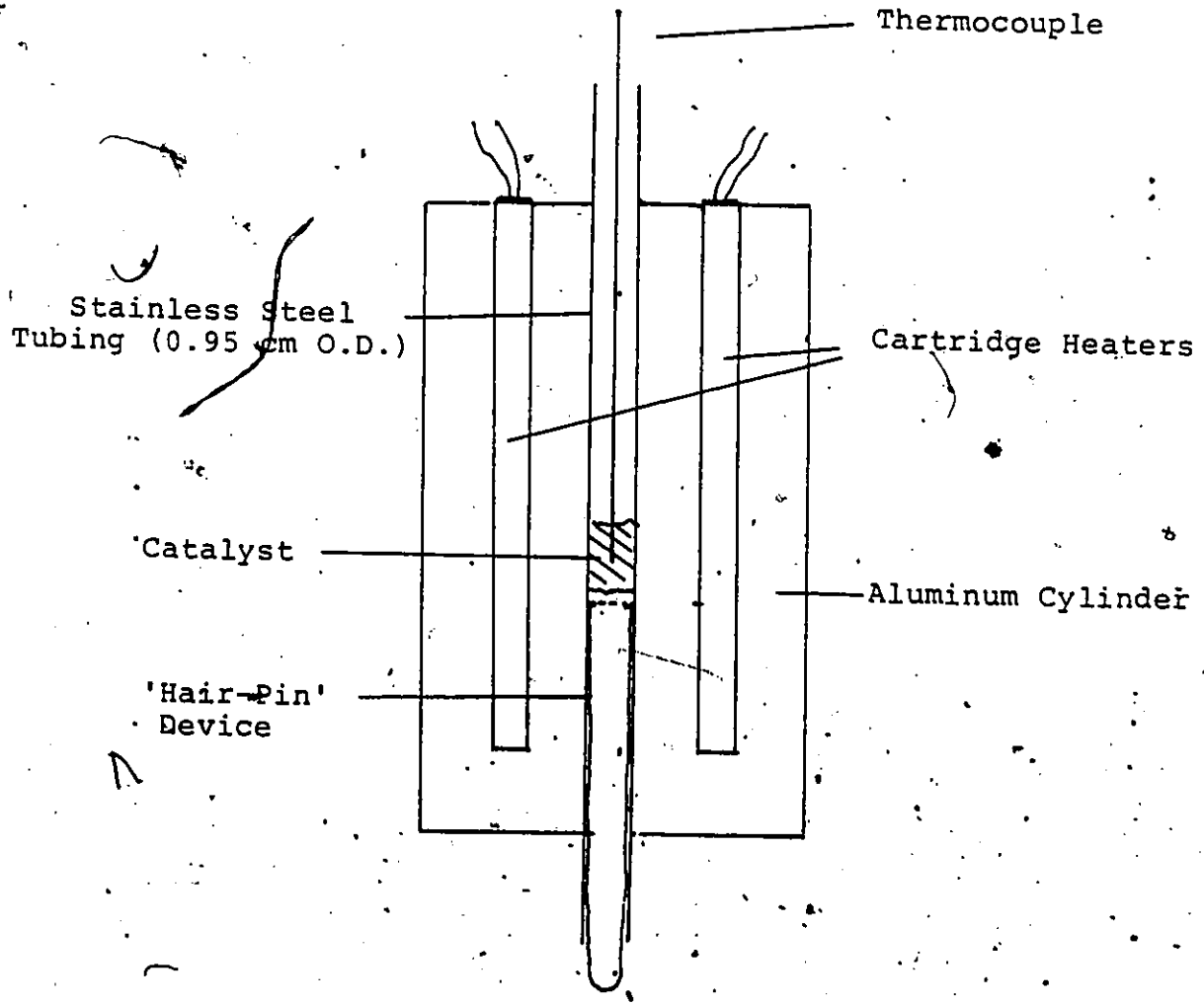

Figure 3-2 Tubular Reactor

horizontal position and permitted its easy removal from the bottom of the reactor tube. The amount of catalyst used was about 0.3 gram, providing an estimated bed length of about 1 cm. The stainless steel gauze was so positioned that the tip of the thermocouple was imbedded in the catalyst bed.

3.4 Operating Procedure

A known amount of Raney nickel was introduced into the reactor from the top. Weighing of the catalyst was done by transferring an appropriate amount of catalyst under water into a weighing tube, connecting the tube to a vacuum system and evacuating overnight at room temperature. The tube with the dry catalyst was weighed. Distilled water was introduced into the tube and the catalyst was transferred wet into the reactor. The weighing tube was again evacuated and weighed. The difference in weight was the amount of dry catalyst placed in the reactor.

After the thermocouple was put in place and the ice trap connected, a slow stream of hydrogen (10 cm^3/min.) was passed through the reactor to remove most of the water. The temperature of the heating block was raised slowly to 623 K. When the temperature reached about 369 K, it would suddenly drop 2 - 3 degrees and then continued to increase again. This phenomenon results from the rapid vaporization of water and indicates that the tip of the thermocouple was indeed imbedded in the catalyst bed. When the temperature reached about 393 K, the flow rate of hydrogen was increased to 60 cm^3/min. The

temperature would usually reach 623 K in about 2.5 hours. Then the system was left overnight.

To begin a kinetic experiment, the reactor temperature and pressure were both set to the desired values with the hydrogen flowing. Then carbon monoxide or carbon dioxide was introduced slowly. As methanation reactions are highly exothermic, the catalyst temperature increased upon introduction of either CO or CO_2. Precaution was taken to ensure that there was no large and sudden rise in temperature. Flow rates of the reactant gases were then adjusted until feed gas of desired composition was obtained. This was achieved by analysing the effluent and making corresponding adjustments in the individual flow rate. Usually only 2 - 3 adjustments were necessary to achieve the desired composition. For a given feed composition the flow rate was set so that the conversion was below 4%.

As the reaction rate is sensitive to temperature, the latter was constantly monitored; usually temperature was constant within 0.2 degree. The product gas was analysed about 30 minutes after the stabilization of temperature. Usually two samples of effluent gas were taken. The effluent flow rate was then measured using one of the two soap-film flowmeters. The temperatures of the reaction and the effluent gas as well as the pressures as indicated by the two pressure gauges were recorded. Then a new experimental condition was chosen and the feed rate and composition changed accordingly.

Usually the temperature was kept constant and only the composition varied for a given set of experimental runs, because the response to feed composition is much faster than to temperature.

For CO hydrogenation the rate increases with H_2/CO ratio and the reaction temperature sometimes jumped by 4 to 5 degrees when the feed composition was changed to higher H_2 or lower CO partial pressures. This transient rise in temperature was monitored carefully to avoid overheating and runaway temperature. Overheating was more likely to occur at higher temperatures such as at 513 K.

The composition of the feed was calculated from the composition of the effluent by means of a carbon balance. The composition used for correlation of kinetic data was the average of both feed and effluent compositions. The pressure drop across the catalyst bed was small, usually less than 1 kPa, and the average of the two pressures recorded was used in calculating the partial pressures of the reactants. The reaction rate was based on the feed rate which was calculated from the conversion and the effluent flow.

When no methane was present in the feed, the conversion was calculated from the mole fraction of methane in the product. When the effect of methane was investigaged, conversion could no longer be obtained from the methane in the effluent. Instead, a control experiment was used in which helium replaced methane in the feed gas. Conversion could be obtained from

a change in H_2/CO or H_2/CO_2 ratios in the effluent as compared to the values obtained in the control experiment.

When the effect of water was investigated, its partial pressures were calculated from the feed of water from the multi-speed pump and the flow of the effluent, as well as the average pressure of the reactor.

As a new catalyst would deactivate significantly during the first hours of reaction, data collection was not attempted until the catalyst was conditioned by running the reaction, usually at 117 kPa with stoichiometric ratios of H_2/CO or H_2/CO_2 feed gas, for two days at 623 K. Overnight the catalyst was kept in hydrogen (60 cm^3/min.), at the temperature of the previous experiment. The first data point of the day was usually collected about 2 hours after experimental conditions had stabilized.

The water condensed in the ice-trap was purged by opening the valve at the bottom of the trap, usually in the morning. It was found that except for runs when water was introduced as feed, the amount of water collected was small, about 0.5 to 1 cm^3/day.

3.5 Interparticle Mass and Heat Transfer

Before reaction can take place, the reactants must reach the catalyst surface. The transfer of reactants from the bulk fluid to the outer surface of the catalyst particles requires a driving force, the concentration difference. Whether this difference in concentration between the bulk

phase and the particle surface is significant or negligible depends on the velocity pattern of the fluid near the surface, and on the intrinsic rate of reaction at the surface. Thus, the concentration gradient depends on the mass transfer coefficient and the rate constant of the reaction. Similarly there is a temperature gradient between the bulk phase and the catalyst surface and its magnitude depends on the heat transfer coefficient, the reaction rate and the heat of reaction.

When a fluid passes over a catalyst particle, a thin boundary layer develops on the solid surface, in which most of the resistance to heat and mass transfer resides. The fluid velocity is zero at the solid surface, but away from the surface, the velocity approaches the bulk velocity. The transport mechanism across this boundary layer may vary from being essentially molecular diffusion near the solid surface to turbulent mixing in the bulk phase. Mass and heat transfer rates across this boundary layer can be expressed in terms of transport coefficients.

$$N_m = k_g a (P_o - P_s) \qquad (3\text{-}1)$$

$$N_H = h a (T_o - T_s) \qquad (3\text{-}2)$$

where N_m = mass transfer rate

N_H = heat transfer rate

k_g, h = mass and heat transfer coefficients

a = area available for transfer

P_o, P_s = partial pressure of component in bulk phase and at the surface

T_o, T_s = temperature in bulk phase and at the surface

The values of these coefficients depend on the hydrodynamics of the fluid flow as well as the intrinsic properties of the gases involved. These transport coefficients are reported as a function of Reynolds number which reflects the prevailing hydrodynamics, and the Schmidt or Prandtl numbers which are measures of the intrinsic properties of the fluids involved. Chilton and Colburn (154) suggested using the j-factor plots. These plots have been widely used by De Acetis and Thodos (155):

$$j_m = f(Re) = \frac{k_m \rho}{G}(Sc)^{2/3} \quad (3\text{-}3)$$

$$j_h = f(Re) = \frac{h}{c_p G}(Pr)^{2/3} \quad (3\text{-}4)$$

where j_m = j-factor for mass transfer

j_h = j-factor for heat transfer

Re = Reynolds number

Pr = Prandtl number

Sc = Schmidt number

G = mass flow rate

It should be noted that heat transfer differs from mass transfer in that heat loss by radiation could be significant and has not been accounted for by the above correlation. However, radiation effects are negligible below 673 K for fixed bed of particles or pellets not greater than 6.35 mm in diameter (156).

The Reynolds number is defined according to the following equation:

$$Re = \frac{d_p G}{\mu} \qquad (3\text{-}5)$$

where d_p = particle diameter

G = mass flow rate

μ = viscosity

From the Reynolds number the j-factors can be easily obtained. Since the j-factors contain Schmidt and Prandtl numbers, the latter two have to be calculated. By definition they are:

$$Sc = \frac{\mu}{\rho D} \qquad (3\text{-}6)$$

$$Pr = \frac{c_p \mu}{k} \qquad (3\text{-}7)$$

where ρ = density

D = diffusivity

c_p = heat capacity

k = thermal conductivity

Knowing the Schmidt and Prandtl numbers as well as the values

of the j-factors corresponding to the calculated Reynolds number will yield values for k_m and h. These coefficients were used to calculate the rate of reaction which could be sustained under a negligible driving force of concentration and temperature difference between the catalyst surface and the bulk gas phase. Concentration and temperature differences of 0.1 kPa and 0.2 K can be regarded as negligible (157). Using equation (3-1) and a value of 500 square cm per gram for "a", the maximum allowable rate supported by the concentration differential can be estimated. Also using the appropriate heats of reaction the maximum reaction rate supported by this 0.2 K temperature difference can also be calculated with equation (3-2). Table 3-1 summarizes the result of these calculations.

For the corresponding carbon oxide hydrogenation reaction, the kinetic experiments were all performed at rates lower than the least allowable values from either heat or mass considerations, corresponding to a reaction region in which the effect of interparticle concentration and temperature gradients are negligible.

3.6 Intraparticle Mass and Heat Transfer

Most of the surface of porous catalyst particles is internal. Since reaction and mass and heat transfer occur simultaneously at any position within the particle, there exist concentration and temperature gradients inside the particle. The effect of intraparticle mass transfer is to

Table 3-1

Summary of Interparticle Mass and Heat Transfer Calculations

Parameter	$H_2/CO = 7$ at one atmosphere	$H_2/CO_2 = 4$ at one atmosphere
$D(cm^2/sec)$	1.99	1.66
C_p(cal./g-K)	1.33	0.75
k (cal./sec-cm-K)	5.2×10^{-4}	4.3×10^{-4}
Pr	0.50	0.38
Sc	0.80	0.54
k_g(mole/cm^2-sec-atm)	1.5×10^{-3}	1.8×10^{-3}
h (cal./cm^2-sec-K)	1.4×10^{-2}	1.9×10^{-2}
$-\Delta H^\circ$ (cal./mole)	51000	40000
N_h(cal./g-sec)	1.4	2.0
Rate(mole/g-sec)	2.7×10^{-5}	5.0×10^{-5}
N_m(mole/g-sec)	7.5×10^{-4}	9.0×10^{-4}

reduce the rate below what it would be if there were no internal concentration gradient. The effectiveness factor η is used to account for the effect of intraparticle gradients, and is defined as the ratio of the actual rate to that which would occur if the temperature and concentration were all constant throughout the particle and have values corresponding to the surface condition. If effectiveness factor approaches unity, the diffusion limitation within the particle is negligible. This factor depends on the particle size, the reaction rate and the intraparticle diffusion rate. By making the following assumptions, the maximum rate at which the effectiveness factor is near unity can be calculated:

(1) the system is isothermal

(2) the active shell of the catalyst particle is considered to be spherical

(3) hydrogen gradient is negligible because of its higher diffusivity

(4) the reaction is first order with respect to CO or CO_2

By writing a mass balance over the spherical-shell volume of thickness dr a second order differential equation is obtained which upon integration yields concentration profile within the particle. From a knowledge of this profile, the effectivness factor can be calculated (110):

$$\eta = 3 \left(\frac{1}{\phi \tan \phi} - \frac{1}{\phi^2}\right) \qquad (3\text{-}8)$$

where Ø is the Thiele modulus defined as

$$\emptyset = R\,(k/D)^{\frac{1}{2}} \qquad (3\text{-}9)$$

where R = radius of particle

k = rate constant

D = effective diffusivity

In pores of 4 nm as found in the Raney nickel, Knudsen diffusion will be operative, and the effective Knudsen diffusivity can be calculated from the following equation (158,159):

$$D = 9700\, r\left(\frac{T}{M}\right)^{\frac{1}{2}}\left(\frac{\Theta}{\tau}\right) \qquad (3\text{-}10)$$

where r = average pore radius

T = temperature

M = molecular weight

Θ = porosity of the catalyst particle

τ = tortuosity factor

From equation (3-8) the maximum allowable value for Ø which corresponds to η greater than 0.95 is $\emptyset \leq 0.9$. Using a particle diameter of 0.04 mm and the effective diffusion coefficient calculated, one can obtain the maximum allowable rate constant k for which diffusion is still fast compared to reaction (equation 3-9). From this the maximum allowable rate can be calculated.

Weisz (160) obtained a convenient criterion by which intraparticle diffusion may be negligible:

$$\frac{R^2 \cdot r \rho}{C_s D} \leqslant 1 \qquad (3\text{-}11)$$

where r = observed reaction rate

R = particle radius

ρ = particle density

C_s = surface concentration

D = effective diffusivity

The above equation is satisfactory as an approximate criterion for most catalytic kinetics even though it was derived for first order kinetics.

The above analysis has been based on the assumption that the porous catalyst particle is isothermal. Since at steady state, the diffusion of reactants across a boundary must be equal to the rate of reaction within that boundary and the heat released must be transferred across the same boundary, the following relationship can be obtained.

$$\Delta T = \frac{-\Delta H \, D \, (C_s - C)}{k} \qquad (3\text{-}12)$$

where ΔT = temperature difference

ΔH = heat of reaction

k = thermal conductivity of the catalyst

C_s = surface concentration

C = concentration within the particle

The maximum temperature difference in a particle occurs when all of the reactant is consumed. Applying the above equation with $C = 0$ gives

$$\Delta T_{max} = \frac{-\Delta H \; D \; C_s}{k} \qquad (3\text{-}13)$$

This temperature increase was calculated to be 0.3 K for this extreme case. Therefore, the assumption of isothermal operation is justified.

Chapter 4

CARBON MONOXIDE METHANATION

4.1 Introduction

The rate of carbon monoxide methanation was examined as a function of temperature and partial pressures of the reactants. The experiments were generally conducted at pressures of less than 202 kPa in the temperature range of 463 - 513 K.

Since the conversions were kept small (less than 4%) the prevailing condition over the catalyst bed was regarded as homogeneous, i.e. the temperature as recorded was taken to be the reaction temperature and the partial pressures of the reactant gases could be obtained from the operating pressure and the effluent gas analysis. The rates were calculated from equation 1-27.

Despite precautions to ensure minimal change in catalytic activity, deactivation did occur occasionally, especially during the adjustment for new reaction conditions, e.g. when carbon monoxide partial pressure was changed to lower values in high temperature runs.

4.2 Preliminary Kinetic Studies

Because of the conflicting information reported in the literature regarding the effect of CO and H_2 concentrations, a preliminary study of the reaction was done at the beginning of this work to confirm the pertinent features of

the reaction. The results are shown in figures 4-1 to 4-3. At 503 K the reaction rate in terms of turnover number defined as:

$$\text{Turnover Number (TON)} = \frac{\text{Molecules of Methane produced}}{\text{Metal Site - second}}$$

was strongly dependent on the partial pressures of H_2 and CO. It increased with H_2 concentration but was inhibited by CO. At sufficiently high CO partial pressures, the order of reaction with respect to hydrogen approached unity but decreased with decreasing CO partial pressure to a value of 0.7 . Figure 4-1 also suggests that when CO partial pressure is sufficiently low, the H_2 order of reaction starts to decrease at sufficiently high H_2 partial pressure.

When the H_2 concentration in the reaction system was maintained constant, the rate decreased with increasing CO partial pressure. This inhibiting effect does not seem to vary significantly with the H_2 concentration in the system. However, at high partial pressures of H_2, the reaction order of CO increased to zero where a maximum in rate was observed. At still lower CO partial pressures, the order with respect to CO was positive. The effect of H_2 and CO on the reaction rate is also illustrated in figure 4-4 where the rate increased with increasing H_2/CO ratio for a constant total pressure.

The positive effect of H_2 concentration on the reaction rate was greater than the inhibiting effect of CO so that the

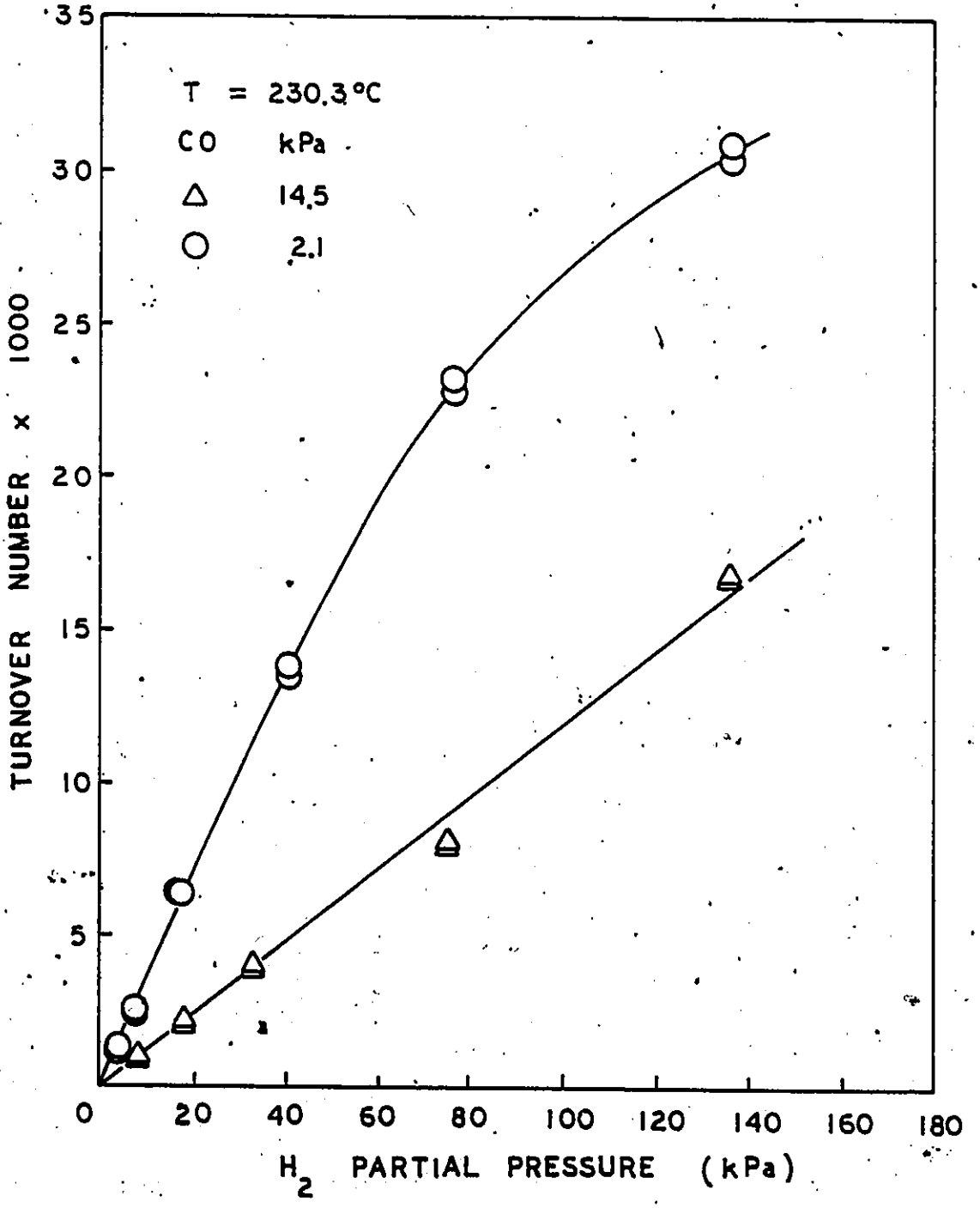

Figure 4-1 Effect of Hydrogen on CO Methanation Rate at 503 K

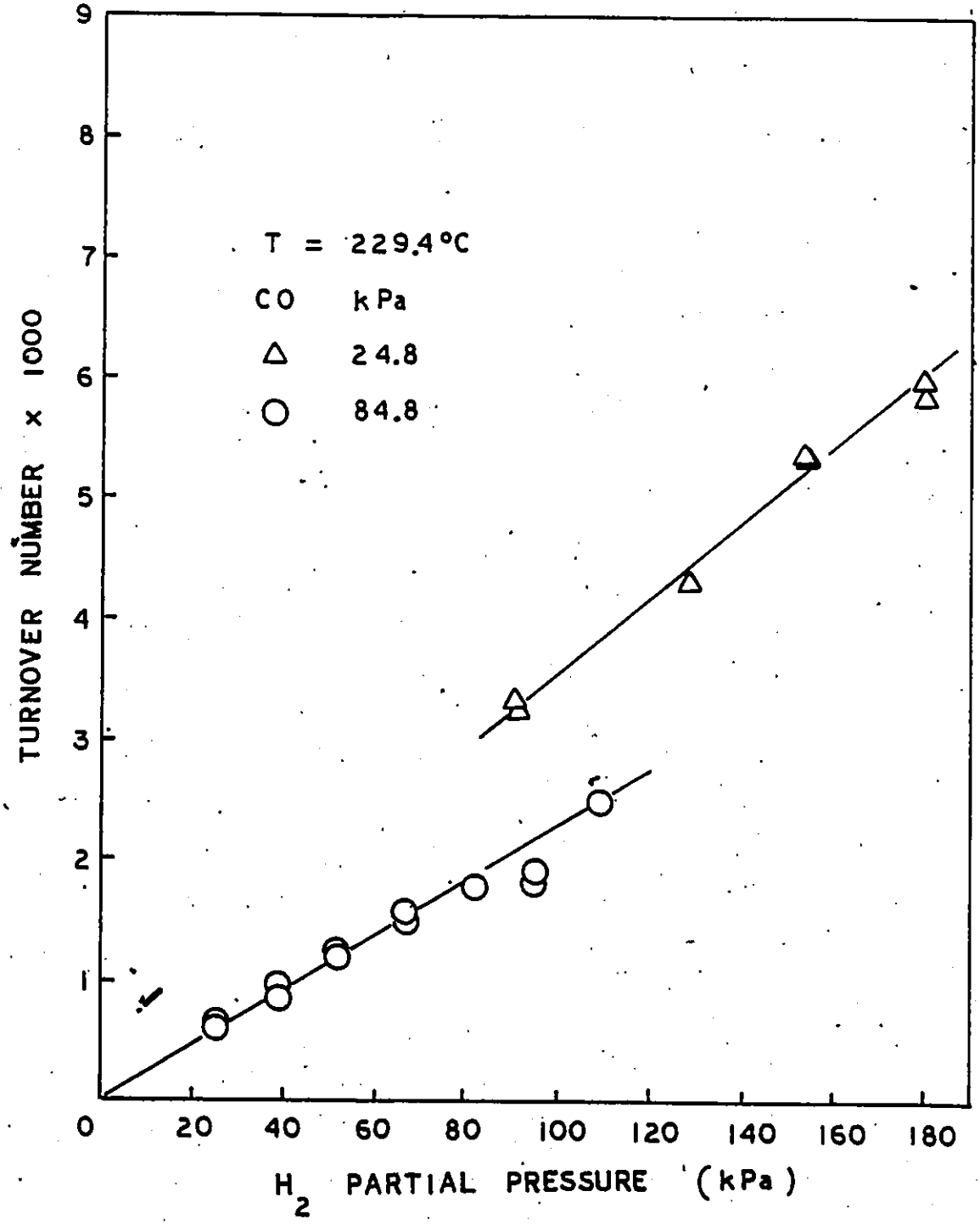

Figure 4-2 Effect of Hydrogen on CO Methanation Rate at 503 K

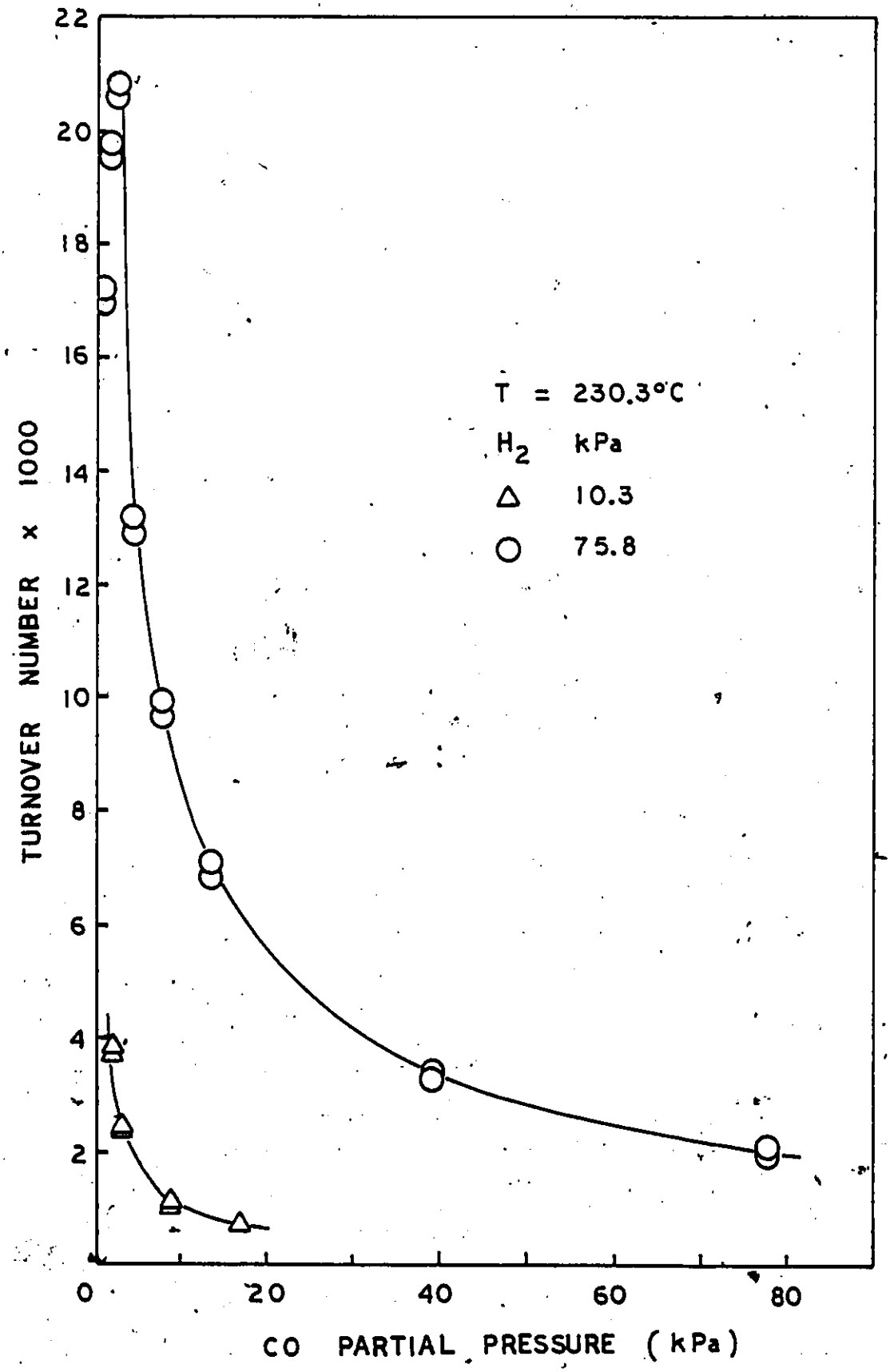

Figure 4-3 Effect of Carbon Monoxide on Methanation Rate at 503 K

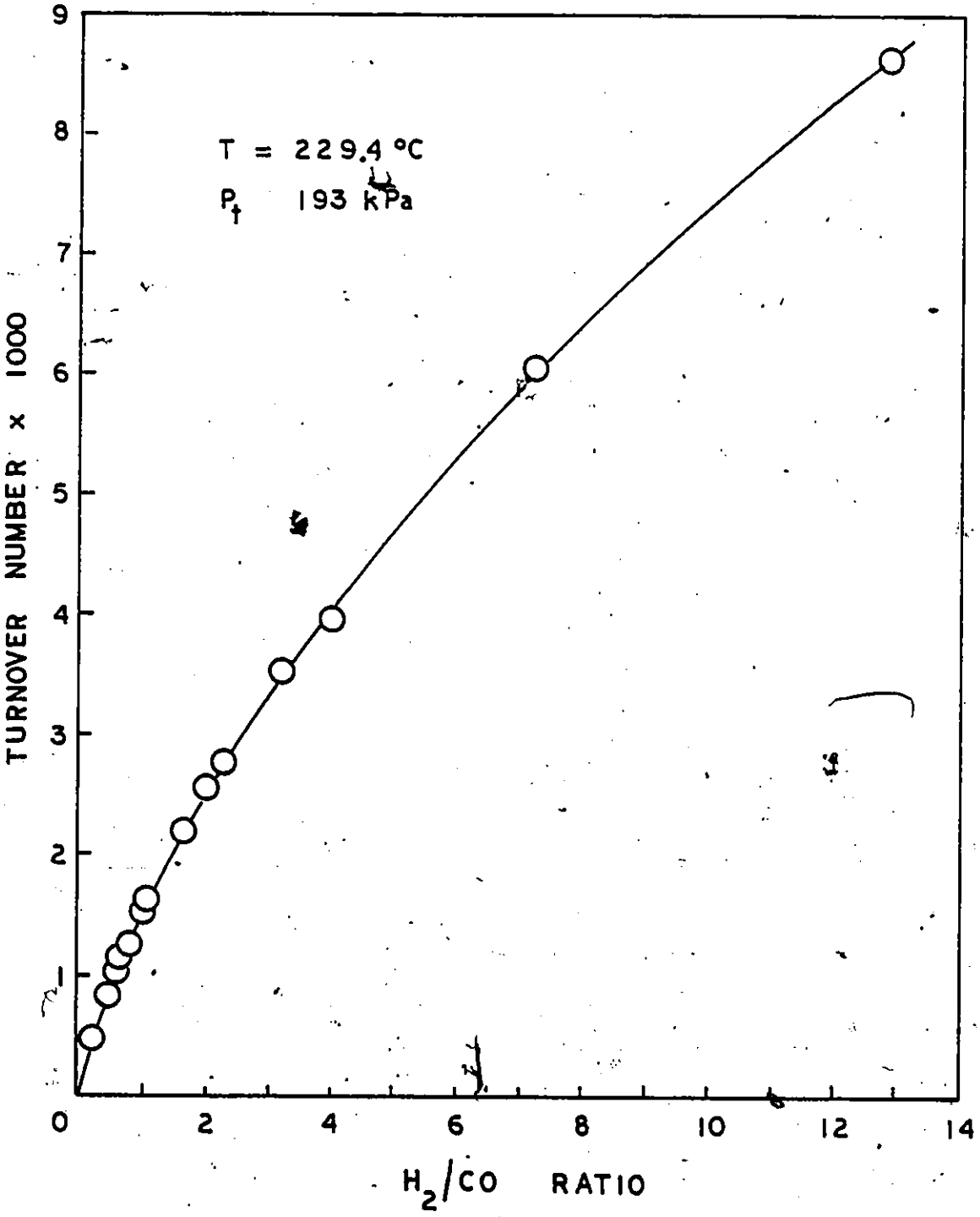

Figure 4-4 Effect of H_2/CO Ratio on Methanation Rate

rate should increase with the total operating pressure, as shown in figure 4-5. For a $3H_2/1CO$ feed gas, the rate increased with total pressure to the power of 0.2, in qualitative agreement with the individual reaction orders obtained before.

In general, the preliminary studies confirmed that the reaction rate increases with H_2 partial pressure to the power of 0.7 - 1.0 . However, there is evidence that the order for H_2 diminishes at sufficiently high concentration. Ho et al. (57) have observed similar decreasing orders for H_2 at high pressures. Goodman et al. (37) reported that the rate remained constant as the H_2/CO ratio became greater than 7 at a constant total pressure of 1.3 kPa; they offered an explanation in terms of saturation of the catalyst surface with adsorbed hydrogen. The results from the present study showed that the rate was still increasing when the H_2/CO ratio was as high as 14 (figure 4-4). One reason for the failure to observe a constant rate with increasing H_2/CO ratio was the much higher total pressure employed in the present study (202 kPa). The lowest partial pressure of CO was 13.5 kPa for H_2/CO ratio of 14 as compared with 1.7 kPa at H_2/CO ratio of 7 where rate started to level off in Goodman's work.

The results from the preliminary studies also confirmed the inhibiting effect of CO on the reaction rate. The rate increased with decreasing CO concentration. At sufficiently low CO partial pressures, the rate reached a maximum. Ho et al.

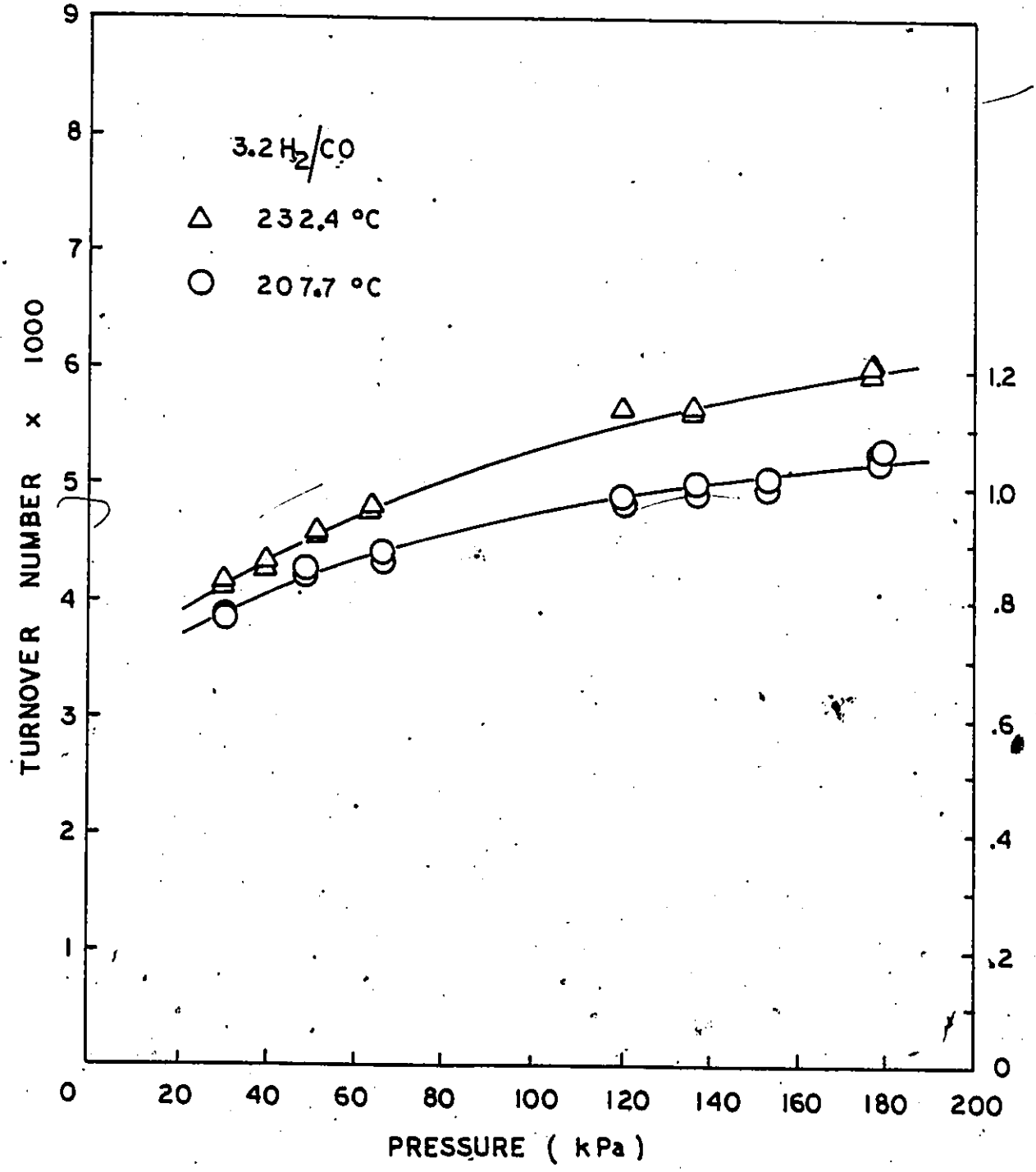

Figure 4-5 Effect of Total Pressure on CO Methanation

(57) observed that at high temperatures, the rate was invariant with respect to CO concentration. Fontaine (161) similarly reported that the maximum in rate obtained at low CO concentrations was rather flat.

4.3 Kinetics

4.3.1 Effect of Temperature

The effect of temperature on the methanation rate was investigated by carrying out the reaction at different temperatures. The results are shown in figure 4- 6 in the form of an Arrhenius plot. For these experiments, the H_2/CO ratio was maintained at 3.2 and the total pressure constant. The activation energy from the slope of the Arrhenius plot was 146 kJ/mol, in agreement with values of 134 kJ/mol and 130 kJ/mol obtained by Uken et al. (162) and Dalla Betta et al. (163), respectively. Earlier work from the Bureau of Mines also yielded a value of 139 kJ/mol. However, lower values of 114 and 103 kJ/mol have been reported by other authors for unsupported nickel catalysis (37). In a study of a series of supported nickel catalysts, Vannice (121) reported that the activation energy lay in the range of 105 - 139 kJ/mol. Still lower values, 84 and 73-80 kJ/mol, were reported by Bousquet and Teichner (1) and Fontaine (161), respectively. Recently Okomoto et al. (164) reported a value of 146 kJ/mol for Raney nickel which agrees very well with the present finding. They showed that the activation energy of methanation reaction increased with decreasing electron density of the

nickel metal with a subsequent decrease in the activity of the catalyst. The results were interpreted by assuming that CO dissociation was the rate determining step. This correlation between catalyst activity and activation energy is, however, not supported by the recent data reported by Vannice (165). Table 4-1 compares the various values of activation energy.

The plots in figures 4-6 and 4-7 show that the activation energy did not depend on the total pressure within the range investigated. This invariance of activation energy with total pressure agrees with the results of Goodman et al. (37) who found that as long as sufficient hydrogen partial pressure was maintained over the catalyst, a linear Arrhenius behaviour was obtained. In mechanistic term the slowest step in the reaction did not change within the pressure range investigated. Figure 4-6 also shows that the activation energy was independent of change in surface area resulting from sintering. Ho et al. (57) found that aging catalysts did not significantly affect the activation energy.

Thus, Raney nickel yielded relatively high values of activation energy compared to other nickel catalysts, in particular the supported ones. Unsupported catalysts have much larger crystallite size. The average crystallite size of the Raney nickel sample used in the present study was found to be 43.4 nm by hydrogen chemisorption. Vannice (123-125)

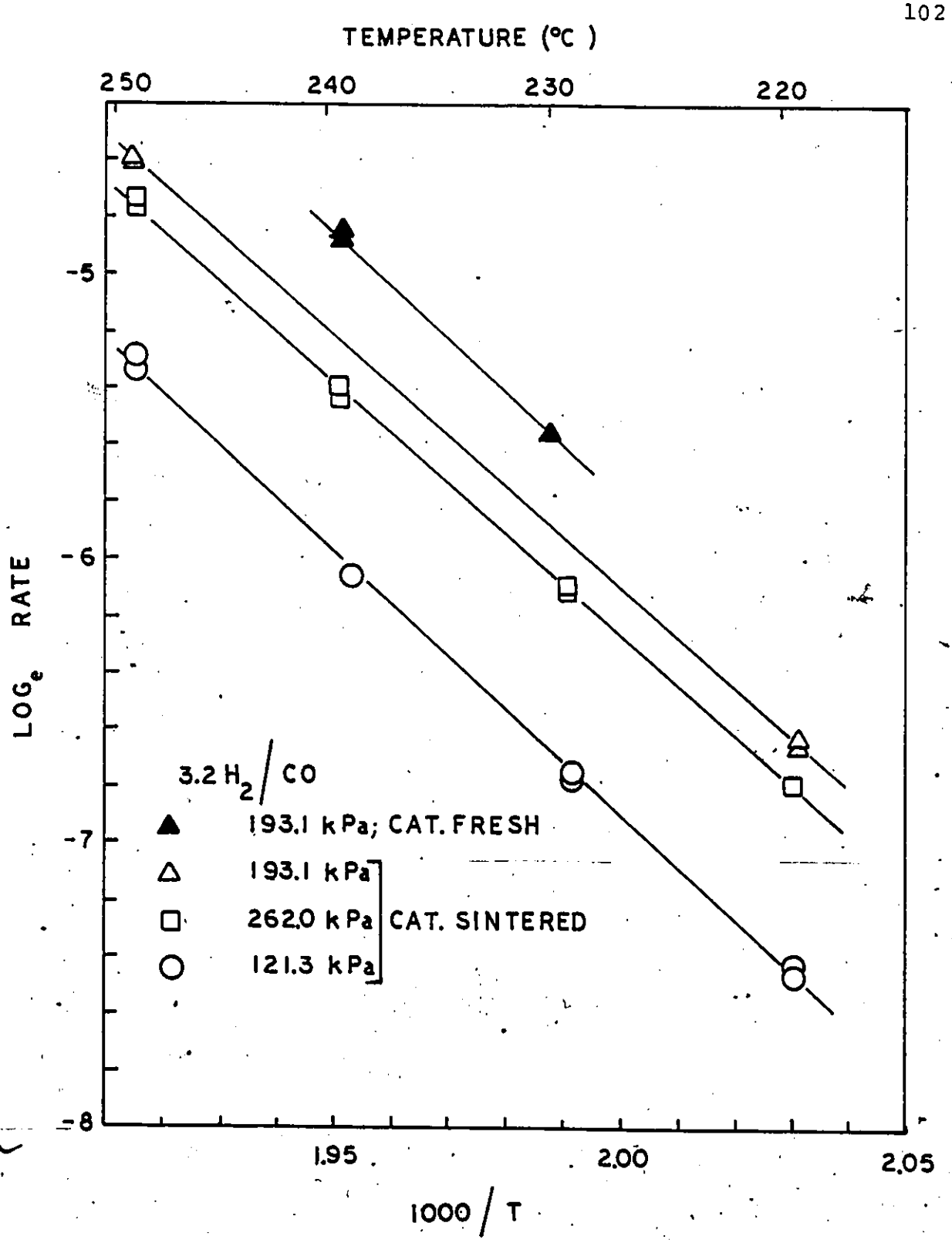

Figure 4-6 Arrhenius Plot for CO Methanation

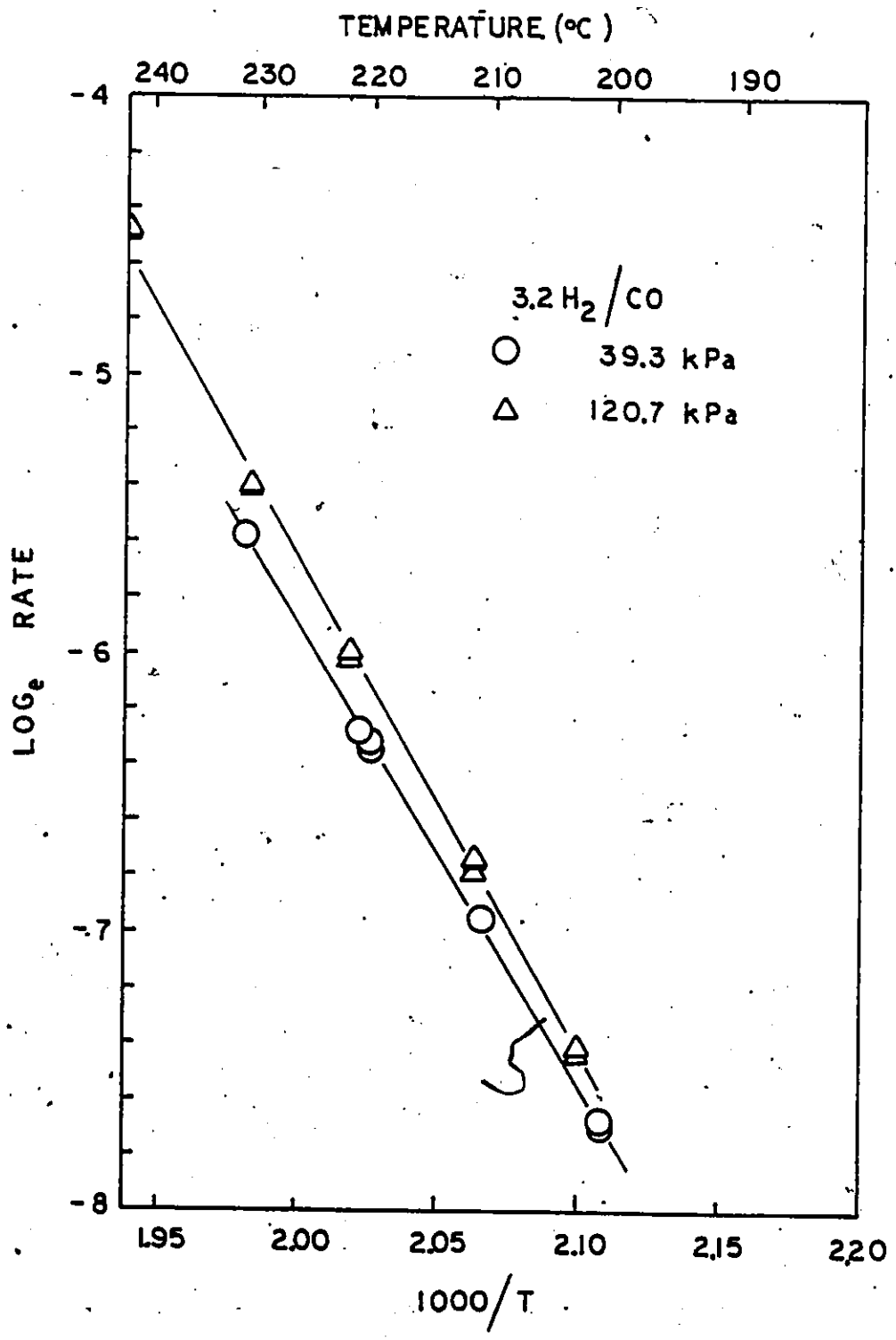

Figure 4-7 Effect of Pressure on Arrhenius Plot

Table 4-1

Activation Energies for CO Methanation

E_{act} (kJ/mol)	Reference
146	This Study
146	(164)
134	(162)
130	(163)
139	(49)
114	(37)
105-139	(121)
84	(1)
73-80	(161)

has pointed out that large unsupported nickel crystallites have lower specific activities than supported catalysts with smaller crystallite sizes. Although Raney nickel is generally regarded as a good catalyst for methanation, finely dispersed nickel on alumina has even higher activity.

The specific activity of the Raney nickel used in this work was compared with samples used by other workers as shown in Table 4-2. The rate of methanation was expressed in terms of turnover number (TON). Expressing reaction rate in TON has proved to be most convenient in comparing rate data, especially for supported catalysts. The number of surface metal sites in the Raney nickel was measured by hydrogen chemisorption. As it would be more relevant for the actual reaction conditions, high temperature chemisorption data were used for defining the number of surface nickel atoms. The merit of this method has been discussed by Ross et al. (151). On this basis, the surface site density was found to be 2.9025×10^{20} sites per gram of catalyst. The activity of the catalyst is shown in Table 4-2 for different temperatures. It was compared with the TON reported by other investigators also using Raney nickel catalyst. The comparison was based on a feed of $H_2/CO = 3$ at a total pressure of 121 kPa. The TON from the different authors were corrected to this conditions using activation energy value of 146 kJ/mol and reaction orders of 0.8 and -0.5 for hydrogen and carbon monoxide, respectively. The Raney nickel used in this study was found

Table 4-2

Comparison of Turnover Number for CO Methanation over Raney Nickel

Temperature (K)	TON* x 10^3	Reference
513	5.2	(163)
513	25.1	(162)
513	11.3	This Study
504	4.5	This Study
493	2.4	This Study
484	1.2	This Study
476	0.6	This Study

* Feed = $3H_2/CO$ at 121 kPa

to be twice as active as that used by Della Betta et al. (163), but only half as active as the sample used by Uken et al. (162). Differences in activity could be attributed to catalytic composition and differences in catalyst pretreatment. The Raney nickel used by Della Betta et al. was a laboratory sample from which only 60% of the aluminum was leached while the catalyst used by Uken et al. was a commercial sample with 82% nickel. The sample used in the present study contained 90% nickel.

4.3.2 Effects of Reactants and Products

The preliminary studies yielded some information on the reaction orders of H_2 and CO. To obtain the kinetics of the reaction in more detail, additional experiments were performed at different temperatures. In these runs, the individual effect of H_2 and CO was studied by carefully maintaining the other reactant at a constant partial pressure. Because of the inhibiting effect of CO, the data set at 475 K was obtained at low CO partial pressure while H_2 was kept at reasonable concentrations to obtain observable conversions.

In these runs, only methane was detected in the effluent in addition to the unreacted H_2 and CO. No ethane was found, in contrast to the results of Vannice (125) who found small quantities of ethane and ethylene. In addition to the difference in reaction conditions, the conversions in the present study were kept at less than 4% in contrast to the 10-20% conversions allowed by Vannice. Trace amounts

of CO_2 were detected when high partial pressures of CO were used or the H_2/CO ratio kept low, but usually the concentration was below the sensitivity of the gas chromatograph for accurate analysis. The low concentration of CO_2 indicated that the reaction was far from equilibrium with respect to the water-gas shift.

The dependence of the methanation rate on the partial pressure of H_2 and CO at the various temperatures was investigated by employing the power rate law:

$$TON = A\, e^{-E/RT}\, P_{H_2}^{x}\, P_{CO}^{y} \qquad (4\text{-}1)$$

where TON = turnover number for methane

A = pre-exponential factor

E = apparent overall activation energy

x,y = order of reaction for hydrogen and carbon monoxide, respectively.

The order of reaction for H_2 from this study was found to vary between 0.7 and 1.0, depending on the temperature (figures 4-8 to 4-10). The H_2 exponent increased slightly with CO partial pressure, but decreased with temperature. The increase in H_2 order with CO partial pressure may be related to the competition of H_2 for chemisorption sites at the surface. However, since CO is much more strongly adsorbed than H_2, the effect should be minimal. The decrease in H_2 order with temperature results from H_2 adsorption becoming

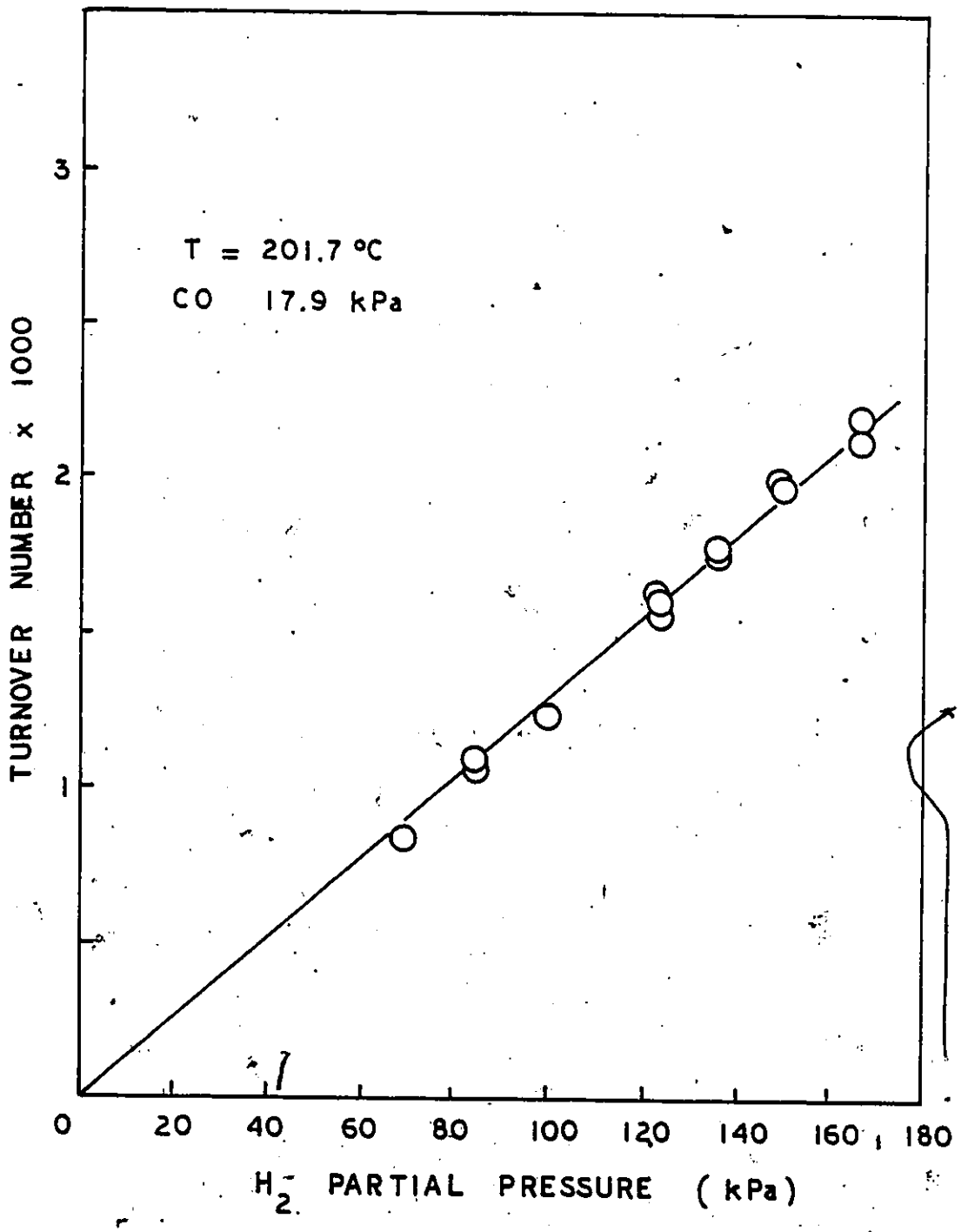

Figure 4-8 Effect of Hydrogen on CO Methanation Rate at 475 K

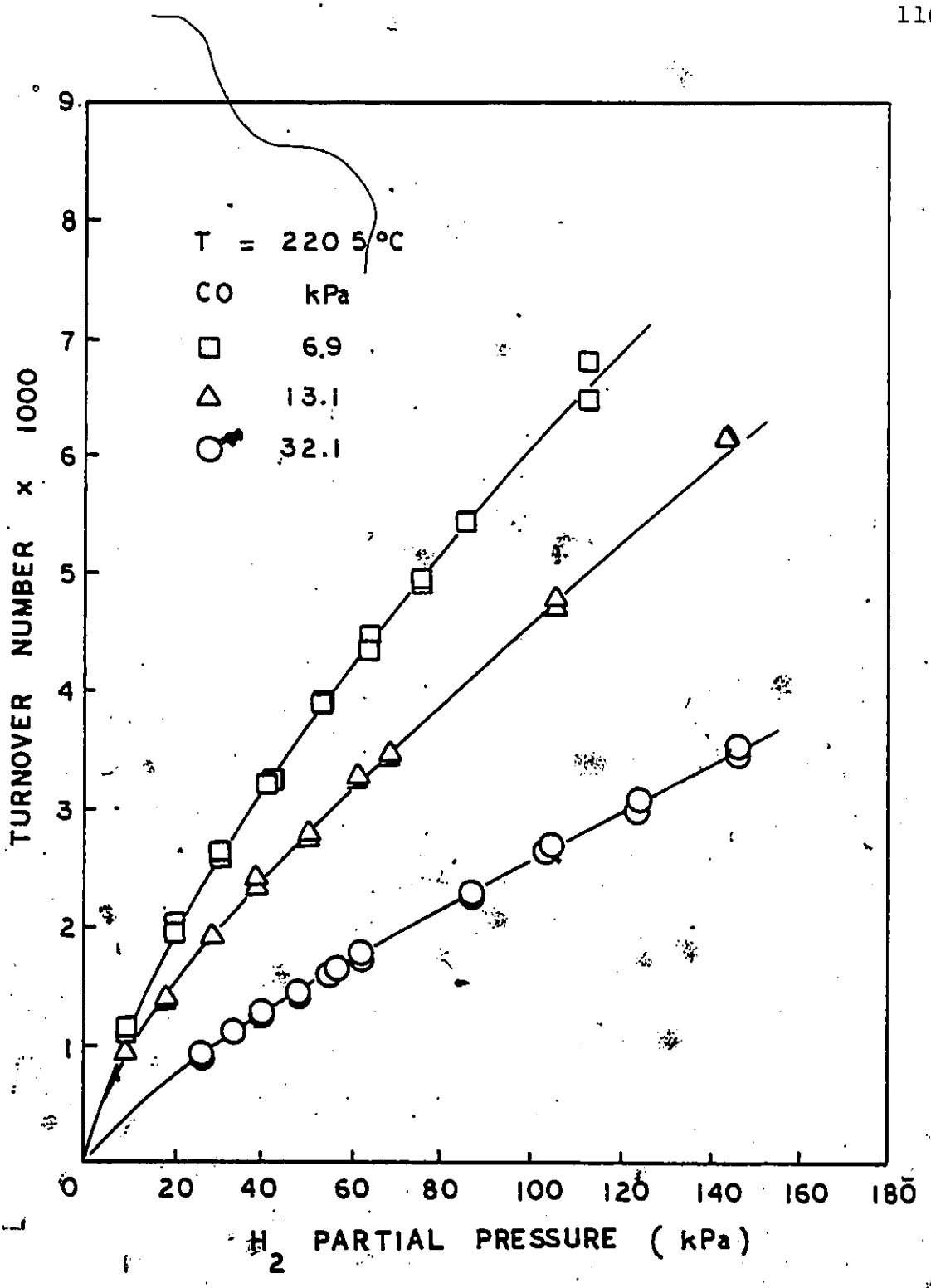

Figure 4-9 Effect of Hydrogen on CO Methanation Rate at 493 K

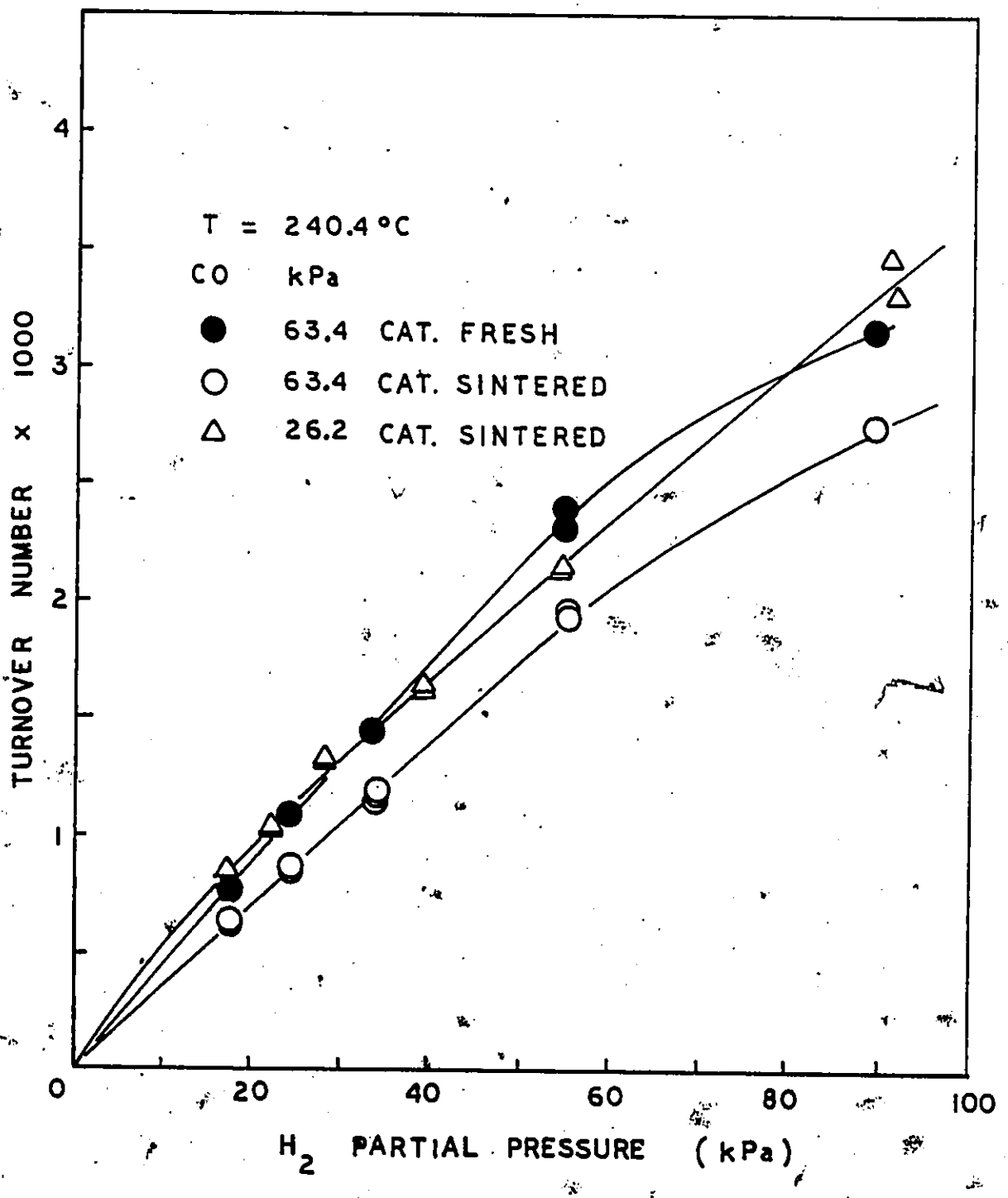

Figure 4-10 Effect of Hydrogen on CO Methanation Rate at 513 K

more competitive at high temperatures. Table 4-3 summarizes the results.

The effect of CO on the reaction rate is shown in figures 4-11 to 4-13. The order of reaction with respect to CO was invariant with the partial pressure of H_2 and varied between -0.53 and -0.64 with temperature. Sughrue and Bartholomew (166) found that CO order increased with temperature. This trend was not observed in the present study, the CO order being -0.53 at 475 K, -0.63 at 494 K, and -0.56 at 513 K (Table 4-4).

The effect of methane on the reaction rate was investigated by introducing methane in the feed gas. The rate was calculated from the change in concentration of CO in the effluent as compared with standard runs in which methane was replaced by helium in the feed. Figure 4-14 shows that there was no definite change in rate even when methane was present in significant amount. Bousquet (1) reported that methane decreased the reaction by product inhibition. However, a more recent study by Elliott and Lunsford (167) revealed that methane had no severely adverse effect on the activity of nickel catalyst. Van Hwerwijnen et al. (52) also investigated the effect of methane on CO methane with CO/CH_4 ratio up to 0.24 and found that methane had no effect on the rate. Satelore and Thomson (53) similarly concluded that methane had no effect on the reaction even at concentration as high as 700 kPa. That methane has no effect

Table 4-3

H_2 Order* of Reaction in CO Methanation

CO Partial Pressure (kPa)	Temperature (K) 475	494	503*	513
6.9	-	0.72	-	-
13.1	-	0.72	-	-
17.9	1.00	-	-	-
24.8	-	-	0.73	-
26.2	-	-	-	0.82
32.1	-	0.78	-	-
63.4	-	-	-	0.92
84.8	-	-	1.00	-

* Result taken from Preliminary Study

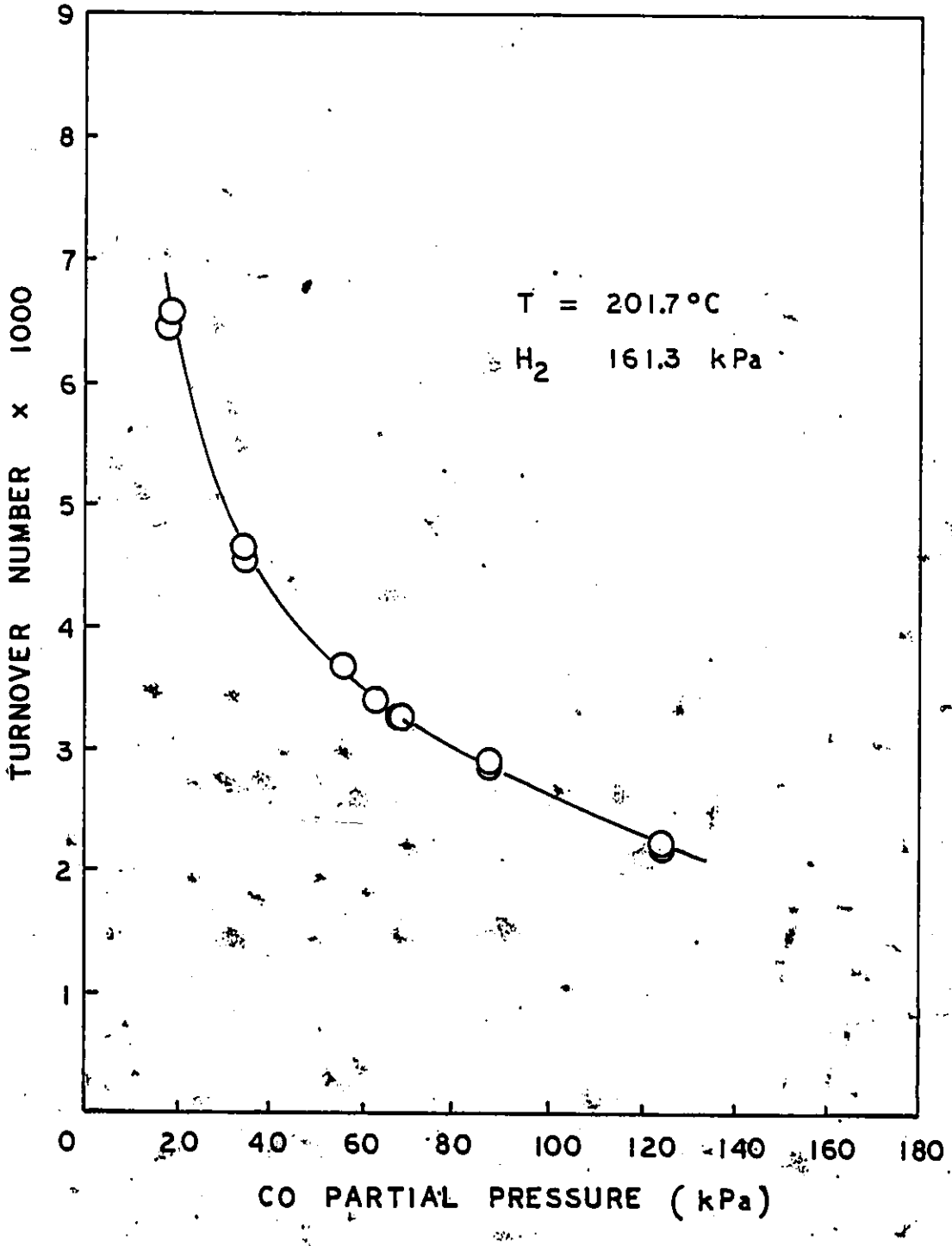

Figure 4-11 Effect of Carbon Monoxide on Methanation Rate at 475 K

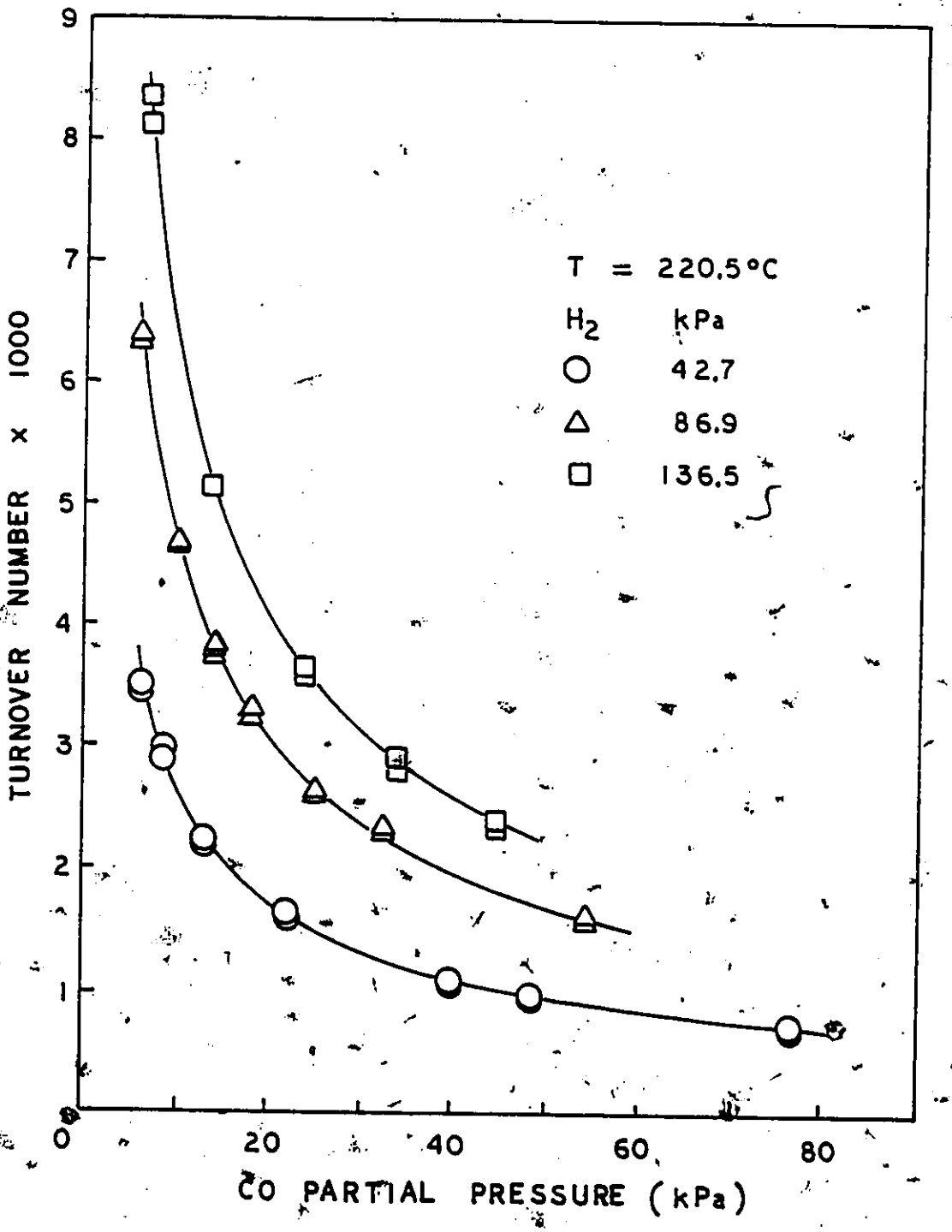

Figure 4-12 Effect on Carbon Monoxide on Methanation Rate at 493 K

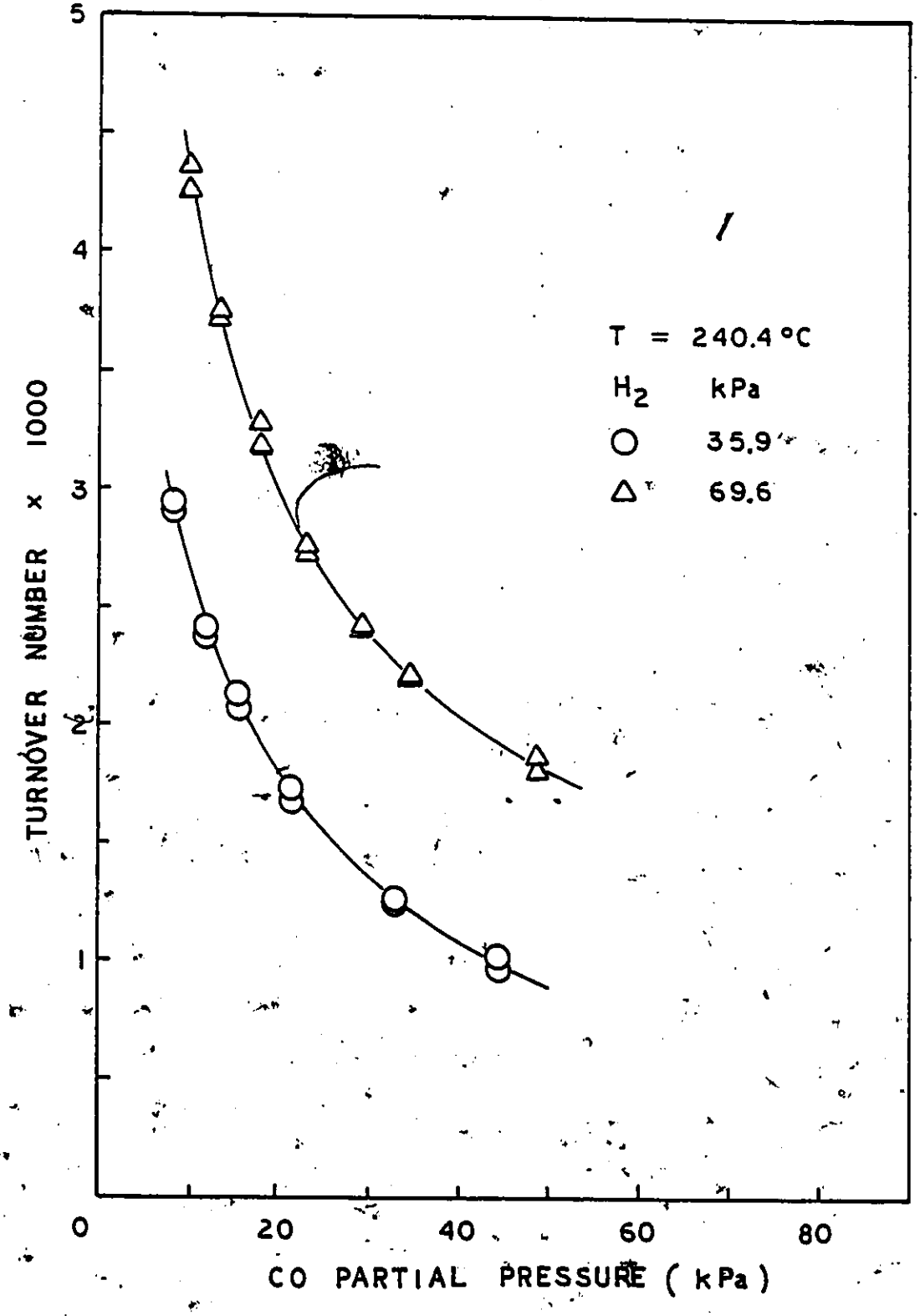

Figure 4-13 Effect of Carbon Monoxide on Methanation Rate at 513 K

Table 4-4

CO Order of Reaction in Methanation

H_2 Partial Pressure (kPa)	Temperature (K)			
	475	494	503*	513
10.3	-	-	-0.68	-
35.9	-	-	-	-0.56
42.7	-0.63	-	-	-
69.6	-	-	-	-0.56
75.8	-	-	-0.68	-
86.9	-	-0.61	-	-
136.5	-	-0.64	-	-
161.3	-0.53	-	-	-

* Result taken from Preliminary Study

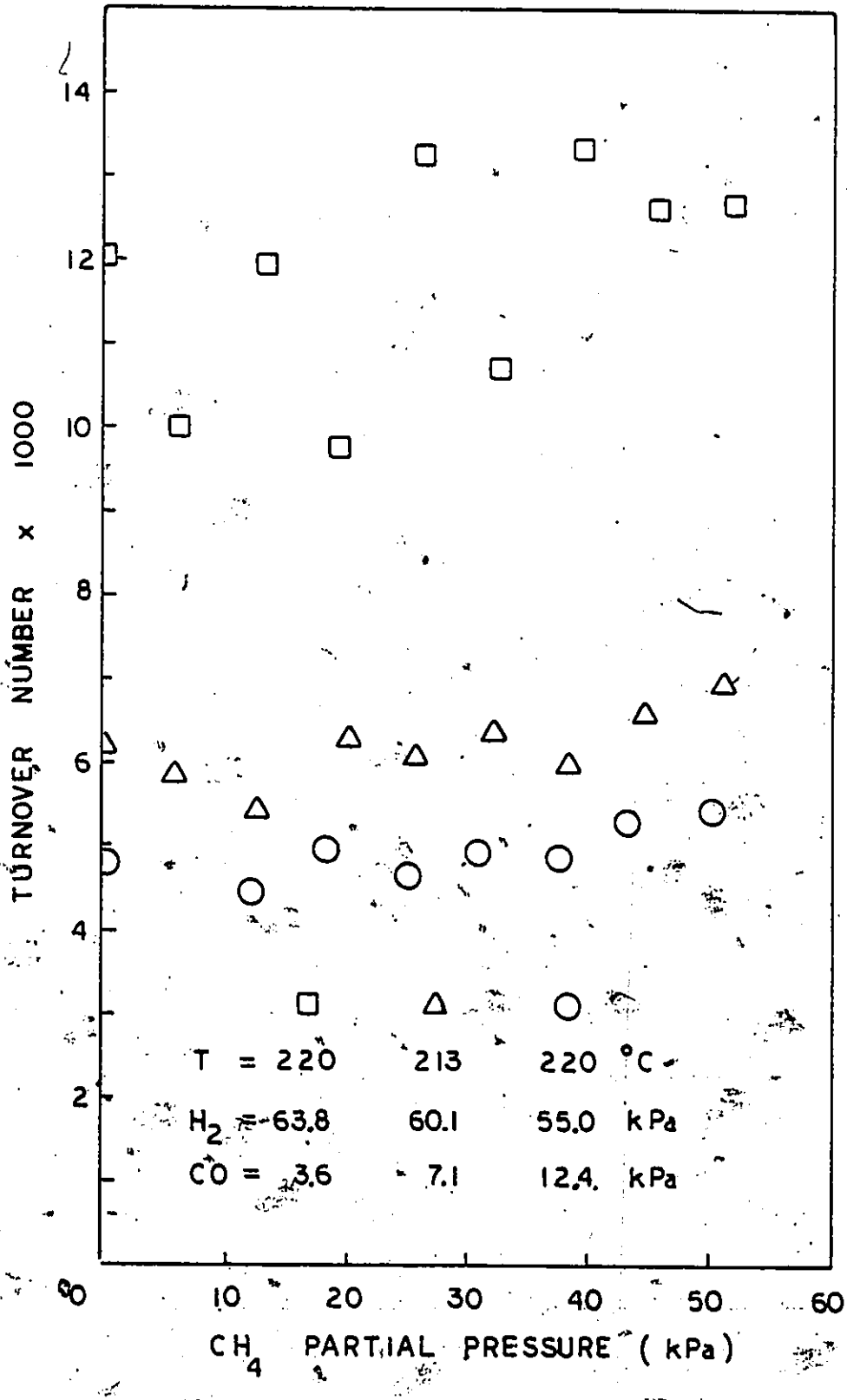

Figure 4-14 Effect of Methane on CO Methanation Rate

on the reaction rate agrees with Fujimoto's finding (72) that adsorption of methane on nickel is very weak and that it desorbs immediately after it is formed.

Contradictory conclusions regarding the effect of water on the reaction rate have been reported. This problem was studied by introducing known concentrations of water vapour into the feed with a $3H_2/1CO$ mixture, the partial pressure of which was kept constant by adjusting the total pressure. The results in figure 4-15 show that water inhibited the reaction rate, in contrast to data reported by Van Herwijnen et al. (52) and Elliott and Lunsford (167). However, Saletore and Thomson (53) reported that the exponent of water was -0.62 which suggests that water strongly inhibits methanation rate. The inhibiting effect of water was examined by fitting the data to the power rate expression. The fitted data are shown in figure 4-16. The exponent obtained at 503 K was -0.08 which suggests that the inhibiting effect was less severe as compared with results from Satelore and Thomson. These authors employed much higher temperatures (above 573 K) in their study, however. King (43) has found that desorption of water was fast relative to its formation and suggested that the effect of water was not due to adsorption equilibrium but possibly to a kinetic effect.

The effect of carbon dioxide on H_2+CO methanation rate was also investigated. Concentrations of H_2 and CO were both maintained at constant values while the partial

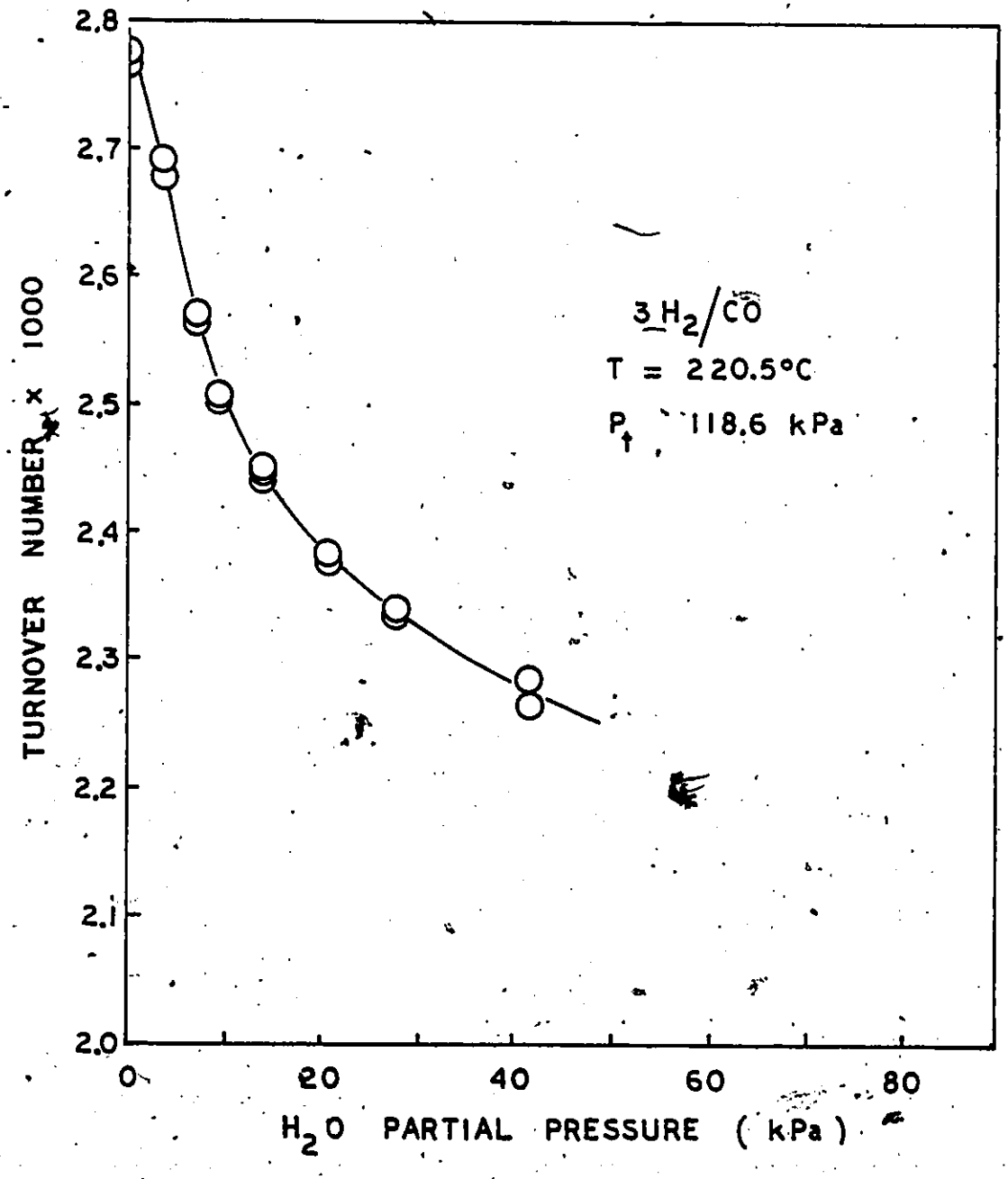

Figure 4-15 Effect of Water on GO Methanation Rate

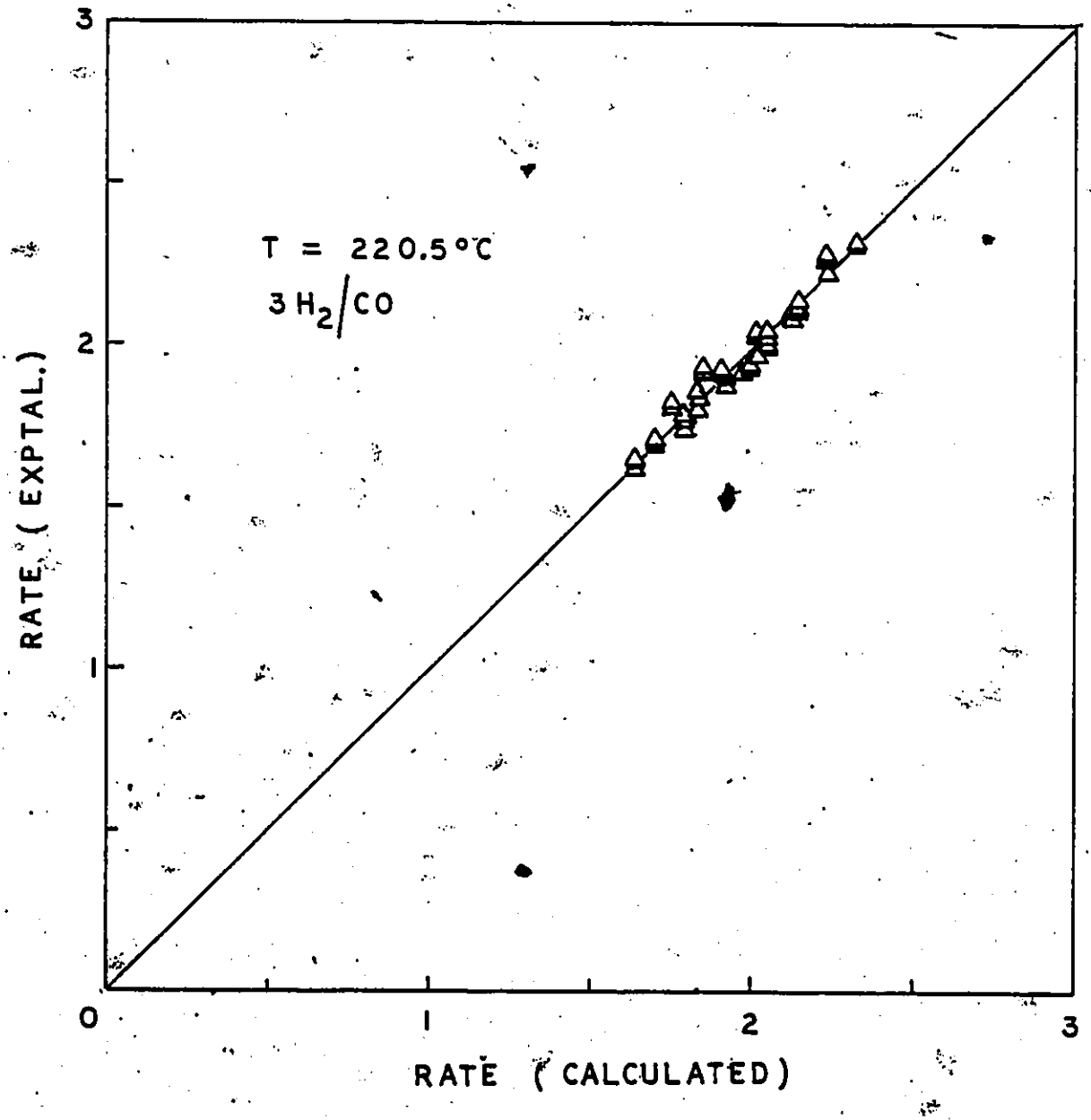

Figure 4-16 Comparison of Experimental and Calculated Rates of CO Methanation - Effect of Water

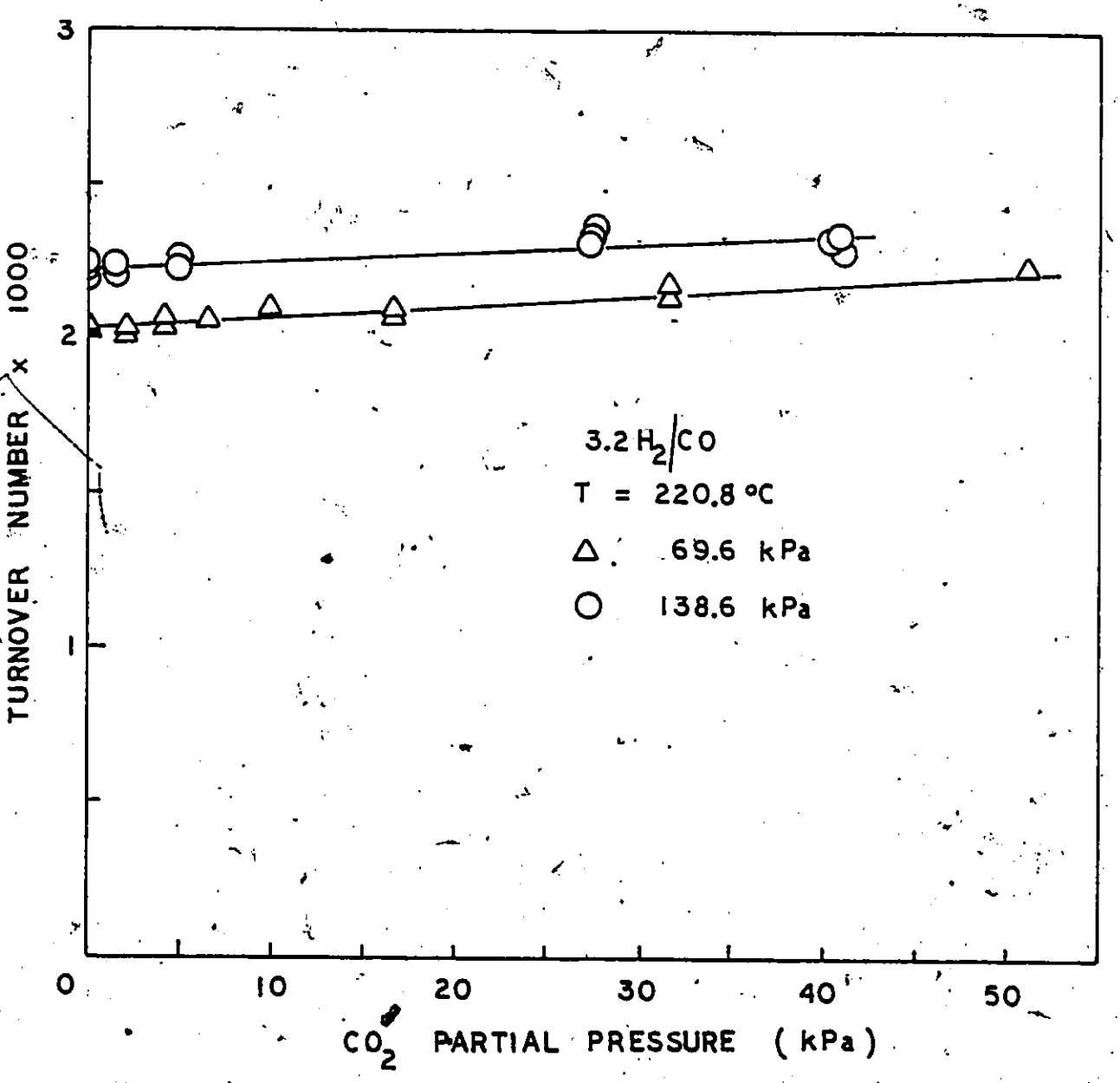

Figure 4-17 Effect of Carbon Dioxide on CO Methanation

pressure of CO_2 was varied. Figure 4-17 shows that the overall methanation rate increased slightly with increasing partial pressure of CO_2. It has been reported that CO_2 could not be hydrogenated in the presence of CO (52). The present result shows that CO_2 could be methanated to a slight extent in the presence of substantial concentrations of CO, suggesting that CO_2 could compete with CO for some of the adsorption sites, especially at high CO_2 partial pressures.

4.4 Reduction of Carbonaceous Residues

It has been reported that carbonaceous species could be an important intermediate in methanation. To investigate this possibility, the surface of the catalyst was examined after a given steady-state run. Generally after the reaction proceeded for an hour, the reactor was flushed with helium until the feed gas could no longer be detected by gas chromatograph analysis; usually this took an hour. Then the helium was replaced by a H_2+He mixture. Upon introduction of H_2, the temperature of the catalyst increased by about one degree and then slowly returned to the initial operating temperature. Methane was formed and its amount was monitored for the next 20 - 30 minutes, depending on the original steady-state experimental conditions. No other higher hydrocarbon was detected in the effluent. Sampling for analysis was started one minute after the observed rise in temperature. However, methane was first

detected 3½ minutes later due to the volume between the catalyst bed and the sampling valve. The initial rate was much higher than the steady-state methanation rate, but it fell quickly with time as the active surface species were depleted. Since CO had been purged before the introduction of H_2+He mixture, it can be deduced that the formation of methane was exclusively due to the hydrogenation of surface carbonaceous species formed in the H_2+CO reaction.

Samples were taken every 2½ minutes for analysis. From the flow rate and the concentration of methane in the effluent, the amount of carbonaceous species left on the catalyst surface could be obtained by integration over the time during which methane was evolved. This amount of surface carbon species was investigated as a function of various steady-state operating conditions, including the effects of temperature, H_2/CO ratio, as well as partial pressures of H_2, CO and water.

The total amount of carbonaceous species removed from the catalyst as methane by hydrogen flushing are shown in figures 4-18 to 4-22. The amount, expressed in terms of moles of carbon, depended on the reaction conditions under which the carbon species was deposited. For constant partial pressures of H_2 and CO, the amount increased with the reaction temperature. In addition, at a constant temperature, the carbon residues increased with the steady-state partial pressure of CO, but decreased with partial pressure of H_2 and increasing H_2/CO

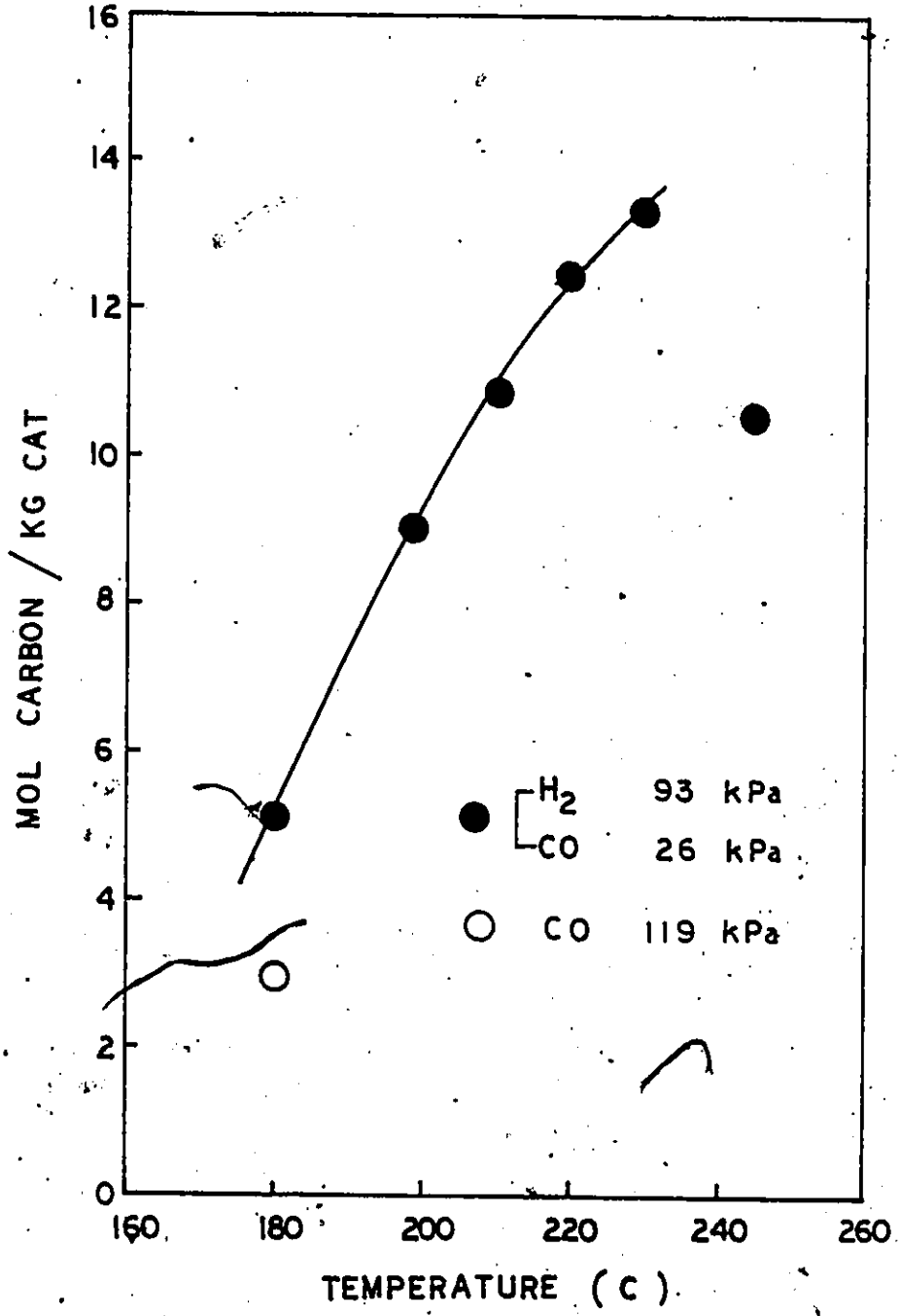

Figure 4-18. Effect of Temperature on the Amount of Residual Carbon

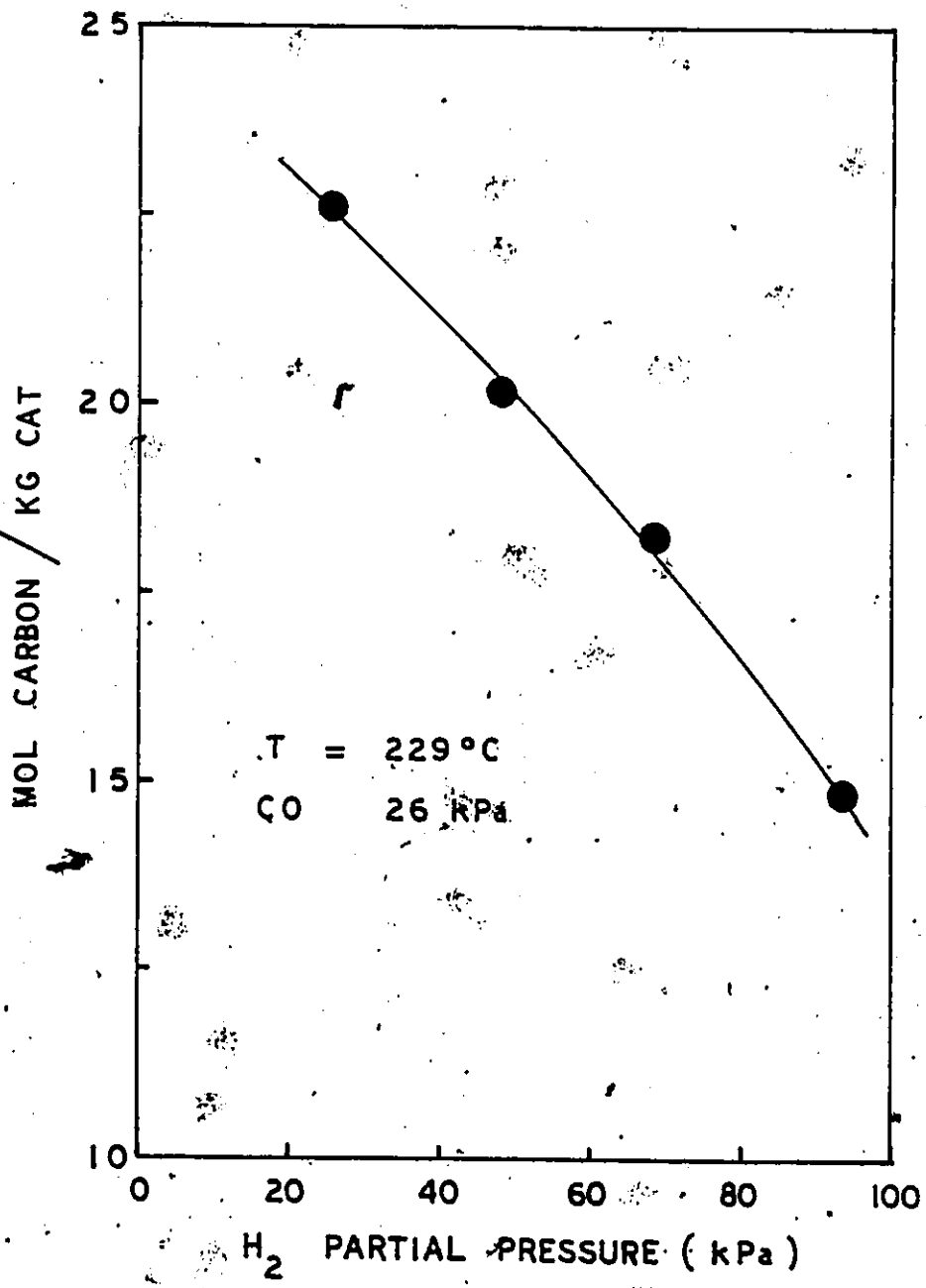

Figure 4-19 Effect of Hydrogen on the Amount of Residual Carbon

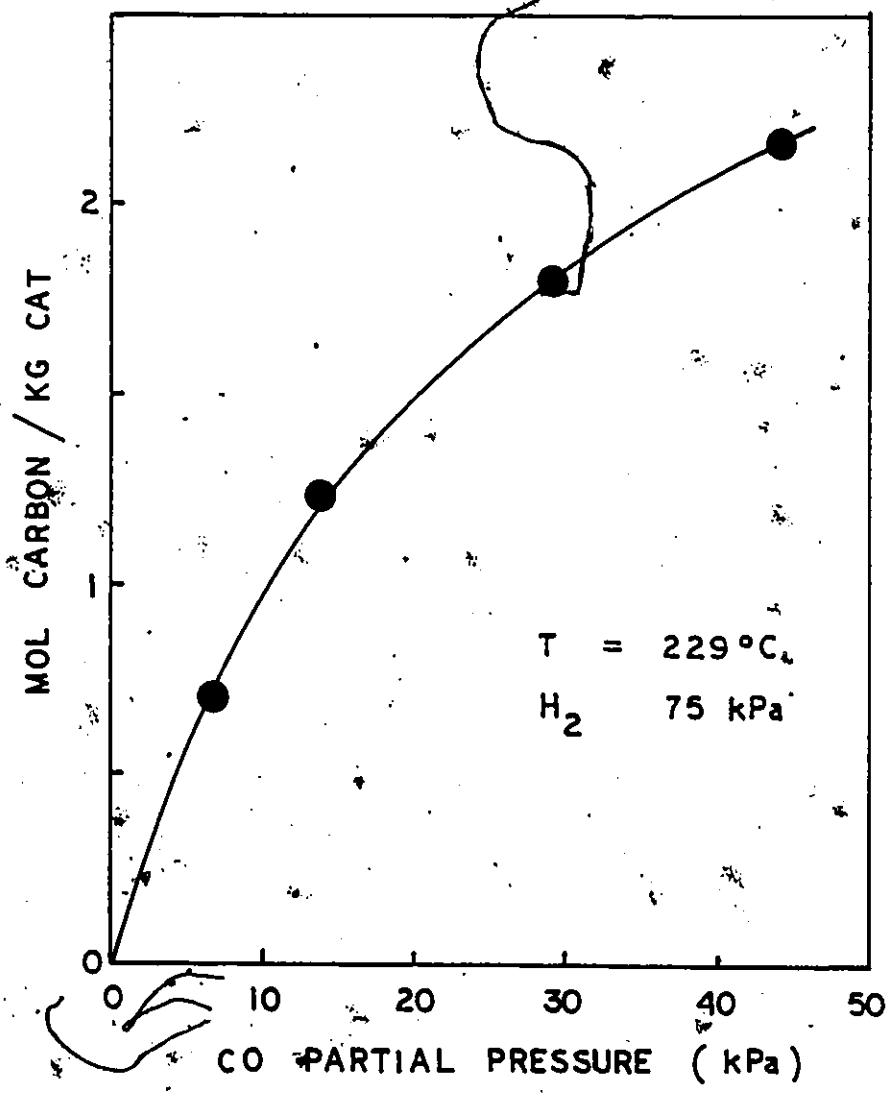

Figure 4-20 Effect of Carbon Monoxide on the Amount of Residual Carbon

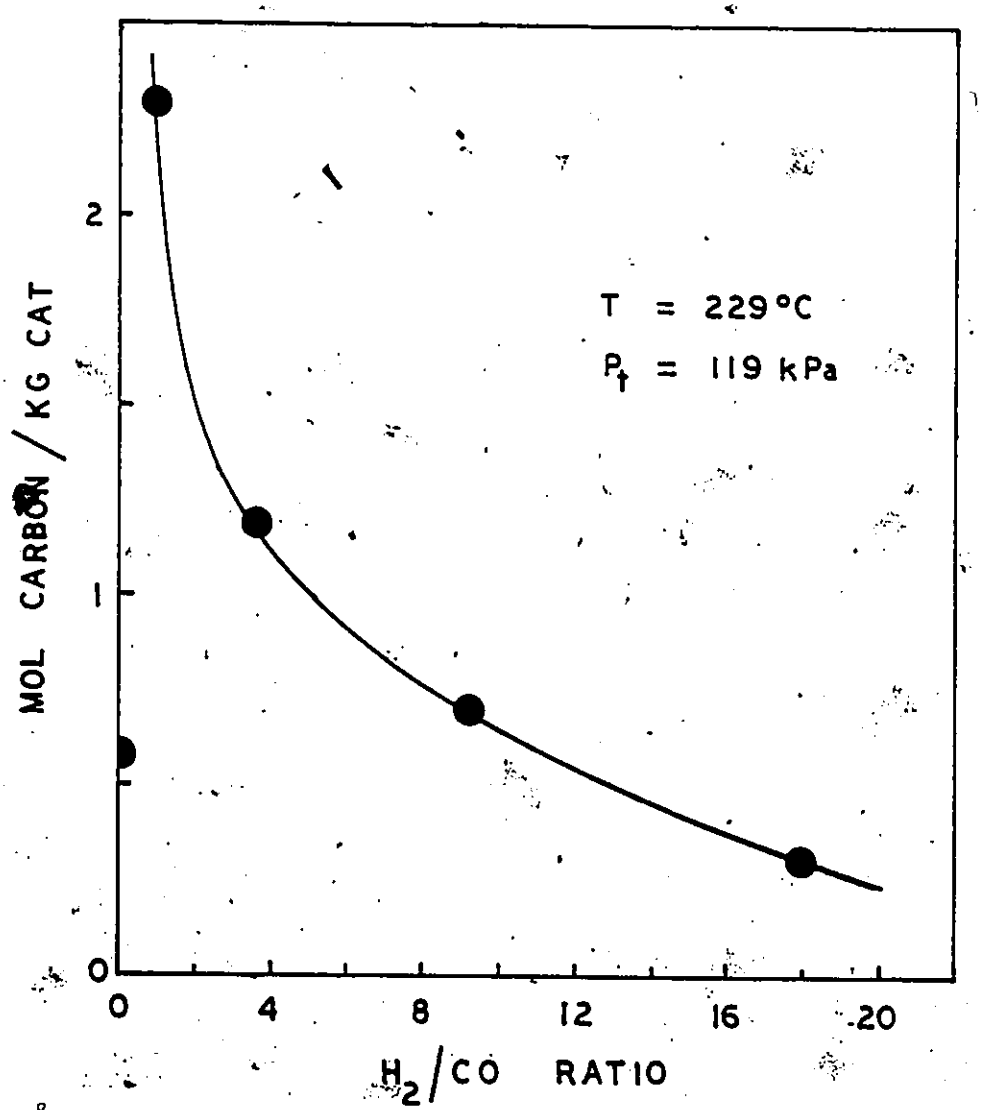

Figure 4-21 Effect of H_2/CO Ratio on the Amount of Residual Carbon

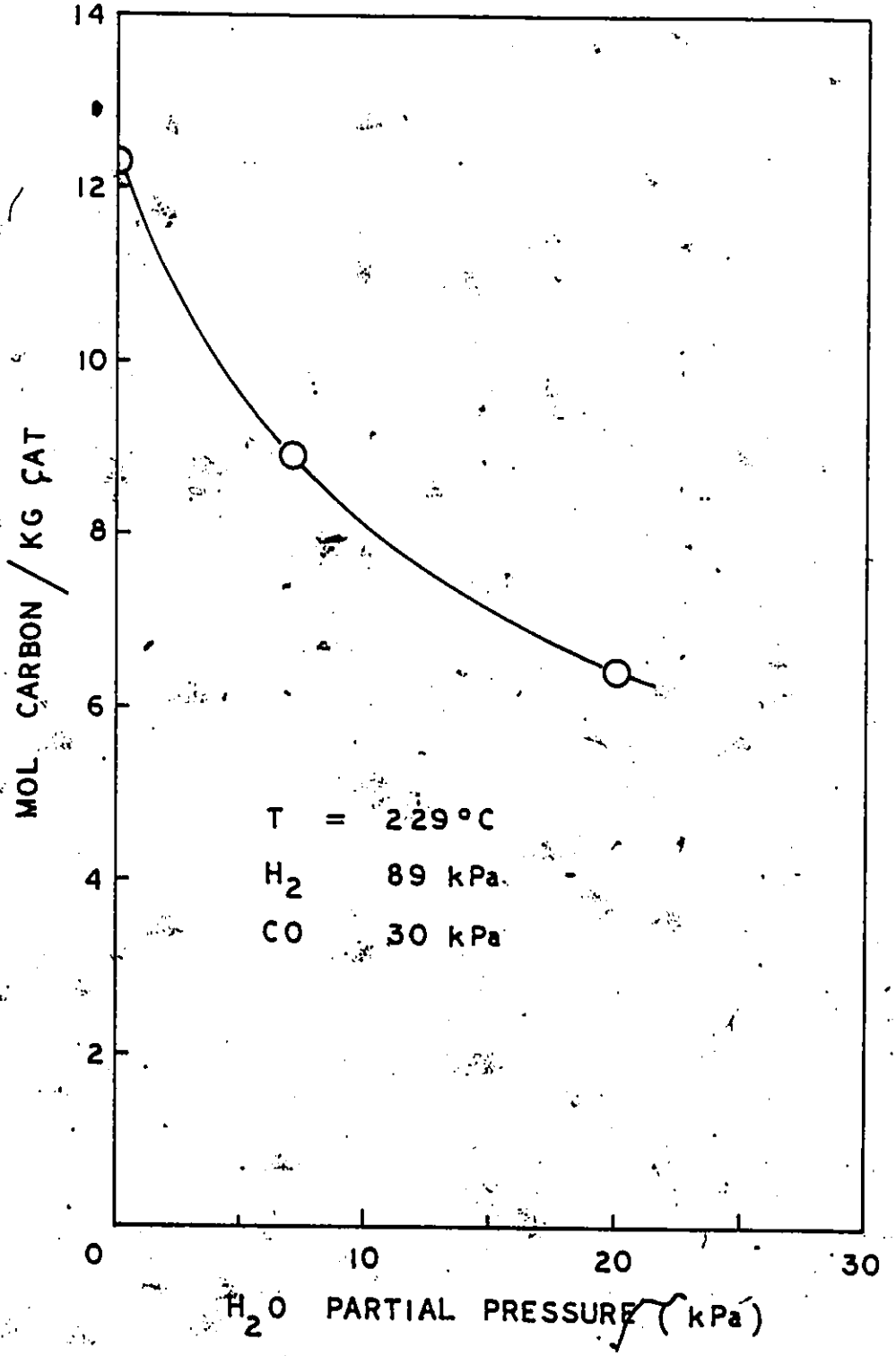

Figure 4-22 Effect of Water on the Amount of Residual Carbon

ratios. Also water decreased the amount of surface carbon residues.

Using 5.4 cm^3 of hydrogen as the monolayer saturation amount per gram catalyst, the calculated number of surface nickel atoms was 48.2×10^{-5} mole per gram of catalyst. Thus, for H_2+CO feed, more than a monolayer of carbon was usually deposited on the used catalyst.

To determine whether the amount of carbon deposited under methanation conditions was different from that deposited upon exposure of the catalyst to CO alone, experiments were carried out in which the catalyst was maintained at the same temperature in a CO+He stream for one hour. Following this exposure, the flow of CO was discontinued and CO was purged with He until no more CO could be detected in the effluent. The catalyst was then flushed with hydrogen. Figure 4-23 shows that the amount of carbon removed as methane was considerably smaller than those after methanation reactions. The effect of CO concentration on the amout of surface carbon was also investigated by adjusting the He diluent flow. The length of these experiments was only 30 minutes, instead of the usual one hour. The amount of carbon deposited was found to increase with the partial pressure of CO.

Assuming that the carbonaceous species was deposited on the catalyst at a constant rate, one can relate the carbon deposition rate to the steady-state methanation conditions.

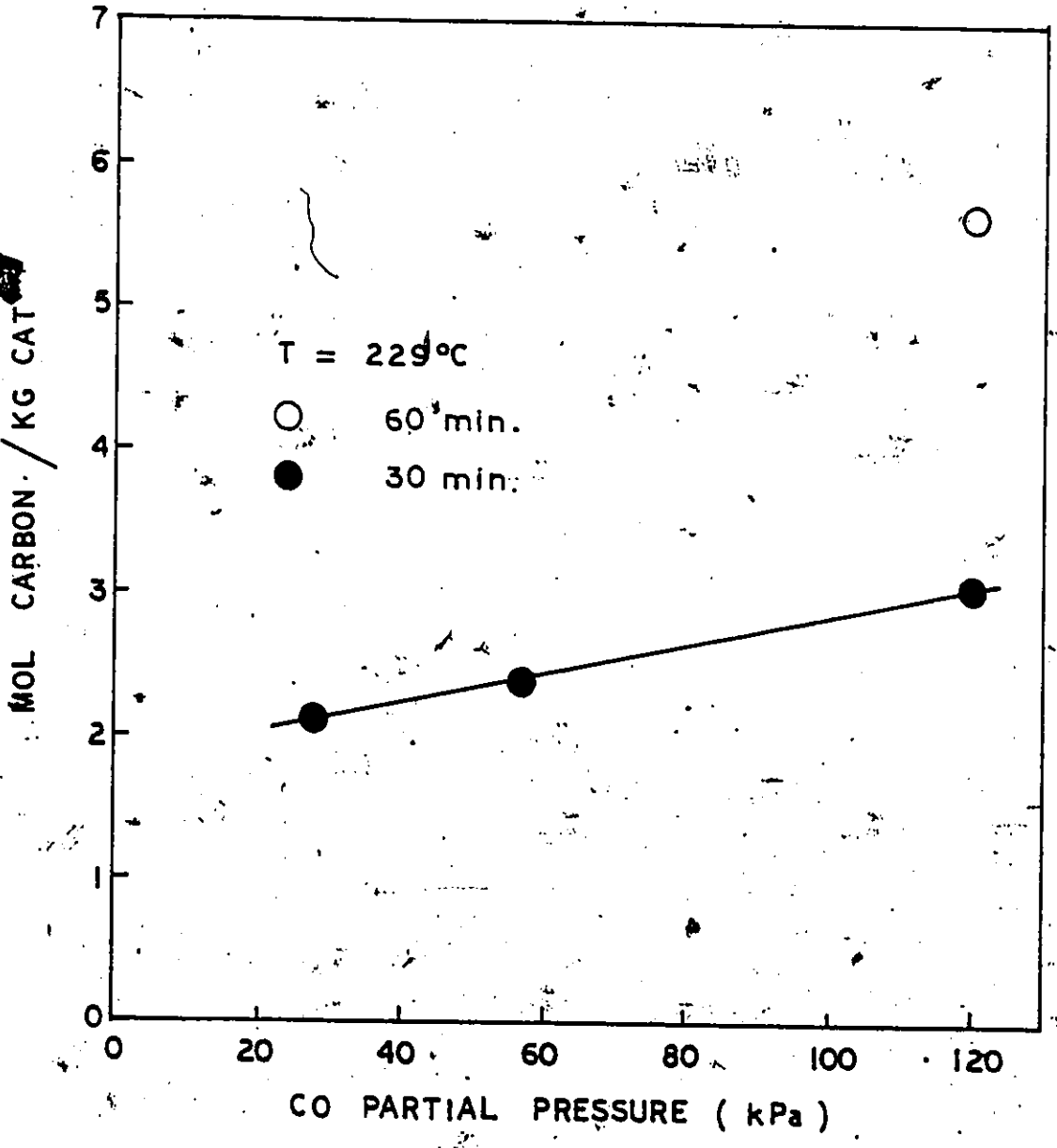

Figure 4-23 Effect of Carbon Monoxide in the Absence of Hydrogen on the Amount of Carbon Deposited

In the power-rate law form, the carbon deposition rate can be expressed as:

$$r_c = k \frac{P_{CO}^{0.6}}{P_{H_2}^{0.3}} \qquad (4-2)$$

where r_c = carbon deposition rate during methanation,

k = constant

P = partial pressures during methanation.

In view of the inaccuracy involved in obtaining methane from the catalyst surface, this expression can best be regarded as semi-quantitative. The exponents of H_2 and CO at 623 K reported by Gardner and Bartholomew (168) were 1.6 and -1.6 for CO and H_2, respectively. The effect of CO in the absence of H_2 on carbon deposition rate was found to be of 0.25 order. The finding agrees with Tøttrup's work which showed that CO dissociation rate increased with increasing CO pressure (29).

The results in figures 4-18 to 4-22 show that under reaction conditions the catalyst maintained a carbon reservoir in excess of a monolayer. Furthermore, this carbonaceous species was very reactive, and in the absence of CO on the surface, could be hydrogenated readily to methane. The rate of methane formation was greater than that measured under steady-state methanation conditons. These observations suggest that carbonaceous species could be an important intermediate in methanation.

Deposition of carbonaceous species during methanation has been reported in the literature (41,170-173). Over ruthenium (41), carbon deposition was greater at higher temperature, in agreement with the present finding over Raney nickel. The decrease in amount of carbon species with increasing H_2 partial pressure or H_2/CO ratio also agrees with results reported by Goodman et al. (37) and other authors (168,173). Apparently under these conditions, a larger fraction of carbon from CO dissociation could react with H_2 to form methane during methanation, resulting in a decrease in residual carbon on the catalyst.

Similar to H_2, water inhibited carbon deposition. It has been suggested that this may result from either the direct reaction of the surface carbon with water or hydrogenation of the carbon species by hydrogen formed via the water-gas shift (168). It was shown recently that methanation of carbon by hydrogen was much slower than by water (174).

The deposition of carbon from CO in the absence of H_2 agrees with the results from Tøttrup (29) and Singh et al. (169). The solid points in figure 4-23 are for steady state runs of 30 minutes duration. It is evident that carbon deposition continued even after one hour. While the amount deposited increased with CO concentration, it was considerably less than that observed in runs with H_2 present (figure 4-21). The present results show that with a feed gas of $H_2/CO = 1$ at a total pressure of 102 kPa, the amount of carbon deposited was

three times of that when pure CO was used.

The present finding suggests that hydrogen plays an important role in controlling the concentration of residual surface carbon. McCarty et al. (41,175) have estimated that the dissociation of CO is thermodynamically unfavourable, and to obtain carbon the equilibrium must be shifted by the removal of surface oxygen from the dissociation. In this regard CO plays an essential role in achieving this shift of equilibrium. However, compared to CO, H_2 is much more effective in removing the surface oxygen, shifting the CO dissociation equilibrium to the right, resulting in a larger amount of carbon deposited (41,176-178). The ease of oxygen removal from nickel surface by hydrogen is supported by the observation in the present study that at low conversions, no CO_2 was observed in the effluent.

4.5 Mechanistic Considerations

There are two major schools of thoughts regarding the mechanism in the hydrogenation of CO. One involves the formation of a CH_xO complex on the catalyst surface, and the other postulates that carbon from the dissociation of CO is the important intermediate. The results discussed in section 4-4 tend to suggest that surface carbon could be a pertinent intermediate.

Most evidence in favour of the CH_xO complex as an intermediate is indirect. It existence has been proposed in order to account for observed adsorption enhancement as

well as kinetics results. Vlaskenko et al (179) proposed the existence of CH_2O complex to explain the enhanced hydrogen adsorption in the presence of CO. Farrauto (180) suggested that the major adsorbed species was of an enolic H-C-OH in order to explain the gravimetric data obtained. From infra-red spectrocopy studies, Blyholder et al. (181) concluded that methane results from hydrogenation of methoxy group CH_3-O-M. Various kinetic models involving CH_xO as intermediate have also been proposed to correlate the kinetic data in methanation. Vannice (4) proposed that the rate determining step involved the reaction between CHOH and H_2, while Huang and Richardson (56) also assumed similar stepwise addition of H to chemisorbed CO, yielding intermediates of CH_xO. It should be noted that the actual existence of CH_xO has not been confirmed despite efforts to identify it by such techniques as infra-red spectroscopy.

The important role of carbon in methanation was first pointed by Wentrcek et al. (31) who found that carbon from dissociation of CO at 553 K was very reactive towards hydrogen. Araki and Ponec (32) proposed a model based on the hydrogenation of surface carbon deposited from CO disproportionation, which was able to explain the reaction order reported for H_2 and CO. Other studies revealed that there were essentially two kinds of carbon. The more reactive form of carbon was believed to be responsible for methanation. This form was unstable and could be transformed into the less reactive form at high temperatures (33, 182).

Given that surface carbon plays an important role in methanation, opinions differ as to the slowest step involved. Zagli et al. (35) using temperature programmed reaction (TPR) technique found that both methane and water left the catalyst surface at the same temperature and concluded that the C-O bond breaking was the rate determining step. Based on infra-red spectroscopy study of the reaction, Dalla Betta et al. (183) also arrived at the same conclusion. In a latter study they reported the absence of H_2-D_2 kinetic isotope effects on nickel, ruthenium and platinum catalysts (36). This observation constitutes an apparent strong case of the involvement of the Boudouard reaction as the slowest step in methanation. McMarthy and Wise (33) also arrived at the same conclusion in their study.

However, the dissociation of CO as the slowest step is at odds with other observations made in methanation studies. If CO dissociation is the slowest step, it would be difficult to explain the positive effect of H_2 on the rate of methanation. Furthermore, the methanation is often inhibited by CO, whereas the present study and others have shown that the rate of CO dissociation increases with the concentration of CO (29). Ho et al. (57) postulated that the slowest step consisted of the reaction between adsorbed CO and H_2 to produce surface carbon. The formation of surface carbon, whether from simple CO dissociation or from reaction of CO with H_2 as the slowest step implies that subsequent reactions are fast and hence

one should not expect the presence of surface carbon after methanation. The present study clearly shows that residual carbonaceous species is left on the catalyst surface, the amount depending on the reaction condition such as temperature, H_2 and CO partial pressures. The presence of surface carbon species also implies that its hydrogenation to methane is slower than its formation.

The strongest evidence for CO dissociation as the slowest step comes from the reported absence of kinetic isotope effect by Dalla Betta et al. (36). However, earlier studies by Jungers et al. (45,46) indicated that over nickel the reaction proceeded more rapidly with D_2 than H_2. This inverse isotope effect was later confirmed by other workers. Mori et al. (184) found that methanation over nickel was 1.4 times faster with D_2 than with H_2. Sakharov and Dokukina (185) also observed an inverse isotope effect for a Co/ThO_2/ kieselguhr catalyst. A normal isotope effect was observed by McKee (186) for methanation over ruthenium powder. Hence the results available thus far have been contradictory. In a comment on Dalla Betta and Shelef's results, Wilson (187) noted that the overall isotope effect could arise from a combination of kinetic and equilibrium isotope effects, the former favouring the reaction of hydrogen and the latter favouring the reaction of deuterium. As a result he concluded that the presence or absence of an isotope effect could not be used to identify the rate determining step. Recently Kellner

and Bell (188) reported an inverse isotope effect for methanation on supported ruthenium catalyst, in contrast to McKee's finding. In addition, it was also reported that the magnitude of the isotope effect depended on the support used. The authors were able to show that the observed isotope effects arose from a complex combination of the kinetic and equilibrium effects associated with the elementary processes occurring on the catalyst surface.

The high activities of carbonaceous species with hydrogen as found in the present study and reported in the literature (30) does not seem to support hydrogenation as the slowest step. On the other hand, carbonaceous species were present on the catalyst surface after methanation. This apparent dilemma is possibly due to the role played by CO. The high activities of the carbon species from CO dissociation is established in the absence of adsorbed CO on the catalyst surface, whereas in actual methanation, adsorbed CO is always present in substantial concentrations. The inhibiting effect of CO was clearly demonstrated in the present study. In Fischer-Tropsch synthesis over ruthenium it was found that higher hydrocarbons were favoured by higher CO/H_2 ratio or higher partial pressure of CO (41). Van Barneveld and Ponec (189) found that over Ni-Cu powders synthesis of higher hydrocarbons required the presence of CO, whereas when the CO feed was stopped, methane formation continued over a considerable time interval, but ethane and propane disappeared from the

effluent gas almost instantaneously. Apparently the presence of CO lowers the hydrogenation rate and the surface species have enough time to grow to higher carbon number species. In this respect, the CO imparts stability to the carbonaceous species. The stability of carbonaceous species to hydrogenation under reaction condition has been ascribed to the presence of CO surrounding the species (41). Once adsorbed CO is removed, the high activity is expected as observed by various investigators and in this work. Thus, the high activities of the carbonaceous species in the absence of CO does not hold in the steady-state operation, and it is justified to say that hydrogenation of these species is a slow process in methanation.

There are observations reported in the literature supporting the hypothesis that hydrogenation of the carbonaceous species is the slowest step in methanation. While the observation of residual carbon on the Raney nickel as found in the present study constitutes a direct and strong evidence, others are less direct and can be derived from various observations which can easily be rationalized in terms of hydrogenation being the slowest step. Bileon et al. (38) have demonstrated that CO dissociation is comparatively fast and hence not a rate determining step, and that CH_x constitutes the most abundant reactive surface carbon species. Gardner and Bartholomew (173) also established that under methanation condition, both the CO adsorption and the desorption of

product were much faster than the formation and hydrogenation of surface carbon. Vannice and Garten (125) studied the activities and selectivities of nickel supported on TiO_2, and found that the catalyst had much higher methanation rate relative to other supported nickel catalyst, and was quite resistant to carbon deposition. The concomitant observations of higher activity and decreased rate of deactivation due to carbon deposition can be rationalized in terms of the faster hydrogenation of surface carbon on the catalyst, which results in the higher methanation rate. The observation of more saturated hydrocarbon formation also suggests the better hydrogenating power of the Ni/TiO_2 catalyst. If the dissociation of CO as the slowest step is assumed, one would expect relatively fast deactivation compared to the other supported nickel catalyst. That hydrogenation is the kinetically significant step in methanation can find support from poisoning studies. Dalla Betta et al. (163) found that the most active methanation catalyst was also the least active one in the presence of hydrogen sulphide. The drop in activity is attributed to the loss of hydrogenation power because sulphur is known to suppress the dissociative adsorption of hydrogen, thus preventing the hydrogenation of surface carbon or partially hydrogenated carbon species. It was also reported that in the presence of hydrogen sulphide poisoning, selectivity towards higher hydrocarbons increased, and that sulphur poisoned the ability of the catalyst to hydrogenate the carbon species

much more severely than the ability to form C-C bonds. Schwarz and Smith (190) also arrived at the conclusion that the sharp decrease in methanation rate was due mainly to the strong suppression of hydrogen chemisorption and not the effect of sulphur on CO adsorption.

The results in this study also provide additional evidence supporting surface carbon species as the important intermediate in methanation. When the Raney nickel catalyst was exposed to CO, carbon species were deposited which reacted with H_2 during the H_2 flushing period to yield methane. This observation is in agreement with Rabo's finding that metals active in CO dissociation were also good methanation catalysts whereas metals that adsorbed CO associatively were generally poor methanation catalysts and were more active for alcohol formation. The results discussed in section 4-4 also suggest that the rate determining step consists of the hydrogenation of carbonaceous species and not of CO dissociation. The decrease in residual carbon with increasing H_2/CO ratio and partial pressure of H_2 at constant CO concentration can be explained in terms of increased removal rate of surface carbon by hydrogenation under these conditions. Increasing the partial pressure of CO inhibited this hydrogenation step, resulting in increased residual carbon level on the catalyst. Thus, under methanation conditions, formation of carbonaceous species is faster than its removal by hydrogenation and its concentration depends on its formation and removal rates.

The increase in the amount of residual carbon with methanation temperature suggests that the rate of formation of surface carbon increases faster with temperature than its rate of removal, and that the activation energy for CO dissociation is higher than that of hydrogenation. Indeed, it has been reported that the activation energy for CO dissociation is some 20 - 30 kJ/mol higher than that of hydrogenation of surface carbon from CO disproportionation (173). This difference in activation energy could result in a change of the slowest step from hydrogenation at high temperatures to CO dissociation at lower temperatures.

The present study also showed that water vapour decreased the methanation rate. While one may attribute this observation to the lowering of the hydrogenation rate by water vapour, it would be difficult to explain the decrease of residual carbon by water vapour. Hence, a more likely explanation is that water vapour curtails the formation of the carbonaceous species, resulting in a decrease in methanation rate. Since methane was found not to affect the methantion rate, the effect of water vapour could not be due to the reverse of methanation, particularly in view of the unfavorable thermodynamics involved. Tøttrup (29) attributed the effect of water vapour on the decrease in rate of CO dissociation to the water-gas shift:

$$CO + H_2O \longrightarrow CO_2 + H_2 \qquad (4\text{-}3)$$

However, according to Araki and Ponec (32), this is unlikely because nickel is a poor catalyst for this reaction. A more likely explanation could be due to water being chemisorbed on the catalyst. Water has been shown to be dissociatively adsorbed on nickel (191,192). Renouprez et al. (191) showed that water dissociated on Raney nickel effectively occupying 2.5 nickel atoms for each molecule of water adsorbed, whereas on nickel prepared from its hydroxide the water molecule occupied six metal sites. Chemisorption of water decreases the concentration of active sites for CO dissociation and results in a lower rate of formation of carbonaceous species as well as the methanation rate.

Thus the findings in the present study strongly suggest that the hydrogenation of carbonaceous species could be the rate determining step in the methanation of CO. To further test this possibility, the kinetic data were fitted to a rate equation based on this assertion.

Fitting kinetic data to Langmuir-Hinshelwood type equations can yield important mechanistic information. While one cannot speak unequivocally about the detailed mechanism, unlikely mechanisms can be ruled out if the fit is poor. On the other hand, a good fit would lend support to the proposed hypothesis. It is important to remember that a good fit of data by a derived equation is a necessary but not sufficient condition for establishing the mechanism. The role of fitting data to Langmuir-Hinshelwood type rate equation in the

interpretation of reaction mechanisms has been discussed by Weller (126).

Based on the evidence from the present study and the literature, the following mechanism is proposed for CO methanation:

$$H_2 + 2S \rightleftharpoons 2H_s \quad (1)$$

$$CO + S \rightleftharpoons CO_s \quad (2)$$

$$CO_s + S \rightleftharpoons C_s + O_s \quad (3)$$

$$O_s + H_s \rightleftharpoons (OH)_s \quad (4)$$

$$(OH)_s + H_s \rightleftharpoons H_2O + 3S \quad (5)$$

$$C_s + H_s \rightleftharpoons (CH)_s \quad (6)$$

$$(CH)_s + H_s \rightleftharpoons (CH_2)_s + 2S \quad (7)$$

$$(CH_2)_s + H_s \rightleftharpoons (CH_3)_s + S \quad (8)$$

$$(CH_3)_s + H_s \rightleftharpoons CH_4 + 2S \quad (9)$$

H_2 and CO adsorptions are assumed to occur rapidly and in equilibrium (steps 1 and 2). Step 3 represents the dissociation of adsorbed CO into carbidic carbon and surface oxygen. In the presence of H_2 the surface oxygen is removed via stepwise hydrogenation to H_2O which desorbs into the gas phase (steps 4-5). The surface carbon is hydrogenated

stepwise to yield finally methane.

The H_2 flushing experiments after steady-state runs showed that carbonaceous species remained on the catalyst surface. These species are non-oxygenated and are at different stages of hydrogenation CH_x (x = 0 - 3) (34,38-41,189,193,194). The slowest step in CO methanation is assumed to be the hydrogenation of the CH species, whose stability has been suggested by various authors. Amenomiya et al. (34) showed that it can withstand evacuation at 373 K and is the most abundant species on the catalyst surface. Dèmuth and Ibach (195) also demonstrated the stability of CH_x fragments on nickel at temperatures greater 300 K. The stability of carbonaceous species under methanation conditions has been previously discussed.

Adsorbed CH species has been suggested to be responsible for chain growth in Fischer-Tropsch synthesis by Joyner (40). While CH species has been suggested as a possible intermediate in CO methanation (34,38,39) and Fischer-Tropsch synthesis (40), the assumption is made here that it occupies two reaction sites. This postulate, together with the various assertions made above, yields the following rate equation (Appendix C):

$$r = \frac{k_1 P_{H_2} P_{CO}^{\frac{1}{2}}}{(1 + k_2^{\frac{1}{2}} P_{H_2}^{\frac{1}{2}} + k_3 P_{CO}^{\frac{1}{2}})^3} \qquad (4\text{-}4)$$

Adsorbed H and surface carbon are assumed to be the most abundant species, while species CH_s and OH_s are each assumed to occupy two reaction sites. The exponent of 3 in the denominator stems from the assumption that hydrogenation of CH_s species is the rate determining step and involves three sites.

The equation predicts a minimum reaction order of -1 for CO and maximum orders of 1.0 and ½ for H_2 and CO, respectively. A maximum rate is predicted as the partial pressure of H_2 is increased sufficiently with the partial pressure of CO kept constant. No such maximum was observed in the present study, possibly due to the H_2/CO ratio's not being high enough. However, Goodman et al. (37) found that the rate is zero order at high H_2/CO ratio.

The fit of the model is shown figures 4-24 to 4-25. Table 4-5 shows the values of the estimated parameters for the model. k_1 and k_3 are products of various constants while k_2 represents the adsorption equilibrium constant of H_2 (See Appendix C). The values of k_2 are compared with those obtained from the high temperature chemisorption (section 2.2.4) in table 4-6. While the values decrease with temperature, they are smaller than the values from chemisorption study. This discrepancy is apparently due to the vastly different catalyst surface conditions. The catalyst surface in the kinetic runs has been shown to contain multilayers of carbon. Falconer et al. (196) showed that surface carbon decreased the sticking

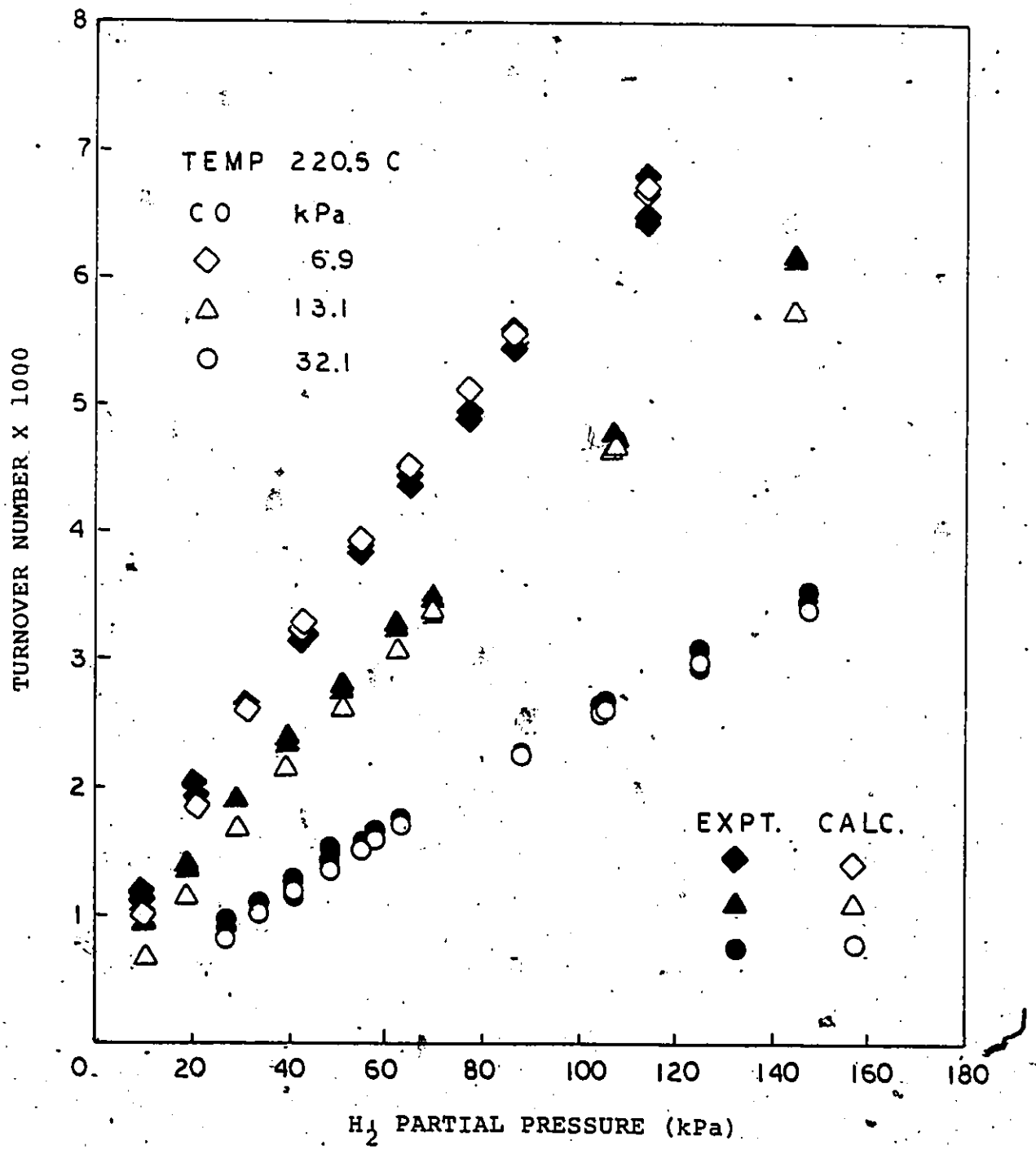

Figure 4-24 Comparison of Experimental and Calculated Rates of CO Methanation

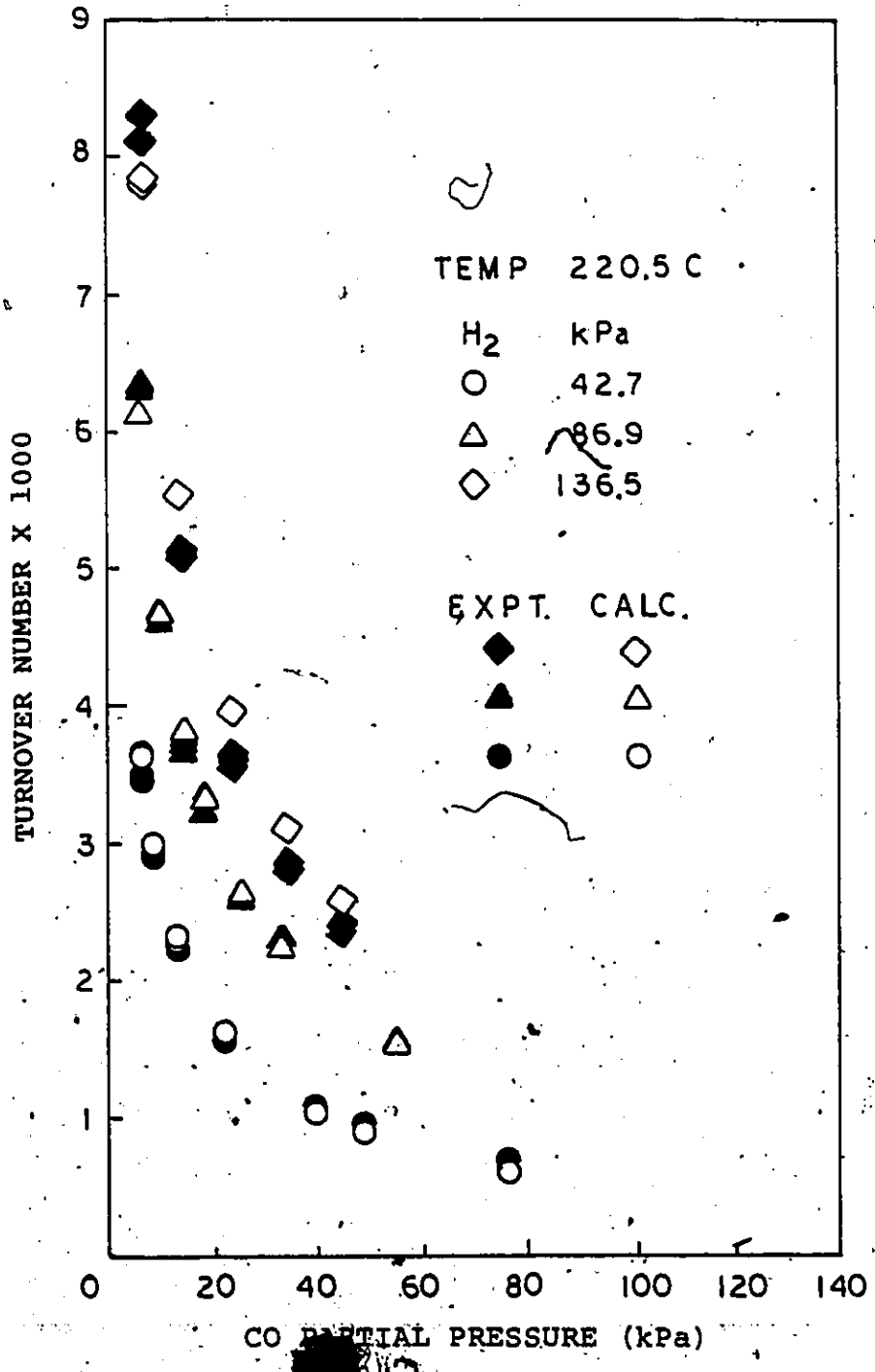

Figure 4— Comparison of Experimental and Calculated Rates of CO Methanation

Table 4-5

Estimated Parameter Values for Langmuir-Hinshelwood Model (Equation 4-4)

Temp (^{o}C)	k_1	$k_2^{\frac{1}{2}}$	k_3
202	0.0145	0.1927	3.3380
220	0.0089	0.1557	1.7713
240	0.0031	0.1151	1.0819

Unit of k_1 = $\frac{\text{molecule}}{\text{Metal site - second - (kPa)}^{1.5}}$

k_2 = kPa^{-1}

k_3 = $kPa^{-\frac{1}{2}}$

Note - The estimated value of parameter k_1 is found to decrease instead of increase with temperature. Since the reaction rate depends on the number of available sites per gram of catalyst, a decrease in reaction sites from catalyst deactivation will result in corresponding decreases in the rate and estimated value of parameter k_1 (e.g. see figure 4-10). Deactivation is attributed to a combination of carbon deposition and sintering, especially at high temperatures. In the absence of deactivation, parameter k_1 would obey the Arrhenius' Law.

Table 4-6

Comparison of H_2 Adsorption Constant k_{H_2}

Temp (°C)	$k_{H_2}^{\frac{1}{2}}$ Values		
	Chemisorption	CO Hydrogenation	CO_2 Hydrogenation
190	0.5404		
202		0.1927	
210	0.4901		0.2148
220		0.1557	
230	0.4324		0.1675
240		0.1151	0.1597
250	0.3424		0.1538

probability of H_2.

Other Langmuir-Hinshelwood equations were also tested against the data (table 4-7). Model 6 (equation 4-4) fitted the data as well as the power-rate law. The fits for models 1, 2, and 9 were poor. Model 1 has been suggested by Ho et al. (57) and Huang et al. (56). Model 9 yields zero order at high partial pressure of H_2. Model 3 yielded a residual sum of squares which was about twice as large as model 6. Models 5 and 7 both gave residual sum of squares about 4 times larger than that from model 6. Of the models tested, model 6 is regarded as adequate in representing the data.

It is difficult if not impossible to obtain a rate equation that will fit the data covering vastly different conditions. The failure of equation 4-4 to predict constant rate at high H_2/CO ratio can be attributed to a change in the slowest step. At the extreme condition of high H_2/CO ratio when constant rate was obtained by Goodman et al. (37), hydrogenation is expected to be fast, and the overall rate may now be determined by the rate of CO dissociation. At even lower CO concentration, the rate will be governed by the adsorption or diffusion process; Randhava et al. (54) found that the order of reaction for CO over nickel to be 0.7 when CO was present in concentration of ppm.

Equation 4-4 does not account for the effect of water vapour since the data used in the regression analysis were

Table 4-7

Rate Equations tested for CO Methanation

No.	Equation
1	$\dfrac{k_1 P_{H_2} P_{CO}}{(1 + k_2^{\frac{1}{2}} P_{H_2}^{\frac{1}{2}} + k_3 P_{CO})^2}$
2	$\dfrac{k_1 P_{H_2} P_{CO}^{\frac{1}{2}}}{(1 + k_2^{\frac{1}{2}} P_{H_2}^{\frac{1}{2}} + k_3 P_{CO}^{\frac{1}{2}})^2}$
3	$\dfrac{k_1 P_{H_2} P_{CO}^{\frac{1}{2}}}{(1 + k_2^{\frac{1}{2}} P_{H_2}^{\frac{1}{2}} + k_3 P_{CO})^2}$
4	$\dfrac{k_1 P_{H_2} P_{CO}}{(1 + k_2^{\frac{1}{2}} P_{H_2}^{\frac{1}{2}} + k_3 P_{CO} + k_4 P_{H_2}^{\frac{1}{2}} P_{CO})^2}$
5	$\dfrac{k_1 P_{H_2} P_{CO}}{(1 + k_2^{\frac{1}{2}} P_{H_2}^{\frac{1}{2}} + k_3 P_{CO})^3}$

Table 4-7 (continued)

No.	Equation
6	$\frac{k_1 P_{H_2} P_{CO}^{\frac{1}{2}}}{(1 + k_2^{\frac{1}{2}} P_{H_2}^{\frac{1}{2}} + k_3 P_{CO}^{\frac{1}{2}})^3}$ (eqn. 4-4)
7	$\frac{k_1 P_{H_2} P_{CO}^{\frac{1}{2}}}{(1 + k_2^{\frac{1}{2}} P_{H_2}^{\frac{1}{2}} + k_3 P_{CO})^3}$
8	$k P_{H_2}^{m} P_{CO}^{n}$ (Power Rate law)
9	$\frac{k_1 P_{H_2}^{3/2} P_{CO}^{\frac{1}{2}}}{(1 + k_2^{\frac{1}{2}} P_{H_2}^{\frac{1}{2}} + k_3 P_{CO}^{\frac{1}{2}})^3}$

obtained under differential conditions when concentration of water was low. However, water has been shown to inhibit the methanation rate, the order being -0.08 at 503 K. Since water dissociates on nickel surface (191,192), its effect on the methanation rate can be attributed to its occupation of active sites. Since the data in figure 4-15 were obtained with constant partial pressures of H_2 and CO, one can test the effect of water with the following equation:

$$r = \frac{K_1}{(K_2 + k P_{H_2O}^{1/n})^m} \qquad (4\text{-}5)$$

The data on the effect of water were analysed by plotting $(1/r)^{1/m}$ versus $P_{H_2O}^{1/n}$ with m and n varying from 1 to 3 and 1 to 6, respectively. It was found that a linear plot was obtained for m = 3 and n = 6. The value of 6 for n is in agreement of Renbuprez's work while the value of 3 for m agrees with the exponent for the denominator for model 6 (equation 4-4). The overall result shows that the effect of water on methanation rate can be explained in terms of its occupying active sites. Thus, to include the effect of water, equation 4-4 can be modified to:

$$r = \frac{k_1 P_{H_2} P_{CO}^{1/2}}{(1 + k_2^{1/2} P_{H_2}^{1/2} + k_3 P_{CO}^{1/2} + k_4 P_{H_2O}^{1/6})^3} \qquad (4\text{-}6)$$

In summary, the mechanism of CO methanation was discussed and evidence in support of surface carbon species as an important intermediate presented. Arguments for the hydrogenation of carbonaceous species as the rate determining step were also detailed. A reaction mechanism was proposed for CO methanation and on this basis, a rate equation was obtained which could represent the data well, lending support to the proposed mechanism.

Chapter 5

CARBON DIOXIDE METHANATION

5.1 Introduction

The rate of carbon dioxide methanation was examined as a function of temperature and partial pressures of the reactants. The experiments were generally conducted at pressures of less than 202 kPa in the temperature range of 483 - 523 K.

The conversions were kept at less than 4%. The reactant concentrations were taken to be the average of the effluent and the inlet concentrations. The temperature was measured directly since the thermocouple was imbedded in the catalyst bed. The rate obtained was differential since the conversions were small, and could be directly applied to various proposed rate equations.

In some of these experimental runs, the catalyst deactivated as a result of sintering or aging. Sintering was more prone to occur in high temperature runs, at temperatures greater than 503 K.

5.2 Preliminary Kinetic Studies

As in the study of CO methanation, preliminary studies were conducted to obtain the pertinent features of methanation of CO_2. This consisted of a brief investigation of the effects of H_2 and CO_2 on the reaction rate. The rate was expressed in terms of methane turnover number as shown in Figure 5-1.

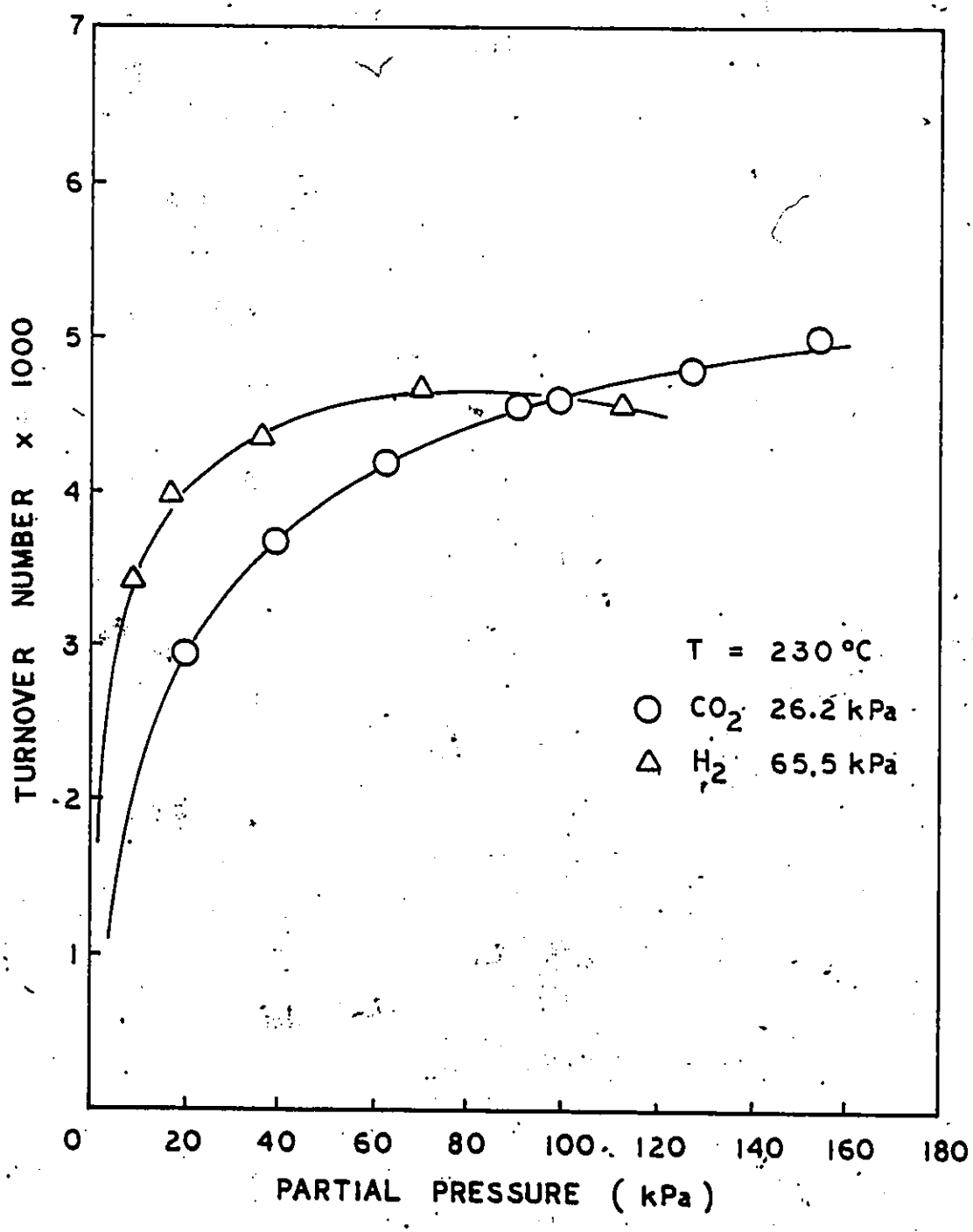

Figure 5-1 Effects of Hydrogen and Carbon Dioxide on Methanation Rate : O CO_2 at 26.2 kPa; Δ H_2 at 65.5 kPa.

The rate increased with the partial pressure of H_2. However, at higher concentrations, the effect of H_2 decreased.

In contrast to the effect of CO on methanation rate, the turnover number (TON) increased with the partial pressure of CO_2. The effect was almost linear at low partial pressures. At higher partial pressures of CO_2, the increase in rate diminished, and a maximum in rate was observed. Further increase in CO_2 concentration decreased the rate slowly. As the partial pressure of CO_2 was increased beyond the maximum, trace amounts of CO were detected in the effluent stream. The maximum rate observed as the CO_2 concentration was increased and the concomitant observation of trace amounts of CO suggest that CO may play a role in suppressing the reaction rate.

The observation of a maximum rate with increasing concentration of CO_2 suggested that the effect of CO_2 on the kinetics may not be adequately represented by using order of reaction. This observation is significant in view of the half (5,7,51) and first orders (97) of reaction reported in the literature.

The preliminary data show that the effects of H_2 and CO_2 on methanation are quite different from those in CO methanation. In contrast to CO, CO_2 increases the rate which reaches a maximum and then decreases with further increase in CO_2 concentration. Hydrogen also increases the rate but there is evidence that its effect diminishes as its concentration is increased. The data question the applicability of power-rate

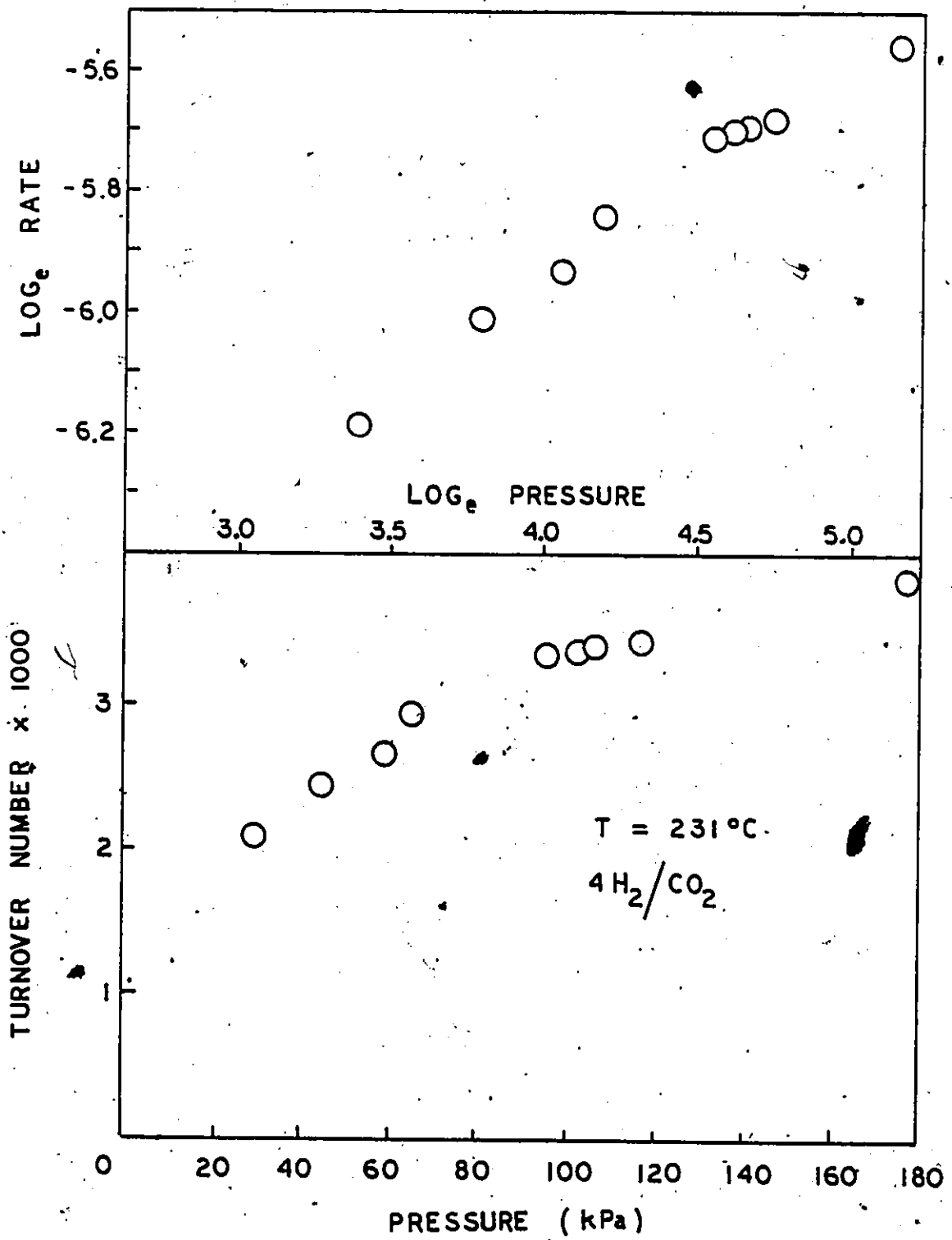

Figure 5-2 Effect of Total Pressure on CO_2 Methanation Rate

law in representing the effects of the reactants, especially as the pressure is increased.

The effect of total pressure on the rate at 503 K is shown in Figure 5-2. The H_2/CO_2 ratio was kept at 4 , and the total pressure increased. Generally the data can be correlated by the power-rate law with an apparent order of 0.4. However, as expected, deviation occurs in the high pressure region where the reaction order is less than 0.4 . This is in agreement with the results on the individual reactant effect at high pressures.

5.3 Kinetics

5.3.1 Effect of Temperature

The effect of temperature on the reaction rate is shown in Figure 5-3 at various total pressures. The H_2/CO_2 ratio was maintained at a stoichiometric ratio of 4. The activation energy obtained from the slope of the Arrhenius plot was 105 kJ/mol. This value is generally 17 - 20 kJ larger than values reported for supported nickel catalysts by various authors. Over Ni/Al_2O_3 catalyst, a value of 88 kJ/mol was reported by Maatman et al. (103) in the temperature range of 483 - 588 K, even though the data showed some scattering. Weatherbee et al. (197) reported a value of 80 kJ/mol over Ni/SiO_2 catalyst. Nicolai et al. (46) also reported a value of 54.4 kJ/mol. However, the value found in the present study agrees well with Herwijnen et al. (52) data (106 kJ/mol). However, of the values reported for

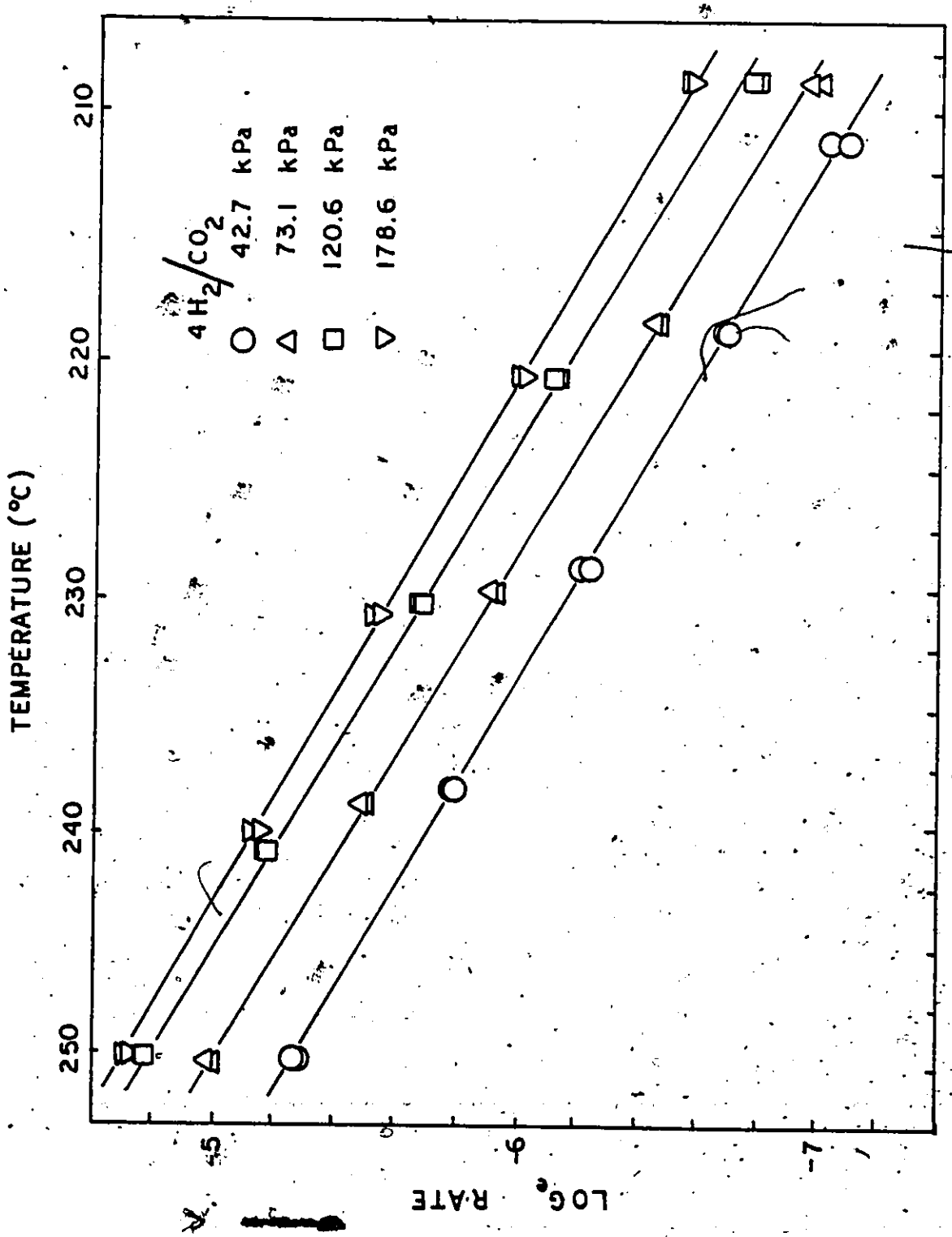

Figure 5-3 Arrhenius Plot for CO_2 Methanation

Raney nickel catalyst, Shultz et al. (49) of the Bureau of Mines found a large value of 125 - 134 kJ/mol, while Okamoto et al. (164) reported a value only half as large (54 kJ/mol).

Activation energies over other catalysts have also been documented, and they generally were smaller. Dwyer and Somorjai (108) reported a value of 71 kJ/mol over iron catalyst, while over rhodium catalyst, both Solymosi et al. (107) and Sexton and Somorjai (84) reported a value of 70 kJ/mol. Over ruthenium, Gupta et al. (106) found that the activation energy value was in the range of 59 - 71 kJ/mol. Table 5-1 compares the activation energy for methanation of CO_2 as reported by various authors.

Figure 5-3 also shows that the activation energy does not depend on the total pressure of the system within the range of 42.7 - 179 kPa. This independence suggests that there is no basic change in mechanism within the pressure range investigated.

Regardless of the exact value of activation energy for CO_2 methanation in comparison with other reported values, the activation energy is generally 40 kJ/mol smaller than that for CO methanation, suggesting two mechanistic interpretations. Different rate determining steps may be involved for the two carbon oxides. On the other hand, the same rate determining step may hold in both methanation reactions, but they react with different rates as a result of the very

Table 5-1

Activation Energies for CO_2 Methanation

E_{act} (kJ/mol)	Reference
105	This Study
125-134	(49)
54	(164)
88.2	(103)
80	(197)
54.4	(46)
105.8	(52)
85.7	(5)

different catalyst surface environments.

The activities of the catalyst in terms of TON are listed in Table 5-2. The data in the Arrhenius plot was based on a catalyst which had been on stream for some time and there was undoubtedly deactivation. Therefore, the TON reported in Table 5-2 were based on two fresh catalyst samples at 484 and 504 K. The TON at other temperatures were obtained by extrapolation using a value of 105 kJ/mol for the activation energy. The condition chosen was H_2/CO_2 ratio of 4 at a total pressure of 138 kPa. The data from Weatherbee et al. (197) were used for comparison. These data were corrected for pressure effect using a total pressure dependency of 0.4 as found previously in the present study.

Table 5-2 shows that Raney nickel is more active than supported nickel catalyst in CO_2 methanation. The low specific activity of supported nickel catalyst could be attributed to the significant amount of CO produced. 9 - 15% of CO was observed in the product gases for the Ni/SiO_2 catalyst employed by Weatherbee et al., which is very high compared with the maximum of 0.08% observed in the present study using Raney nickel. Since CO was found to inhibit methanation, the lower rate observed for supported nickel catalyst was reasonable. Raney nickel is a more active methanation catalyst than supported nickel catalysts for CO methanation. This high activity obviously also holds for the methanation of CO_2.

Table 5-3 shows a comparison of the methanation rate over

Table 5-2

Specific Activity of Nickel Catalyst for CO_2 Methanation[a]

Temperature (K)	TON x 1000 (This Study)	TON x 1000 (Ni/SiO_2)
525	64.1[b]	7.0[c]
513	36.6[b]	
504	24.1	3.3[c]
495	15.0[b]	
484	7.0	

a) $H_2/CO_2 = 4$ at a total pressure of 138 kPa

b) Extrapolated by using $E_{act} = 105$ kJ/mol

c) Corrected to condition (a) by expression $r = k P_t^{0.4}$

TON = molecules of methane produced per metal site per second

Table 5-3

Comparison of Specific Rate for CO and CO_2 Methanation over Raney Nickel

Temperature (K)	TON x 1000 $3H_2/CO$[a]	TON x 1000 $4H_2/CO_2$[b]
525	24.8[c]	64.1[d]
513	11.3	36.6[d]
504	4.5	24.1
495	2.8	15.0[d]
484	1.2	7.0

a) Total pressure = 121 kPa

b) Total pressure = 138 kPa

c) Extrapolated by using E_{act} = 146 kJ/mol

d) Extrapolated by using E_{act} = 105 kJ/mol

TON = molecules of methane produced per metal site per second

Raney nickel for both CO and CO_2. It is obvious that at the same temperature, CO_2 methanation proceeded at a higher rate than CO, in agreement with observations reported in the literature. Table 5-3 is probably the first comparison of methanation rates over Raney nickel for both carbon oxides. Weatherbee et al. (197) reported that the specific rate was higher for CO_2 at temperatures less than 550 K. However, at temperatures above 550 K the specific rate for CO methanation was higher than for CO_2 methanation because of the higher activation energy for CO methanation. The present result agrees with their finding in that at temperatures less than 550 K, the specific rate is higher for CO_2 methanation.

5.3.2 Effects of Reactants and Products

To obtain the kinetics of the reaction in more details, additional experiments were performed at different temperatures. In these runs, the individual effects of H_2 and CO_2 were studied by carefully maintaining one reactant at a constant partial pressure. Data for four different temperatures were obtained. The data sets at 513 and 523 K were obtained before the mass flowmeter was available. Because of the difficulties in keeping the individual reactant partial pressures constant, the data show some scattering. In addition, due to the large activities at higher temperatures, the catalysts used were deactivated by accidental temperature runaways. The prolonged use of the catalysts also resulted

in aging of the catalyst. Hence, the rates as turnover numbers were lower than those at 484 K and 504 K for which two separate catalyst samples were used and the individual feed concentrations could be kept constant relatively easily by using the now available mass flowmeter.

In these experimental runs, the hydrocarbon product consisted of only methane; no higher hydrocarbons were observed. This contrasts the results of Weatherbee et al. (197) who found small amounts of C_2^+ hydrocarbons over a Ni/SiO_2 catalyst. In most cases, no CO could be detected. However, for conditions where the H_2/CO_2 ratio was kept low, trace amounts of CO could be detected. The exact value of this ratio below which CO could be detected was difficult to estimate accurately due to the small amount of CO involved. However, CO appeared at H_2/CO_2 ratios between 1 and 3 depending on the temperature used. Nevertheless, the amount of CO detected in the effluent seldom exceeded 0.08%. This concentration was much less than the value expected from the reverse water-gas shift if equilibrium were attained. It has been reported that CO_2 methanation occurs at a lower temperature than the shift reaction (101). Weatherbee et al. (197) found that at high feed rates and low conversions, substantial yields of CO were observed, and they suggested that the production of CO is governed by equilibrium phenomenon. However, in their study, much higher conversions were allowed compared with the present study, and the H_2/CO_2 ratio

was kept constant at 4. The finding in the present study suggests that H_2/CO_2 ratio is important in governing the formation of CO. The formation of CO at relatively low H_2/CO_2 ratio indicates that CO may be an intermediate in the reaction. CO as an intermediate in CO_2 methanation has been suggested by Falconer and Zagli (104,105).

The effect of H_2 on methanation rate is shown in Figures 5-4 to 5-9. At constant CO_2 partial pressures, H_2 increased the rate at low concentrations. However, the rate reached a maximum and remained constant with further increases in H_2 partial pressure. The minimum partial pressure of H_2 at which this maximum rate was reached increased with CO_2 concentration. At high partial pressures of CO_2 (69 and 138 kPa) the rate increases with H_2 almost coincided as shown in Figures 5-4 and 5-7. To ascertain if the rate would decrease at sufficiently high H_2/CO_2 ratio, the partial pressure of CO_2 was maintained at 9 kPa and that of H_2 increased to 180 kPa (Figure 5-5). Even when the H_2/CO_2 ratio reached a value of 20, there was no observable drop in rate.

It is to be noted that for CO_2 concentration in the range of 13.4 to 28 kPa, the maximum rate was reached when the H_2 concentration reached 80 - 100 kPa for all four temperature sets. It is suspected that similar maximum in rate can be obtained for other higher CO_2 partial pressure runs when the H_2 partial pressure is raised sufficently high.

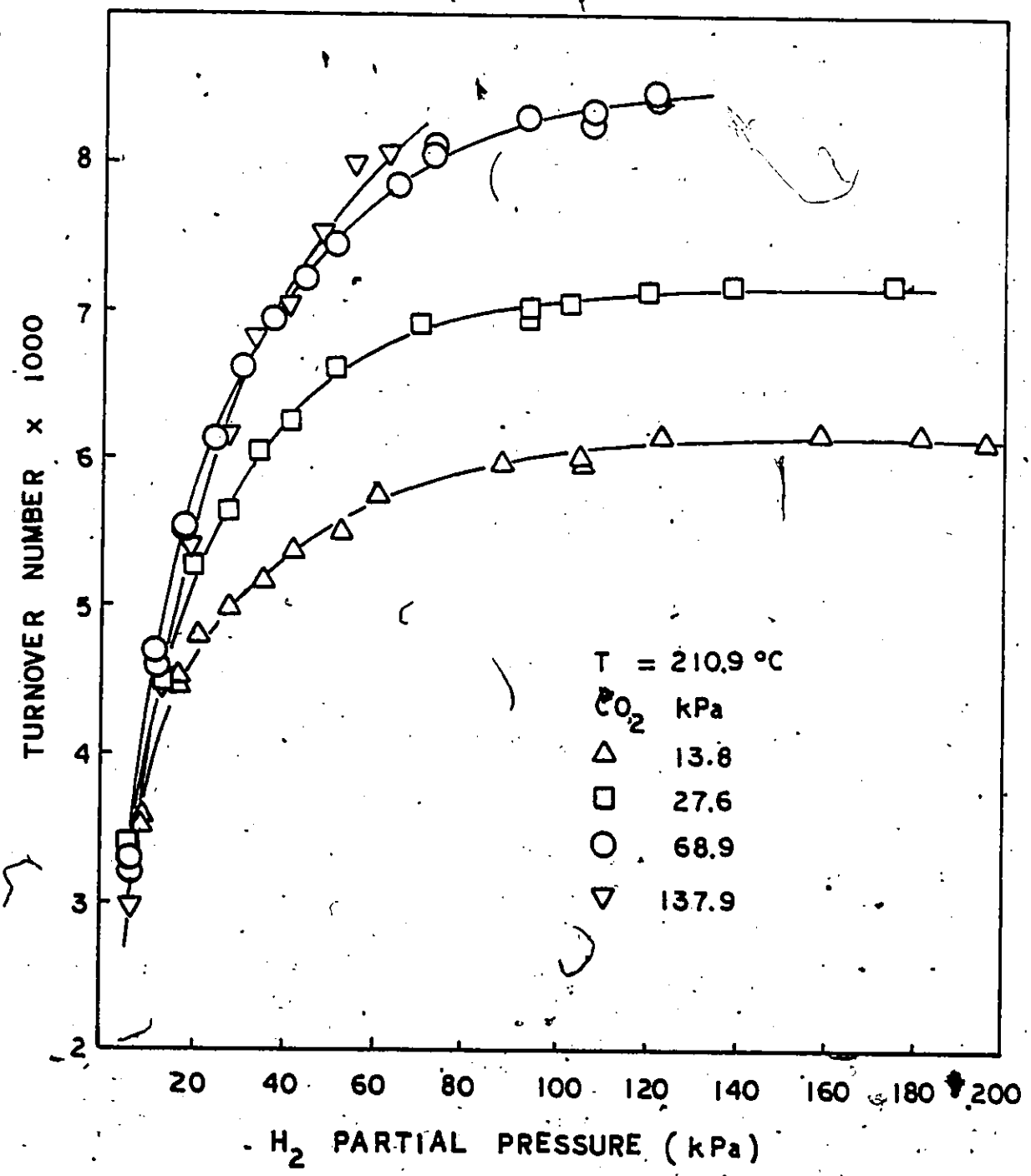

Figure 5-4 Effect of Hydrogen on CO_2 Methanation Rate at 484 K

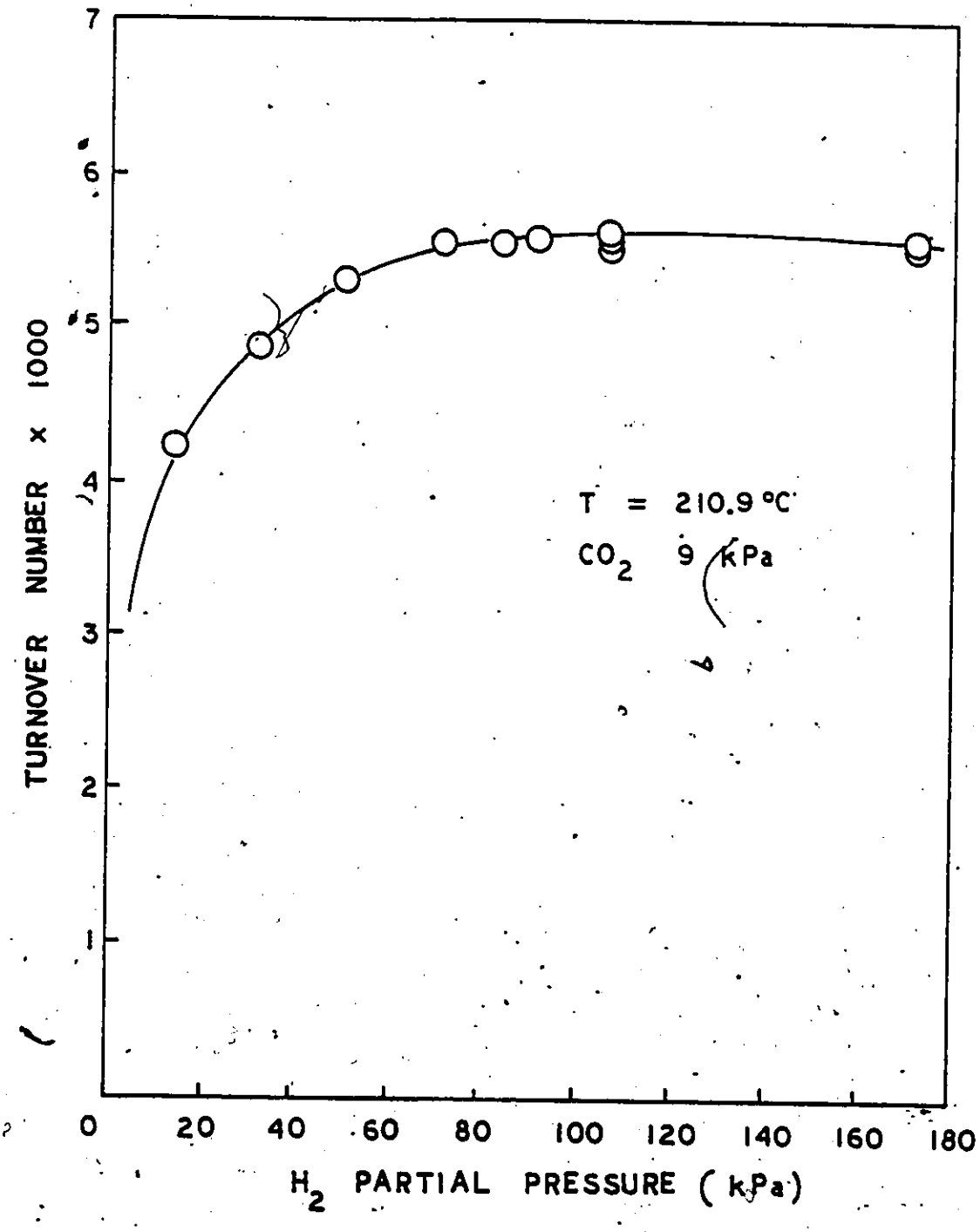

Figure 5-5 Effect of Hydrogen on CO_2 Methanation Rate at 484 K

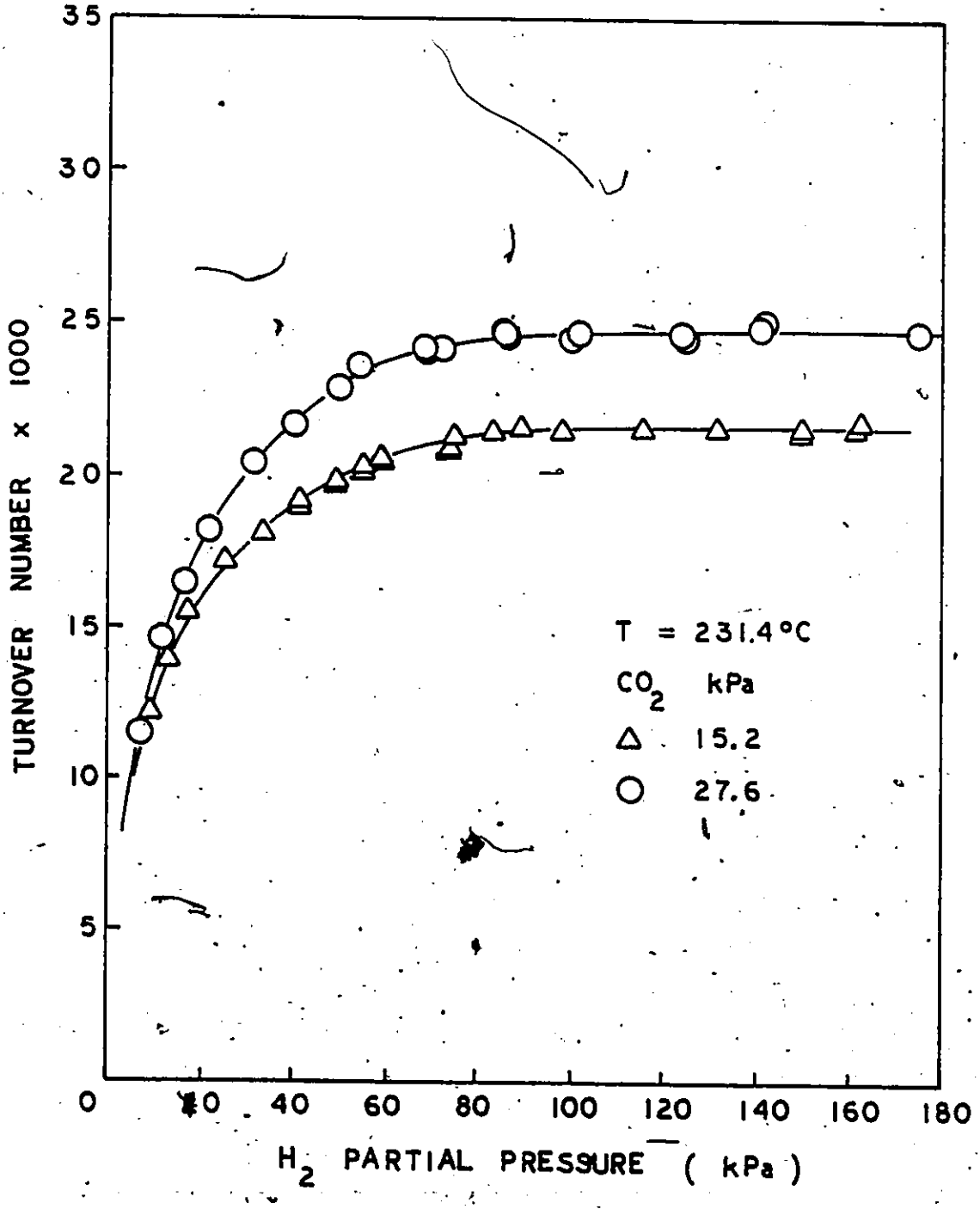

Figure 5-6 Effect of Hydrogen on CO_2 Methanation Rate at 504 K

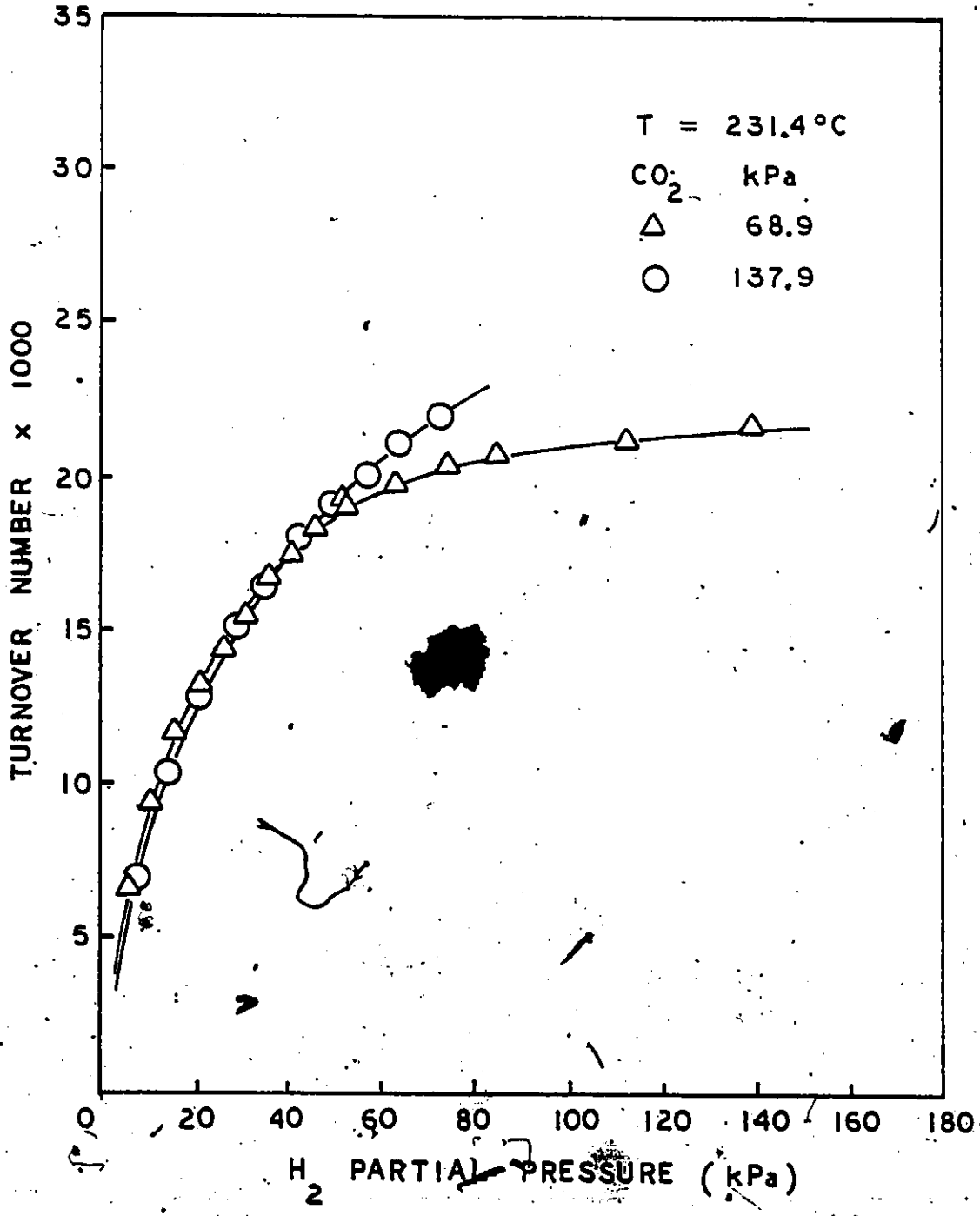

Figure 5-7 Effect of Hydrogen on CO_2 Methanation Rate at 504 K

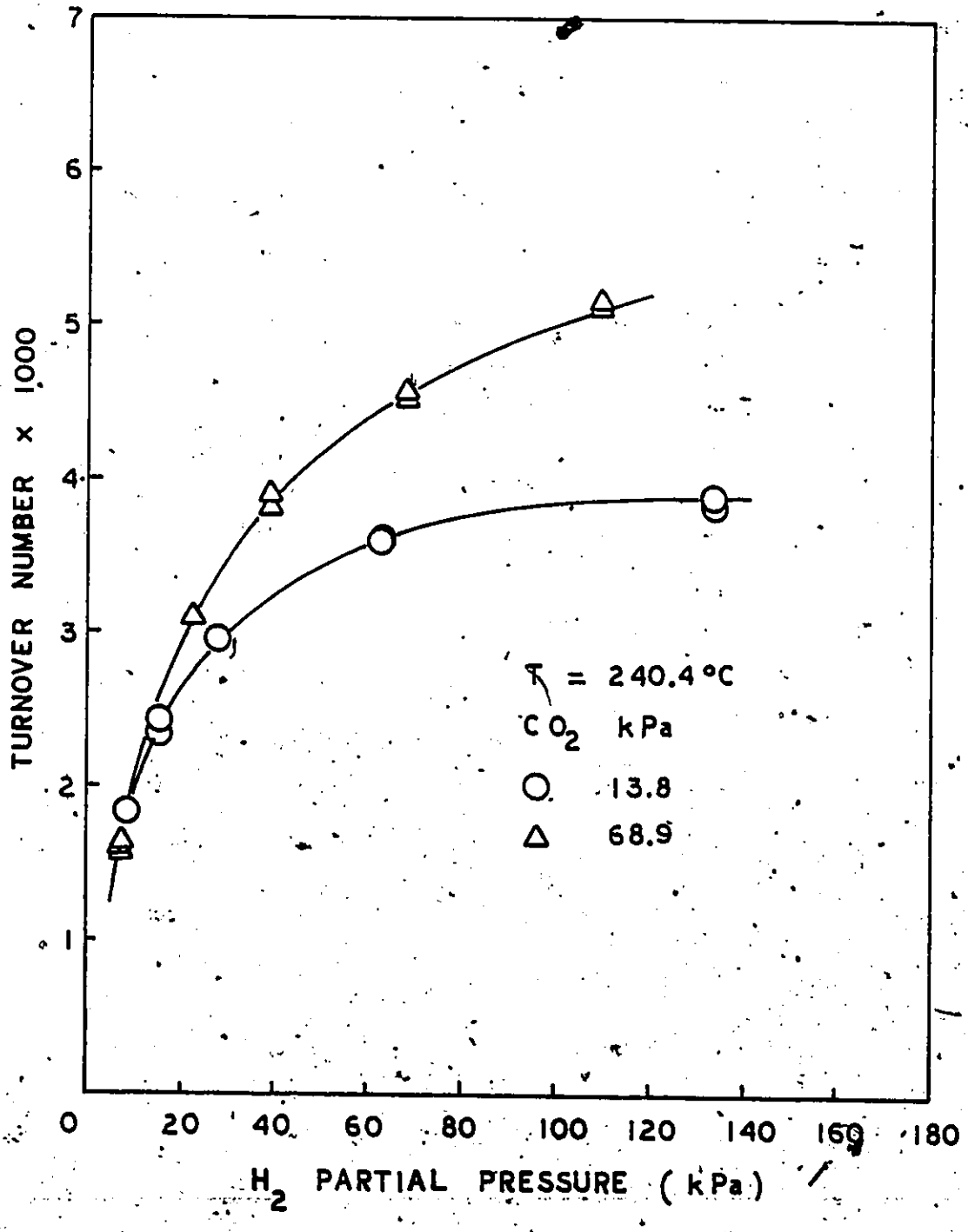

Figure 5-8 Effect of Hydrogen on CO_2 Methanation Rate at 513 K

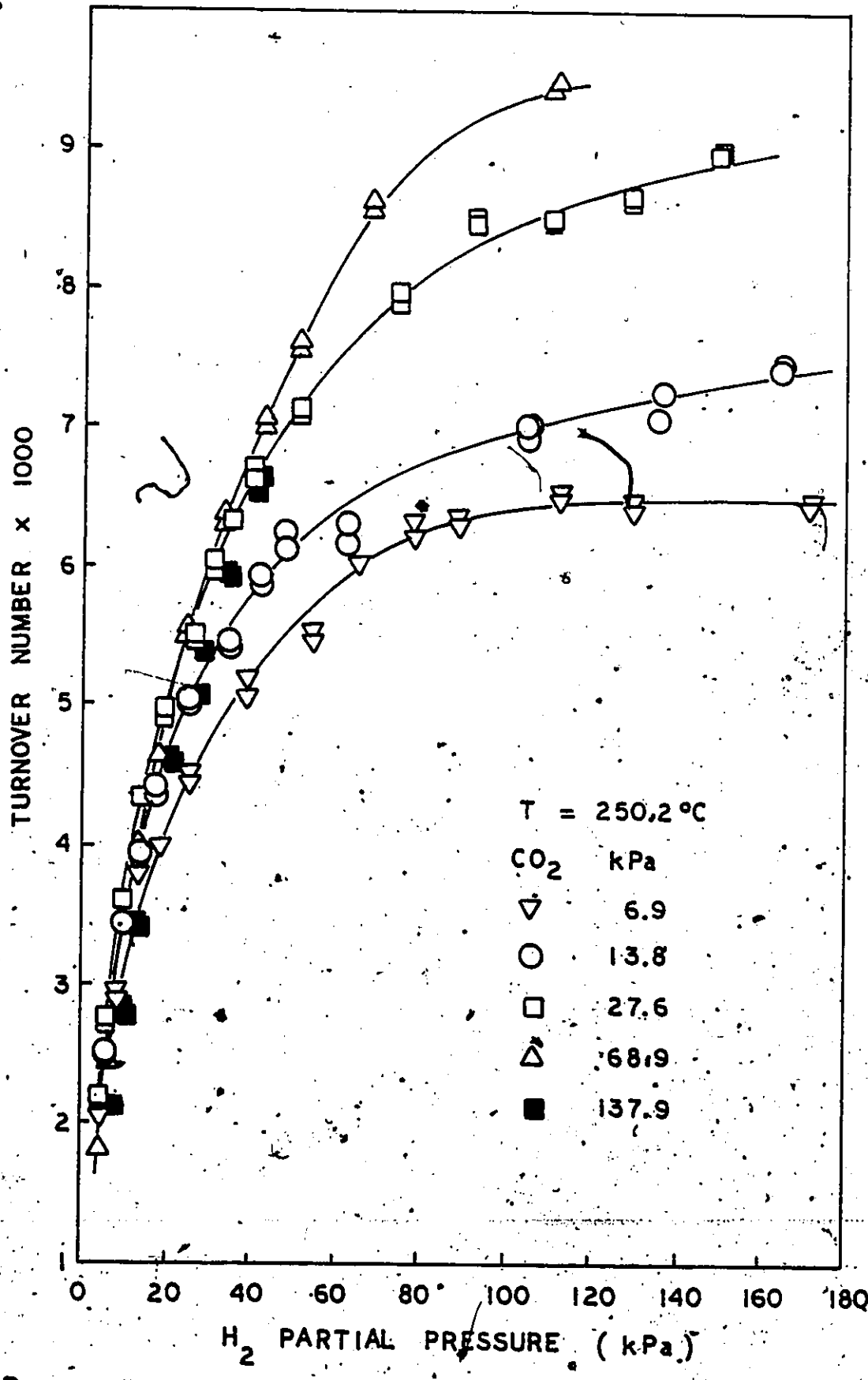

Figure 5-9 Effect of Hydrogen on CO_2 Methanation Rate at 523 K

The effect of CO_2 on the rate is show in figures 5-10 to 5-14. When the partial pressure of H_2 was kept constant, the rate increased with partial pressure of CO_2, especially when H_2 concentration was high. At higher CO_2 partial pressures, the rate reached a maximum and then decreased as CO_2 was further increased. The partial pressure of CO_2 corresponding to the maximum rate increased with the partial pressure of H_2, as shown in figures 5-10 and 5-14. For a given H_2 partial pressure, the CO_2 partial pressure for maximum rate decreased with temperature. For example, when H_2 partial pressure was kept at 14 kPa, the CO_2 partial pressure corresponding to maximum rate decreased from 70 kPa at 484 K to 30 kPa at 523 K.

The results from these experiments confirm that CO_2 methanation rate passes through a maximum as the CO_2 partial pressure is increased as noted in the preliminary study. This is the first reported observation of maximum in rate with increasing CO_2 concentration. Maatman et al. (103) has reported a maximum in rate by varying the H_2/CO_2 ratio at atmospheric pressure; this maximum occurred at a concentration of CO_2 of about 38%. However, since the rate must be zero at both 0 and 100% CO_2, this maximum in rate in the 38% CO_2 region is not surprising. By maintaining the partial pressure of H_2 constant while increasing CO_2 concentration, the present results show that the rate goes through a true maximum in rate, when the H_2/CO_2 ratio is

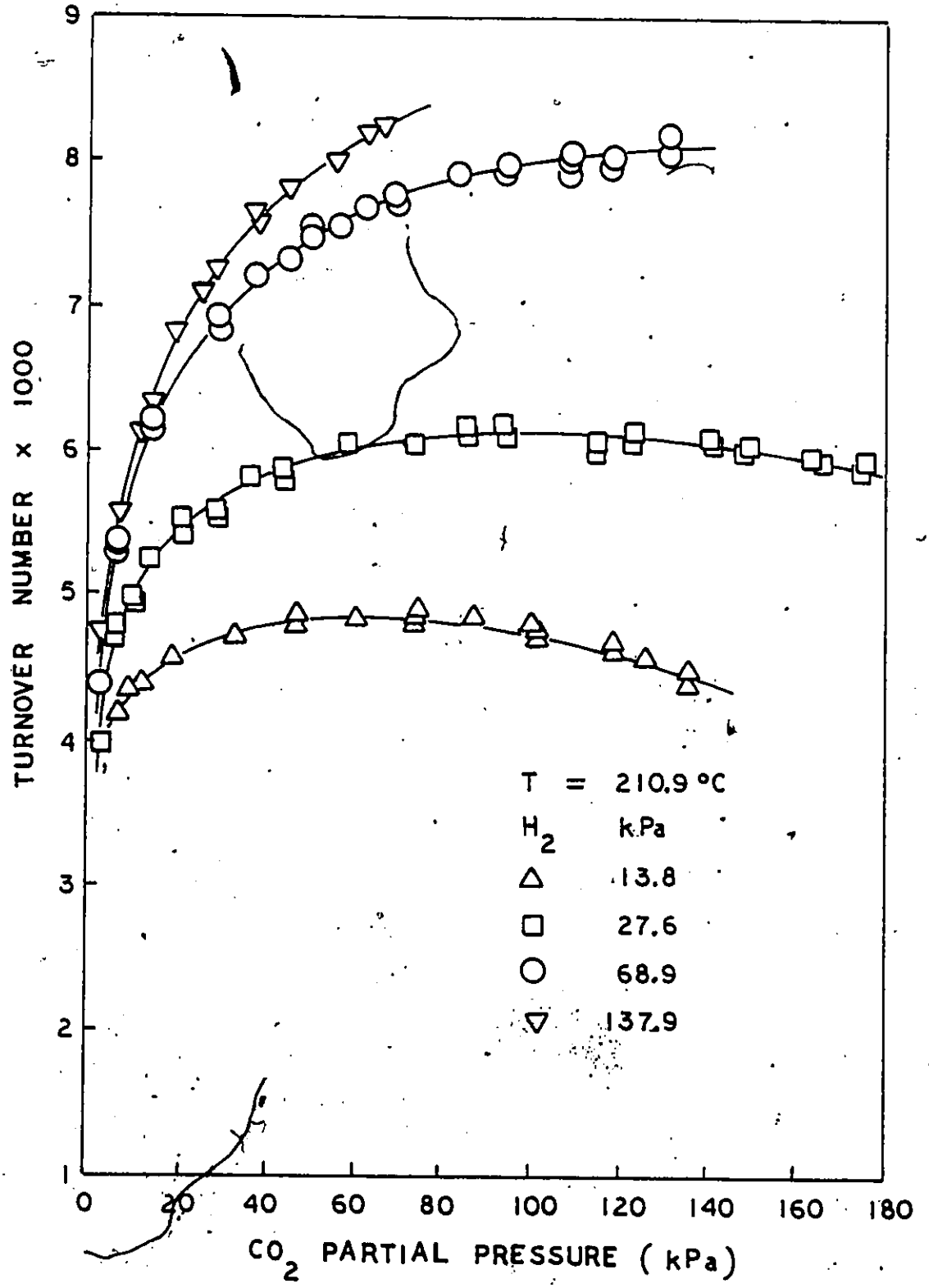

Figure 5-10 Effect of Carbon Dioxide on Methanation Rate at 484 K

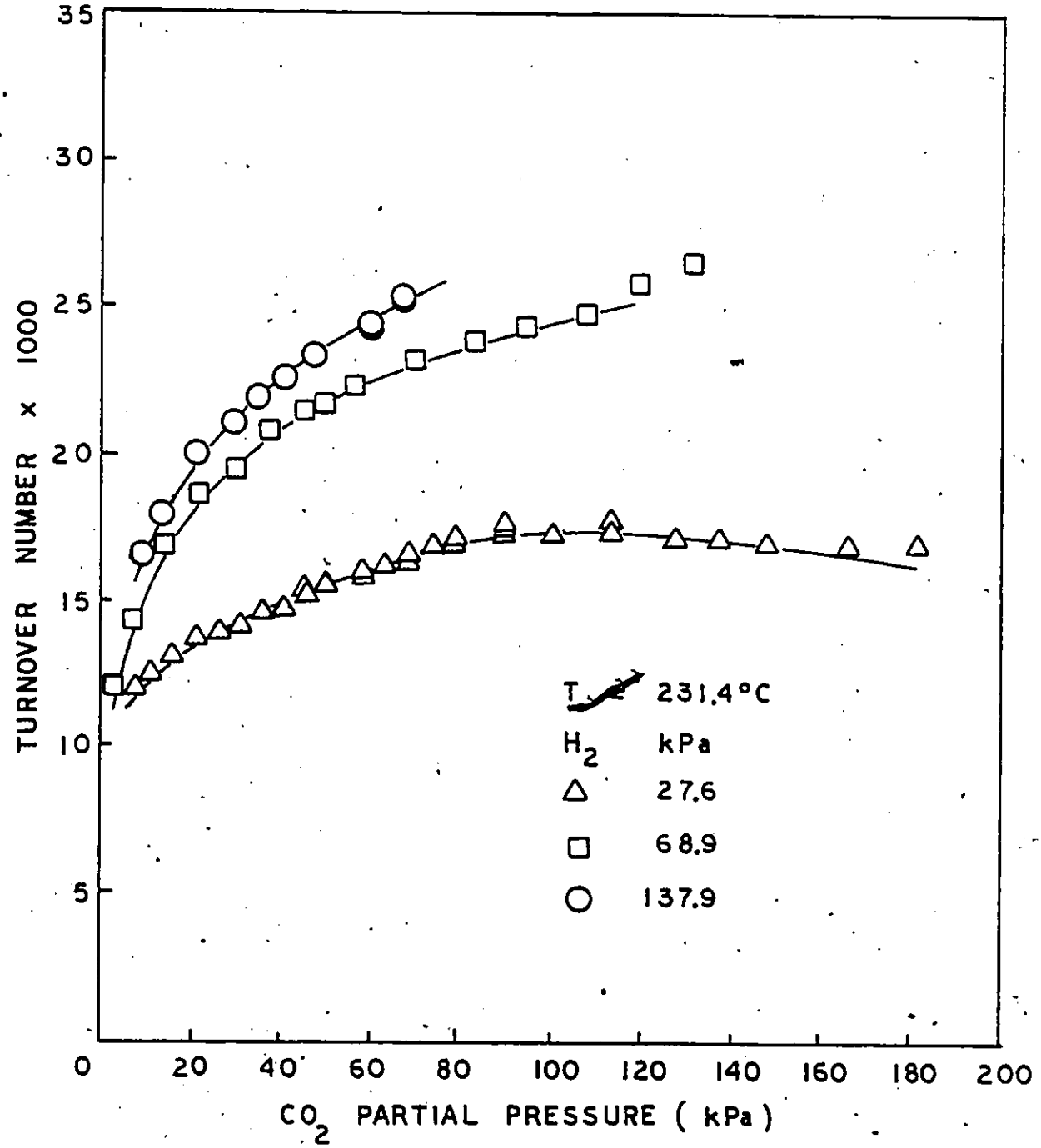

Figure 5-11 Effect of Carbon Dioxide on Methanation Rate at 504 K

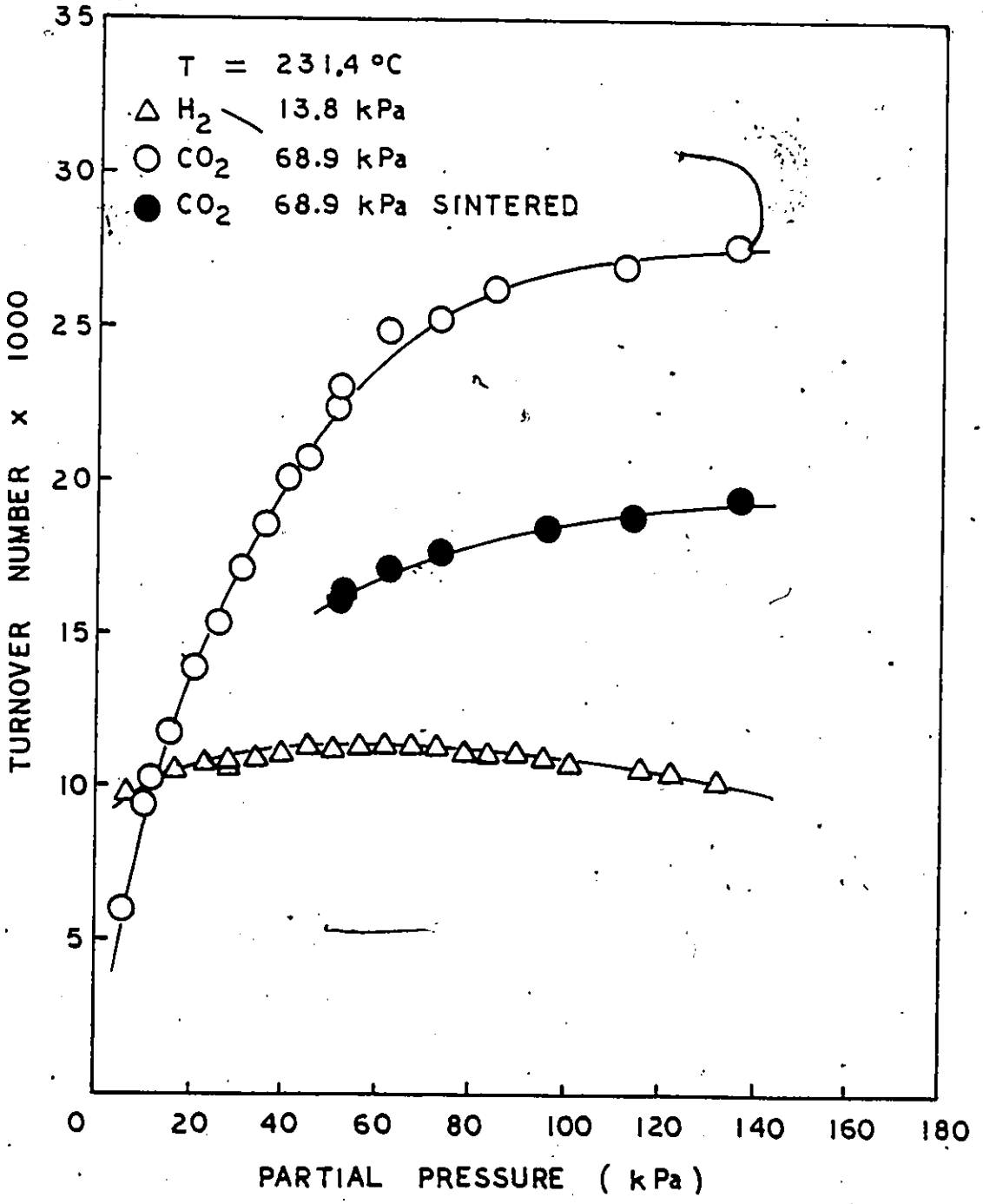

Figure 5-12 Effect of Carbon Dioxide and Hydrogen on Methanation Rate at 504 K

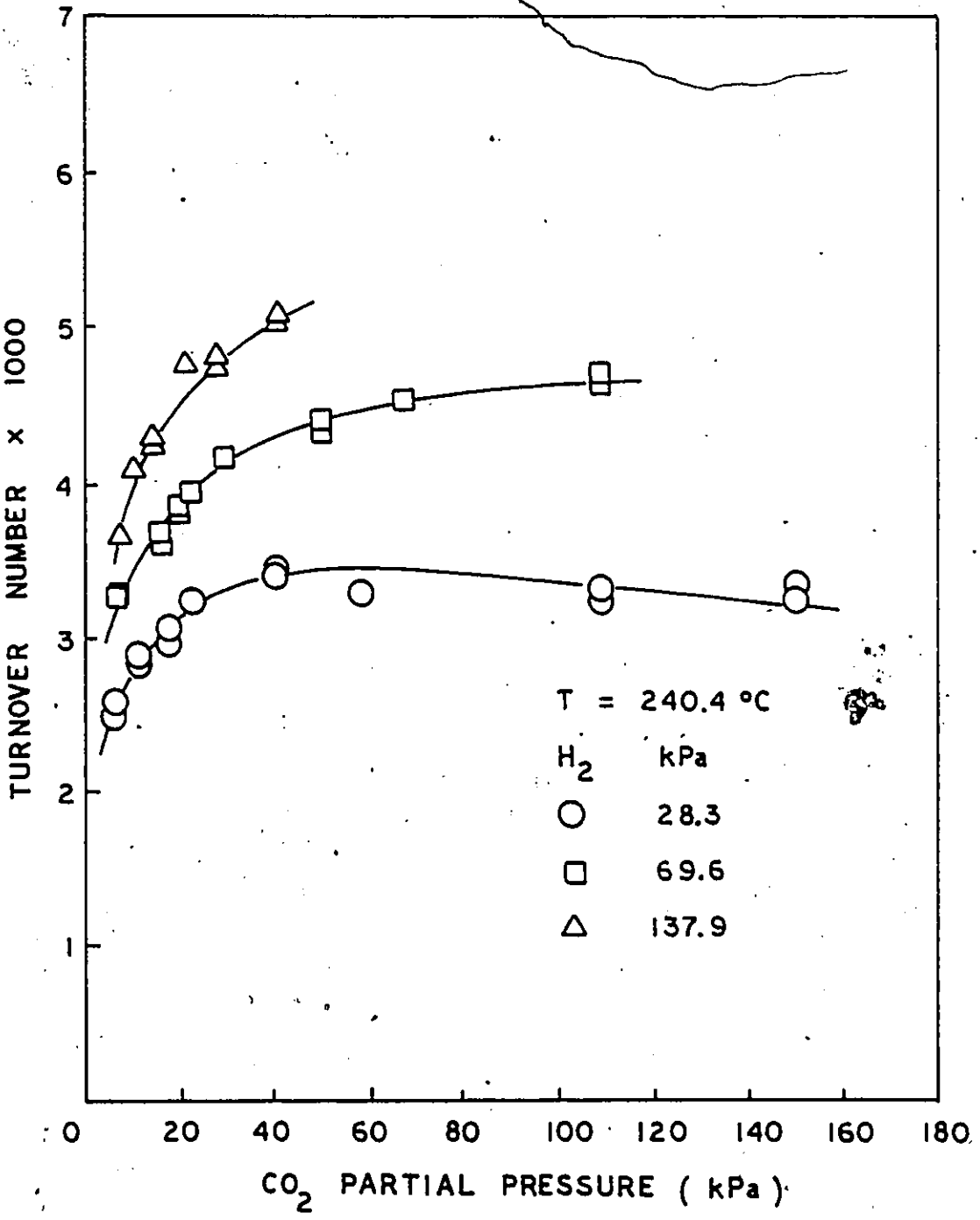

Figure 5-13 Effect of Carbon Dioxide on-Methanation Rate at 513 K

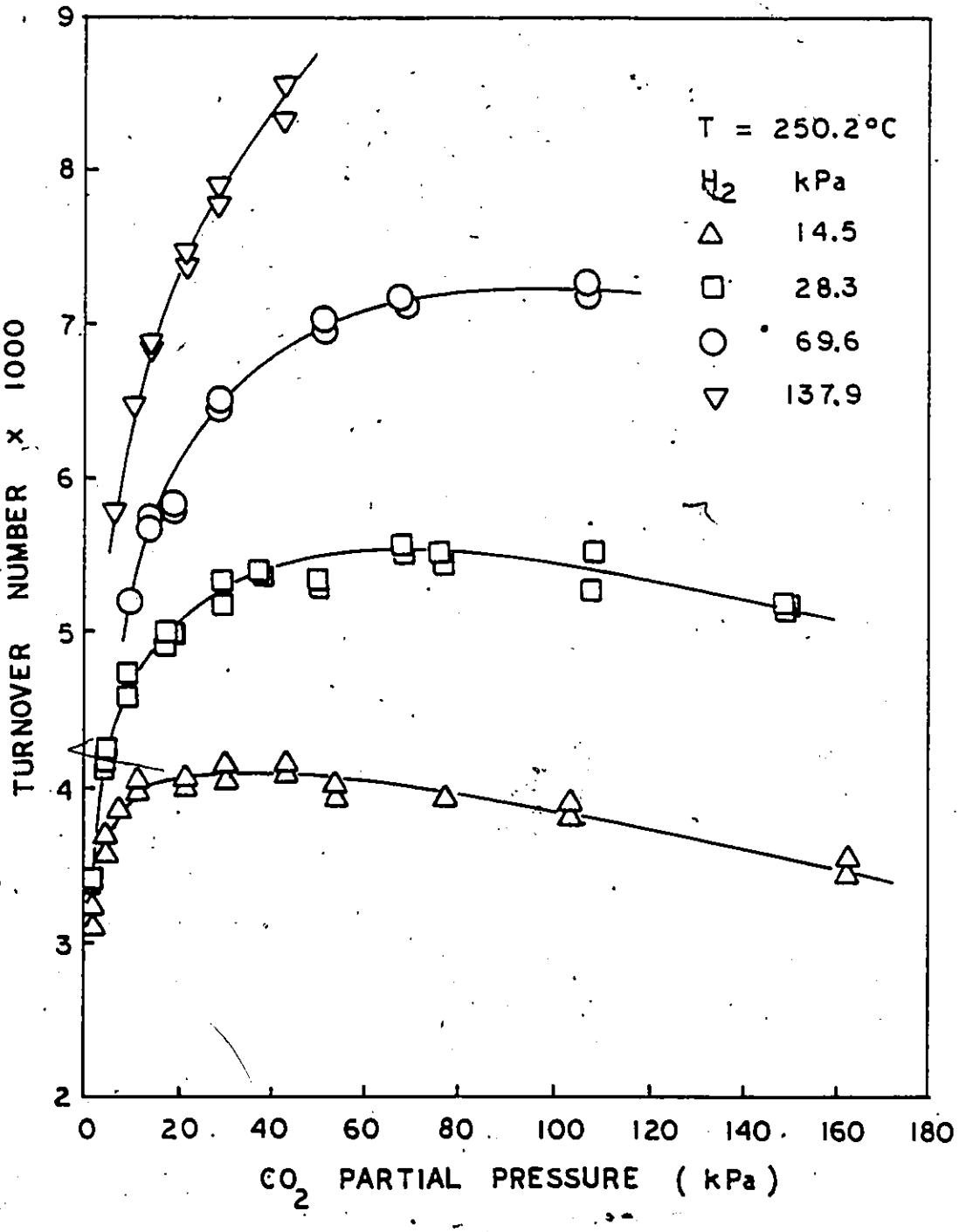

Figure 5-14 Effect of Carbon Dioxide on Methanation Rate at 523 K

greater than one, in qualitative agreement with Maatman's results.

The results also show that the rate increases with the partial pressure of H_2. However, it increases to a maximum value and remains invariant with further increases with H_2 partial pressure.

The results obtained above clearly demonstrate that the kinetics of CO_2 methanation needs a more complicated description than using order of reaction as expressed by the power-rate law equations, a significant finding in view of the common practice of reporting the kinetics by reaction order. The present work also indicates that these reported orders of reaction, e.g. ½ order for CO_2, first or zero order for H_2 etc., is at best representative of only part of the kinetic picture.

Despite the obvious inadequacy of the power-rate law, attempts were made to determine the ranges of operating parameters over which the simple equation was valid. For data in figure 5-15, except for high CO_2 concentrations, the power-rate law is adequate to represent the effect of CO_2 on the rate, especially when the H_2 partial pressure is kept high. The orders of reaction for CO_2 obtained in this manner are summarized in table 5-4 for various temperatures and partial pressures of H_2. The order is never close to the generally accepted ½ order, and does not vary much with temperature. However, the CO_2 order depends on the H_2 partial pressure,

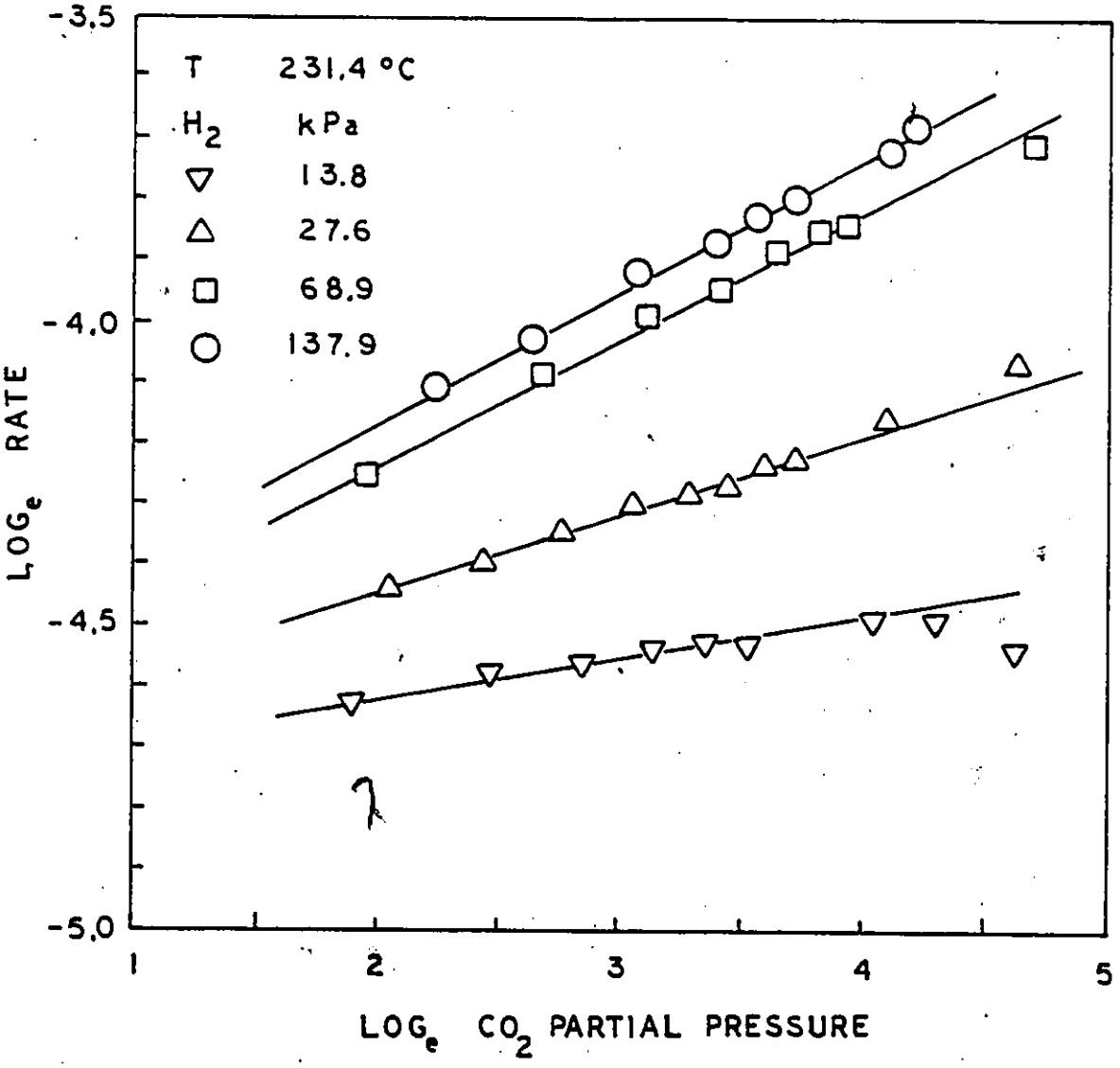

Figure 5-15 Power Rate Law Plot for the Effect of Carbon Dioxide

Table 5-4

CO_2 Order of Reaction in Methanation

H_2 Partial Pressure (kPa)	Temperature (K)			
	483	503	513	523
13.8	0.08	0.07	-	0.12
27.6	0.11	0.13	0.15	0.13
68.9	0.17	0.21	0.19	0.20
137.9	0.20	0.22	0.25	0.22

increasing from a value of about 0.1 to 0.22 as the partial pressure of H_2 increases from 13.8 to 138 kPa. The change of CO_2 order suggests that at high enough H_2 concentration or H_2/CO_2 ratio, CO_2 order may increase to 0.5 . However, this would require much higher H_2/CO_2 ratios than those used in the present study. High H_2/CO_2 ratios were used by Solc (5), Pour (7), and recently by Maatman et al. (103); all of them concluded that the order of reaction for CO_2 was 0.5. Solymosi et al. (107) studied CO_2 methanation over rhodium catalyst and arrived at an order of reaction of 0.26 for CO_2. The present finding of changing order of reaction with hydrogen concentration clearly shows that the effect of CO_2 on the kinetics cannot be represented by any fixed value for the order of the reaction.

The H_2 orders similarly obtained are shown in table 5-5. Usually only the first few data points at low partial pressure of H_2 can be represented by the power-rate law, especially when CO_2 partial pressure was kept at about 7-14 kPa, because the rate levels out at higher H_2 pressures (figure 5-16). Nevertheless, the order of reaction can be seen to depend on both temperature as well as the CO_2 partial pressure. The order increases with CO_2 partial pressure. At a given CO_2 concentration, the order decreases with decrease in reaction temperature. This contrasts the order of reaction for CO_2 which is independent of temperature. This change in H_2 order

Table 5-5

H_2 Order of Reaction in CO_2 Methantion

CO_2 Partial Pressure (kPa)	Temperature (K)			
	483	503	513	523
6.9	0.18	-	-	0.35
13.8	0.31	0.35	0.40	0.44
27.6	0.39	0.44	-	0.47
68.9	0.48	0.53	0.50	0.66
137.9	0.50	0.58	-	0.75

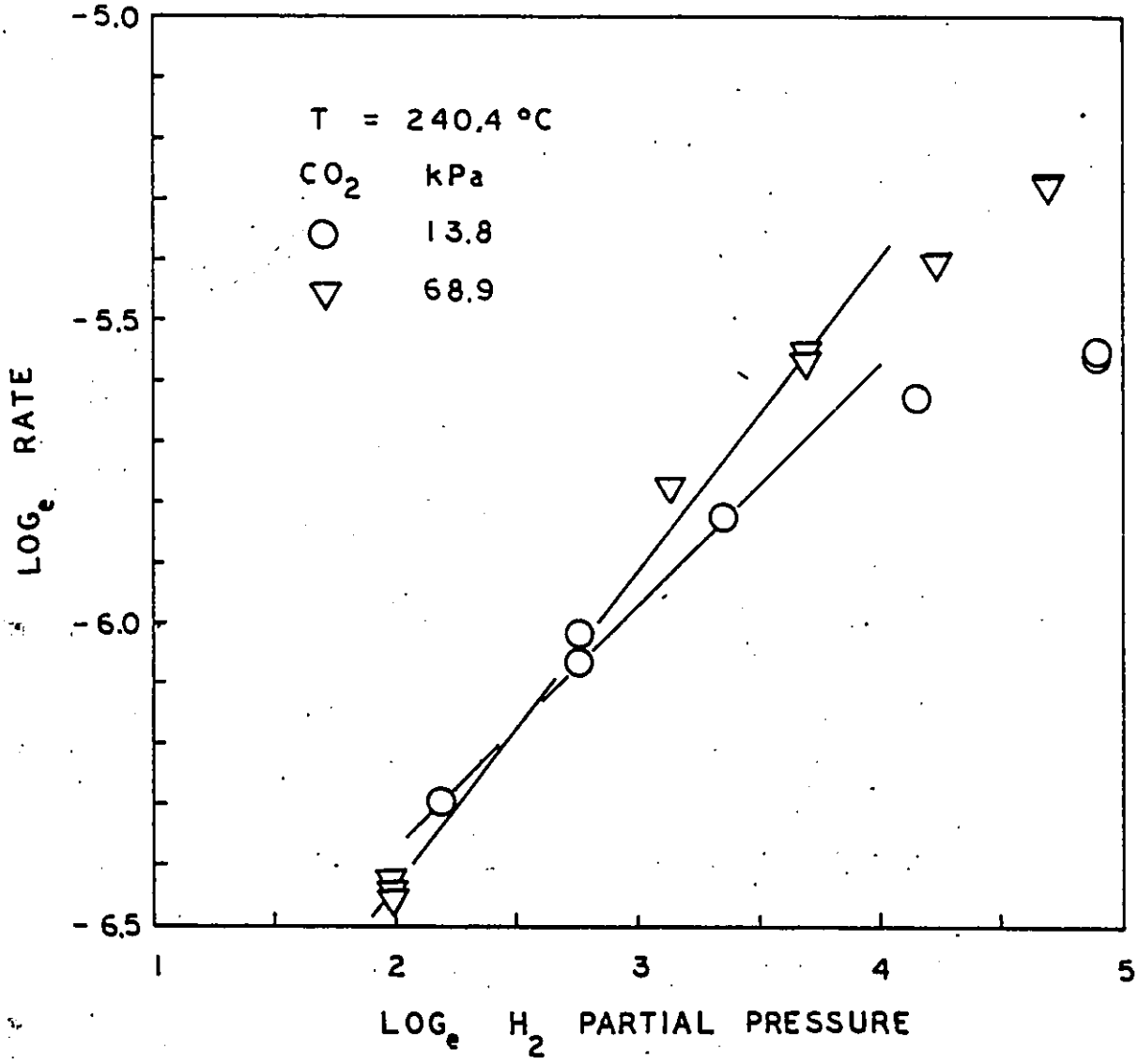

Figure 5-16 Power Rate Law Plot for the Effect of Hydrogen

may be a result of decrease in H_2 chemisorption at higher temperatures.

The effect of water vapour on CO_2 methanation rate was also investigated. As in the case of CO methanation, a known amount of water was introduced into the reactor using a $H_2/CO_2 = 4$ feed gas. The partial pressure of the feed gas was kept constant by appropriately raising the total reactor pressure. The results are shown in figure 5-17 for two temperatures and two pressures. Water had an inhibiting effect on the reaction rate. Its effect was reversible at low concentrations; and could be quantified by a power-rate law expression. The order of reaction depended on the reaction conditions. The inhibiting effect of water increased with temperature; with the feed gas at 120 kPa, the order changed from -0.06 at 483 K to -0.11 at 493 K. When the temperature was kept constant, its effect was independent of total pressure, the order being -0.11 at both pressures of 63 and 120 kPa. Additional data on the effect of water were obtained and fitted to a power-rate law. The result is shown in figure 5-18 which shows that the effect of water on methanation can be adequately represented by a power-rate law.

The effect of methane was investigated at two temperatures by introducing methane into the feed. As in the case of CO methanation, the rate was calculated from change in the H_2/CO_2 ratio as compared to the ratio in the

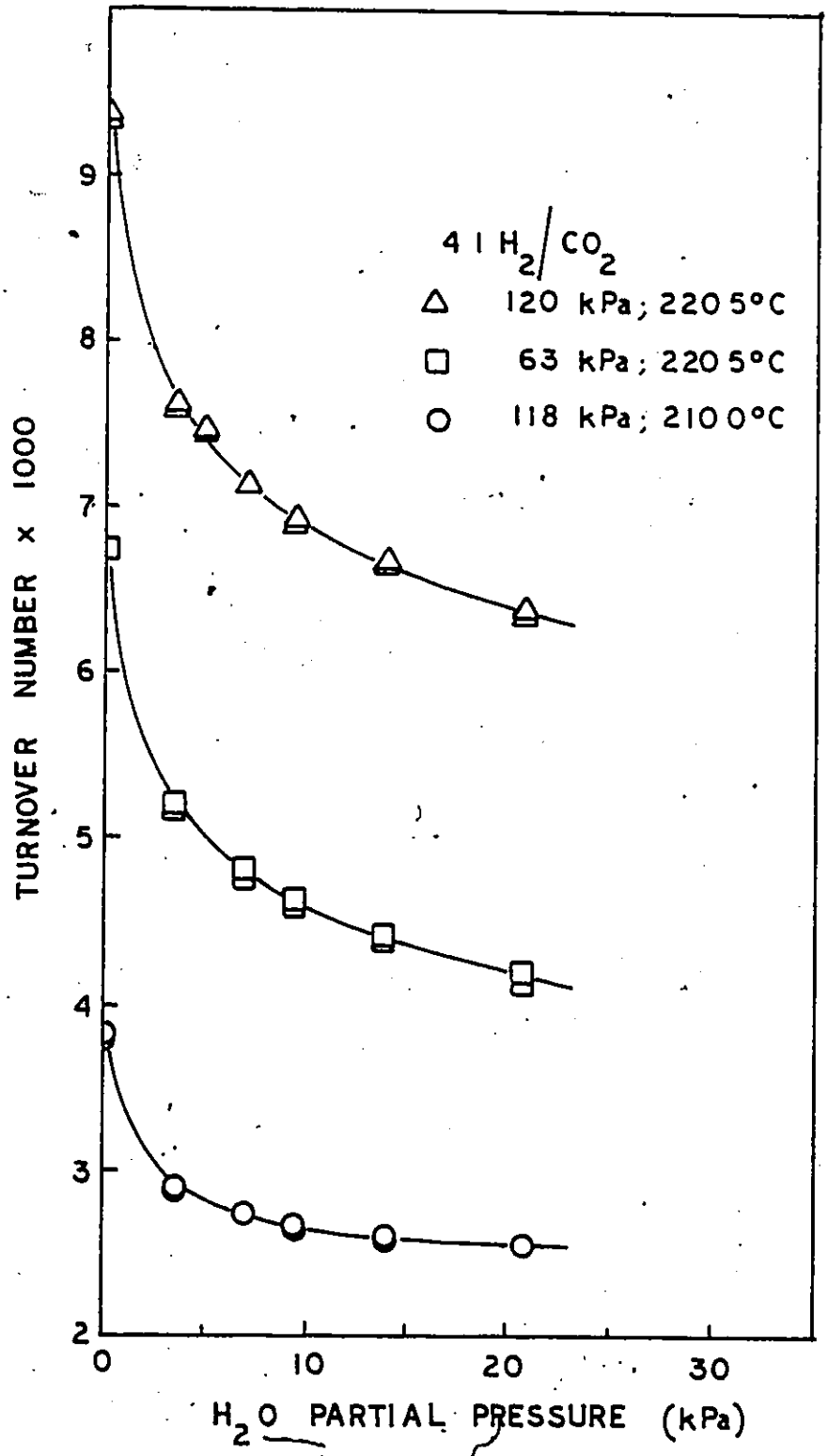

Figure 5-17 Effect of Water on CO_2 Methanation Rate

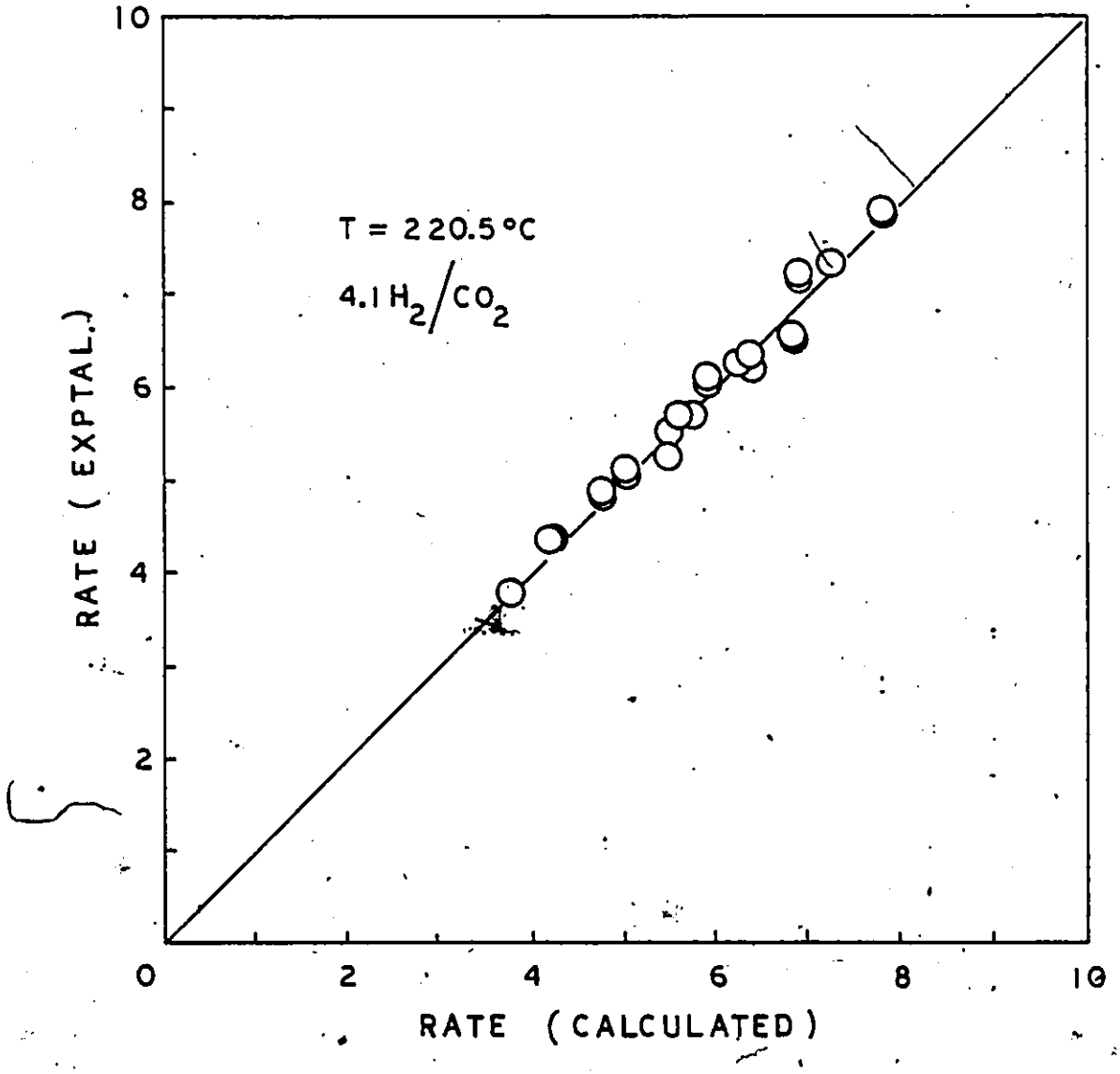

Figure 5-18 Comparison of Experimental and Calculated Rate of CO_2 Methanation - Effect of Water

controlled runs in which methane was replaced by inert helium gas. Methane was found to have no significant effect on the reaction rate, similar to CO methanation (Figure 5-19). That methane has no effect is not surporising in view of its weak adsorption on nickel surface (72). In addition, steam reforming of methane is thermodynamically unfavorable at the low concentration of water and the low temperature employed. The present finding agrees with the results reported by Herwijnen et al. (52).

The effect of CO on CO_2 methanation was studied by introducing CO in various amounts into the reactor while the partial pressures of H_2 and CO_2 were kept constant. Two cases are shown in Figure 5-20 for two total pressures at 523 K. In low concentrations, CO increased the methanation rate. However, at higher concentrations of CO, the rate decreased for the two pressures of H_2 and CO_2. The partial pressure of CO for which the rate was the same as the case with no CO present increased with the total H_2+CO_2 pressure. That the methanation rate is increased in the presence of small amounts of CO is important from a mechanistic viewpoint. Undoubtedly, most of the methane comes from the CO in view of the stronger chemisorption of CO compared to CO_2. Since CO and CO_2 can both dissociate on nickel the result suggests that the concentration of carbon species is increased by the presence of CO with the concomitant increase in reaction rate. However, as the CO concentration increases, the rate decreases as a result of CO inhibition of H_2 chemisorption.

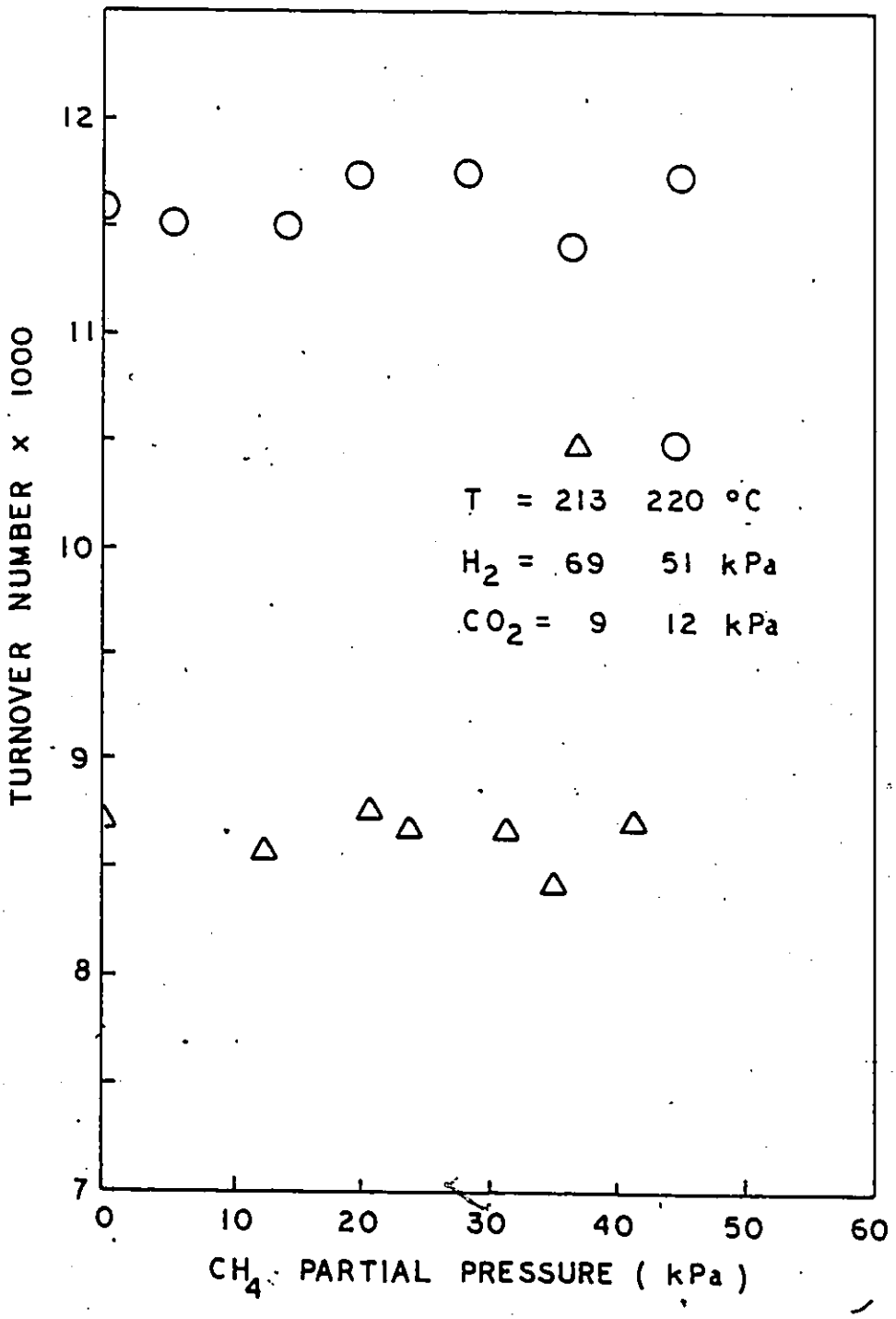

Figure 5-19 Effect of Methane on CO_2 Methanation Rate

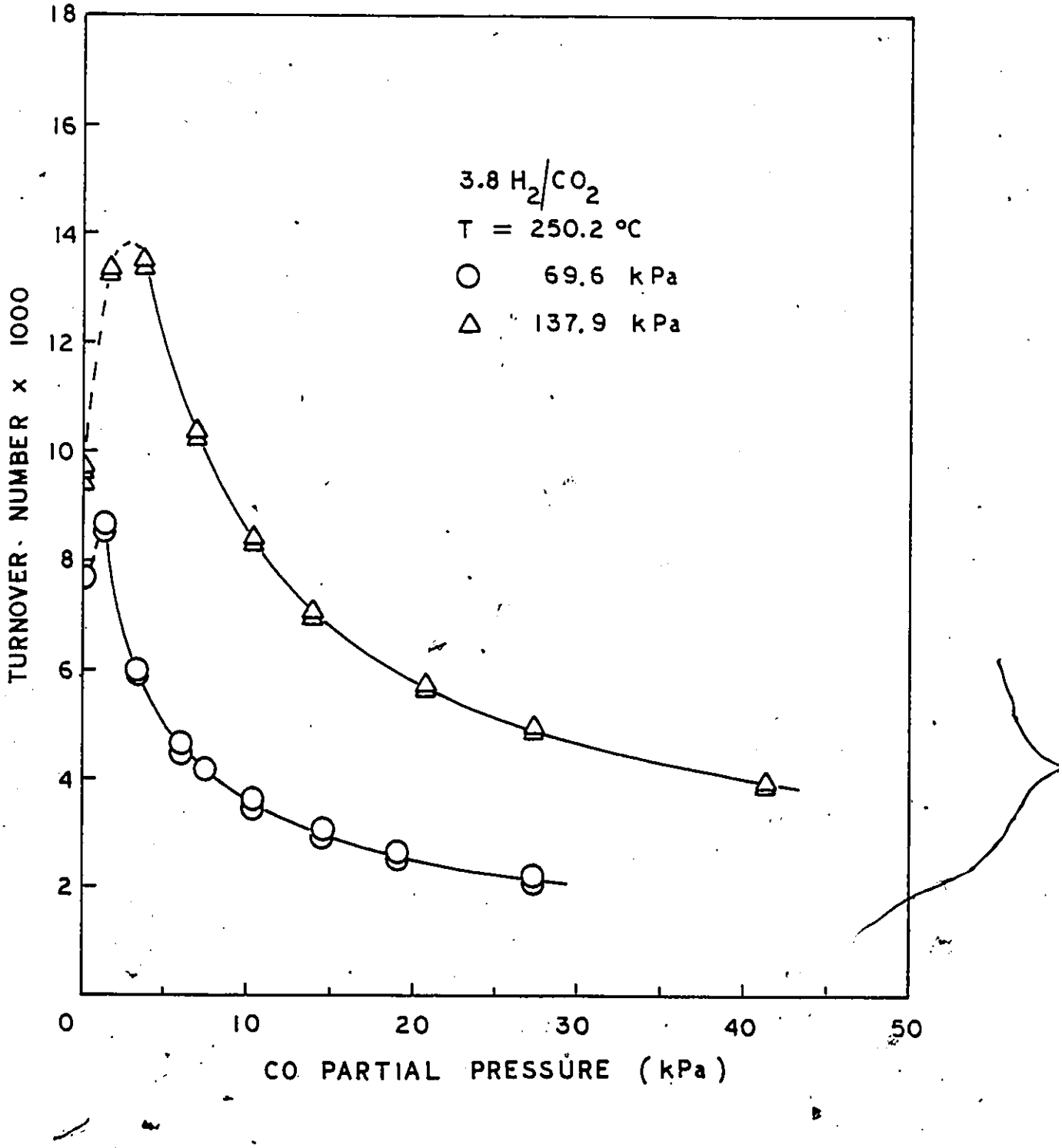

Figure 5-20 Effect of Carbon Monoxide on CO_2 Methanation Rate

5.4 Reduction of Carbonaceous Residues

It has been reported that CO_2 can dissociate into carbon and oxygen species on nickel surface (73). The possible presence of carbonaceous species on the catalyst surface was investigated by hydrogenating the catalyst after a steady-state methanation run. The procedure employed has been detailed in section 4.4 .

The total amount of carbonaceous species removed from the catalyst as methane by hydrogen flushing are shown in figures 5-21 to 5-24. This amount, expressed in terms of moles of carbon, depended on the reaction conditions under which it was deposited. As in CO methanation, at constant partial pressures of H_2 and CO_2, the amount of carbon species increased with the reaction temperature. At a constant temperature, the carbon residue increased with the partial pressure of CO_2 but decreased with the partial pressure of H_2 and increasing H_2/CO_2 ratios. When water vapour was introduced in the steady-state methanation run, the amount of methane produced during hydrogen flushing was so small that the methane peak could not be integrated. Water obviously suppressed the deposition of surface carbon.

Thus, the amount of surface carbon deposited during CO_2 methanation was affected in the same way by the various steady-state conditions as the CO methanation. Despite these qualitative similarities, the amount of surface carbon was

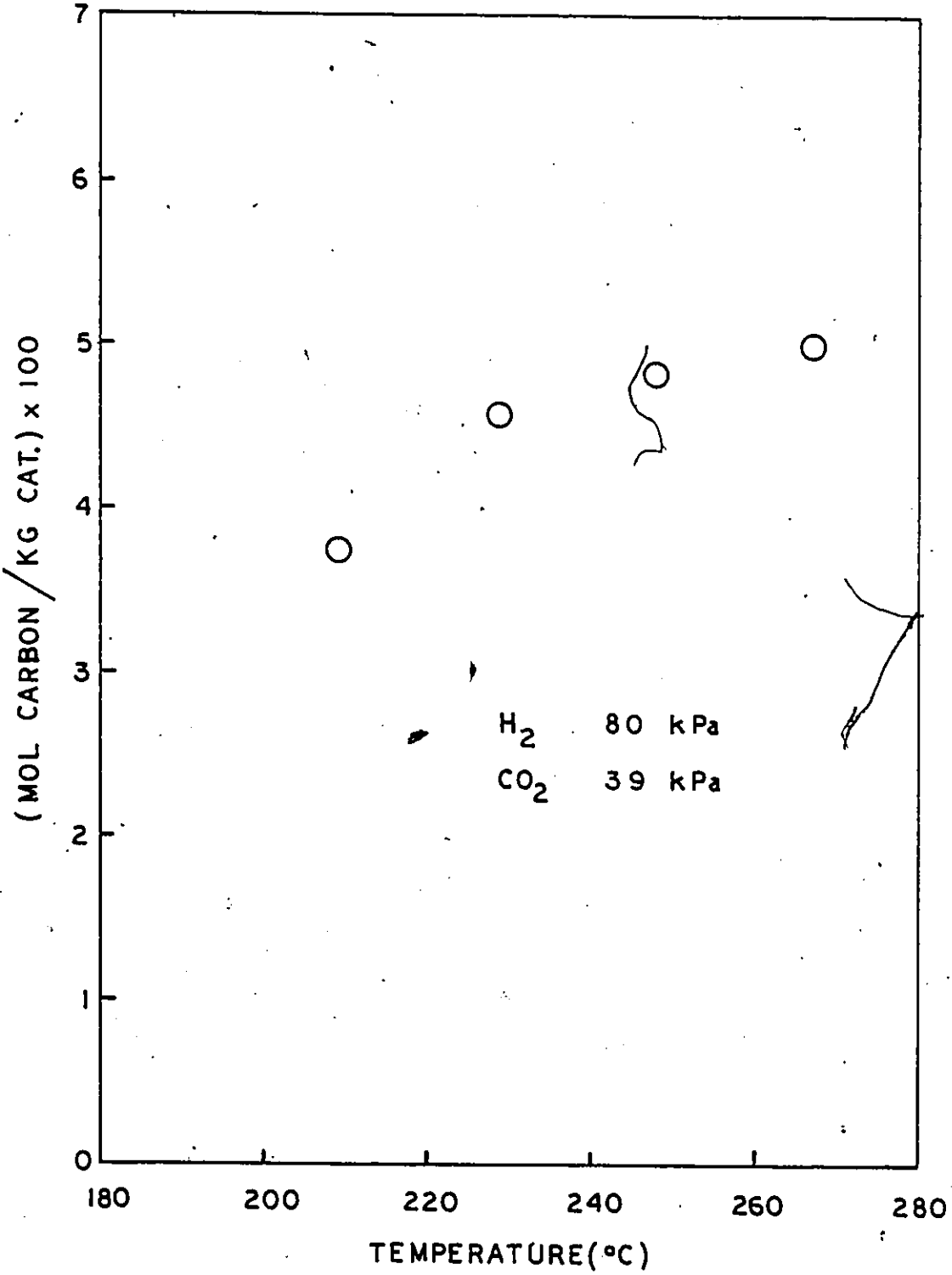

Figure 5-21 Effect of Temperature on the Amount of Residual Carbon

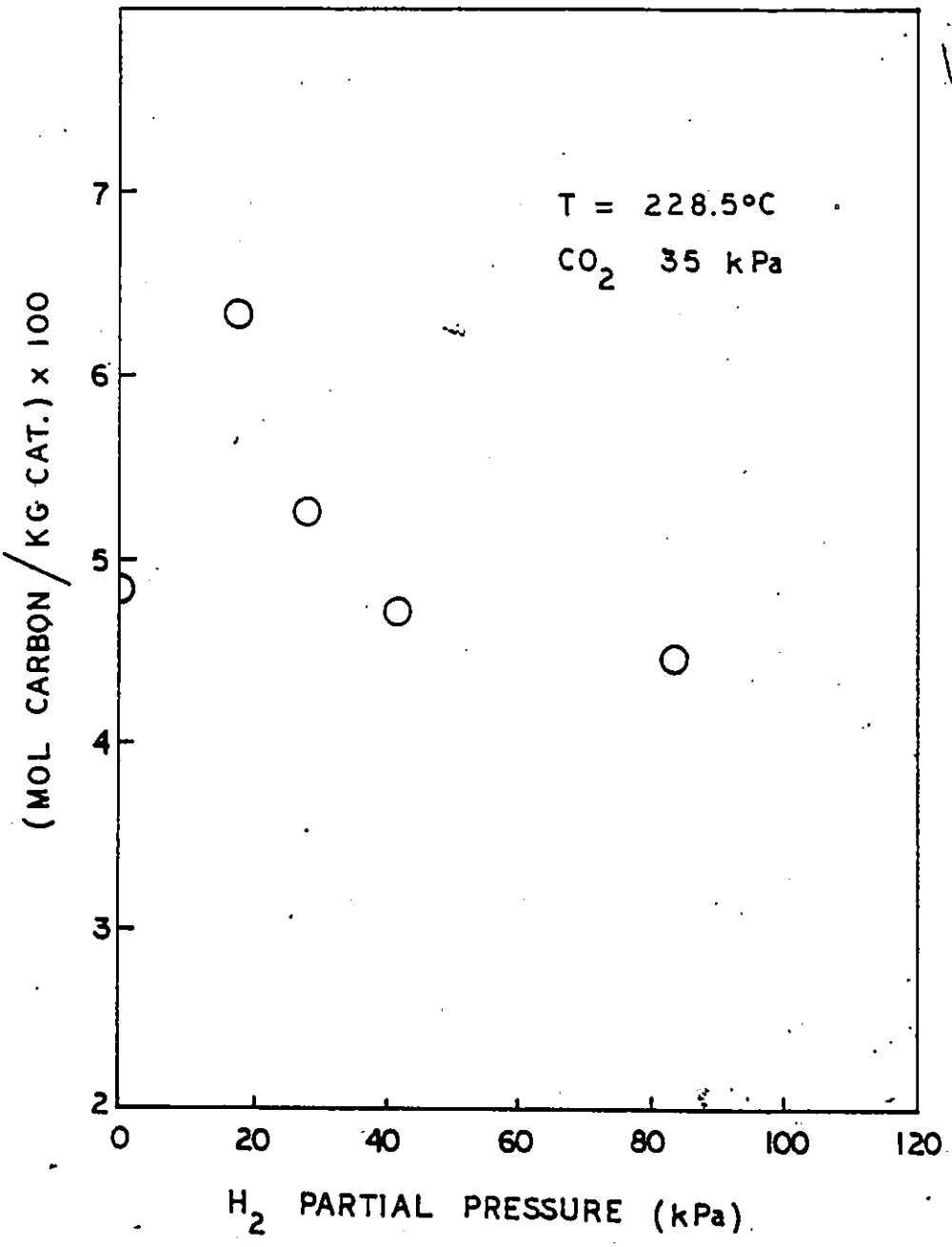

Figure 5-22 Effect of Hydrogen on the Amount of Residual Carbon

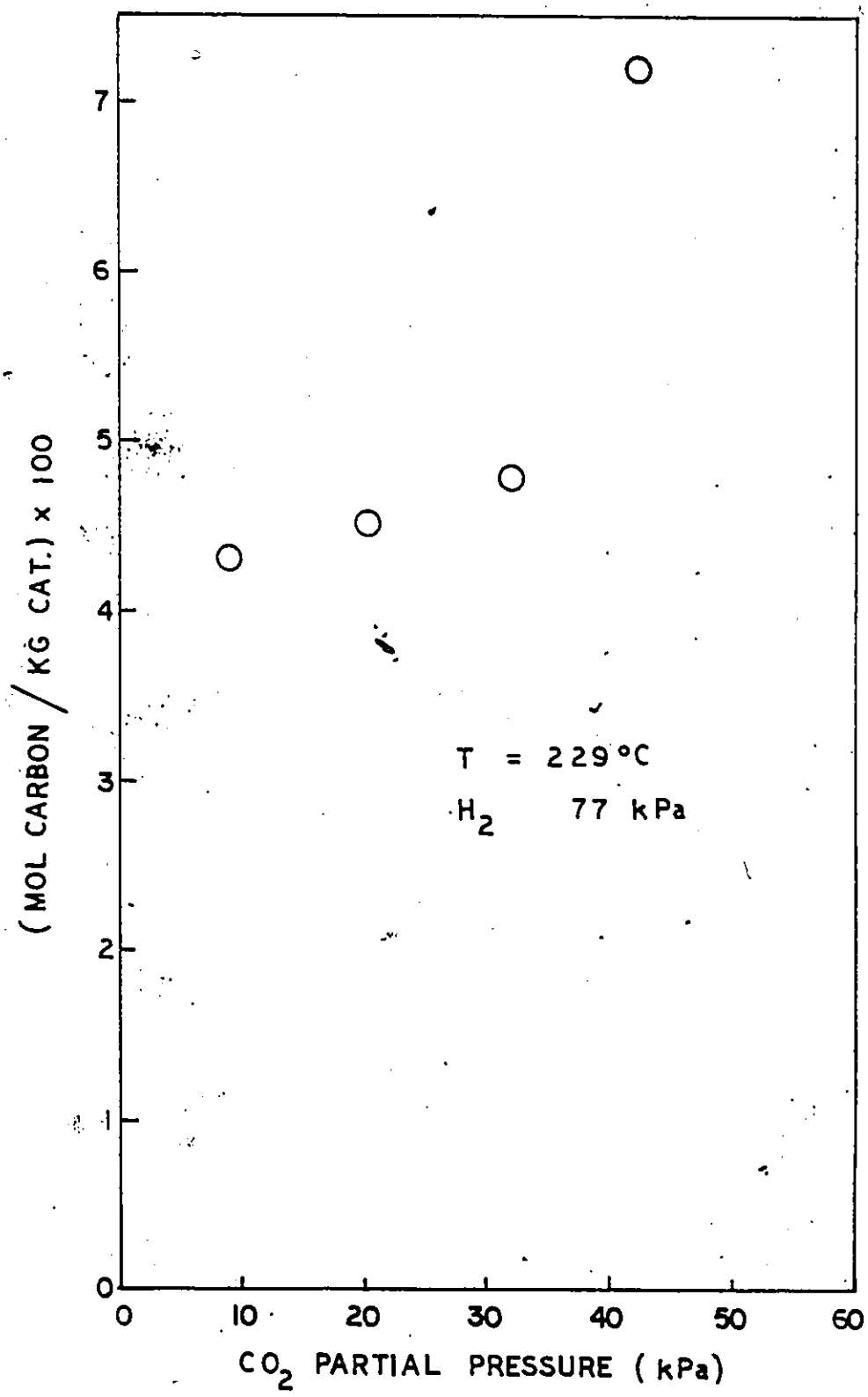

Figure 5-23 Effect of Carbon Dioxide on the Amount of Residual Carbon

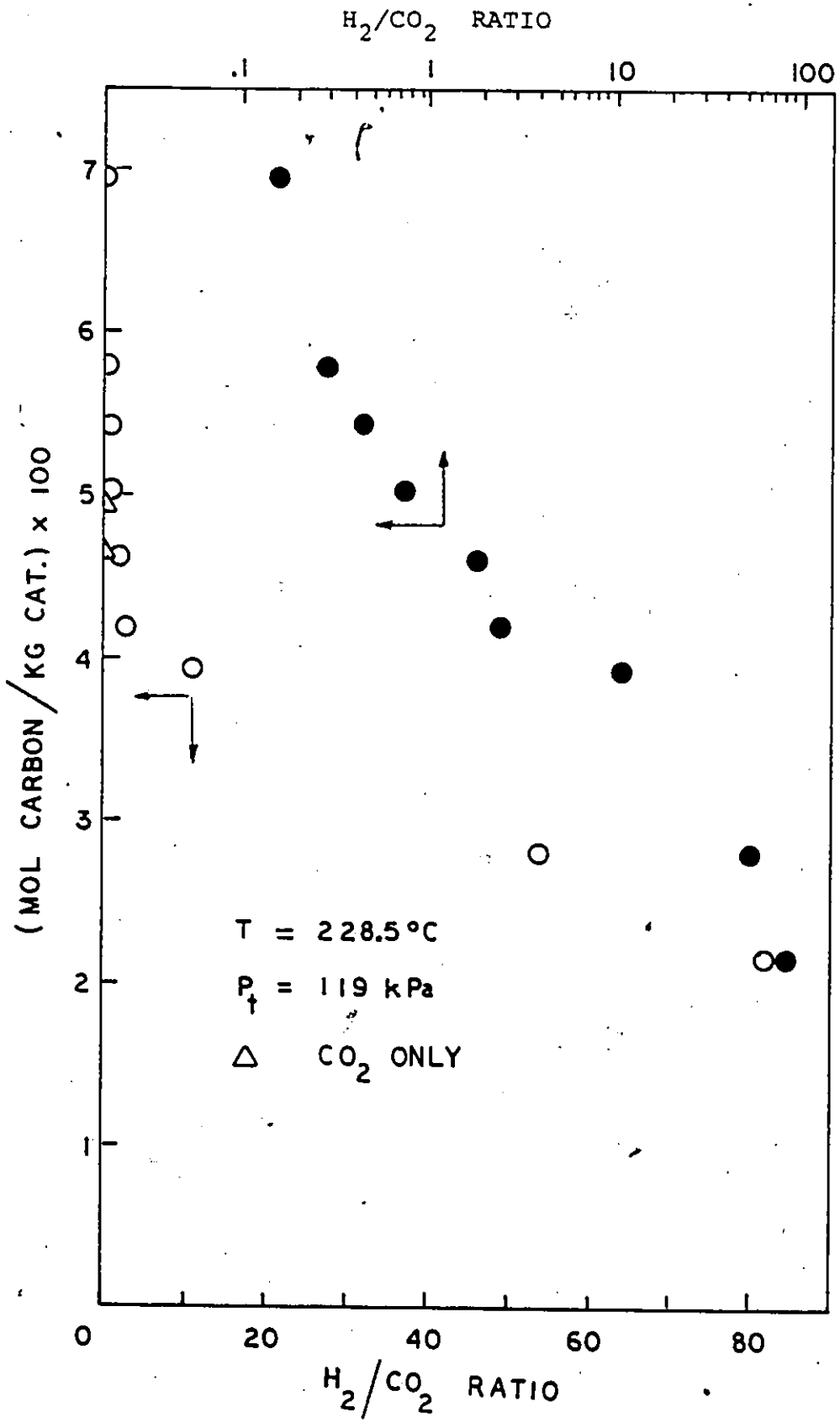

Figure 5-24 Effect of H_2/CO_2 Ratio on the Amount of Residual Carbon

consistently much lower for CO_2 methanation than for CO methanation, indicating that the catalyst in methanation of CO_2 was much 'cleaner'.

In quantitative terms, less than a monolayer of surface carbon was found on the catalyst after an hour of methanation. Under all the steady-state conditions investigated, the surface carbon concentration varied from 0.04 to 0.15 monolayer, in sharp contrast to CO hydrogenation where the surface carbon concentration was much larger, often exceeding a monolayer. Solymosi et al. (107) have made similar observations over rhodium catalyst. For CO_2 methanation a limiting carbon concentration of 0.31 monolayer was reported; carbon concentration was 3 to 5 times higher in CO hydrogenation.

The amount of carbon deposited on the catalyst surface in the absence of H_2 was also investigated as a function of CO_2 partial pressure. Figure 5-25 shows that the amount increases with the partial pressure of CO_2, but does not exceed a monolayer. The result supports the assertion that CO_2 dissociates on nickel surfaces leaving carbon and oxygen species on the surface. Hirato et al. (100) and Falconer et al. (105) have suggested that CO_2 may completely dissociate on nickel surfaces at high temperatures.

The carbon deposition rate was correlated with the steady-state methanation conditions by the equation:

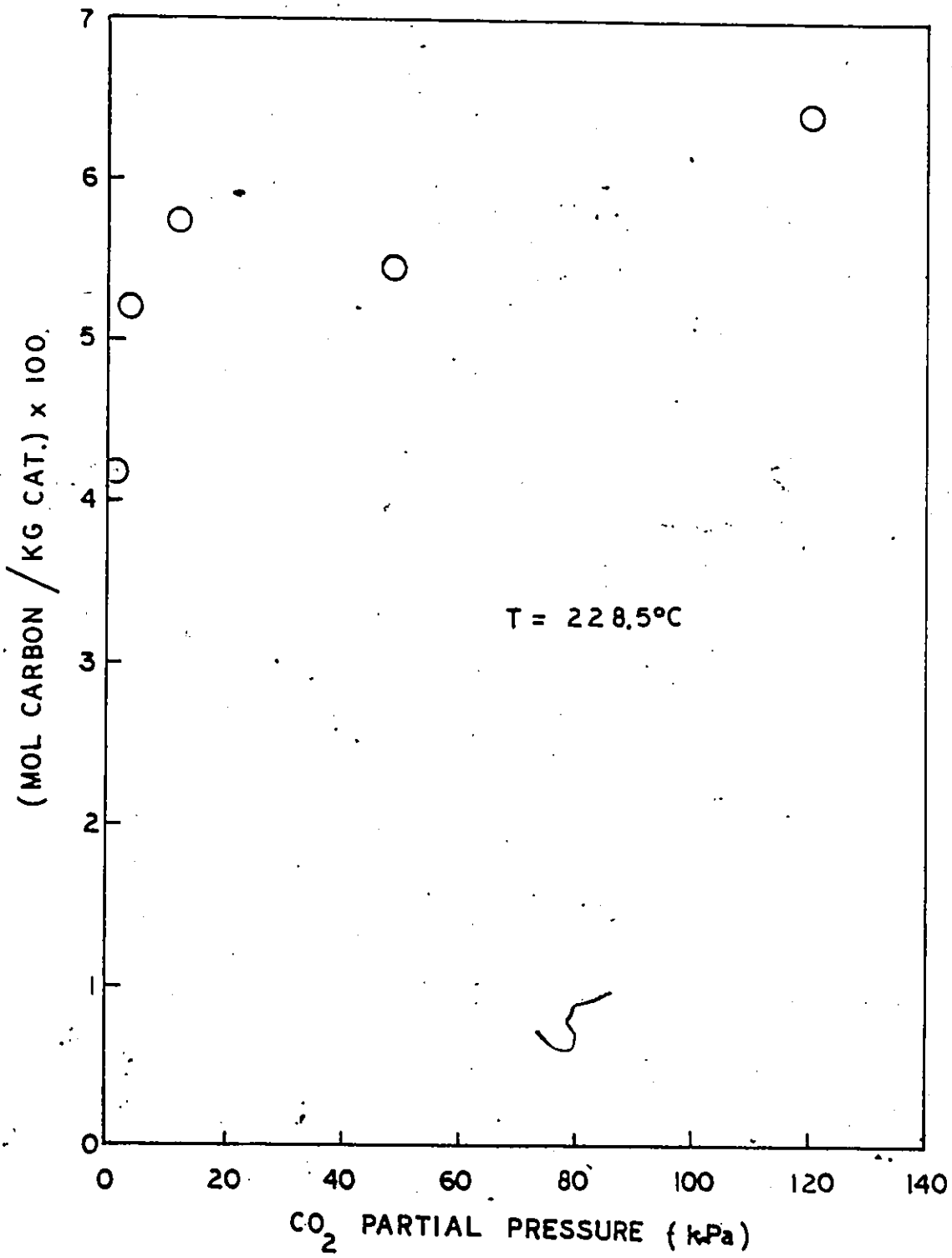

Figure 5-25 Effect of Carbon Dioxide in the Absence of Hydrogen on the Amount of Carbon Deposited

$$r_c = k \frac{P_{CO_2}^{0.1}}{P_{H_2}^{0.4}} \qquad (5\text{-}1)$$

where r_c = carbon deposition rate during methanation

k = constant

P = partial pressure during methanation

The effect of CO_2 in the absence of H_2 on the deposition rate was found to be of 0.1 order.

The results in figures 5-21 to 5-24 show that under CO_2 methanation condition the catalyst maintained less than a monolayer of carbonaceous species. Furthermore, this surface carbon was very reactive, and in the absence of CO_2 or CO on the surface, could be hydrogenated readily to methane. The rate of methane formation was greater than that measured under steady-state conditions. These observations lead to the consideration of carbonaceous species as an important intermediate in CO_2 methanation.

The observation of less than monolayer accumulation of carbon taken together with the continuous formation of methane in the steady-state runs implies that, on the average, most of the catalyst surface is free of the carbon species, which contrasts sharply the case of CO methanation where more than a monolayer of carbon was found.

Although the buildup of surface carbon during CO methanation has been reported for various transition metals,

it is believed that the present finding is the first reported presence of residual carbon on nickel surface for CO_2 methanation. Solymosi et al.(107) reported the presence of less than monolayer carbon on rhodium for CO_2 methanation. However, the authors did not investigate the effects of steady-state conditions on the amount of surface carbon deposited. The present results show that the amount decreases with increasing partial pressure of H_2 or H_2/CO_2 ratio. Apparently under these conditions, hydrogenation rate of surface carbon from CO_2 dissociation is relatively fast, resulting in a decrease in residual carbon on the catalyst surface.

Similar to H_2, water inhibited carbon deposition during methanation. The decrease in residual carbon could result from the direct reaction of the surface carbon with water (168). However, water has been shown to be dissociatively adsorbed on nickel (191,192). Chemisorption of water could decrease the concentration of active sites for CO_2 dissociation and result in a lower rate of formation of carbonaceous species.

In the absence of H_2, increasing concentrations of CO_2 increased the amount of carbon deposited, similar to the case of CO dissociation. However, the amount was less than that observed in runs with H_2 present. The importance of H_2 in the dissociation of CO_2 has been pointed out by various investigators. Gupta et al. (106) showed that CO_2 did not

directly decompose on ruthenium surface, but when H_2 was passed over the adsorbed CO_2, carbon was formed. Solymosi et al.(107) found that CO_2 dissociation to CO and O was promoted by H_2. The results in the present study also demonstrate the presence of H_2 assists in the deposition of carbon from CO_2. Figures 5-22 and 5-23 show that a small amount of H_2 could result in 40% more surface carbon deposited. The results also suggest that the dissociation of CO_2 is thermodynamically unfavourable. To obtain surface carbon the equilibrium must be shifted by the removal of surface oxygen from the dissociation. In this respect H_2 plays an important role in achieving this shift of equilibrium towards the formation of surface carbon. The ease of removal of surface oxygen by hydrogen has been demonstrated by Zagli and Falconer (104,105).

5.5 Mechanistic Considerations

Data currently available suggest that CO_2 methanation proceeds through the intermediate formation of CO. Weatherbee et al. (197) have reported the observation of CO in the effluent over Ni/SiO_2 catalyst. Falconer and Zagli (103) concluded that following adsorption on nickel catalyst, CO and CO_2 methanation proceeded by the same mechanism. They suggested that CO_2 dissociates upon adsorption at elevated temperature into surface oxygen and CO. Solymosi et al.(107) also concluded that over rhodium CO is formed first, possibly assisted by the presence of H_2, and then CO further dissociates into surface carbon and oxygen.

The findings in this study also provide further evidence supporting CO as an intermediate in CO_2 methanation. The observation of trace amounts of CO at low H_2/CO_2 ratio indicates that CO_2 methanation possibly goes through the formation of CO. Whereas Weatherbee et al. (197) concluded that adsorbed CO from dissociative adsorption of CO_2 is in equilibrium with the CO in the gas phase, the present study suggests that the H_2/CO_2 ratio plays an important role in governing the concentration of CO in the gas phase. The decrease in methanation rate and the concomitant observation of CO at low H_2/CO_2 ratio is in agreement with the assertion that CO_2 dissociates to form first adsorbed CO and then surface carbon. The role of CO in CO_2 methanation is further illustrated in figure 5-20 which shows that CO in small concentrations can increase the reaction rate.

The present study also shows that in CO_2 methanation reactive carbonaceous species are formed on the nickel surface, which can be hydrogenated to form methane, indicating that dissociation of CO_2 is an inherent part of the reaction. However, the dissociation of CO_2 cannot be the rate determining step in methanation since within the temperature range considered, the rate of CO_2 hydrogenation is higher than that of CO. This assertion is also supported by the observation of residual carbon on the catalyst which suggests that the rate determining step consists of the hydrogenation of carbonaceous species and not of CO_2 dissociation. The decrease in the amount of residual carbon with increasing H_2/CO_2 ratio and partial pressure of

H_2 at constant CO_2 concentration can be explained in terms of increased removal rate of surface carbon by hydrogenation under these conditions. The increase in residual carbon with the partial pressure of CO_2 is probably due to the increase in adsorbed CO concentration and hence an increase in surface carbon. In addition, the increase in adsorbed CO may also lower the hydrogenation rate of surface carbon.

The increase in the amount of residual carbon with methanation temperature suggests that the rate of formation of surface carbon increases faster with temperature than its rate of removal. Higher temperature lowers the surface coverage of H_2 resulting in lower rate of hydrogenation. On the other hand, higher temperature also increases the rate of CO_2 dissociation. Overall the depletion of surface carbon by hydrogenation is lower than its formation at higher temperature, resulting in an increase of residual carbon.

That water retards the methanation rate as well as decreases the amount of surface carbon suggests the importance of surface carbon in kinetic consideration. Apparently water lowers the deposition rate of surface carbon by occupying active sites for CO_2 dissociation, similar to its effect on CO methanation as discussed in Chapter 4. It is believed that water has only minimal effect on the hydrogenation step; otherwise one would expect an increase in the amount of residual carbon. This in turn suggests that at least in the presence of water, the slowest step involves the hydrogenation of deposited surface

carbon. The effect of water on the methanation rate contrasts with that of CO in low concentrations which increases the rate, possibly due to the increased formation of surface carbon (figure 5-20).

The above discussion leads to a reaction mechanism for CO_2 methanation which is similar to that for CO methanation. The reaction is perceived to proceed through the dissociation of CO_2 first to CO and then to surface carbon which is then hydrogenated to yield methane. Given that the slowest step consists of the hydrogenation of surface carbon in both reactions, one would then expect similar activation energies and reaction rates. However, the results in the present study show that CO_2 methanation has a lower activation energy and proceeds at a faster rate than CO methanation. According to Solymosi et al. (107), this apparent contradiction can be related to the difference in the amounts of adsorbed CO and surface carbon on the catalyst during methanation. For CO_2 methanation, the concentration of adsorbed CO is relatively low and the concentration of surface carbon is less than a monolayer. The carbon can react quickly with the large excess of H_2, and the possibility of accumulation and aging of surface carbon is minimized. In contrast, for CO methanation, the concentration of adsorbed CO is much higher and the formation of surface carbon is greatly increased. Consequently, not all the surface carbon can be hydrogenated immediately. The unreacted carbon is transformed into a less reactive form

which will be subsequently hydrogenated but with a higher activation energy and hence a lower rate. The aging of surface carbon has been demonstrated by Gupta et al. (106) and McCarty and Wise (33).

The lower concentration of surface carbon in CO_2 methanation is also related to the higher methane selectivity compared to the case of CO methanation. The relatively low concentration and short lifetime of the carbon on the catalyst surface make the formation of C - C bond, and hence the formation of higher hydrocarbons, difficult (107).

From the discussion above, the following mechanism is proposed for CO_2 methanation:

$$H_2 + 2S \rightleftharpoons 2H_s \quad (1)$$

$$CO_2 + S \rightleftharpoons (CO_2)_s \quad (2)$$

$$(CO_2)_s + S \rightleftharpoons CO_s + O_s \quad (3)$$

$$CO_s + S \rightleftharpoons C_s + O_s \quad (4)$$

$$O_s + H_s \rightleftharpoons (OH)_s \quad (5)$$

$$(OH)_s + H_s \rightleftharpoons H_2O + 3S \quad (6)$$

$$C_s + H_s \rightleftharpoons (CH)_s \quad (7)$$

$$(CH)_s + H_s \longrightarrow (CH_2)_s + 2S \quad (8)$$

$$(CH_2)_s + H_s \rightleftharpoons (CH_3)_s + S \quad (9)$$

$$(CH_3)_s + H_s \rightleftharpoons CH_4 + 2S \quad (10)$$

CO_2 adsorption and dissociation are assumed to be in equilibrium (steps 2 and 3). The adsorbed CO further decomposes to yield surface carbon and oxygen. Steps 2 to 4 can be simplified to:

$$CO_2 + 3S \rightleftharpoons C_s + 2O_s \quad (11)$$

In the presence of H_2 the surface oxygen is removed via stepwise hydrogenation to H_2O which desorbs into the gas phase (steps 5 and 6). The surface carbon is hydrogenated stepwise to yield finally methane. Species CH_s and OH_s are each assumed to occupy two surface sites. As in the case of CO hydrogenation, the carbonaceous species on the surface are assumed to be non-oxygenated of the type CH_x (x = 0 - 3). The proposed mechanism is very similar to that for CO methanation, and the following rate equation can be derived (Appendix C):

$$r = \frac{k_1 P_{H_2} P_{CO_2}^{1/3}}{(1 + k_2^{1/2} P_{H_2}^{1/2} + k_3 P_{CO_2}^{2/3})^3} \quad (5\text{-}2)$$

The equation is very similar in form to equation (4-4) for CO methanation. The exponent 3 in the denominator results from the assumption that the hydrogenation of CH_s species is the rate determining step and involves three sites.

The equation predicts a maximum in rate as CO_2 concentration is increased at a constant partial pressure of

H_2. It also yields maximum order of 0.33 and 1.0 for CO_2 and H_2, respectively. The model does not yield a constant rate as the partial pressure of H_2 is increased sufficiently with the partial pressure of CO_2 kept constant.

The fit of the model is shown in figures 5-26 to 5-30. Table 5-6 shows the values of the estimated parameters for the model. k_1 and k_3 are products of various constants; k_2 is the adsorption equilibrium constant of H_2. These k_2 values are compared with those from the high temperature chemisorption study (section 2.2.4) and from equation (4-4) for CO methanation. The values decrease with temperature and are comparable to but slightly larger than those from the CO kinetics. This observation is in agreement with the interpretation put forward in section 4.5 regarding the catalyst surface condition. In CO_2 methanation the concentrations of adsorbed CO and carbonaceous carbon have been shown to be much lower than those in CO methanation. The value of k_1 should increase with temperature as it reflects the temperature dependency of the reaction rate. The low values of k_1 at 513 and 523 K is a result of catalyst deactivation, as shown in figures 5-8 and 5-9 where it can be seen that the turnover numbers are much lower than those at 503 K (figures 5-6 and 5-7).

Other Langmuir-Hinshelwood equations were also tested against the data (table 5-7). Models 1 and 2 which predict

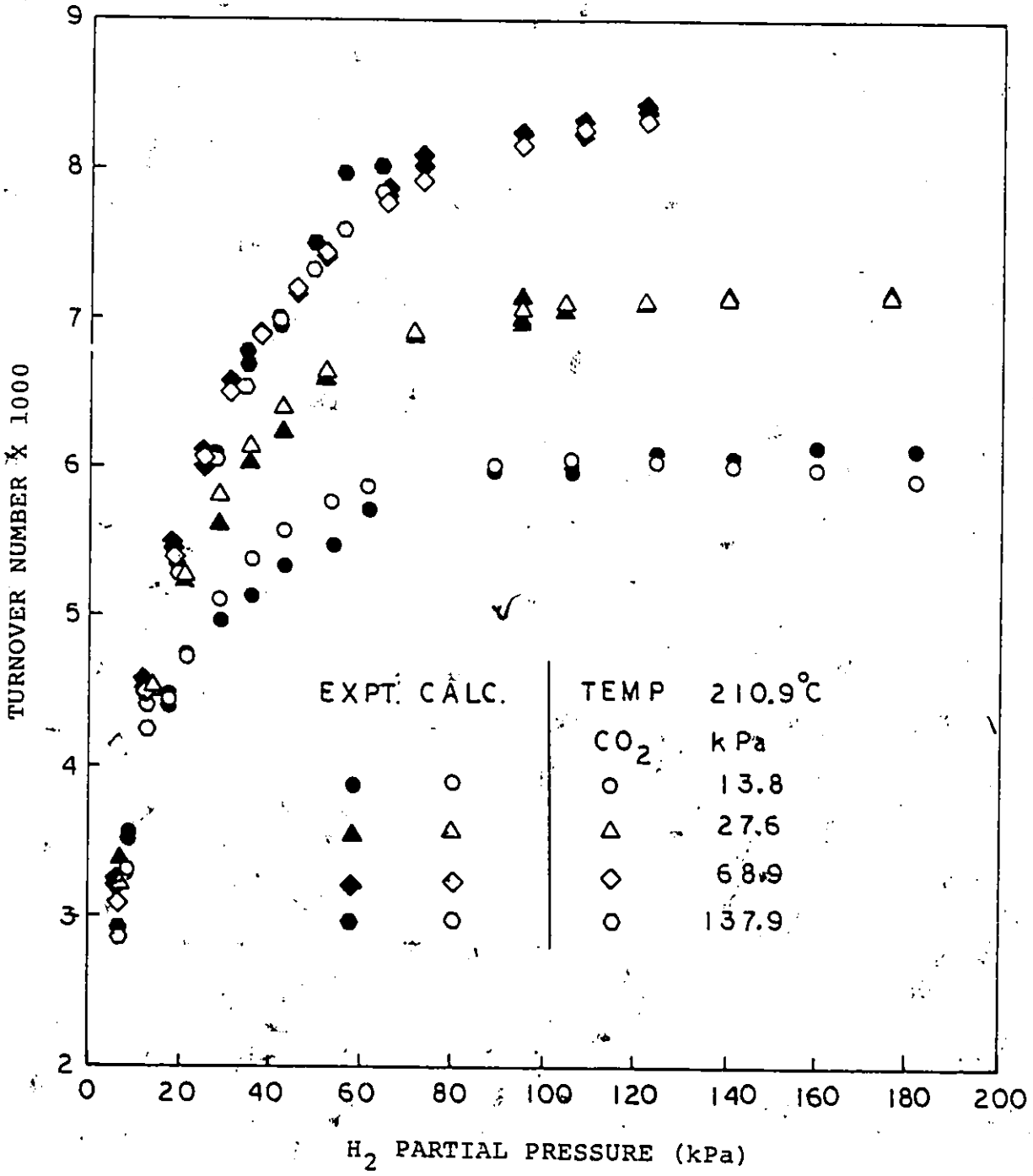

Figure 5-26 Comparison of Experimental and Calculated Rates of CO_2 Methanation at 484 K

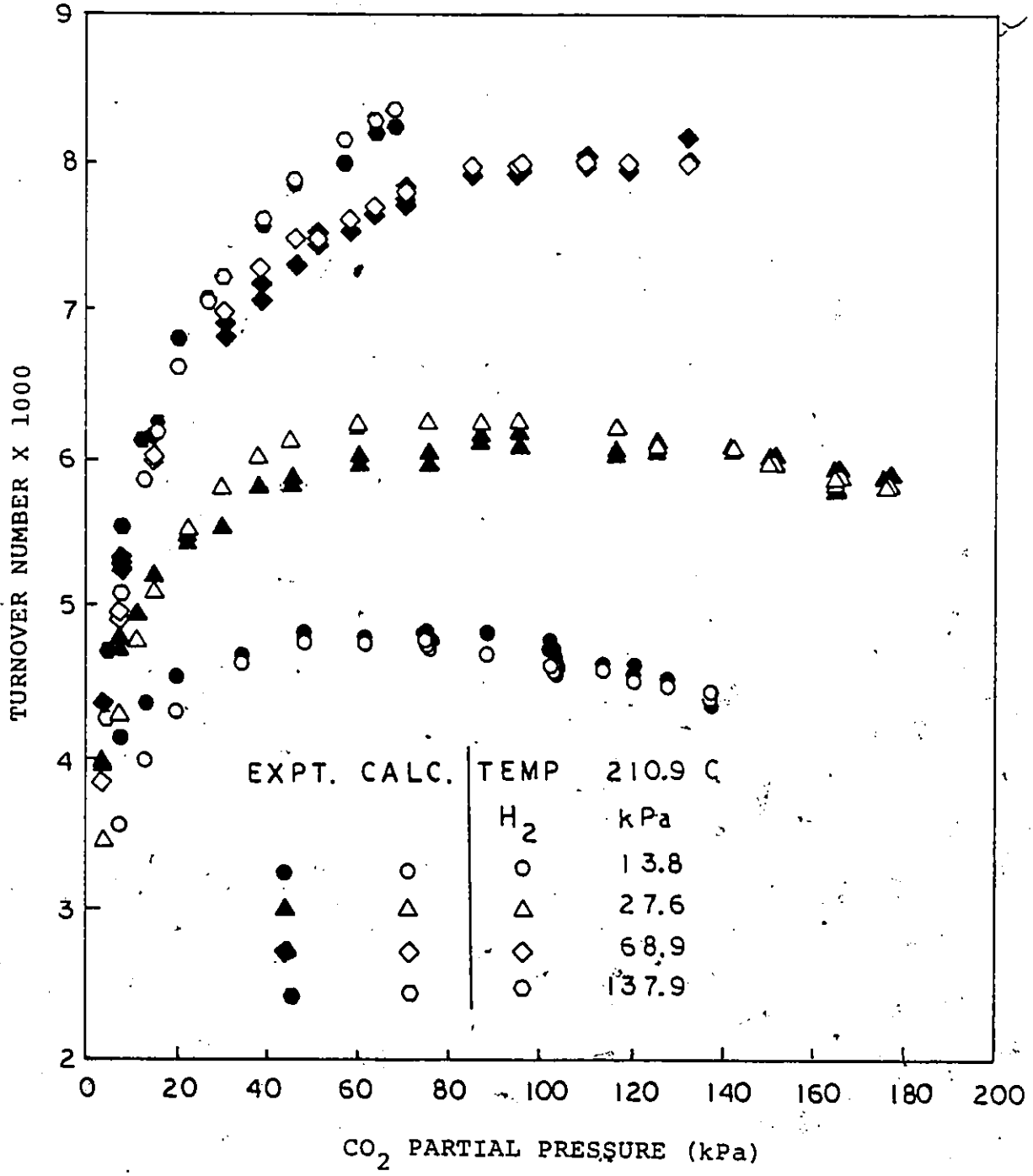

Figure 5-27 Comparison of Experimental and Calculated Rates of CO_2 Methanation at 484 K

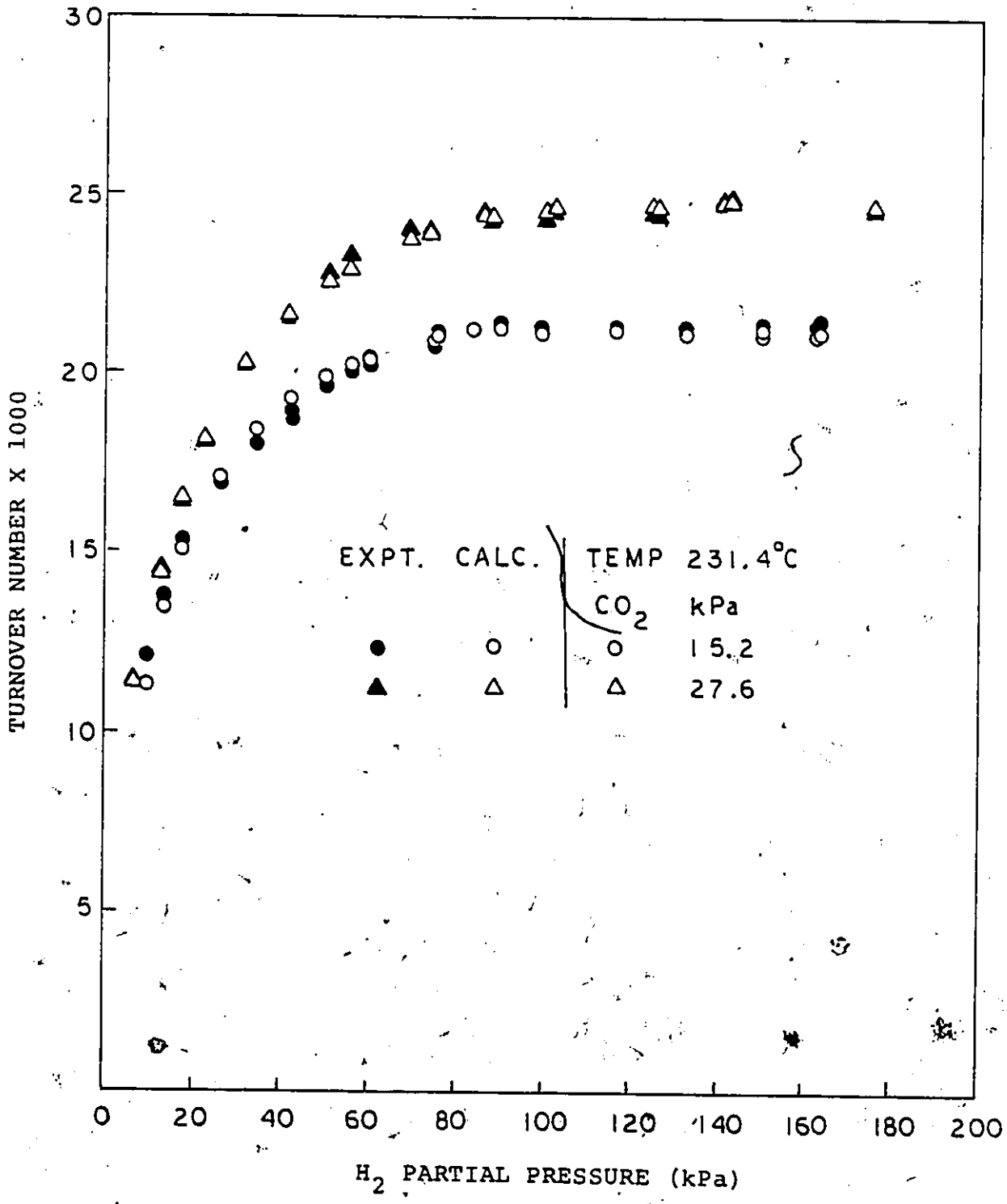

Figure 5-28 Comparison of Experimental and Calculated Rates of CO_2 Methanation at 504 K

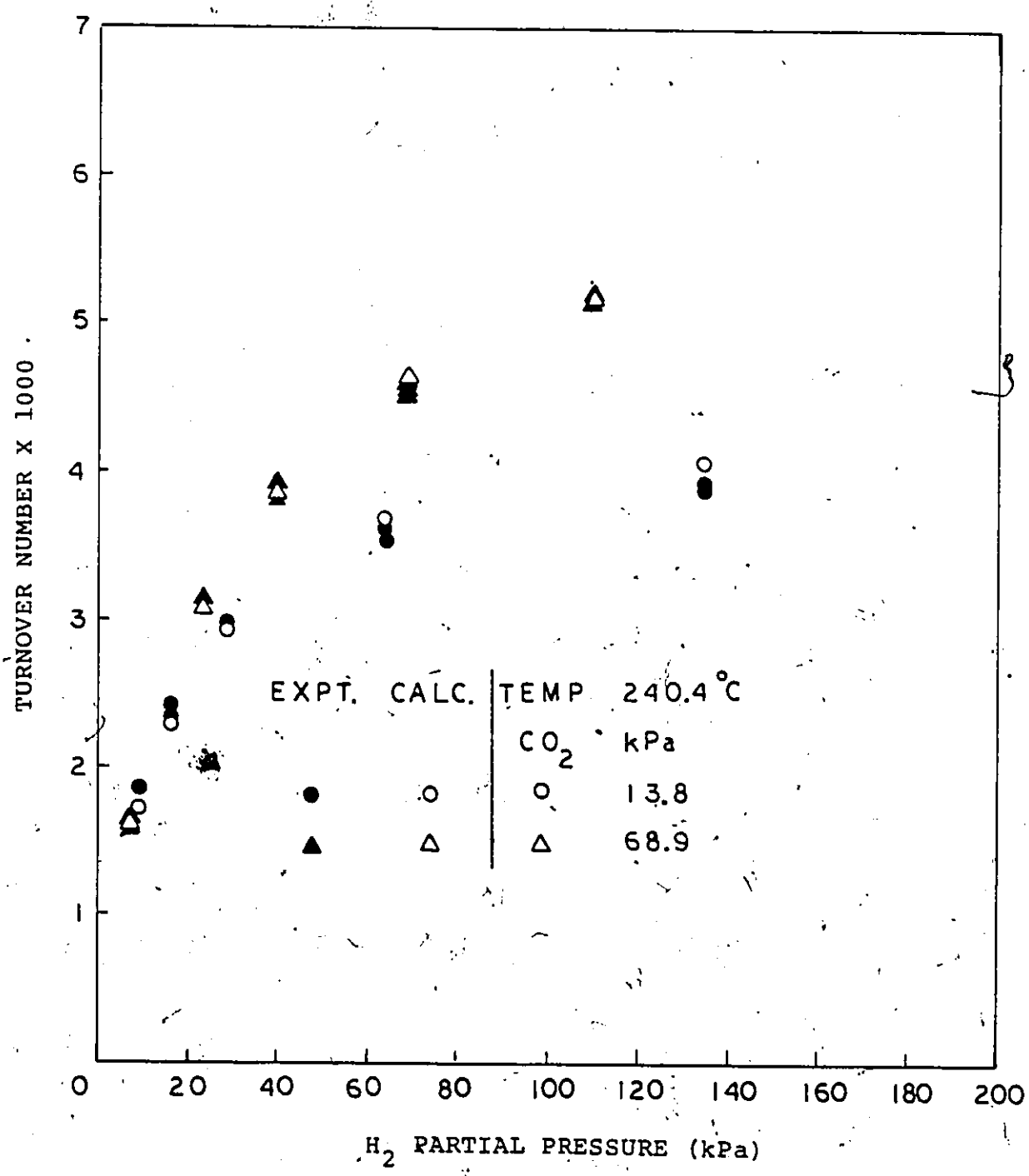

Figure 5-29 Comparison of Experimental and Calculated Rates of CO_2 Methanation at 513 K

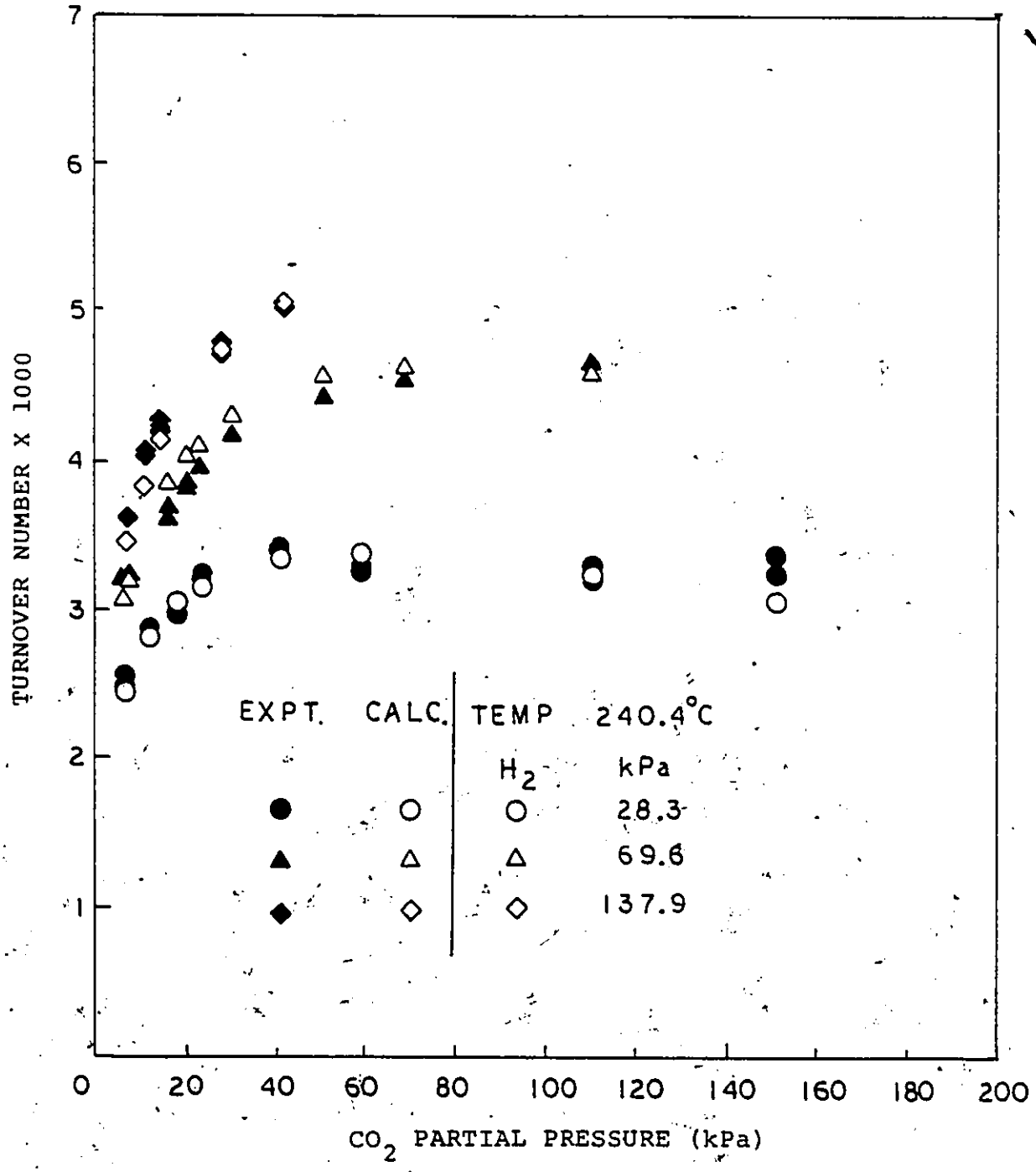

Figure 5-30 Comparison of Experimental and Calculated Rates of CO_2 Methanation at 513 K

Table 5-6

Estimated Parameter Values for Langmuir-Hinshelwood Model

(Equation 5-2)

Temp (^{o}C)	$k_1 \times 10^3$	k_2	$k_3 \times 10$
210	0.895	0.2148	0.238
230	1.367	0.1675	0.174
240*	0.340	0.1597	0.252
250*	0.595	0.1538	0.274

Unit of $k_1 = \dfrac{\text{molecule}}{\text{Metal site} - \text{second} - (\text{kPa})^{4/3}}$

$k_2 = \text{kPa}^{-1}$

$k_3 = \text{kPa}^{-2/3}$

* The estimated values of parameter k_1 are found not to obey the Arrhenius' Law. Since the reaction rate depends on the number of available sites per gram of catalyst, a decrease in reaction sites from catalyst deactivation will result in corresponding decreases in the rate and estimated value of parameter k_1. Deactivation is attributed to a combination of carbon deposition and sintering, especially at high temperatures. In the absence of deactivation, parameter k_1 would obey the Arrhenius' Law.

Table 5-7

Equations tested for CO_2 Methanation

No.	Equation
1	$\dfrac{k_1 P_{H_2} P_{CO_2}^{1/2}}{(1 + k_2^{1/2} P_{H_2}^{1/2} + k_3 P_{CO_2}^{1/2})^2}$
2	$\dfrac{k_1 P_{H_2} P_{CO_2}^{1/3}}{(1 + k_2^{1/2} P_{H_2}^{1/2} + k_3 P_{CO_2}^{1/3})^2}$
3	$\dfrac{k_1 P_{H_2}^{1/2} P_{CO_2}^{1/2}}{(1 + k_2^{1/2} P_{H_2}^{1/2} + k_3 P_{CO_2}^{1/2})^2}$
4	$\dfrac{k_1 P_{H_2}^{1/2} P_{CO_2}^{1/3}}{(1 + k_2^{1/2} P_{H_2}^{1/2} + k_3 P_{CO_2}^{1/3})^2}$
5	$\dfrac{k_1 P_{H_2} P_{CO_2}^{1/2}}{(1 + k_2^{1/2} P_{H_2}^{1/2} + k_3 P_{CO_2}^{1/2})^3}$

Table 5-7 (continued)

No.	Equation	
6	$\dfrac{k_1 P_{H_2} P_{CO_2}^{1/3}}{(1 + k_2^{\frac{1}{2}} P_{H_2}^{\frac{1}{2}} + k_3 P_{CO_2}^{1/3})^3}$	
7	$\dfrac{k_1 P_{H_2} P_{CO_2}^{1/3}}{(1 + k_2^{\frac{1}{2}} P_{H_2}^{\frac{1}{2}} + k_3 P_{CO_2}^{2/3})^3}$	(eqn. 5-2)

a constant rate at high partial pressure of H_2 do not fit the data well. Models 3 and 4 assume the rate determining step to be the first stepwise hydrogenation of surface CO and carbon, respectively, and predict a maximum rate with respect to H_2 concentration. Models 5 and 6 assume the second hydrogenation step to be the rate determining step. Model 7 (equation 5-2) differs from model 6 by assuming the adsorbed CO completes for reaction sites with H_2. In the process of fitting the data, it became clear that a better fit could generally be obtained if the exponent for CO_2 in the numerator of the rate equation is 1/3 instead of ½, and if the exponent for the denominator is 3 instead of 2. Of the equations tested, equation 5-2 (model 7) gives the best fit.

Equation 5-2 does not account for the effect of water which has been shown to inhibit the reaction rate. The data on the effect of water (figure 5-17) were analysed by using equation 4-5 as was done for the effect of water on CO methanation. When $(1/r)^{1/m}$ was plotted versus $P_{H_2O}^{1/n}$, linear plots were obtained for m = 3 and n = 6. The same value of n was also obtained for the effect of water on CO methanation (equation 4-5). Thus to include the effect of water, equation 5-2 can be modified to:

$$r = \frac{k_1 P_{H_2} P_{CO_2}^{1/3}}{(1 + k_2 P_{H_2}^{1/2} + k_3 P_{CO_2}^{2/3} + k_4 P_{H_2O}^{1/6})^3} \quad (5\text{-}3)$$

In summary, the mechanism of CO_2 methanation was discussed. It involves the dissociation of CO_2 to adsorbed CO and surface carbon. Hydrogenation of the surface carbon leads to the formation of methane. Based on the mechanism which is very similar to that of CO methanation, a rate equation was obtained which could represent the data well.

Chapter 6

CHAIN GROWTH IN THE FISCHER-TROPSCH SYNTHESIS

6.1 Introduction

Knowledge of the composition of the hydrocarbons from the Fischer-Tropsch process is essential in determining its applicability as fuel. It is also important in understanding the reaction mechanism involved. A significant amount of work has been done in this area, notably that of the U.S. Bureau of Mines (11,197,198). In the Fischer-Tropsch synthesis the products are not in thermodynamic equilibrium with each other or with the reactants. If equilibrium were established, the product would consist mainly of methane, which is the most favoured product thermodynamically (199). In view of this, an analysis of the carbon number and isomer distributions would provide pertinent clues in the interpretation of the mechanism, in particular, the chain growth process. In this regard the present work is an investigation of the chain growth process .

6.2 Literature Survey

Fischer-Tropsch synthesis is undoubtedly a complicated process. After nearly sixty years of investigations, there is still no general consensus as to the nature of the intermediate or the mechanism involved. The large amount of work that has been done in this effort is well documented.

Generally, the process can be regarded essentially as a polymerization process not unlike that in free radical polymerization. The propagation steps consist of the stepwise addition of one-carbon units. However, the exact mechanism and structure of the intermediate essential in this addition step is still the subject of much controversy. The theories proposed include the condensation type reaction of enolic intermediate due to Anderson et al. (11), the insertion and hydrogenation of carbon monoxide by Pichler and Schulz (20, 200,201), and the more recently held view of active carbon species, similar to the original methylene species from the Fischer and Tropsch's carbide theory (8). Irrespective of the exact nature of these 'monomer' units, the accepted view is that chain growth is a result of the stepwise addition of these units. The relevant concern is the mode of addition and its relationship to the product and isomer distributions.

Herington (202) was the first to introduce the idea of the ratio of chain termination rate r_t to the chain propagation rate r_p, and laid the foundation of organizing the data in a form that can relate various carbon fraction amounts with respect to the carbon number, i.e. the product distribution with respect to carbon number. Thus,

$$\beta_n = \frac{r_t}{r_p} = \frac{1 - \alpha_n}{\alpha_n} \qquad (6\text{-}1)$$

where α_n is the probability of growth of a chain of length n. Friedel and Anderson (203) extended the idea and showed that

if α_n is constant for $n \geqslant x$, a recursion formula is obtained:

$$\phi_n = \phi_x \alpha^{n-x} \qquad (6\text{-}2)$$

where ϕ_n is the moles of hydrocarbons with n carbon atoms. On the other hand, in the thirties, Flory (204) and Schulz (205) arrived independently at the equation:

$$w_n = (1-\alpha)^2 \, n \, \alpha^{n-1} \qquad (6\text{-}3)$$

where w_n is the weight fraction of polymer containing n carbon atoms. Equation (6-3) is traditionally used to explain the molecular weight distribution in polymerization. Recently, it was applied by Henrici-Olive' and Olive' (206) to analyse the Fischer-Tropsch data on cobalt and iron catalysts, and the authors discussed the mechanism by comparing similar reactions in homogeneous and heterogeneous catalytic systems. Much debate followed regarding the validity of such an approach (207-210). Madon (211) showed that equations (6-2) and (6-3) are mathematically equivalent. Putting the exact mechanistic details aside, since similar ideas and statistics such as ratios of propagation and termination are involved, that the equations are equivalent is not surprising.

Anderson et al. (212) went beyond mere hydrocarbons distribution and extended the model to account for the distribution of isomers in various carbon fractions. This

was achieved by introducing a branching probability factor f which is the ratio of the rate of appearance of C_n upon addition to the penultimate carbon of C_{n-1} to the rate of appearance of C_n upon addition to the end carbon of C_{n-1}. This can account for the presence of isomers with methyl groups. This model, subsequently known as simple chain growth (SCG) model, was much used in the U.S. Bureau of Mines, and was found to predict well the isomer distributions of various catalytic systems. The SCG model, embodied in the equation :

$$\phi_n = k F_n a^{n-2} \qquad (6-4)$$

where a and k are constants and F_n is a function of branching probability factor f, which also yields information on the carbon number distribution.

In Fischer-Tropsch products quaternary carbon species are not observed. Hence, addition to a tertiary carbon is not allowed. The SCG model, however, does not yield any isomers with ethyl groups. Blaustein et al. (213) found that ethyl-substituted carbon chains were present in the same concentrations as dimethyl substituted hydrocarbons. Therefore, in order to account for the presence of ethyl species, the SCG model needs to be modified.

There is growing evidence that olefins such as ethylene can be incorporated into the growing hydrocarbon chain during Fischer-Tropsch synthesis (214). This raises the possibility

that the chain growth process may also involve two-carbon units addition at a time, in addition to the generally accepted one-carbon addition. Recently, Pichler et al. (215) have analysed Fischer-Tropsch products by capillary gas chromatography for carbon fractions up to C_{17}. In the hydrogenated hydrocarbon fractions, virtually all isomers up to C_9 were separated and many of the isomers up to C_{17} were identified. In particular, the concentrations of ethyl-substituted species were obtained. This analysis is perhaps the most comprehensive and detailed of any Fischer-Tropsch product composition. This detailed knowledge with respect to isomer composition provides an unique opportunity to test some more complicated chain growth schemes. The excellent work of Anderson and Chan (216) is an attempt in this regard. However, the work has been limited to the range of carbon fractions C_6 to C_9. The abundant information provided by the composition in the higher carbon fractions was not utilized. The present work is an attempt to apply the various chain growth models to all carbon fractions.

6.3 Formalism of Chain Growth Schemes

In interpreting the various chain growth schemes to be investigated, the SCG scheme involving stepwise addition of single carbon units is given here to illustrate the formalism involved.

The following assumptions are made:

(1) hydrocracking reactions do not occur to a significant extent;

(2) one carbon addition only is allowed;

(3) carbon addition is allowed only at one end of the carbon chain;

(4) addition to tertiary carbons is prohibited;

(5) rates of addition to the end carbon or to the penultimate carbon are independent of carbon chain length.

Assuming that desorption of isomers species is first order, the rate of formation of these species is proportional to their respective surface concentrations, i.e.

$$M_n = k_1 C_n \qquad (6\text{-}6)$$

where M_n = amount of isomer produced

C_n = surface species concentration

k_1 = desorption rate constant

Thus, one needs only to focus on the concentration of the surface species. For a hydrocarbon species of carbon number n with end group ---CC, its concentration on the surface can be obtained from a consideration of rates of formation and disappearance. For example, with n = 5, one has the following:

$$CCCC \xrightarrow{k_2} CCCCC \xrightarrow{k_2} CCCCCC$$

$$CCCCC \xrightarrow{k_3} \underset{C}{C}CCCC$$

It can be formed only from its predecessor of one less carbon by end-on addition:

$$R_f = k_2 C_4 \qquad (6\text{-}7)$$

where R_f = rate of formation

C_4 = surface concentration

k_2 = end-on addition rate constant

However, C_5 can disappear by desorption, by end-on addition to the end carbon, as well as by addition to the penultimate carbon:

$$R_d = (k_1+k_2+k_3)\, C_5 \qquad (6\text{-}8)$$

where R_d = rate of disappearance

k_3 = penultimate carbon addition rate constant

For steady state, the rates are equal and hence one obtains the ratio:

$$\frac{C_5}{C_4} = \frac{k_2}{k_1+k_2+k_3} = a \qquad (6\text{-}9)$$

However, for a species with the end group --$\overset{C}{C}$C, there are only two ways of disappearance, i.e. by desorption and end-on addition. It can be formed only from its predecessor of one less carbon by addition to the penultimate carbon. For example, with n = 4, one has the following:

$$CCC \xrightarrow{k_3} C\overset{C}{C}C \xrightarrow{k_2} CC\overset{C}{C}C$$

Similar consideration gives the following ratio:

$$\frac{C_4}{C_3} = \frac{k_3}{k_1 + k_2} = b \qquad (6\text{-}10)$$

Since the amount of hydrocarbon obtained is proportional to the surface species concentration, there emerges a relationship between the concentration of hydrocarbon growing and the concentration of its predecessor, depending on the species under consideration. If one defines

$$b = af \qquad (6\text{-}11)$$

one can represent the growth scheme by the following:

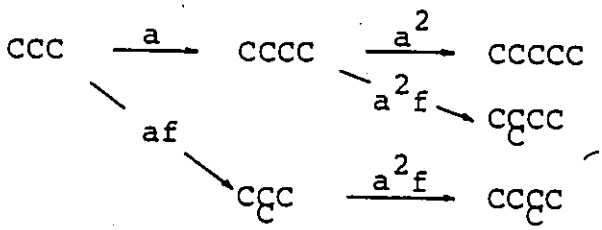

Thus, it is clear that the concentration of a given species can be obtained easily from the predecessor by using the factor a or af, depending on whether the species has end group CC-- or $\overset{C}{C}$C--. According to this scheme, the exponent of f is equal to the number of methyl units -$\overset{C}{C}$- in the hydrocarbon chain.

6.4 Computer Simulation of Chain Growth Schemes

It is obvious that as the chain propagates the number of species of different structures increases rapidly with the carbon number. This large number of species makes hand

calculations tedious and prone to error. Hence, there should be a way by which this 'bookkeeping' of all the species formed can be automated. This can be conveniently achieved with a computer. The idea involved is to find means of describing and storing the isomers as they are formed, and subject them to further growth according to the rules of the chain growth scheme under study. This will entail a method of describing, storing and identifying the isomer molecules.

To describe the aliphatic hydrocarbon molecules from the Fischer-Tropsch products, one can utilize the fact that there are only three kinds of carbon atoms in the molecules: primary or secondary carbon atoms with only hydrogen atoms attached; tertiary carbon atoms with a methyl group attached; and tertiary carbon atoms with an ethyl group attached. To designate these carbon units one can use numbers. Thus, numbers 1, 2, and 3 are used to represent units of -C- , -C- and -C- , respectively. Thus, a vector of description (1111000000000000) is used to represent a normal butane molecule. Similary one can use vectors (1210000000000000) and (1131111000000000) to represent isobutane and 3-ethyl heptane, respectively. The zeros are to fill up the vector space. Thus, the molecules of the hydrocarbons are represented by numbers and stored in a vector form.

As the isomers are generated, not only their nature must be known but also their concentrations. This latter information can also be stored in the same vector which has

now dimension 18. The first 17 spaces are used for representing the isomer, and the 18th space for storing the information on its concentration. Thus two pieces of information are stored in each vector: the nature of the isomer and the concentration. Hence x moles of normal butane can be stored in the vector as (11110000000000000 x).

With the isomer and its concentration stored in a vector, the chain growth process can be conveniently represented by successive generation of new vectors according to the given chain growth rule. Table 6-1 and 6-2 summarize the chain growth rules for the various one carbon addition and one- and two-carbon additions growth schemes, respectively. Each of these growth schemes has two growth constants, f and g, which empirically measure the extent of branching. Examples of how two of these schemes work are given in tables 6-3 and 6-4.

While some of the isomers of a given carbon number may appear to be different in the vector forms, they are the same products in the Fischer-Tropsch product. Thus, species (11121000000000000 x) and (12111000000000000 y) stored in two separate vectors both represent the same compound 2-methyl pentane. Species such as (11111000000000000 a) and (11300000000000000 b) may be obtained in the growth process, but they represent the same compound, normal pentane. Thus these species, after they have been subjected to the growth

Table 6-1

Chain Growth Rules for One-Carbon Addition

Scheme	Growth Rules[+]		
1A	U —— a ⟶ 1U	(all species)	1
	11W —— af ⟶ 21W		2
	111X —— ag ⟶ 112*X		3
	112*X —— a ⟶ 113X		4
1B	Same as scheme 1A except that step 4 is replaced by		
	112*X —— ag ⟶ 113X		4'
1C	Same as scheme 1A except that steps 3 and 4 are replaced by		
	111X —— ag ⟶ 1*1*2*X	(only)	3''
	1*1*2*X —— a ⟶ 113X		4''
1D	U —— a ⟶ 1U	(all species)	1
	11W —— af ⟶ 12W		2
	112X —— ag ⟶ 113X		3

After all growth steps on the species are completed, the following transformations are made: 2X = 11X, 3X = 111X, 13X = 112X, 112*X = 112X, and 1*1*2*X = 112X

+ U, W, and X are parts of a carbon chain that may have any size or configuration.

Table 6-2

Chain Growth Rules for One- and Two-Carbon Additions

Scheme	Growth Rules[+]		
2A	$U \xrightarrow{a} 1U$	(all species)	1
	$1W \xrightarrow{af} 2W$		2
	$1W \xrightarrow{a^2g} 3W$		3
	$1W \xrightarrow{a^2g} 21W$		4
2B	Same as scheme 2A except that step 4 is replaced by		
	$X \xrightarrow{a^2g} 2X$		4'
2C	Same as scheme 2A except that step 3 is replaced by		
	$1W \xrightarrow{a^2fg} 3W$		3'
2D	Same as scheme 2A except that step 4 is replaced by		
	$1W \xrightarrow{a^2f} 21W$		4''
2E	An extension of scheme 2C; all steps are shown.		
	$U \xrightarrow{a} 1U$	(all species)	1
	$1W \xrightarrow{af} 2W$		2
	$1W \xrightarrow{a^2fg} 3W$		3
	$1W \xrightarrow{a^2g} 21W$		4
	$3W \xrightarrow{a^2fg} 23W$		5
	$2W \xrightarrow{a^2g} 22W$		6

Table 6-2 (continued)

Scheme	Growth Rules[+]
2P	Same as scheme 2A except that step 4 is prohibited.

After all growth steps on the species are completed, the following transformations are made: 2W = 11W, 3W = 111W, and 13W = 112W.

+ U, W, and X are parts of a carbon chain that may have any size or configuration.

Table 6-3

The Initial Part of Growth Scheme $1A^+$

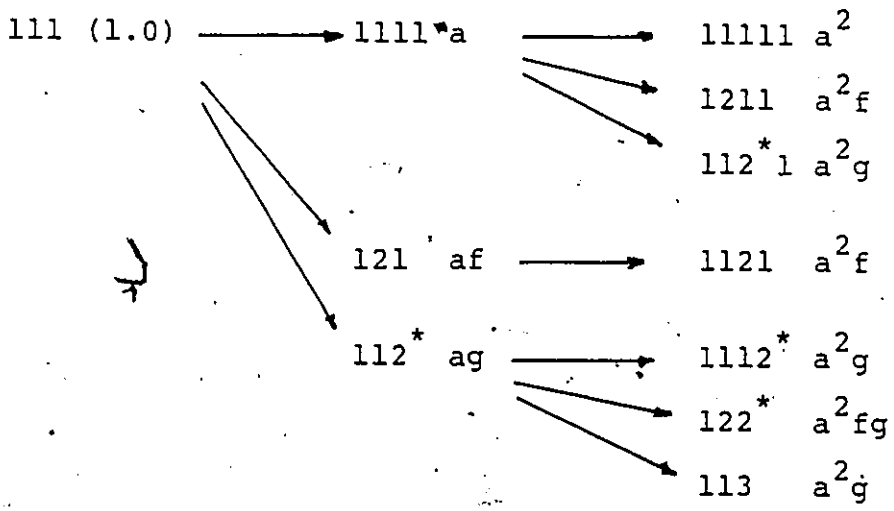

Transformations after the growth steps : 112^* = 1111, 1112^* = 11111, 122^* = 1211, and 113 = 11111

+ Steps yielding species larger than C_5 are not shown.

Table 6-4

The Initial Part of Growth Schemes 2A and $2B^+$

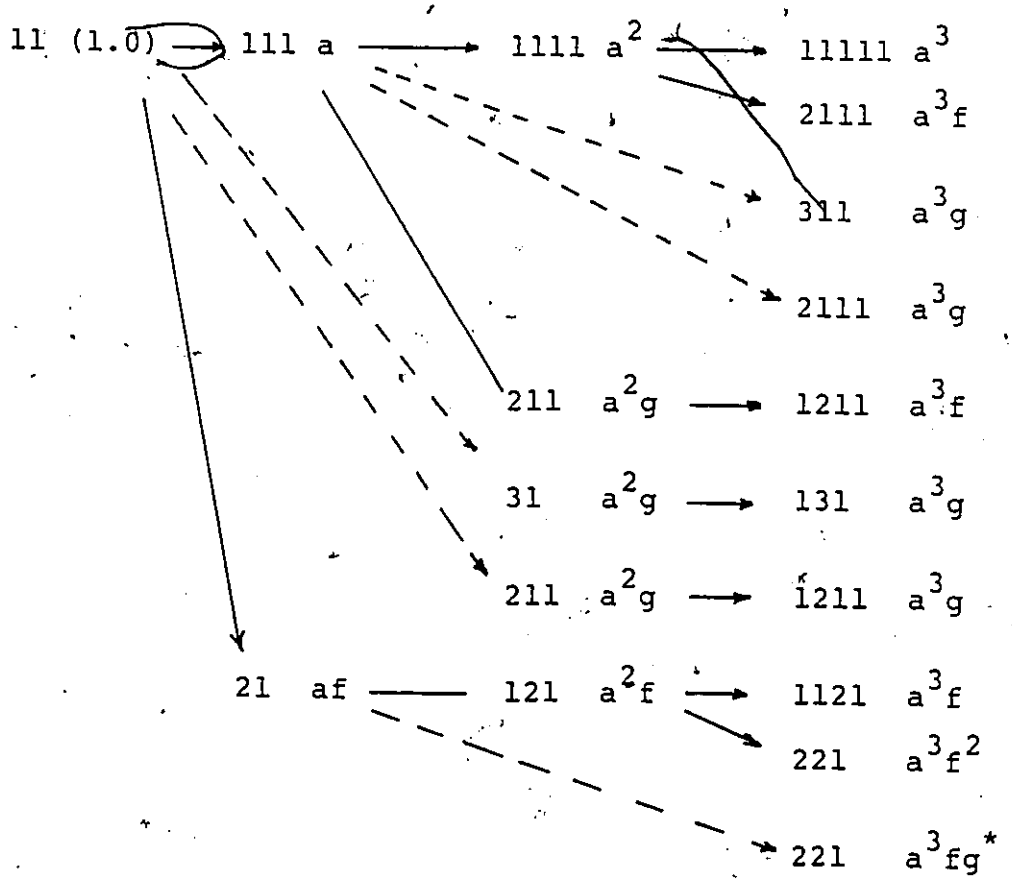

Transformations after the growth steps: 21 = 111, 211 and 31 = 1111, 2111 and 311 = 11111, 131 = 1121, and 221 = 1121.

+ Steps yielding species larger than C_5 are not shown

* This growth step is not permitted in Scheme 2A

process, should be rearranged to the proper product form. This procedure, called isomer intermediate rearrangement, consists of examining and identifying each isomer intermediate and re-describing it in the final product form. Thus vector (1130000000000000 b) is changed to (1111100000000000 b). these isomers will still be stored in their original vector and their concentrations remain unchanged. Isomer intermediate rearrangement is not initiated until the intermediate has been used for generating higher hydrocarbon of one or two more carbon number.

After an isomer of carbon number n has been subjected to the growth process and isomer intermediate rearrangement, if necessary, its concentration is accumulated. This is achieved by storing the isomer in one storage area reserved only for this compound and its concentration. This process, called isomer grouping, consists of examining the various isomers which are now in the product form, by a set of rules, and if k of them refer to compound nn, they will be stored in the matrix S(n,nn) and their concentrations accumulated. Figure 6-1 is a flow diagram relating growth process, isomer intermediate rearrangement, and isomer grouping.

The above is essentially concerned with the event sequences of one intermediate isomer, say the jth one of carbon chain length n. For every intermediate isomer the event sequence is always (1) chain growth, (2) intermediate

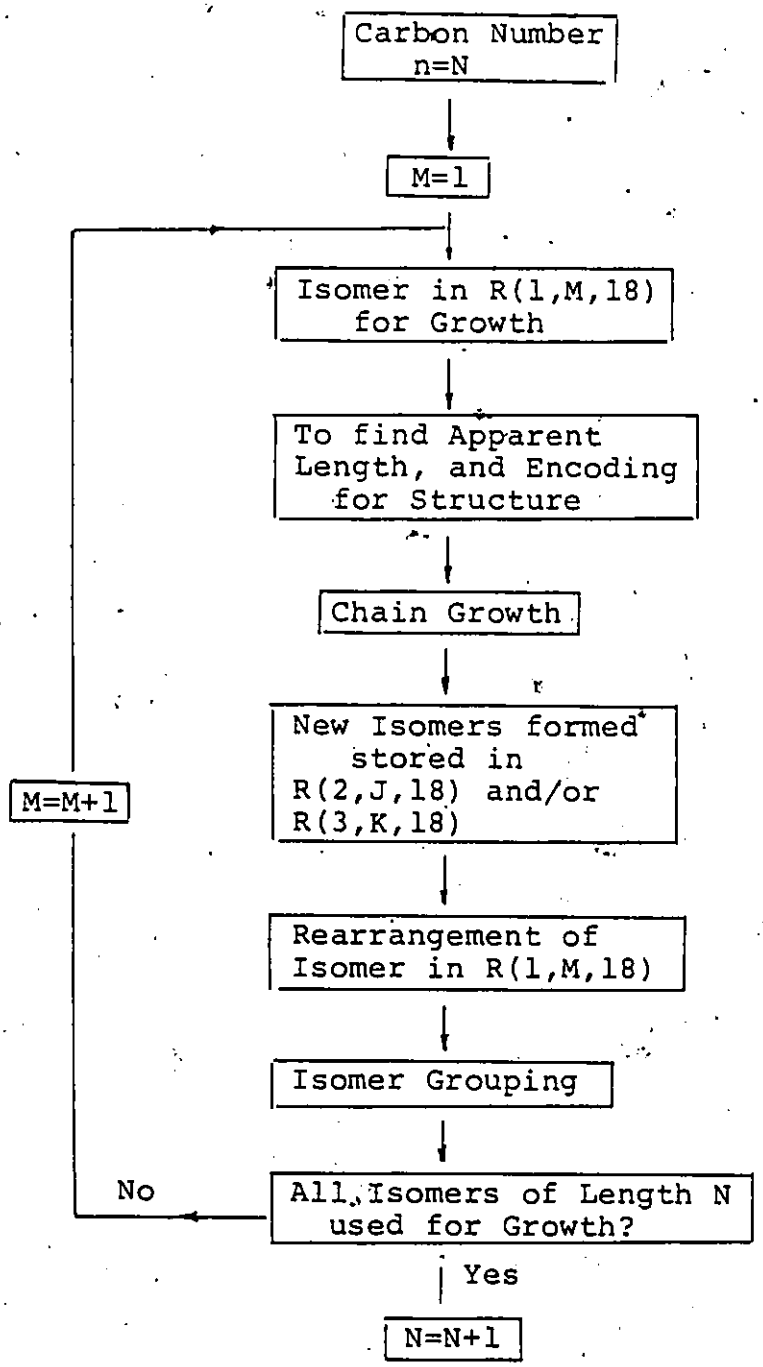

Figure 6-1 Chain Growth Simulation Flow Diagram

rearrangement (if applicable), and (3) isomer grouping. However, there are many intermediate isomers as the carbon number increases. Thus, one has to have means of recording and ordering all these various isomers of carbon number n. It is convenient to use a two-dimensional array or matrix of dimension m by 18. Hence, there are m vectors representing m isomer species and their concentrations. The isomers are stored in these vectors sequentially as they are formed. The maximum number of isomer species that can be obtained depends on the carbon number n as well as on the particular growth scheme under consideration.

In the chain growth process, isomers of carbon number n are employed to generate various isomers of carbon number n+1 for single carbon addition, and of carbon number n+2 for two-carbon addition. In view of this, three matrices have to be present, one for chain growth process, and the other two to store the new isomers and their respective concentrations. Thus, one needs a three dimensional array or matrix block for this purpose. This block R will have dimension of 3 by m by 18. In R(1,m,18) will be stored all the ordered isomers with their respective concentrations of carbon number n. Each of these isomers will be examined, tested and subjected to the chosen set of chain growth rules, generating m2, say, of isomer intermediates of carbon number n+1, and m3, say, of isomers of carbon number n+2. These isomers of carbon numbers n+1 and n+2 and their concentrations are now stored in matrices R(2,m,18) and

R(3,m,18), respectively. Isomers in matrix R(1,m,18) are then subjected to the process of isomer intermediate rearrangement and isomer grouping, and their concentrations are accumulated.

Information in matrix R(1,m,18) is no longer useful and is erased. Information from R(2,m,18) is then transferred to R(1,m,18). Similarly information in matrix R(2,m,18) is erased and used to store information transferred from matrix R(3,m,18). Finally, all information in matrix R(3,m,18) is also erased. Now isomers of carbon number n+1 in R(1,m,18) are subjected to the process of chain growth giving further isomers of carbon number n+2, which are then stored in matrix R(2,m,18). Similarly two carbon addition rules will yield isomers of carbon number n+3 to be stored in the blank matrix R(3,m,18). These processes are illustrated by the flow diagrams in figure 6-2.

The above is concerned with the methods of storing information about the isomers, and how this can be achieved by using three matrices. The actual implementation is complicated by the fact that there could be a shortage of computer space if certain modifications are not taken. The main reason that Chan's work (216) was limited to data on carbon numbers 6 - 9 is that overflow of information occurs. By imposing extra constraints on the various growth schemes, this storage problem can be avoided. These constraints and the other details of calculation are contained in the subroutine FUN. This program FUN performs, given values of branching probabilities f and g, the calculation of the

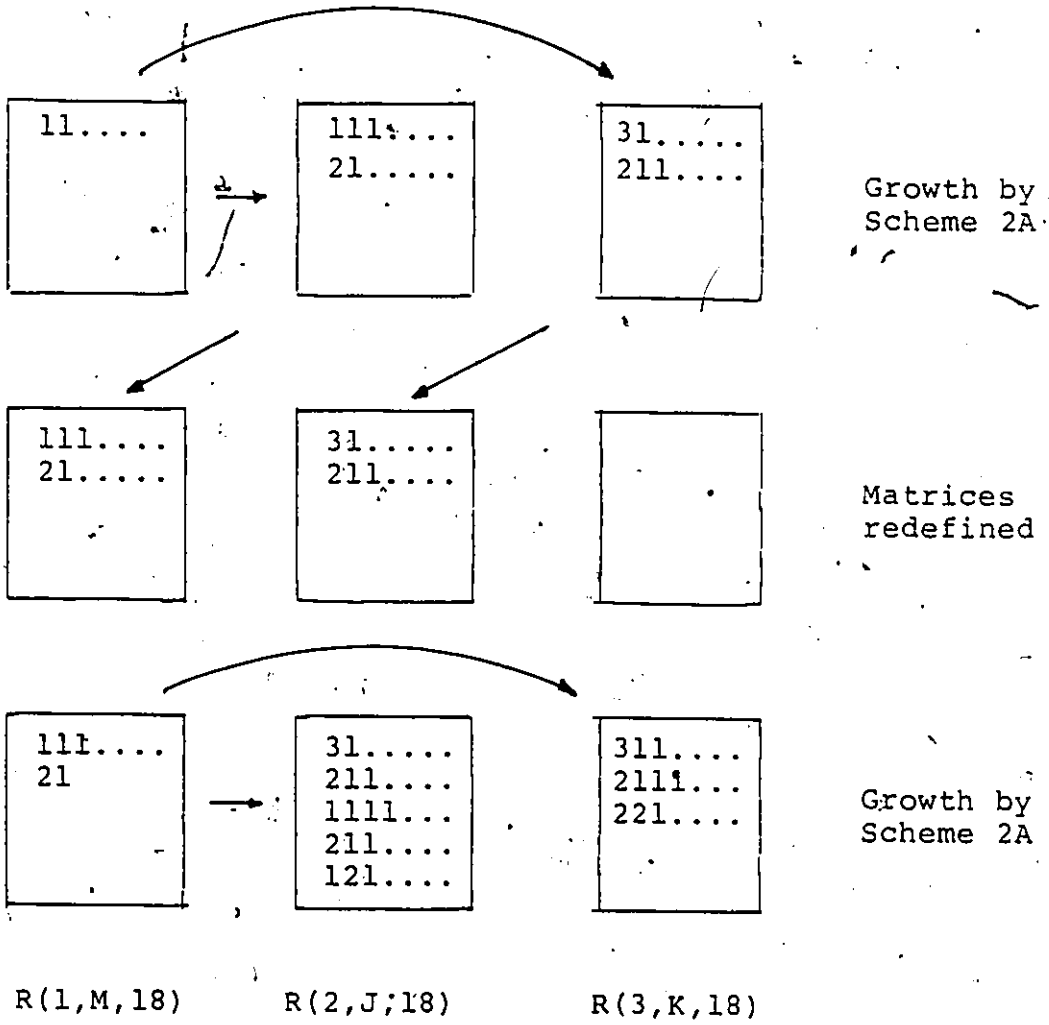

Figure 6-2 Chain Growth and Storage of Information on Matrices

normalized concentrations of various isomers in all carbon fractions, up to carbon number 17.

The program performs the following steps:

(1) to find the apparent length of the intermediate isomers and encode the structure of the growing end of the carbon chain;

(2) to perform the actual isomer growth process;

(3) to rearrange the isomers to the proper product form;

(4) to identify the product isomers and to calculate their concentrations by isomer grouping.

Whether an isomer can grow according to a chosen chain growth scheme depends on the structure of this isomer. Thus, in all the growth schemes considered, one does not allow addition at the penultimate carbon by single carbon addition if this carbon has already a methyl group. However, storage problem will be encountered if the growth rules are strictly followed. Extra constraints or rules have to be implemented to circumvent this problem. These constraints consist of prohibiting chain growth which would result in an isomer that is absent in the product. In this regard knowledge of the growing isomer structure and carbon number is important.

Information on the 'expected' length of the carbon chain is important and is stored as LEM. To find LEM the apparent length LIM of the isomer is found first. This is given by the number of spaces in the description vector that store non-zero numbers. Thus, isomer (11213100000000000 z) has apparent length of 6. The 'expected' length LEM is 7 since the

non-growing end ---31... will be rearranged to give ---21100..., thereby increasing the length by one. For this particular isomer, growth at the penultimate carbon is curtailed since trimethyl species are absent in carbon numbers of 10 or larger.

In addition to the 'expected' length, additional information on the structure of the non-growing end of the chain is also necessary. Codes are assigned to describe the structure at the non-growing end. Thus, species of structure such as (11113100...) or (112111300...) are assigned codes of SIGNAL = 5 and SIGNAL = 2, respectively. Other species such as (1211100...) or (112112100...) etc. are all assigned SIGNAL = 0. These codes are necessary to account for the fact that some of these end groups are no longer ethyl species after rearrangement. Both the values of LEM and SIGNAL are used in controlling the growth of species in the one-carbon addition schemes. The structure of the growing species is also examined to see if it contains an apparent methyl or ethyl group in the carbon chain. Presence of a methyl group is signified by TT = 2 and an ethyl group by TE = 3. Otherwise they are assigned values of 0.

For chain growth schemes in which two-carbon addition is allowed, codes also have to be assigned to describe the structure of the growing end, because of the possible presence of structures such as (31121100...) or (2311100...) etc. The presence of unit 3 at the growing end may conflict with its presence elsewhere in the carbon chain, particularly

the non-growing end. Thus, a new coding system is necessary in this case. The presence of unit ....3100.... at the non-growing end, e.g. (112113100....) is coded as SIGL = 3; otherwise SIGL = 0. When unit such as 3... appears at the growing end such as (3112100....), code SIGR = 3 is assigned; otherwise SIGR is given value of 0. The presence of unit 3 anywhere in the carbon chain is given by TE = 3. Values assigned to LEM are obtained as in the case of one-carbon addition chain growth schemes.

Whether a certain growth step is allowed or not depends on the particular chain growth scheme under consideration as well as the extra constraints imposed by the absence of certain isomers in the products. By monitoring the carbon number and the apparent structure of the species through the use of different codes and the expected length LEM, chain growth is prohibited if it results in a compound which is not identified in the product.

To test the validity of the different chain growth schemes with the extra constraints, the isomer intermediates generated are printed out in their vector forms. The number of isomers obtained and their structures are checked against those generated manually for isomers up to carbon number 8. The number of isomer intermediates generated by this controlled growth depends on the carbon number and the growth scheme under consideration as shown in table 6-5.

After an intermediate has been subjected to the

Table 6-5

Number of Isomer Intermediates Generated as a Function of Carbon Number

	Growth Schemes					
Carbon No.	1A,1B	1C	1D	2A,2C,2D	2B,2E	2F
2				1	1	1
3	1	1	1	2	2	2
4	3	3	2	5	5	4
5	7	5	3	9	10	7
6	15	9	6	18	22	13
7	32	17	11	37	47	24
8	69	31	20	73	101	44
9	146	56	36	145	215	80
10	155	56	32	183	232	81
11	220	73	41	264	326	106
12	297	92	51	363	436	134
13	75	36	19	101	104	54
14	84	40	21	113	116	60
15	93	44	23	125	128	66
16	102	48	25	137	140	72
17	111	52	27	149	152	78

growth processes, it is rearranged to its proper product form. For one-carbon addition schemes, one needs to be concerned only with the non-growing end of the chain. Thus, species such as (1113100....) and (11211300....) are rearranged to (11121100....) and (1121111100....), respectively. Since for one-carbon additions, species such as (3121$\bar{1}$00....) or (2112100....) with an apparent ethyl or methyl group at the growing end are not generated, further rearrangement is not necessary.

However, when two-carbon addition is allowed, further rearrangement at the growing end of the carbon chain is necessary. This is due to the fact that species such as (3112100....) or (221100....) etc. can be generated. These are rearranged to their product forms. Usually only the first or last three carbon units of the chain need to be examined for rearrangement.

Now all the isomers are in their final product forms but stored at different locations with different concentrations. They have to be identified and their respective concentrations accumulated. Thus 2-methyl-pentane could be stored as (1211100....) at x different vectors, and as (1112100....) in y vectors. Since all these species represent only one product, the total concentration has to be summed. Essentially the logic involved is governed by the actual isomers isolated experimentally. For example, no ethyl substituted isomer is possible until carbon number 7 is reached. Also trimethyl

species are only found in carbon number 8 and 9. These relationships are used in identifying the different isomers of a given carbon number n. The sequences involved are as follows:

(1) identification of normal hydrocarbons;

(2) identification of species with two ethyl groups, or with one ethyl group and two methyl groups;

(3) identification of species with trimethyl or methyl-ethyl groups;

(4) identification of species with only one ethyl or two methyl groups;

(5) identification for species with only one methyl group.

The above identifications can be easily achieved by finding the actual carbon chain length and comparing it with the carbon number n. Identification of various methyl substituted isomers such as 2-methyl, 3-methyl isomers can be done by locating the position of the unit -2- in the carbon chain.

When an isomer of carbon number n is identified, it is placed in the matrix S(n,nn) where n refers to the carbon number, and nn refers to the particular isomer. For example, nn = 7 is reserved for 2,3 -dimethyl substituted isomers; nn = 1 is for normal isomers; and nn = 23 is for 3-ethyl substituted isomers (Table 6-6). The respective concentrations for these identified isomers are accumulated and divided by the concentration of the normal isomer of this

Table 6-6

Identification Number nn of Isomers in Matrix S(n,nn)

nn	Isomer
1	Normal
2	2M
3	3M
4	4M
5	5M
6	6M
7	23DM
8	24DM
9	25DM
10	26DM
11	27DM
12	28DM
13	29DM
14	34DM
15	35DM
16	36DM
17	37DM
18	38DM
19	45DM
20	46DM
21	47DM
22	56DM
23	3E
24	4E
25	5E
26	TM
27	E-M
28	Quadra-M
29	DM-E
30	DE
31	7M
32	8M

M=methyl; DM=dimethyl; TM=trimethyl; E=ethyl, E-M=ethyl-methyl; DM-E=dimethyl-ethyl; DE=diethyl

carbon number. These normalized predicted concentrations are compared with the normalized experimental concentrations. The sum of squares of errors for all available species and for all carbon numbers (nn = 1 to 32; n = 4 to 17) are calculated to give the objective function which is to be minimized by choosing appropriate values of f and g.

$$SS = \sum_{n=4}^{17} \sum_{nn=1}^{32} (y_{n,nn} - y'_{n,nn})^2 \qquad (6\text{-}12)$$

where SS = error sum of squares

y = normalized experimental concentration

y' = normalized predicted concentration

6.5 Estimation of Growth Constants

In testing the various chain growth schemes, values of the growth constants f and g are searched by optimization techniques to give minimum values for the error sum of squares (equation 6-12). One of the powerful techniques in optimization is the conjugate gradient methods (217 - 220). In any minimization (or maximization) problem, two fundamental steps can be identified: the choice of direction of search in the parameter space, and the distance moved in the chosen direction. In the Fletcher and Reeves method (219), after a direction is chosen, a linear search will proceed until a minimum in the objective function along that chosen direction is obtained. Then a new direction which is conjugate to the previous one is generated. Linear search is again done

along this newly generated direction until a minimum is obtained. Thus, each move consists of a linear search for a minimum for a chosen direction, and the generation of a new direction conjugate to the previous one to be used in the next move. After p moves (for a function involving p parameters), p linear searches would have been done in p conjugate directions, and for a quadratic function, the minimum will be located at the p th linear search.

In the conjugate gradient methods, the generation of a new direction of move involves the calculation of the gradients of the objective function. According to Fletcher and Reeves (219), the conjugate direction can be obtained by the recursion relationship:

$$\underline{z}^{(k)} = - \nabla\psi(\underline{x}^{(k)}) + \beta^{(k-1)}\, \underline{z}^{(k-1)} \qquad (6\text{-}13)$$

where

$$\beta^{(k-1)} = \frac{\nabla\psi(\underline{x}^{(k)})^T \nabla\psi(\underline{x}^{(k)})}{\nabla\psi(\underline{x}^{(k-1)})^T \nabla\psi(\underline{x}^{(k-1)})} \qquad (6\text{-}14)$$

$\underline{z}$ = direction vector;

$y = \psi(\underline{x})$, the objective function to be minimized;

$\underline{x}$ = parameter vector.

The derivations depend on the properties of conjugacy as well as the following relationship:

$$(\underline{z}^{(k)})^T \nabla\psi(\underline{x}^{(k+1)}) = 0 \qquad (6\text{-}15)$$

The latter relationship implies that the linear search along direction $\underline{z}^k$ is continued until a point is found at which the gradient of the objective function is orthogonal to the direction of search, i.e. search until the optimum is located in this direction.

A linear search for the minimum along a chosen direction can be divided into two parts. First, the region in which the minimum lies is located. In this regard, a direct search due to Swann (221) is used. The objective function is evaluated at a sequence of points along the chosen direction $\underline{z}$:

$$\underline{x}^{(0)},\ \underline{x}^{(1)} = \underline{x}^{(0)} + s\underline{z},\ \underline{x}^{(2)} = \underline{x}^{(1)} + 2s\underline{z},\ \ldots, \underline{x}^{(k)} = \underline{x}^{(k-1)} + 2^{(k-1)}s\underline{z}$$

where s is the step size, and $\underline{x}^{(k)}$ is the first position tested which fails to yield a decrease in the value of the objective function:

$$y^{(0)} > y^{(1)} > y^{(2)} > \ldots\ldots y^{(k-1)} \leqslant y^{(k)}$$

Thus the minimum lies in the interval between $\underline{x}^{(k-1)}$ and $\underline{x}^{(k)}$. The step size s should be the same order of magnitude as that of $\left|\underline{x}^* - \underline{x}^{(0)}\right|$ where $\underline{x}^{(0)}$ is the starting point and $\underline{x}^*$ is the optimal value of $\underline{x}$.

The second part of the linear search consists of finding the optimal $\underline{x}^*$ (to within a given tolerance) in the region in which the optimal is located. To this end, the modified Fibonacci (222) search technique proves to be very efficient.

This method has the merit that only one additional test point is needed each time the values of the objective function are to be compared.

6.6 Organization of programs

The simulation of the Fischer-Tropsch chain growth process according to the various schemes was done with a CDC 6400 computer. The computer programs consist of one executive program and four subprograms. The executive program essentially reads in trial values of growth constants f and g. Operation is then transferred to the program CONJUG the function of which is to generate the gradient directions and to test for convergence. It calls on program UNISER for linear search for minimum in the objective function along the generated gradient direction. Program DIREC is also called by CONJUG to calculate the gradient of the objective function. Both programs UNISER AND DIREC call the program FUN to calculate the value of the objective function. Program FUN was developed by Anderson and Chan (216). It has been modified so as to extent its applicability up to carbon number 17. When convergence is obtained operation is passed back to the executive program and results printed. Figure 6-3 shows how the programs interact with each other.

To ensure that global minimum value for the error sum of squares is obtained, different trial values of f and g are used. In all cases studied, they all converge to the same optimal values for the respective growth schemes and data set.

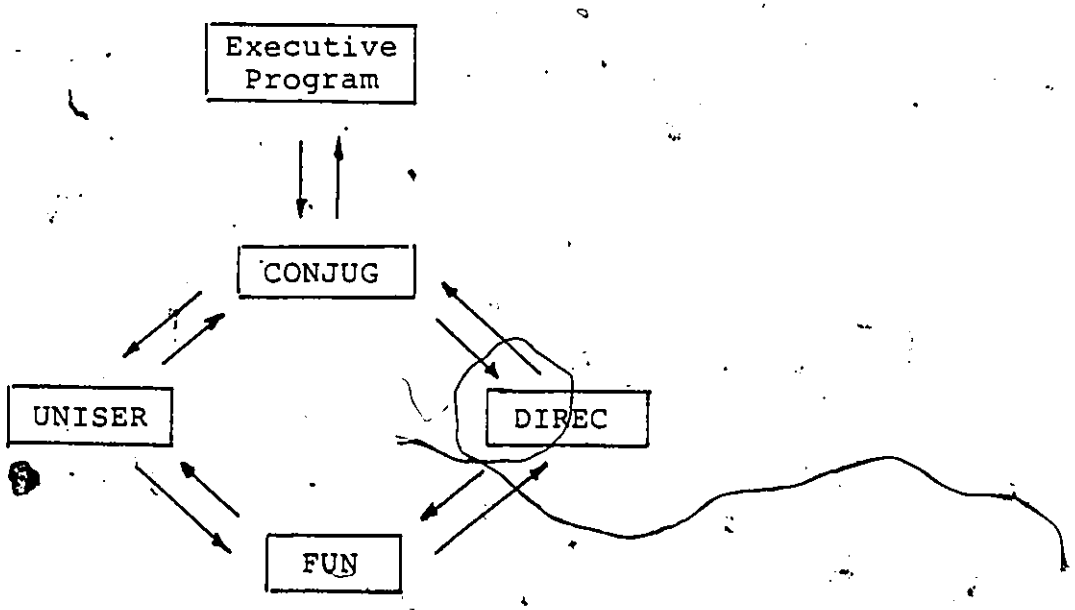

Figure 6-3 Organization of Programs

6.7 Results and Discussion

6.7.1 General

To test the different proposed chain growth schemes, data of Pichler et al. (215) were used. The data consist of hydrogenated hydrocarbon from a fixed-bed reactor with precipitated cobalt catalyst at atmospheric pressure and 463 K, and from the entrained reactors with reduced fused iron catalyst at 22 atmospheres and 593 K. The hydrocarbons included olefins which were saturated by hydrogenation before capillary gas chromatography analysis. The cobalt catalyst yielded all aliphatic compounds while the products from the iron catalyst contained, in some carbon number fractions, significant portion of aromatics and naphthenes. The iron data also showed a higher percentage of unknowns. Only the aliphatic hydrocarbons from both catalysts were used for testing the various chain growth schemes. It is believed this is the only readily available data in the literature of detailed isomer distribution of Fischer-Tropsch synthesis of hydrocarbons up to carbon number 17.

The amount of branched isomers relative to the normal hydrocarbons (hereafter termed 'normalized' amount) increases with carbon number, from some 5 to 55 and 70 % for cobalt and iron data, respectively. Though the fraction of normal hydrocarbon decreases with increasing carbon number they still constitute a significant portion even at carbon number 17. This points to the fact that branching is not favorable

compared to the formation of straight chain species. Weber (222) first noticed a regular increase in branched isomer content with increasing carbon number, and proposed a definite probability of branching at each carbon addition. Figures 6-4 and 6-5 show the change of normal hydrocarbon percentage with carbon number.

As the carbon chains grow, the percentage of the monomethyl substituted species (MSS) in a given carbon number fraction increases. This increase of branched species with carbon number is also true for dimethyl substituted species (DMSS). These trends are shown in figures 6-6 to 6-9.

The isomer distributions from both cobalt and iron catalysts show similarities. In general the normalized amount of 2-methyl (2M) isomer for carbon number fraction 4 is smaller than those of higher carbon numbers, usually about one-half of the subsequent somewhat constant normalized amounts. This observation is also true for any newly formed mono-methyl isomers. For example, the normalized 3-methyl (3M) isomer amounts for iron catalyst have the following values:

Carbon No.	6	7	8	9
Normalized amount	0.143	0.285	0.230	0.218

The normalized amounts of DMSS are much smaller, usually about 1/20 - 1/10 th of those of MSS, and seem to

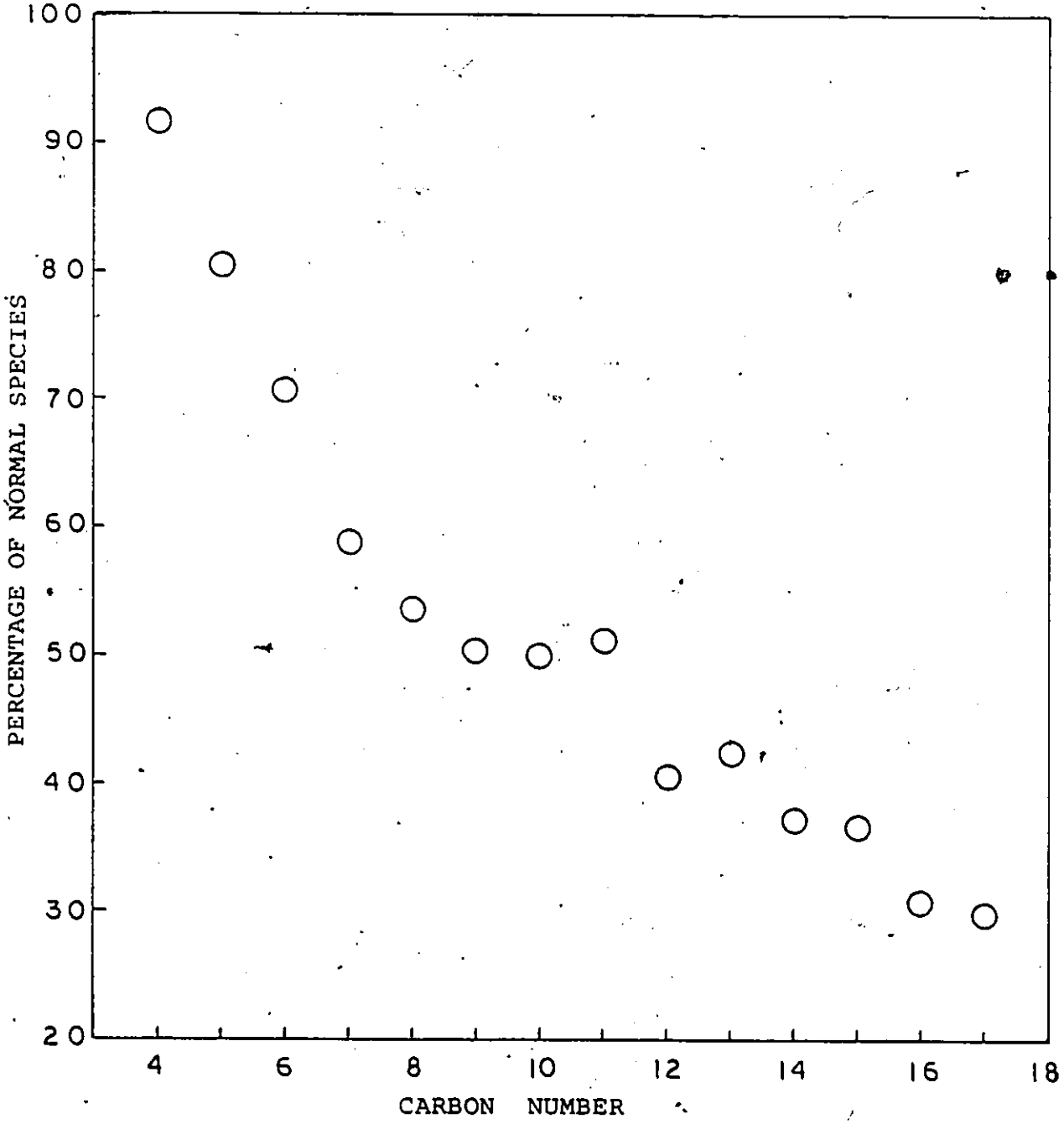

Figure 6-4 Variation of Normal Species with Carbon Number - Iron Data

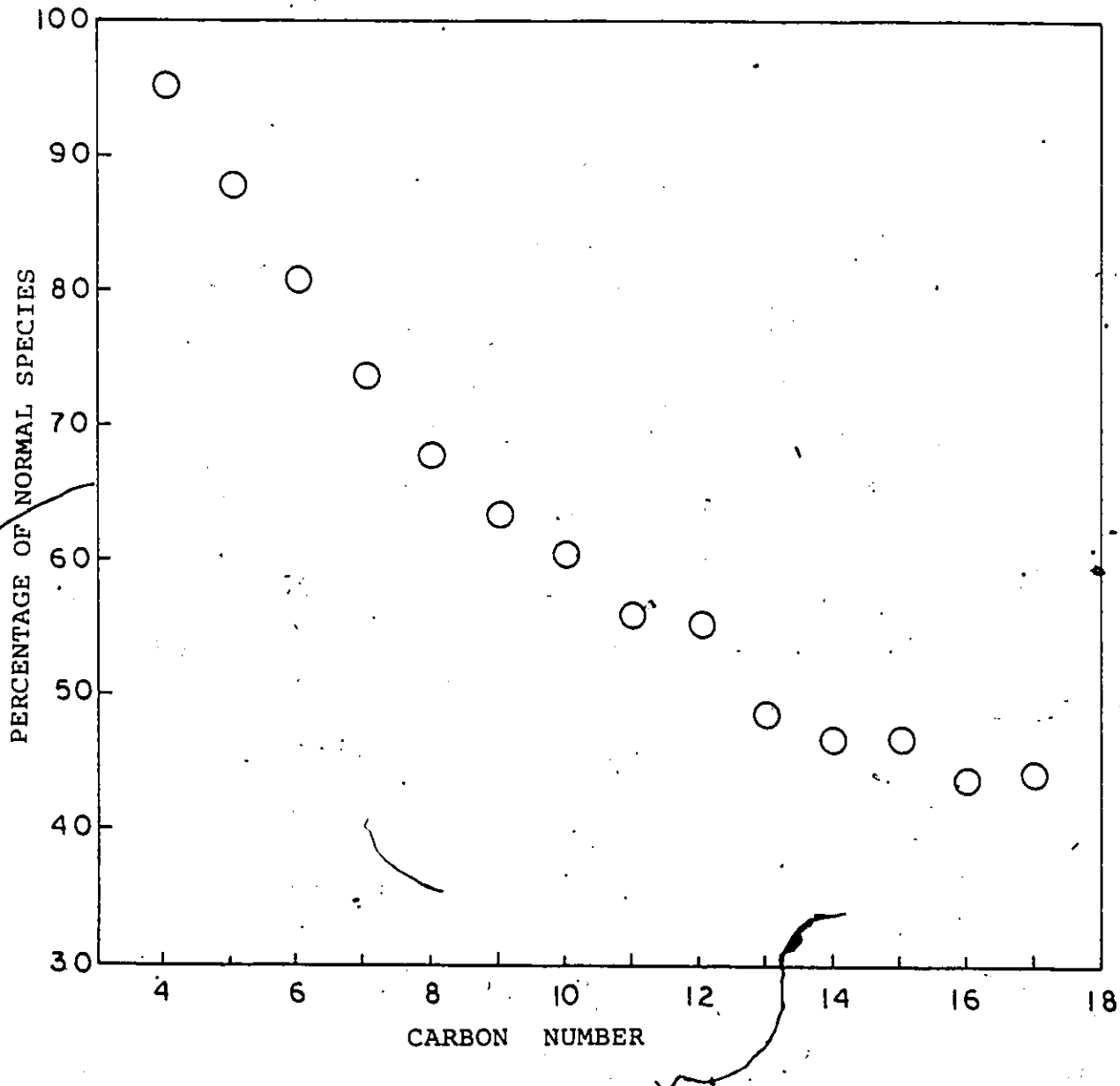

Figure 6-5 Variation of Normal Species with Carbon Number - Cobalt Data

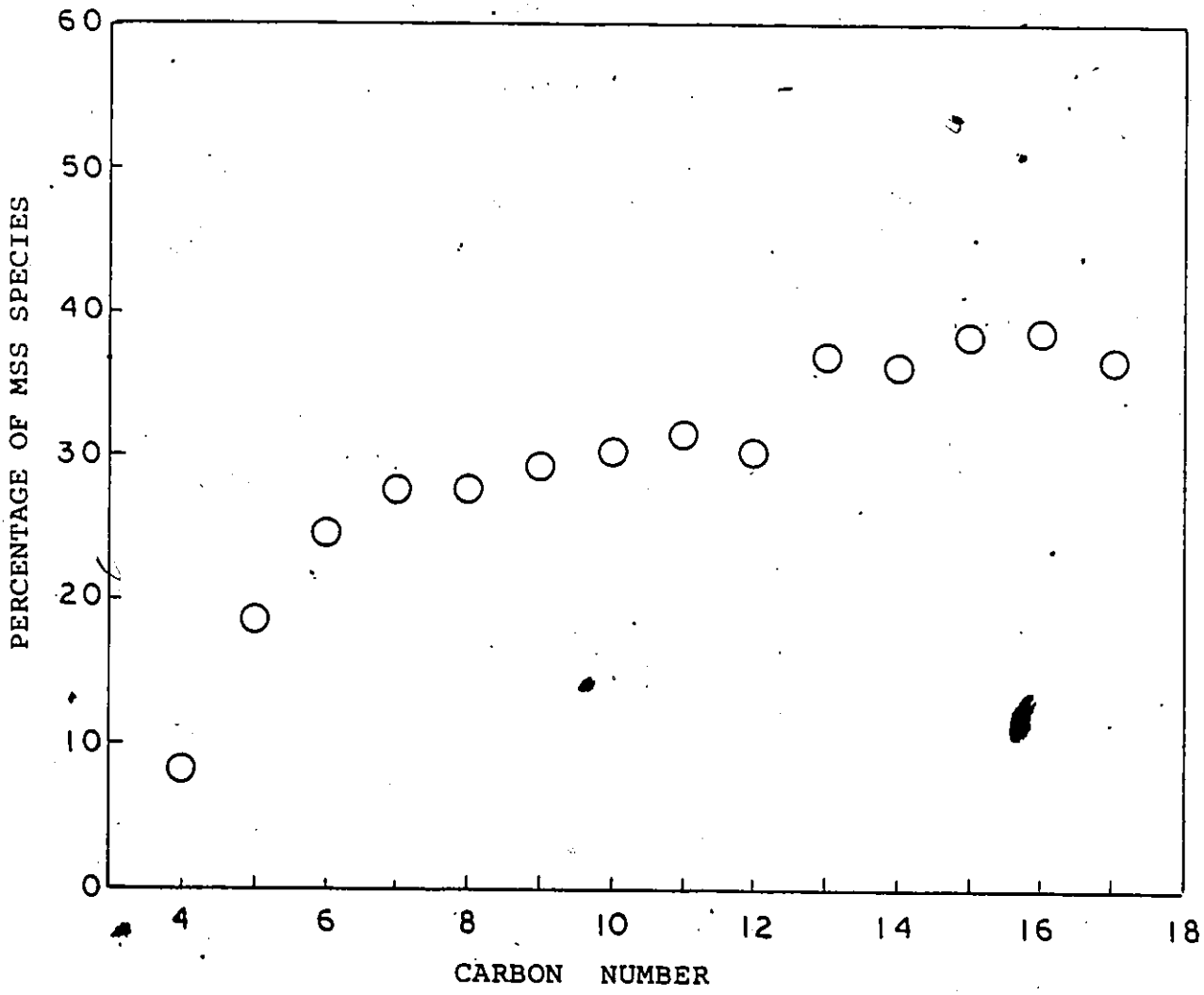

Figure 6-6 Variation of Methyl Substituted Species with Carbon Number - Iron Data

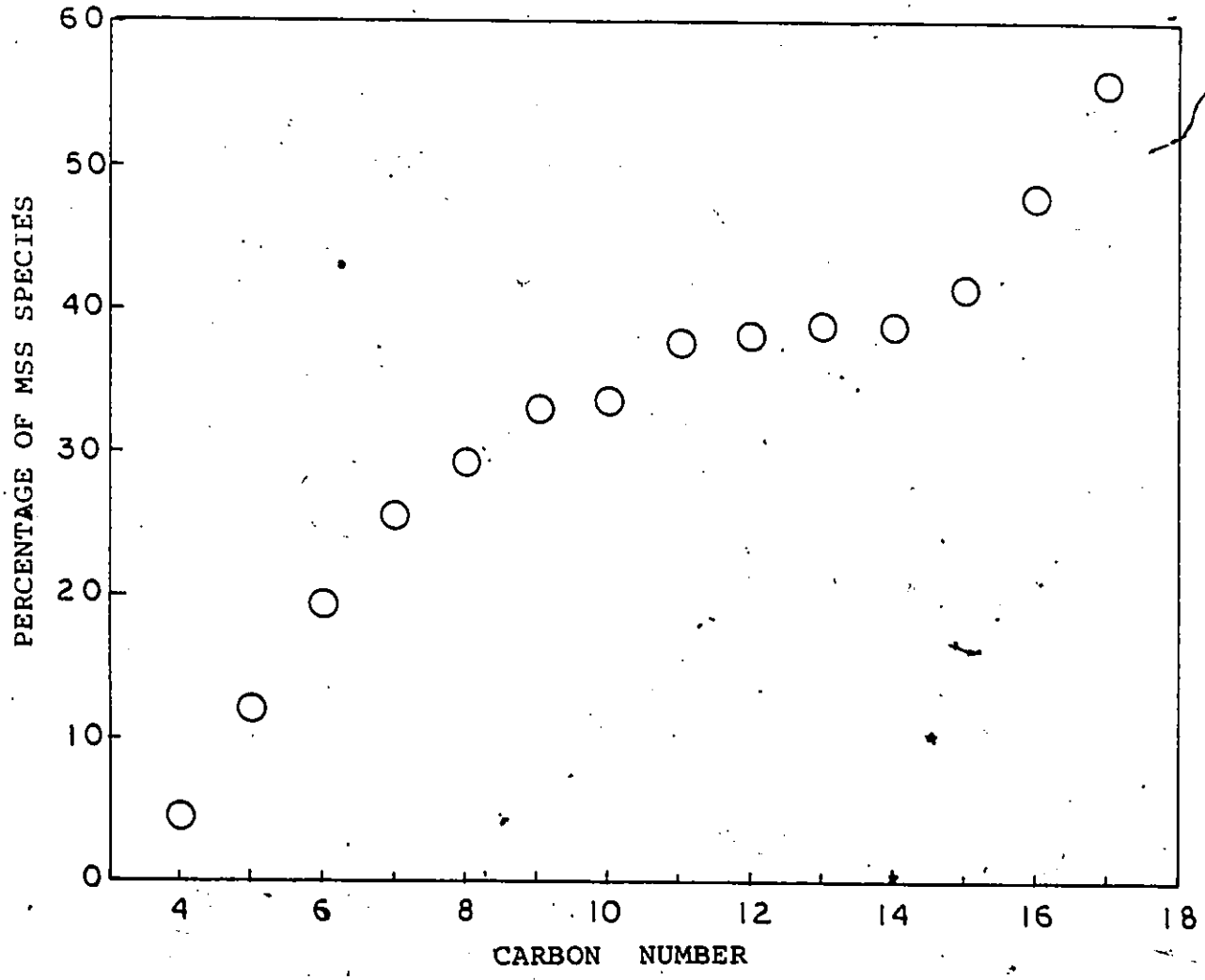

Figure 6-7 Variation of Methyl Substituted Species with Carbon Number - Cobalt

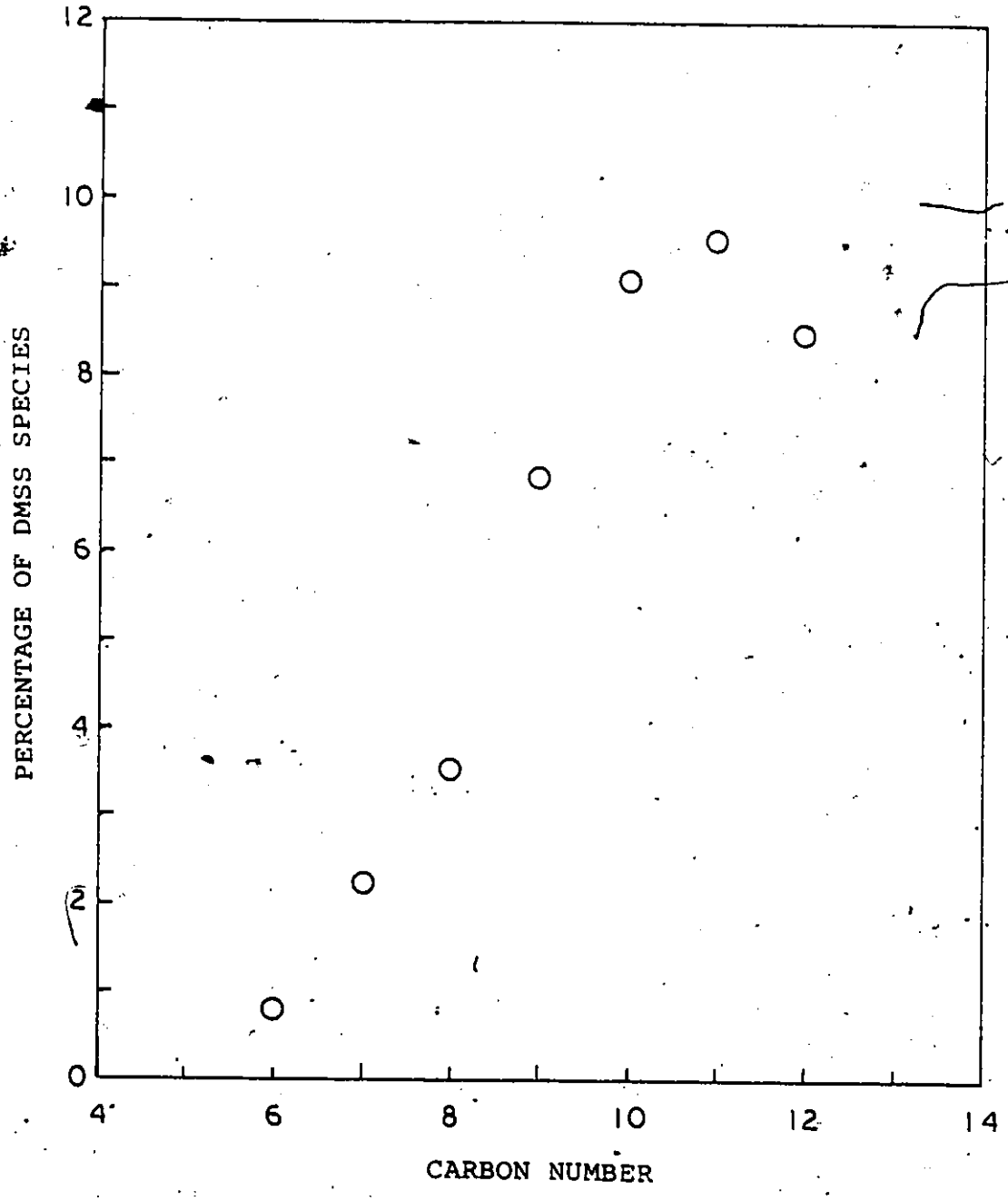

Figure 6-8 : Variation of Dimethyl Substituted Species with Carbon Number - Iron Data

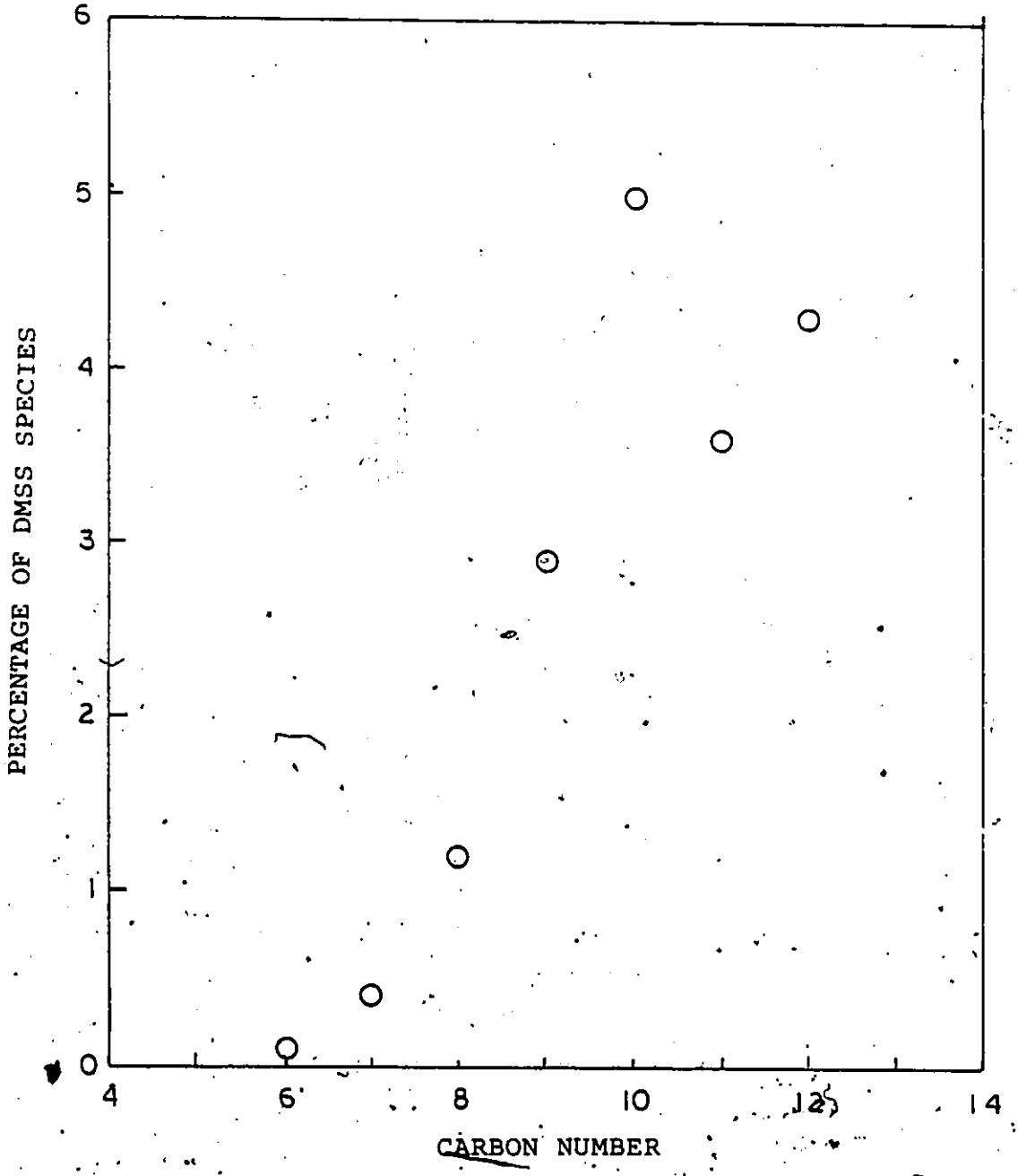

Figure 6-9 Variation of Dimethyl Substituted Species with Carbon Number - Cobalt Data

show a maximum with respect to carbon numbers. However it is difficult to say whether this is a definite trend or a mere result of inaccuracy in the analysis since low concentrations are involved.

The first ethyl substituted species (ESS) appear in the heptane fraction. The normalized amounts of 3-ethyl (3E) isomers show a maximum with respect to carbon numbers for the cobalt data. For the iron data, except for 3-ethyl pentane, the amounts generally decrease with carbon number.

For a meaningful discussion of the performance of the various growth schemes investigated, one must have criteria by which this can be judged. These criteria have to be more than just a mere examination of the error sum of squares. A reasonable scheme should be able to produce the trends reflected by the experimental data as discussed above. Since one of the main concerns is the amount of ESS, an important criterion is that the scheme should be able to predict reasonably well the amounts of ESS.

Generally speaking all the growth schemes were able to predict the analytical data quite well, often to within the experimental uncertainties of separating and identifying the various isomers in these complex hydrocarbon mixtures, especially the higher carbon number fractions. The results of the various chain growth schemes are shown in Tables 6-7 and 6-8 for iron and cobalt data, respectively.

Of the four one-carbon addition schemes tested with

Table 6-7

Predicted Isomer Distribution for Product from Entrained Iron

Ratio of Branched-to-Normal Species

Carbon No.	Isomer	Expt.	1A	1B	1C	1D	2A	2B	2C	2D	2E	2F
4	2M	.0917	.0763	.0865	.0858	.0893	.0692	.0688	.0800	.0419	.0824	.0798
5	2M	.2335	.1659	.1787	.1911	.1786	.1705	.1711	.1726	.1445	.1750	.1847
6	2M	.2065	.1670	.1787	.1733	.1786	.1591	.1585	.1726	.1302	.1748	.1682
	3M	.1429	.1051	.0922	.1247	.1098	.1168	.1185	.0936	.1223	.0931	.1246
	23DM	.0113	.0069	.0080	.0075	.0080	.0053	.0063	.0070	.0020	.0076	.0071
7	2M	.1891	.1670	.1787	.1733	.1786	.1591	.1585	.1726	.1302	.1748	.1682
	3M	.2845	.1972	.1845	.2126	.1991	.2086	.2099	.1867	.2165	.1858	.2133
	23DM	.0307	.0164	.0165	.0184	.0178	.0141	.0166	.0151	.0075	.0162	.0179
	24DM	.0068	.0069	.0080	.0075	.0080	.0063	.0063	.0075	.0039	.0076	.0071
	3E	.0136	.0145	.0000	.0194	.0206	.0145	.0149	.0005	.0177	.0002	.0197
8	2M	.1940	.1670	.1787	.1733	.1786	.1591	.1585	.1726	.1302	.1748	.1682
	3M	.2295	.1972	.1845	.2126	.1991	.2086	.2096	.1867	.2165	.1858	.2133
	4M	.0970	.0921	.0922	.0875	.0893	.0914	.0912	.0931	.0931	.0927	.0884
	23DM	.0243	.0154	.0165	.0152	.0159	.0122	.0145	.0151	.0061	.0162	.0149
	24DM	.0187	.0164	.0165	.0184	.0178	.0166	.0166	.0161	.0142	.0162	.0179
	25DM	.0093	.0069	.0080	.0075	.0080	.0063	.0063	.0075	.0039	.0076	.0071
	34DM	.0131	.0097	.0085	.0113	.0098	.0093	.0110	.0082	.0068	.0086	.0114
	TM	.0037	.0006	.0007	.0007	.0007	.0004	.0006	.0006	.0001	.0007	.0006
	EM	.0037	.0024	.0000	.0034	.0037	.0021	.0024	.0001	.0016	.0000	.0033
	3E	.0280	.0291	.0001	.0393	.0411	.0293	.0300	.0010	.0366	.0005	.0398

Table 6-7 (continued)

Carbon No.	Isomer	Expt.	1A	1B	1C	1D	2A	2B	2C	2D	2E	2F
9	2+4M	.3658	.3512	.3631	.3484	.3571	.3419	.3408	.3589	.3164	.3602	.3450
	3M	.2167	.1972	.1845	.2126	.1991	.2086	.2099	.1867	.2165	.1858	.2133
	23DM	.0219	.0154	.0165	.0152	.0159	.0122	.0145	.0151	.0061	.0162	.0149
	24DM	.0139	.0154	.0165	.0152	.0159	.0145	.0145	.0161	.0121	.0162	.0149
	25+35DM	.0378	.0261	.0250	.0297	.0276	.0275	.0276	.0248	.0259	.0249	.0293
	26DM	.0199	.0069	.0080	.0075	.0080	.0063	.0063	.0075	.0039	.0076	.0071
	34DM+4E	.0418	.0328	.0170	.0384	.0383	.0310	.0342	.0168	.0297	.0175	.0389
	3E	.0239	.0291	.0001	.0393	.0411	.0293	.0300	.0010	.0366	.0005	.0398
	TM	.0032	.0028	.0030	.0029	.0030	.0020	.0027	.0026	.0007	.0029	.0028
10	2M	.1620	.1670	.1787	.1733	.1786	.1591	.1585	.1726	.1302	.1748	.1682
	3M	.1960	.1972	.1845	.2126	.1991	.2086	.2096	.1867	.2165	.1858	.2133
	4M	.1680	.1843	.1844	.1750	.1786	.1827	.1823	.1863	.1861	.1854	.1768
	5M	.0800	.0921	.0922	.0875	.0893	.0914	.0912	.0931	.0931	.0927	.0884
	23+34DM +4E	.0680	.0629	.0335	.0734	.0748	.0581	.0634	.0324	.0546	.0339	.0738
	24DM	.0120	.0154	.0165	.0152	.0159	.0145	.0145	.0161	.0121	.0162	.0149
	25+35DM	.0360	.0336	.0335	.0338	.0337	.0336	.0336	.0335	.0323	.0334	.0337
	26DM	.0300	.0164	.0165	.0184	.0178	.0166	.0166	.0161	.0142	.0162	.0179
	27DM	.0140	.0069	.0080	.0075	.0080	.0063	.0063	.0075	.0039	.0076	.0071
	36DM	.0200	.0097	.0085	.0113	.0098	.0109	.0110	.0088	.0117	.0086	.0114
	3E	.0220	.0291	.0001	.0393	.0411	.0293	.0300	.0010	.0366	.0005	.0398
11	2M	.1487	.1670	.1787	.1733	.1786	.1591	.1585	.1726	.1302	.1748	.1682
	3M	.2016	.1972	.1845	.2126	.1991	.2086	.2096	.1867	.2165	.1858	.2133
	4M	.1389	.1843	.1844	.1750	.1786	.1827	.1823	.1863	.1861	.1854	.1768
	5M	.1311	.1843	.1844	.1750	.1786	.1827	.1823	.1863	.1861	.1854	.1768
	23+34DM	.0646	.0336	.0335	.0338	.0337	.0283	.0336	.0314	.0169	.0334	.0337

Table 6-7 (continued)

Carbon No.	Isomer	Expt.	1A	1B	1C	1D	2A	2B	2C	2D	2E	2F
11	24DM	.0098	.0154	.0165	.0152	.0159	.0145	.0145	.0161	.0121	.0162	.0149
	25+35DM	.0313	.0336	.0335	.0338	.0337	.0336	.0336	.0335	.0323	.0334	.0337
	26DM	.0176	.0154	.0165	.0152	.0159	.0145	.0145	.0161	.0121	.0162	.0149
	27DM	.0254	.0164	.0165	.0184	.0178	.0166	.0166	.0161	.0142	.0162	.0179
	28+36DM	.0294	.0251	.0250	.0261	.0257	.0254	.0254	.0248	.0240	.0249	.0259
	37DM	.0078	.0097	.0085	.0113	.0098	.0109	.0110	.0087	.0117	.0086	.0114
	3E	.0196	.0291	.0001	.0393	.0411	.0293	.0300	.0010	.0366	.0005	.0397
	4E	.0098	.0293	.0001	.0397	.0411	.0297	.0302	.0010	.0377	.0005	.0401
	5E	.0137	.0147	.0000	.0198	.0206	.0149	.0151	.0005	.0189	.0002	.0200
12	2M	.1605	.1670	.1787	.1733	.1786	.1591	.1585	.1726	.1302	.1748	.1682
	3M	.1951	.1972	.1845	.2116	.1991	.2086	.2099	.1867	.2165	.1858	.2133
	4M	.1580	.1843	.1844	.1750	.1786	.1827	.1823	.1863	.1861	.1854	.1768
	5M	.1531	.1843	.1844	.1750	.1786	.1827	.1823	.1863	.1861	.1854	.1768
	6M	.0840	.0921	.0922	.0875	.0893	.0914	.0912	.0931	.0931	.0927	.0884
	24DM	.0469	.0154	.0165	.0152	.0159	.0145	.0145	.0161	.0121	.0162	.0159
	25+35DM +26DM	.0469	.0489	.0500	.0490	.0497	.0481	.0480	.0495	.0444	.0496	.0486
	27DM	.0198	.0154	.0165	.0152	.0159	.0145	.0145	.0161	.0121	.0162	.0149
	28DM	.0346	.0164	.0165	.0184	.0178	.0166	.0166	.0161	.0142	.0162	.0179
	29+37DM	.0395	.0251	.0250	.0261	.0258	.0254	.0254	.0248	.0240	.0249	.0259
	36DM	.0022	.0182	.0170	.0186	.0178	.0191	.0191	.0174	.0201	.0172	.0189
	38DM	.0173	.0097	.0085	.0113	.0098	.0109	.0110	.0087	.0117	.0086	.0114
	3E	.0196	.0291	.0001	.0393	.0411	.0293	.0300	.0010	.0366	.0005	.0397
	4E	.0617	.0293	.0001	.0397	.0411	.0297	.0302	.0010	.0377	.0005	.0401
	5E	.0395	.0293	.0001	.0397	.0411	.0297	.0302	.0010	.0377	.0005	.0401

Table 6-7 (continued)

Carbon No.	Isomer	Expt.	1A	1B	1C	1D	2A	2B	2C	2D	2E	2F
13	2M	.1840	.1670	.1787	.1733	.1786	.1591	.1585	.1726	.1302	.1748	.1682
	3M	.2005	.1972	.1845	.2126	.1991	.2086	.2099	.1867	.2165	.1858	.2133
	4M	.1698	.1843	.1844	.1750	.1786	.1827	.1823	.1863	.1861	.1854	.1768
	5M	.1627	.1843	.1844	.1750	.1786	.1827	.1823	.1863	.1861	.1854	.1768
	6M	.1680	.1843	.1844	.1750	.1786	.1827	.1823	.1863	.1861	.1854	.1768
	3E	.0189	.0291	.0001	.0393	.0411	.0293	.0300	.0010	.0366	.0005	.0397
14	2M	.1671	.1670	.1787	.1733	.1786	.1591	.1585	.1726	.1302	.1748	.1682
	3M	.1887	.1972	.1845	.2126	.1991	.2086	.2099	.1867	.2165	.1858	.2133
	4M	.1752	.1843	.1844	.1750	.1786	.1827	.1823	.1863	.1861	.1854	.1768
	5M	.1483	.1843	.1844	.1750	.1786	.1827	.1823	.1863	.1861	.1854	.1768
	6+7M	.2992	.2764	.2767	.2626	.2678	.2741	.2735	.2794	.2792	.2781	.2653
	3E	.0647	.0291	.0001	.0393	.0411	.0293	.0300	.0010	.0366	.0005	.0397
15	2M	.1662	.1670	.1787	.1733	.1786	.1591	.1585	.1726	.1302	.1748	.1682
	3M	.2125	.1972	.1845	.2126	.1991	.2086	.2099	.1867	.2165	.1858	.2133
	4M	.1717	.1843	.1844	.1750	.1786	.1827	.1823	.1863	.1861	.1854	.1768
	5M	.1526	.1843	.1844	.1750	.1786	.1827	.1823	.1863	.1861	.1854	.1768
	6M	.1635	.1843	.1844	.1750	.1786	.1827	.1823	.1863	.1861	.1854	.1768
	7M	.1771	.1843	.1844	.1750	.1786	.1827	.1823	.1863	.1861	.1854	.1768
	3E	.0109	.0291	.0001	.0393	.0411	.0293	.0300	.0010	.0366	.0005	.0397

Table 6-7 (continued)

Carbon No.	Isomer	Expt.	1A	1B	1C	1D	2A	2B	2C	2D	2E	2F
16	2M	.2190	.1670	.1787	.1733	.1786	.1591	.1585	.1726	.1302	.1748	.1682
	3M	.2941	.1972	.1845	.2126	.1991	.2086	.2099	.1867	.2165	.1858	.2133
	4M	.1961	.1843	.1844	.1750	.1786	.1827	.1823	.1863	.1861	.1854	.1768
	5M	.1961	.1843	.1844	.1750	.1786	.1827	.1823	.1863	.1861	.1854	.1768
	6M	.1863	.1843	.1844	.1750	.1786	.1827	.1823	.1863	.1861	.1854	.1768
	7+8M	.1732	.2764	.2767	.2626	.2678	.2741	.2735	.2794	.2792	.2781	.2653
17	2M	.1717	.1670	.1787	.1733	.1786	.1591	.1585	.1726	.1302	.1748	.1682
	3M	.2323	.1972	.1845	.2126	.1991	.2086	.2096	.1867	.2165	.1858	.2133
	4M	.1818	.1843	.1844	.1750	.1786	.1827	.1823	.1863	.1861	.1854	.1768
	5M	.1650	.1843	.1844	.1750	.1786	.1827	.1823	.1863	.1861	.1854	.1768
	6M	.1381	.1843	.1844	.1750	.1786	.1827	.1823	.1863	.1861	.1854	.1768
	7+8M	.3468	.3685	.3689	.3501	.3571	.3655	.3647	.3725	.3723	.3707	.3537

M=methyl, DM=dimethyl, TM=trimethyl, E=ethyl, and EM=ethyl-methyl

Table 6-8

Predicted Isomer Distribution from Fixed-Bed Cobalt Catalyst

Ratio of Branched-to-Normal Species

Carbon No.	Isomer	Expt.	1A	1B	1C	1D	2A	2B	2C	2D	2E	2F
4	2M	.0482	.0711	.0472	.0810	.0817	.0688	.0692	.4991	.0404	.0507	.0761
5	2M	.1389	.1524	.1335	.1680	.1634	.1576	.1582	.1348	.1277	.1368	.1628
6	2M	.1551	.1532	.1336	.1625	.1634	.1513	.1517	.1349	.1250	.1353	.1589
	3M	.0844	.0933	.0890	.0929	.0898	.0973	.0972	.0883	.0938	.0904	.0912
	23DM	.0012	.0059	.0042	.0066	.0067	.0052	.0058	.0027	.0018	.0044	.0063
7	2M	.1535	.1532	.1336	.1625	.1634	.1513	.1617	.1349	.1250	.1353	.1589
	3M	.1943	.1764	.1768	.1744	.1715	.1806	.1804	.1761	.1825	.1777	.1740
	23DM	.0041	.0135	.0118	.0142	.0140	.0124	.0137	.0074	.0059	.0120	.0138
	24DM	.0014	.0059	.0042	.0066	.0067	.0057	.0058	.0044	.0038	.0044	.0063
	3E	.0054	.0111	.0015	.0059	.0081	.0080	.0076	.0018	.0048	.0017	.0046
8	2M	.1488	.1532	.1336	.1625	.1634	.1513	.1517	.1349	.1250	.1353	.1589
	3M	.1812	.1764	.1768	.1744	.1715	.1806	.1804	.1761	.1825	.1777	.1740
	4M	.1002	.0832	.0877	.0815	.0817	.0832	.0831	.0877	.0884	.0872	.0828
	23DM	.0044	.0127	.0117	.0132	.0134	.0114	.0126	.0073	.0055	.0118	.0132
	24DM	.0074	.0135	.0118	.0142	.0140	.0137	.0137	.0119	.0115	.0120	.0138
	25DM	.0059	.0058	.0042	.0066	.0067	.0057	.0058	.0044	.0036	.0044	.0063
	3E	.0250	.0224	.0030	.0119	.0162	.0161	.0153	.0036	.0099	.0035	.0091
9	2+4M	.3428	.3196	.3091	.3255	.3268	.3177	.3179	.3103	.3018	.3097	.3245
	3M	.1785	.1764	.1768	.1744	.1715	.1806	.1804	.1761	.1825	.1777	.1740
	23DM	.0016	.0127	.0117	.0132	.0134	.0114	.0126	.0073	.0055	.0118	.0132
	24DM	.0095	.0127	.0117	.0132	.0136	.0126	.0126	.0118	.0111	.0118	.0132
	25+35DM	.0221	.0212	.0196	.0218	.0214	.0218	.0218	.0197	.0198	.0199	.0214

Table 6-8 (continued)

Carbon No.	Isomer	Expt.	1A	1B	1C	1D	2A	2B	2C	2D	2E	2F
9	26DM	.0032	.0059	.0042	.0066	.0067	.0057	.0058	.0044	.0038	.0044	.0063
	34DM+4E	.0095	.0259	.0170	.0202	.0221	.0217	.0227	.0114	.0133	.0172	.0190
	3E	.0126	.0024	.0030	.0119	.0162	.0161	.0153	.0036	.0099	.0035	.0091
10	2M	.1308	.1532	.1336	.1625	.1634	.1513	.1517	.1349	.1250	.1353	.1589
	3M	.1705	.1764	.1768	.1744	.1715	.1806	.1804	.1761	.1825	.1777	.1740
	4M	.1722	.1663	.1755	.1630	.1634	.1664	.1663	.1754	.1768	.1744	.1656
	5M	.0828	.0832	.0877	.0815	.0817	.0832	.0831	.0877	.0884	.0872	.0828
	23+34DM +4E	.0348	.0499	.0302	.0394	.0436	.0412	.0429	.0206	.0239	.0308	.0367
	24DM	.0066	.0127	.0117	.0132	.0134	.0126	.0126	.0118	.0111	.0118	.0132
	25+35DM	.0248	.0274	.0272	.0275	.0274	.0276	.0276	.0273	.0272	.0273	.0276
	26DM	.0099	.0135	.0118	.0142	.0140	.0137	.0137	.0119	.0115	.0120	.0138
	27DM	.0033	.0059	.0042	.0066	.0067	.0057	.0058	.0044	.0036	.0044	.0063
	36DM	.0033	.0078	.0078	.0076	.0073	.0082	.0081	.0078	.0083	.0079	.0076
	3E	.0166	.0224	.0030	.0119	.0162	.0161	.0153	.0036	.0099	.0035	.0091
11	2M	.1431	.1532	.1336	.1625	.1634	.1514	.1517	.1349	.1250	.1353	.1589
	3M	.1771	.1764	.1768	.1744	.1715	.1806	.1804	.1761	.1825	.1777	.1740
	4M	.1878	.1663	.1755	.1630	.1634	.1664	.1663	.1754	.1768	.1744	.1656
	5M	.1646	.1663	.1755	.1630	.1634	.1664	.1663	.1754	.1768	.1744	.1656
	24DM	.0036	.0127	.0117	.0132	.0134	.0126	.0126	.0118	.0111	.0118	.0132
	25+35DM	.0107	.0274	.0272	.0275	.0274	.0276	.0276	.0273	.0272	.0273	.0276
	26DM	.0143	.0127	.0117	.0132	.0134	.0126	.0126	.0118	.0111	.0118	.0132
	27DM	.0107	.0135	.0118	.0142	.0140	.0137	.0137	.0119	.0115	.0120	.0138
	28+36DM	.0197	.0205	.0197	.0208	.0207	.0208	.0208	.0198	.0197	.0199	.0207
	37DM	.0054	.0078	.0078	.0076	.0073	.0082	.0081	.0078	.0083	.0079	.0076
	3E	.0215	.0224	.0030	.0119	.0162	.0161	.0153	.0036	.0099	.0035	.0091

Table 6-8 (continued)

Carbon No.	Isomer	Expt.	1A	1B	1C	1D	2A	2B	2C	2D	2E	2F
11	4E	.0197	.0225	.0030	.0120	.0162	.0162	.0153	.0036	.0101	.0035	.0092
	5E	.0107	.0113	.0015	.0060	.0081	.0081	.0077	.0018	.0050	.0018	.0046
12	2M	.1214	.1532	.1336	.1625	.1634	.1513	.1517	.1349	.1250	.1353	.1590
	3M	.1739	.1764	.1768	.1744	.1715	.1806	.1804	.1761	.1825	.1777	.1740
	4M	.1649	.1663	.1755	.1630	.1634	.1664	.1663	.1754	.1768	.1744	.1656
	5M	.1540	.1663	.1755	.1630	.1634	.1664	.1663	.1754	.1768	.1744	.1656
	6M	.0761	.0832	.0877	.0815	.0820	.0832	.0831	.0877	.0884	.0872	.0828
	24DM	.0018	.0127	.0117	.0132	.0134	.0126	.0126	.0118	.0111	.0118	.0132
	25+35+26DM	.0236	.0402	.0390	.0407	.0407	.0402	.0402	.0391	.0382	.0391	.0407
	27DM	.0109	.0127	.0117	.0132	.0134	.0126	.0126	.0118	.0111	.0118	.0132
	28DM	.0127	.0135	.0118	.0142	.0140	.0137	.0137	.0119	.0115	.0120	.0138
	29+37DM	.0163	.0205	.0197	.0208	.0207	.0208	.0208	.0198	.0197	.0199	.0207
	36DM	.0091	.0147	.0155	.0142	.0140	.0150	.0150	.0154	.0161	.0155	.0144
	38DM	.0036	.0078	.0078	.0076	.0073	.0082	.0081	.0078	.0083	.0079	.0076
	3E	.0181	.0024	.0030	.0119	.0162	.0161	.0153	.0036	.0099	.0035	.0091
	4E	.0163	.0225	.0030	.0120	.0162	.0162	.0153	.0036	.1008	.0035	.0092
	5E	.0091	.0225	.0030	.0120	.0162	.0162	.0153	.0036	.1008	.0035	.0092
13	2M	.1320	.1532	.1336	.1625	.1634	.1513	.1517	.1349	.1250	.1353	.1589
	3M	.1691	.1762	.1768	.1744	.1715	.1806	.1804	.1761	.1825	.1777	.1740
	4M	.1773	.1663	.1755	.1630	.1634	.1664	.1663	.1751	.1768	.1744	.1756
	5M	.1670	.1663	.1755	.1630	.1634	.1664	.1663	.1751	.1768	.1744	.1756
	6M	.1567	.1663	.1755	.1630	.1634	.1664	.1663	.1751	.1768	.1744	.1756
	3E	.0144	.0224	.0030	.0119	.0162	.0161	.0153	.0036	.0099	.0035	.0091
14	2M	.1266	.1532	.1336	.1625	.1634	.1513	.1517	.1349	.1250	.1353	.1589
	3M	.1567	.1764	.1768	.1744	.1715	.1806	.1804	.1761	.1825	.1777	.1740

Table 6-8 (continued)

Carbon No.	Isomer	Expt.	1A	1B	1C	1D	2A	2B	2C	2D	2E	2F
14	4M	.1717	.1663	.1755	.1630	.1634	.1664	.1663	.1754	.1768	.1744	.1656
	5M	.1567	.1663	.1755	.1630	.1634	.1664	.1663	.1754	.1768	.1744	.1656
	6+7M	.2232	.2495	.2632	.2445	.2451	.2500	.2494	.2631	.2652	.2617	.1484
	3E	.0107	.0224	.0030	.0119	.0162	.0161	.0153	.0036	.0099	.0035	.0091
15	2M	.1133	.1532	.1336	.1625	.1634	.1513	.1517	.1349	.1250	.1353	.1589
	3M	.1517	.1764	.1768	.1744	.1715	.1806	.1804	.1761	.1825	.1777	.1740
	4M	.1667	.1663	.1755	.1630	.1634	.1664	.1663	.1754	.1768	.1744	.1656
	5M	.1560	.1663	.1755	.1630	.1634	.1664	.1663	.1754	.1768	.1744	.1656
	6M	.1432	.1663	.1755	.1630	.1634	.1664	.1663	.1754	.1768	.1744	.1656
	7M	.1517	.1663	.1755	.1630	.1634	.1664	.1663	.1754	.1768	.1744	.1656
	3E	.0086	.0224	.0030	.0119	.0162	.0161	.0153	.0036	.0099	.0035	.0091
16	2M	.1236	.1532	.1336	.1625	.1634	.1513	.1517	.1349	.1250	.1353	.1589
	3M	.1556	.1764	.1768	.1744	.1715	.1806	.1804	.1761	.1825	.1777	.1740
	4M	.1945	.1663	.1755	.1630	.1634	.1664	.1663	.1754	.1768	.1744	.1656
	5M	.1945	.1663	.1755	.1630	.1634	.1664	.1663	.1754	.1768	.1744	.1656
	6M	.1602	.1663	.1755	.1630	.1634	.1664	.1663	.1754	.1768	.1744	.1656
	7+8M	.2655	.2495	.2630	.2445	.2451	.2496	.2494	.2631	.2652	.2617	.2484
17	2M	.1179	.1532	.1336	.1625	.1634	.1513	.1517	.1349	.1250	.1353	.1589
	3M	.1383	.1764	.1768	.1744	.1715	.1806	.1804	.1761	.1825	.1777	.1740
	4M	.1859	.1663	.1755	.1630	.1634	.1664	.1663	.1755	.1768	.1744	.1756
	5M	.1406	.1663	.1755	.1630	.1634	.1664	.1663	.1755	.1768	.1744	.1756
	6M	.2018	.1663	.1755	.1630	.1634	.1664	.1663	.1755	.1768	.1744	.1756
	7+8M	.4830	.3326	.3509	.3259	.3268	.3327	.3325	.3508	.3536	.3489	.3311

M=methyl, DM=dimethyl, and E=ethyl

the iron data, scheme 1C gives the smallest sum of square 0.0477 while scheme 1B gives a value of 0.0841, and also predicts very little ESS. All the four schemes are able to produce the pattern of yielding about one half of the final normalized amount when a new mono-methyl species is formed. The 3M species have the highest concentration of the other mono-methyl species within the individual carbon number fraction. The DMSS are also predicted in the experimental order of magnitude. Scheme 1B produces effectively no ESS while scheme 1A gives a good prediction of these isomers. Both schemes 1C and 1D predict about twice the experimental amount. In terms of ESS consideration, scheme 1A is the best. However, scheme 1C is better in terms of other general predictions such as MSS species in particular, and DMSS.

For the one- and two-carbon addition schemes 2A to 2F, all except schemes 2E and 2F predict low 2M species in the carbon number 4 cut. All the schemes are able to predict the initial one half amount trend for mono-methyl species. Schemes 2A and 2B give the best representation of ESS. In contrast, schemes 2C and 2E both predict low concentrations of these species. Scheme 2F produces twice the experimental amount of ESS, but yields the smallest sum of squares. As a matter of fact, its performance is very similar to those of schemes 1C and 1D. These three schemes give similar values of growth constants f and g (Table 6-9).

For the cobalt data, all the schemes are able to

Table 6-9

Optimal Values of Growth Constants f and g for Iron Data

Scheme	f	g	Least Sum of Squares
1A	0.07746	0.01473	0.06615
1B	0.08692	0.00532	0.08409
1C	0.08752	0.01991	0.04769
1D	0.08928	0.23050	0.05711
2A	0.07650	0.01493	0.06222
2B	0.07606	0.01517	0.06095
2C	0.08746	0.00570	0.08540
2D	0.04653	0.01893	0.09677
2E	0.09003	0.00267	0.08440
2F	0.08842	0.02011	0.05068

predict the general trends such as the one half amount for newly formed mono-methyl species, and 3M species having the highest concentrations of MSS in the individual carbon number fractions. In terms of the sum of squares, scheme 1B and 2C are the best (Table 6-10). However, schemes 1A, 2A and 2B again give the best prediction in terms of ESS amounts. All the schemes, however, predict higher DMSS amounts than the experimental values for low carbon number fractions.

As the ability of the various chain growth schemes to predict ethyl substituted species is one of the reasons behind this investigation, it should be an important consideration in assessing the schemes. Since the concentrations of ESS form but a small portion of the different carbon number fractions, judging the schemes by the values of sum of squares alone would be to neglect a very important piece of information. It has been noted that schemes 1B, 2C and 2E effectively produce no ESS for both cobalt and iron. Schemes 1C, 2D and 2F give too low concentrations of ESS for cobalt data on the one hand, and too high concentrations for iron data on the other. While scheme 1D behaves practically the same as scheme 1C in predicting low concentrations of ESS for the iron data, it yields reasonably accurate ESS concentrations for cobalt. Schemes 2A and 2B are very similar in terms of least sum of squares as well as the values of f and g. Schemes 1A, 2A and 2B are considered the 'best' schemes in that they show consistency in their general predictions, such as amounts of MSS,

Table 6-10

Optimal Values of Growth Constants f and g for Cobalt Data

Scheme	f	g	Least Sum of Squares
1A	0.07190	0.01131	0.04347
1B	0.04925	0.03861	0.03611
1C	0.08149	0.00601	0.05107
1D	0.08170	0.09964	0.05063
2A	0.07510	0.00812	0.04300
2B	0.07547	0.00770	0.04328
2C	0.05437	0.03344	0.03570
2D	0.04420	0.00507	0.03731
2E	0.05518	0.03215	0.03632
2F	0.08279	0.00460	0.04652

DMSS, and in particular, ESS, as well as giving reasonable values of sum of squares, for both sets of data. Figures 6-10 to 6-13 show the predicted amounts of MSS and ESS in comparison with the experimental values.

The 2M species in carbon number 4 fraction in the cobalt data have a much lower concentration than those in higher carbon number fractions. Instead of about one half of the final concentrations as in the case of iron, its value is about only 1/3 of the final amouht. The concentrations of MSS in the cobalt data is generally smaller than those in the iron data. In addition, the DMSS concentrations are only about 1/4 of those in the hydrocarbons from iron catalyst. These generally lower concentrations of branched hydrocarbons in the products from the cobalt catalyst is reflected in the lower values of growth constants f and g as shown in Tables 6-9 and 6-10. This is also shown in figures 6-4 and 6-5 which show that the normal hydrocarbon percentage decreases much faster with carbon number for iron than for cobalt.

The increase in branched isomers with carbon number is a consequence of an increasing number of ways by which the branched species can be formed. Table 6-5 shows the number of intermediate isomers (before the process of isomer rearrangment), including the normal ones, for different carbon numbers. The number of isomers generated depends on the schemes under consideration and on the carbon number. The

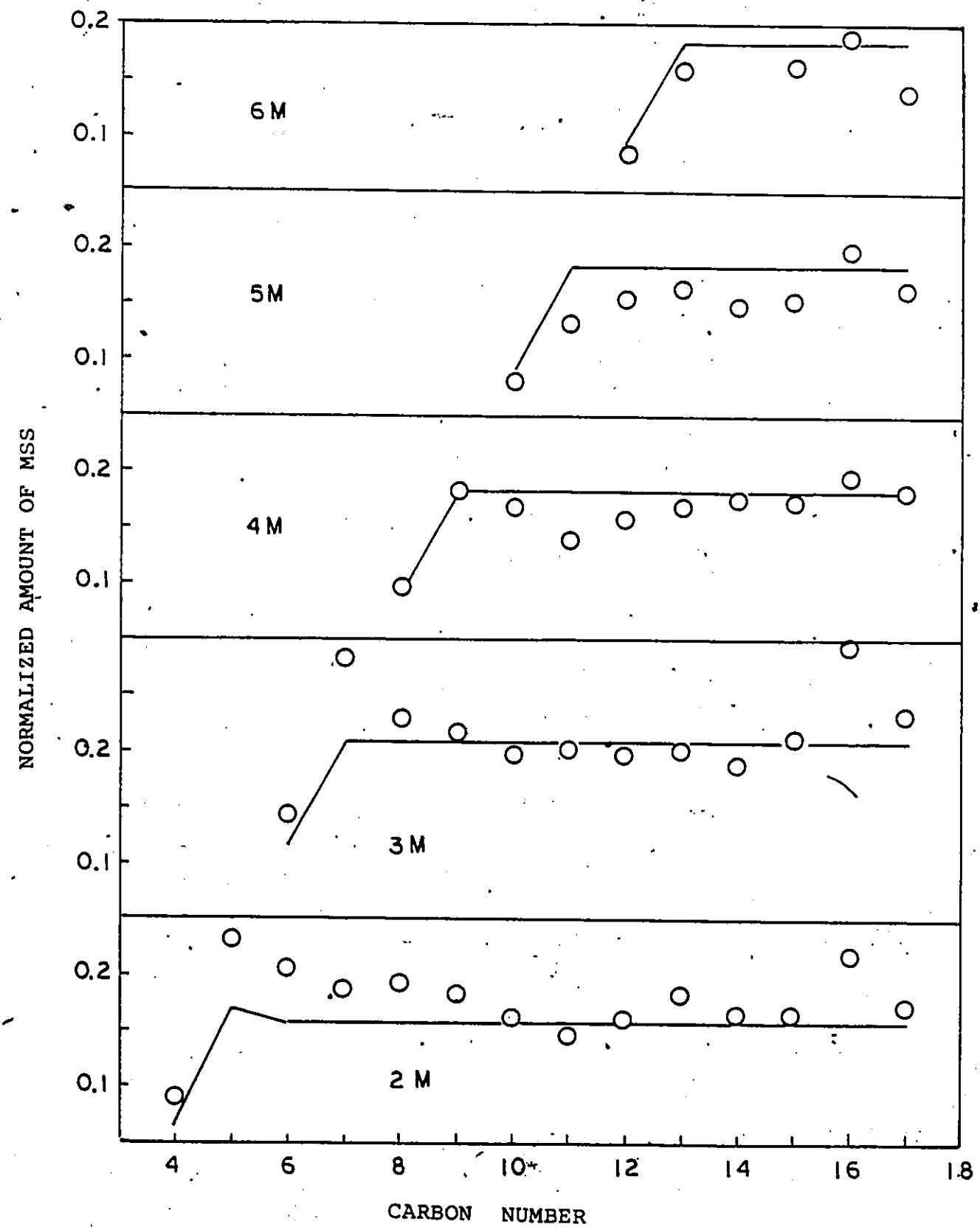

Figure 6-10 Comparison of Experimental and Calculated Amount of Methyl Substituted Species (Schemes 2A and 2B) for Iron Data

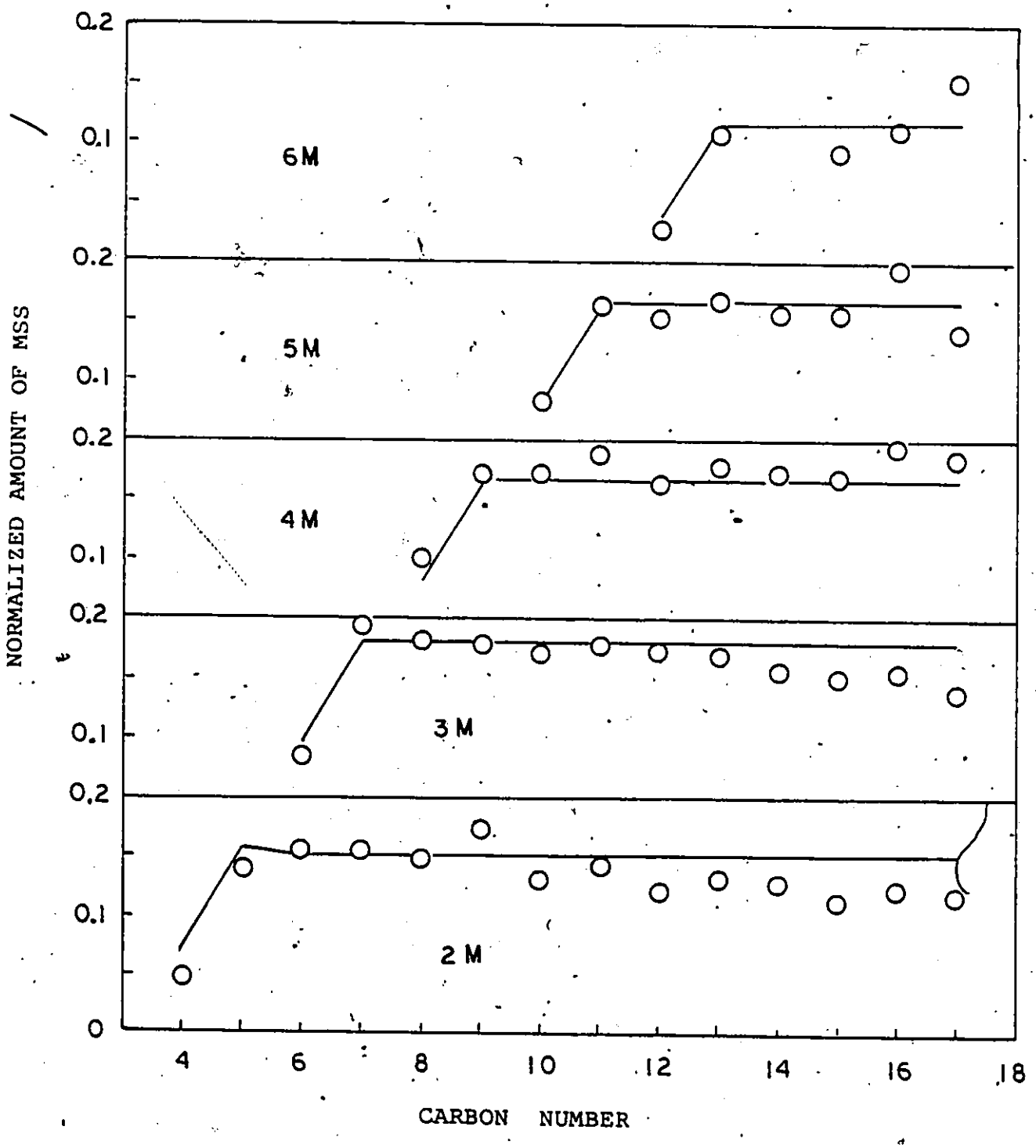

Figure 6-11 Comparison of Experimental and Calculated Amount of Methyl Substituted Species (Schemes 2A and 2B) for Cobalt Data

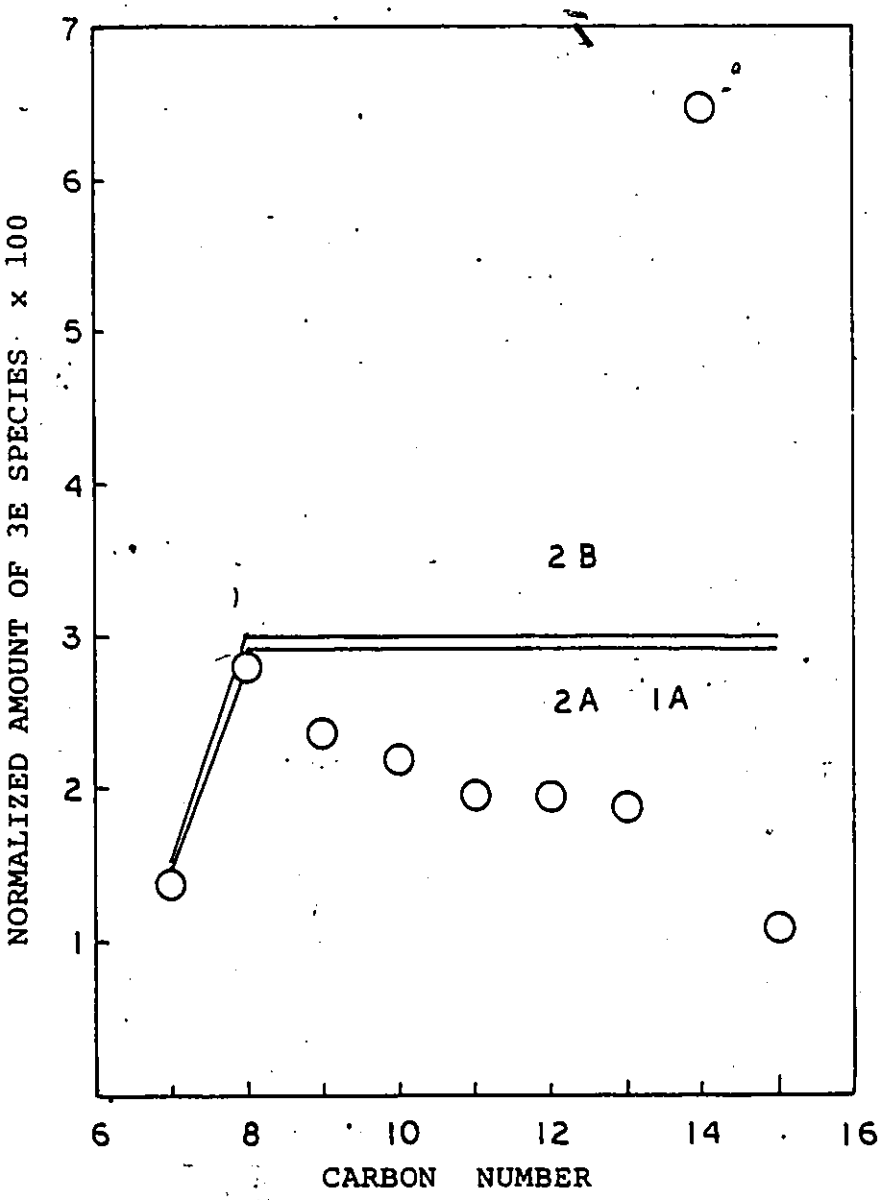

Figure 6-12 Comparison of Experimental and Calculated Amount of 3E Species for Iron Data

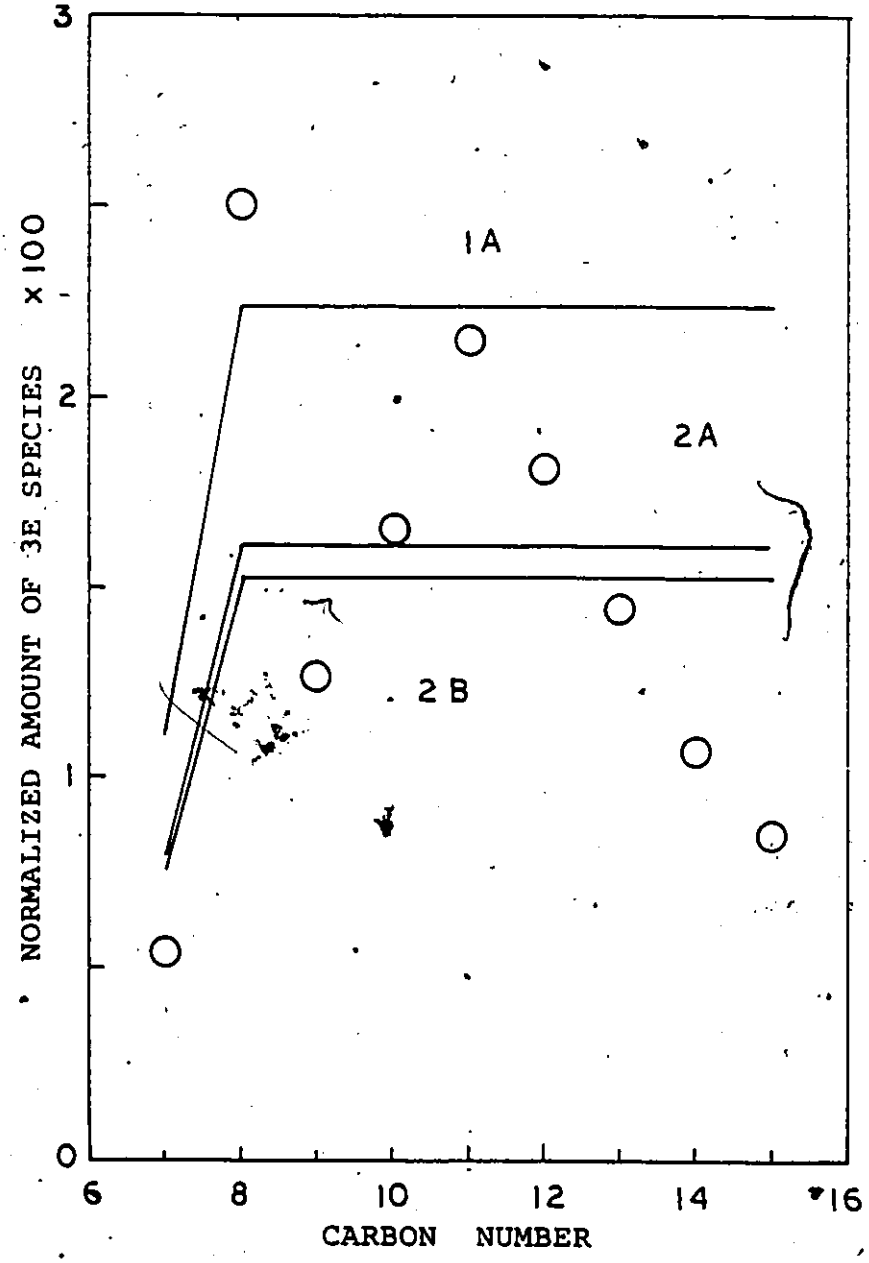

Figure 6-13 Comparison of Experimental and Calculated Amount of 3E Species for Cobalt Data

more ways one-carbon or two-carbon units are allowed to add to the growing chain, the larger will be the number of intermediate species produced. It can be seen that schemes 2B and 2E give a maximum of 436 species. Theoretically, the number of species should increase with the carbon number. The decrease in the number of species at carbon number 13 results from the imposed constraints that some isomers derived from intermediates in carbon number 12 or 11 fractions would yield isomers that are absent in carbon number 13 or higher cuts. Hence, these isomers are not allowed to form resulting in a decrease of total number of isomer intermediates.

In all of the schemes investigated, the growth constants f and g are assumed to be independent of carbon number as well as the structure of the growing chain. While one expects the growth kinetic constants to vary with carbon chain length, the result obtained in the present study shows that it is the ratio of these growth constants that are relevant in the consideration of isomer distributions. Hence, it is the relative kinetic constants and not the absolute values that are important. Thus, the governing parameters for isomer distributions are the relative rates of branching versus normal addition as exemplified by the values of f and g which can be taken to be effectively independent of carbon chain length and structure. This is an important observation because the number of kinetic parameters is reduced by one.

6.7.2 Chain Growth

Although the mechanism of Fischer-Tropsch synthesis is still a subject of much controversy, the reaction can be regarded essentially as a polymerization process not unlike that in free radical polymerization. The carbon chain is perceived to grow by stepwise addition of one-carbon units (223,224). Anderson et al. (212) developed in the early fifties an isomer distribution model that represents these propagation steps by one-carbon addition scheme.

Evidence is accumulating which suggests that the carbon chain growth process may involve more than just one-carbon unit at a time. The early work of Kummer and Emmett (225), as well as that of Hall (226) suggested that ethylene acts as a chain initiator over iron catalyst. Similar work by Eidus et al. (227) showed that 25% of the ethylene introduced was converted to higher hydrocarbons with constant molar radioactivity. The extent to which ethylene participates as chain initiator increases in proportion to the amount of ethylene in the gas phase. It was suggested that ethylene is present in the initial surface complex which is responsible for chain growth. Olefins are generally regarded as the primary products in Fischer-Tropsch synthesis, and the paraffins are formed therefrom by hydrogenation. This conclusion has been confirmed by Pichler et al. (215) who were able to show that the olefin content of the product increased with increasing space velocity of the synthesis gas feed. Presumably, with low space velocity

the primary olefins are transformed into secondary products such as paraffins and methyl-substituted products. Friedel and Anderson (203) arrived at the same conclusion from thermodynamic equilibrium considerations. Pichler and Schulz (200) showed that α-olefins can be incorporated into the growing chain under Fischer-Tropsch conditions, leading to branching. The ability of α-olefins to be incorporated decreases with increasing molecular weight, incorporation being significant only for ethylene and propylene. King (228), in studying the reaction of H_2 and CO over ruthenium catalyst, suggested that ethylene was the precursors of saturated hydrocarbons, except for methane. It was also suggested that the insertion of olefinic species into the growing carbon chain is difficult relative to hydrogenation, except for ethylene the abnormally low yield of which indicates the relative ease of incorporation into the carbon chain as well as to saturate. Dwyer and Somorjai (108) also showed that ethylene acts not only as a chain initiator but also participates in chain propagation, and that readsorption and subsequent secondary reactions of terminal olefins readily occur in Fischer-Tropsch synthesis.

The present work shows that the assumption of one- and two-carbon units addition is in agreement with the expermental evidence, and that it is indeed possible to represent Fischer-Tropsch synthesis by stepwise addition of 'monomer' and 'dimer' such as CH_2 (223,224) and ethylene. Regardless

of the exact nature of these intermediates, the propagation step can be perceived as involving two-carbon units in addition to the usually accepted one-carbon addition. The ability of these chain growth schemes to predict the concentrations of complicated species such as 2,3,4-trimethyl isomers to within experimental accuracy is significant in terms of mathematical description of the isomer growth process and distribution.

While the nature of the intermediate for one-carbon addition is still very much a matter of debate, one can only speculate at this stage as to the nature of the 'dimer' units. Biloen et al. (38) concluded that for low temperature hydrocarbon synthesis over nickel catalyst, a mechanism is operative that proceeds via insertion of carbidic species CH_x into the growing hydrocarbon chain. Ekerdt and Bell (229) suggested that ethylene can react with methylene, and that Fischer-Tropsch synthesis can be perceived as polymerization of ethylene by insertion of the olefin into the metal-alkyl bond. The work of Kibby et al. (230) suggests that olefins are adsorbed and used for branching and chain growth. The results from the present work shows that, regardless of the nature of the adsorbed intermediate, branching can be rationalized by assuming the addition of one-carbon and/or two-carbon addition to the growing end of the carbon chain.

While one can always attach interpretations to the various chain growth schemes in rationalizing the mechanism

of Fischer-Tropsch synthesis, the discussion here will be concentrated on schemes 1A, 2A and 2B because of their performances. According to scheme 1A, steps 1 and 2 are the typical end-on (or normal) and penultimate one-carbon addition in the simple chain growth scheme (212), respectively. Step 3 and 4 combine to give ethyl species. Weitkamp (231) suggested that addition to the third carbon from the growing end of the carbon chain is possible to account for the presence of ethyl species. However, it was not mentioned that two addition steps each involving one-carbon unit were needed to produce the ethyl group.

Essentially schemes 2A and 2B are very similar except for step 4 where the two-carbon unit can add to the carbon chain at the growing end only when there is a primary carbon in scheme 2A, while there is no such restriction in scheme 2B. In the latter scheme, the 'dimer' unit can add to the carbon chain with a primary or secondary carbon at the growing end. This addition step is equivalent to the ethylene insertion step where only one carbon of the 'dimer' unit is used for bonding between the metal and the alkyl group. Step 3 in both schemes 2A and 2B involves no insertion type reaction but addition effectively of a two-carbon unit to the carbon atom which is still attached to the metal surface. This is similar to the penultimate one-carbon addition to give methyl species except now a two-carbon unit is involved. This is a variant of the condensation mechanism proposed by Anderson et al. (11).

The incorporation of olefins involves both carbon atoms separated by the double bond. Hence, no branching occurs when ethylene is incorporated whereas incorporation of propylene and 1-butene results in the formation of methyl and ethyl groups on the carbon chain, respectively (200,206). According to step 4 in schemes 2A and 2B, addition of a two-carbon unit will result in methyl species. This addition step is equivalent to the incorporation of ethylene except that only one carbon of the 'dimer' unit is used for bonding between the metal and the alkyl group. It is consistent with the generally accepted one-carbon addition in that only one carbon atom is involved in bond formation between the metal and the alkyl group, not unlike that of CO insertion where only the carbon is involved while the oxygen atom is removed by subsequent hydrogenation.

6.7.3 Carbon Number Distribution

In the chain growth schemes considered, there are three growth constants, f, g and a. Constant a is the end-on addition probability and, by definition, is less than one. It was given a value of unity in the simulation studies since the data were analysed using the relative or normalized amounts of isomers, i.e. ratios of branched isomers to normal isomer in each carbon number fraction. To obtain the value of constant a, it is necessary to utilize information on the carbon number distribution. Since the amount of hydrocarbons of

carbon number n is related to the value of constant a by equation 6-4:

$$\phi_n = k F_n a^{n-2} \qquad (6-4)$$

a plot of $\ln (\phi_n / F_n)$ versus carbon number n will yield value of a.

Growth constant a is related to the growth probability by the following relationship:

$$\alpha = \frac{a F_{n+1}}{F_n} \qquad (6-12)$$

According to equation 6-2, the growth probability α is in turn related to the amount of hydrocarbons in different carbon number fractions:

$$\phi_n = \phi_x \alpha^{n-x} \qquad (6-2)$$

Thus, there are two ways of obtaining the value of α, which should yield consistent results. Table 6-11 shows the values of α obtained. The carbon number distribution for cobalt and iron data are shown in figures 6-14 and 6-15, respectively. The ratio (F_{n+1} / F_n) in equation 6-12 was obtained by averaging the values obtained from the simulation runs. The values of α obtained by the two methods agree with each other. This is particularly so for the cobalt data which give a straight

Table 6-11

Values of Growth Probability α and Growth Constant a for Iron and Cobalt Data*

Catalyst	a	F_{n+1}/F_n (average)	α (eqn.6-12)	α (expt.)
Iron	0.625	1.061	0.663	0.653
Cobalt	0.662	1.056	0.699	0.705

* Values of F_n are for Scheme 2B.

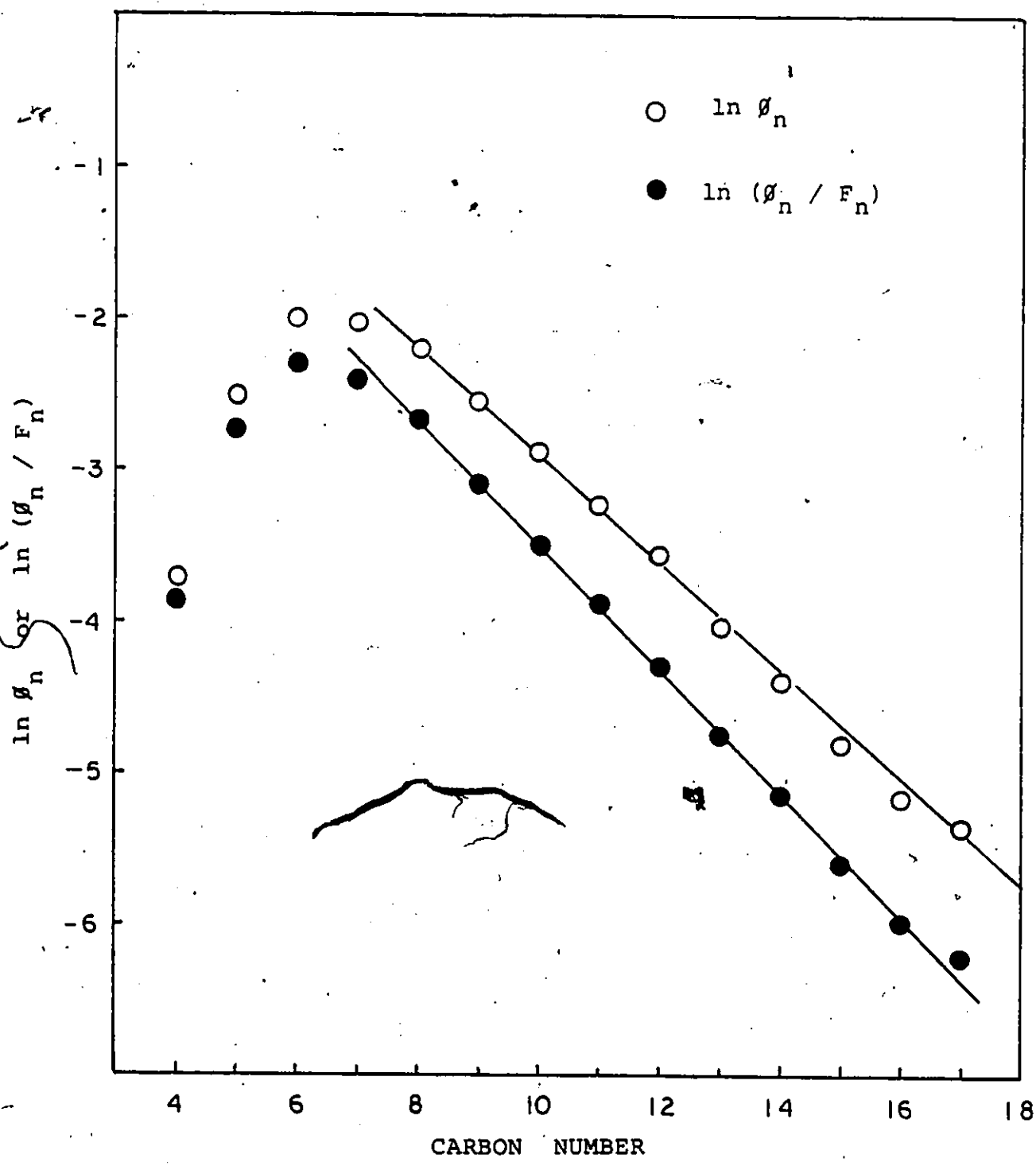

Figure 6-14 Carbon Number Distribution for Cobalt Data

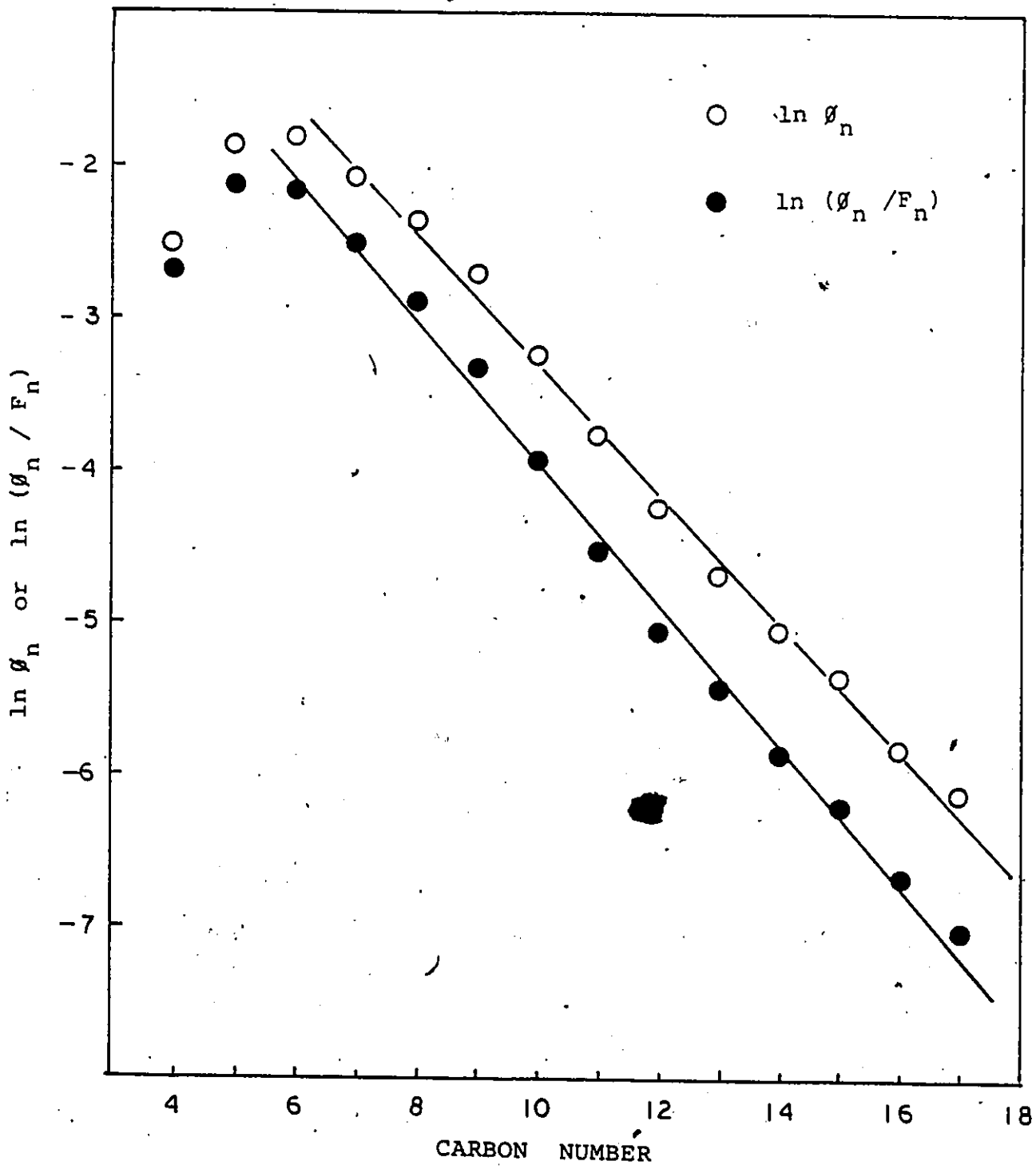

Figure 6-15 Carbon Number Distribution for Iron Data

line in the carbon number distribution plot. For data from iron catalyst there are some deviations. This somewhat non-linear plot has been reported by Storch et al. (11), and seems to be typical of product distributions from iron catalysts. The deviations at the low carbon numbers are typical in product distribution plots. Ruthenium catalysts are especially notorious for this kind of deviation (211). The deviation at low carbon numbers is probably due to the further reactions of the lower unsaturated hydrocarbons. It may also be due to losses since volatile components are involved.

The agreement in the values of growth probability obtained from carbon number distribution on the one hand, and from carbon number and isomer distributions on the other, is significant in that it supports the modes by which the isomer intermediates propagate according to the schemes considered. It also reflects the complexities of 'polymerization' on heterogeneous systems as compared to the homogeneous systems in which the molecules grow by 'end-on' addition of monomers.

Chapter 7

CONCLUSIONS

The hydrogenation reactions of carbon monoxide and carbon dioxide were studied over commercial Raney nickel. The physical properties of the catalyst were determined by physical adsorption and chemisorption using nitrogen, carbon monoxide, carbon dioxide, and hydrogen. The surface area and pore size distribution were measured by nitrogen adsorption at 77 K, and the metal surface area and crystallite size were determined by hydrogen chemisorption at both 77 K and reaction temperatures. Carbon monoxide and carbon dioxide chemisorptions were also studied.

A single-pass plug-flow reactor was used for kinetic study; conversions were kept below 4% to ensure differential conversions and to minimize transport limitations. A gas chromatographic system was able to separate and measure all of the reactants and products to provide rate data.

Carbon monoxide hydrogenation rate was found to increase with hydrogen partial pressure but decrease with carbon monoxide concentration. Methane had no significant effect on the rate but water inhibited the reaction

reversibly. The reaction orders ranged from 0.7 to 1 for hydrogen and -0.5 to -0.6 for carbon monoxide. Temperature had no significant effect on the order. Water decreased the methanation rate but its effect is much less than that of CO, the reaction order being -0.1 . During methanation carbonaceous species equivalent to a multilayer of carbon were deposited on the catalyst surface. Its concentration decreased with hydrogen and water but increased with carbon monoxide and temperature. Hydrogen in low concentrations facilitated the deposition of these carbonaceous species.

The steady-state reaction produced methane and water; trace amounts of carbon dioxide were detected which decreased with the aging of the catalyst. No ethane was detected.

The apparent activation energy of carbon monoxide hydrogenation was 146 kJ/mol and was independent of total pressure. The specific activity of the catalyst was found to compare favourably with other Raney nickel catalysts.

The mechanism is perceived to involve the dissociation of carbon monoxide and the stepwise hydrogenation of deposited surface carbon. A rate equation was derived which was able to represent the data well.

Carbon dioxide hydrogenation rate increased with hydrogen partial pressure but reached a maximum value

and remained constant with further increase in hydrogen concentration. The rate also increased with carbon dioxide and reached a maximum; further increase in carbon dioxide concentration decreased the rate slowly. Methane had no effect on the rate while water inhibited the rate reversibly.

Power rate law was not able to represent the data over the whole range of reaction conditions; it could only represent the data in low hydrogen and carbon dioxide concentrations. Exponents thus obtained depend on the temperature and concentrations of the other reactant.

During methanation, less than a monolayer of carbonaceous carbon was deposited on the catalyst. Surface carbon concentration decreased with hydrogen and water, but increased with temperature and carbon dioxide concentration. Presence of hydrogen in low concentration facilitated the deposition of carbonaceous species.

The steady state reaction products were methane and trace amount of carbon monoxide was obtained at low H_2/CO_2 ratios. The apparent activation energy of CO_2 methanation was 105 kJ/mol. and was independent of H_2/CO_2 ratio. The specific activity was an order of magnitude higher than that of CO hydrogenation. The mechanism is perceived to involve the dissociation of carbon dioxide

into carbon and oxygen, and their subsequent hydrogenation. Kinetic data support this mechanism. A kinetic model based on these was derived and was able to represent the data well.

The similar kinetic models for CO and CO_2 hydrogenation were able to not only fit the data but also yield comparable adsorption constant values for H_2. This result provides an indirect evidence supporting the hypothesis that CO and CO_2 proceed via similar mechanism.

The detailed compositions of Fischer-Tropsch hydrocarbon isomers up to carbon number 17 were used to examine the carbon chain growth process and isomer distribution. The carbon chain growth process was simulated on a computer for various growth schemes, involving one-carbon as well as one- and two-carbon additions. The simulation was able to predict reasonably well the carbon number and isomer distributions. The results provided evidence that the chain growth steps in the Fischer-Tropsch synthesis could involve stepwise additions of both one-carbon and two-carbon units.

REFERENCES

1. Bousquet, J.L. and Teichner, S.J., Bull. Soc. Chim. Fr., 2963 (1969).

2. Bousquet, J.L., Gravelle, P. and Teichner, S.J., Bull. Soc. Chim. Fr., 3693 (1972).

3. Lee, A.L., Feldkirchner, H.L. and Tajbl, D.G., Preprints, Div. Fuel Chem., Amer. Chem. Soc., 14(4), Part 1, p. 126, Sept. 1970, paper 31.

4. Vannice, M.A., J. Cat., 37, 462 (1975).

5. Solc, M., Collection Czechoslov. Chem. Commun., 27, 2621 (1962).

6. Muller, J., Pour, V. and Regner, A., J. Cat., 11, 326 (1968).

7. Pour, V., Collection Czechoslov. Chem. Commun., 34, 45 (1969).

8. Fischer, A. and Tropsch, H., Brennst. Chem., 7, 97 (1926).

9. Craxford, S.R. and Rideal, E.K., J. Chem. Soc., 1604 (1939).

10. Craxford, S.R. and Rideal, E.K., Trans. Faraday Soc., 42, 576 (1946).

11. Storch, H.H., Golumbic, H. and Anderson, R.B., "The Fischer-Tropsch and Related Synthesis", Wiley, N.Y., 1951.

12. Weller, S., Hofer, L.J.W., and Anderson, R.B., J. Amer. Soc., 70, 799 (1948).

13. Eidus, Y.T., and Zelinskii, N.D., Izv. Akad. Nauk SSSR Otd. Khim. Nauk., 190 (1942).

14. Vlasenko, V.M., Kukhar', L.A., Rusov, M.T., and Samchenko, N.P., Kinetika i Kataliz, 5, 337 (1964).

15. Weller, S., J. Amer. Chem. Soc., 69, 2431 (1947).

16. Elvius, O.C., and Nash, A.W., Fuel, 5, 263 (1926).

17. Tropsch, H., Schellenberg, A., and A. von Philippovich, Ges. Abhandl, Kenntnis Kohle, 1, 63 (1925).

18. Schoubye, P., J. Cat., 14, 238 (1969).

19. Fischer, F., Tropsch, H., and Dilthey, P., Brennst-Chem., 6, 265 (1925).

20. Pichler, H., Chem. Tech. (Berlin), 18, 392 (1966).

21. Orlov, E.I., Zh. Russ. Khim. Obskh., 40, 1142, 1588 (1908).

22. Eidus, Y.T., and Zelinskii, N.D., Izv. Akad. Nauu SSSR, Otd. Khim. Nauk, 289 (1940).

23. Eidus, Y.T., Usp. Khim, 20(1), 54-70 (1951); translated to English in U.S. Bur. Mines Inform. Circ., 7821, 7-10 (1958).

24. Hamai, S., Bull. Chem. Soc., Japan, 16, 213 (1941); J. Chem. Soc. Japan, 62, 516 (1941).

25. Nijs, H.H., and Jacobs, P.A., J. Cat., 66, 401 (1980).

26. Vlasenko, V.M., and Yuzefovich, G.E., Russian Chem. Rev., 38(9), (1969), U.D.C. 541, 128 and 547, 211, p. 728, English Translation.

27. Blyholder, G., Shihabi, D., Wyatt, W.V., and Bartlett, R., J. Catal., 43, 122 (1976).

28. Tracy, J.E., J. Chem. Phys., 56, 2736 (1972).

29. Tøttrup, P.B., J. Catal., 42, 29 (1976).

30. Rabo, J.A., Risch, A.P., and Poutsma, M.L., J. Catal., 53, 295 (1978).

31. Wentrcek, P.R., Wood, B.J., and Wise, H., J. Catal., 43, 363 (1976).

32. Araki, M., and Ponèc, V., J. Catal., 44, 439 (1976).

33. McCarty, J.G., and Wise, H., J. Catal., 57, 406 (1979).

34. Galuszka, J., Chang, J.R., and Amenomiya, Y., Proceeding of the 7th Inter. Congress on Catalysis, Tokyo, Vol. 1, p. 529, 1980.

35. Zagli, A.E., Falconer, J.L., and Keenan, C.A., J. Catal., 56, 453 (1979).

36. Dalla Betta, R.A., and Shelef, M., J. Catal., 49, 383 (1977).

37. Goodman, D.W., Kelley, R.D., Madey, T.E., and Yates, J.T., Jr., J. Catal., 63, 226 (1980).

38. Biloen, P., Helle, J.N., and Sachtler, M.H., J. Catal., 58, 95 (1979).

39. Matsumoto, H., and Bennett, C.O., J. Catal., 53, 331 (1978).

40. Joyner, R.W., J. Catal., 50, 176 (1977).

41. Ekerdt, J.G., and Bell, A.T., J. Catal., 58, 170 (1979).

42. Sexton, B.A., and Somorjai, G.A., J. Catal., 46, 167 (1977).

43. King, D.L., J. Catal., 61, 77 (1980).

44. Mills, G.A., and Steffgen, F.W., Catal. Rev., 8, 159 (1973).

45. Luyten, L., and Jungers, J.C., Bull. Soc. Chim. Belg., 54, 303 (1945).

46. Nicolai, J., d'Hont, M., and Jungers, J.C., Bull. Soc. Chim. Belg., 55, 160 (1946).

47. Akers, W.W., and White, R.R., Chem. Eng. Progr., 44, 553 (1948).

48. Karn, F.S., Shultz, J.F., and Anderson, R.B., Ind. Eng. Chem. Prod. Res. & Dev., 4, 265 (1965).

49. Shultz, J.F., Karn, F.S., and Anderson R.B., U.S. Bur. Mines Rept. Invest. 6941 (1967).

50. Vlasenko, V.M., Yuzefovich, G.E., and Ruso, M.T., Kinet. Katal., 6, 688 (1965).

51. Cagnion, J.M., and Marguerin, J., Kinet. Katal., 16, 1552 (1975), English Translation.

52. van Herwijnen, T., van Doesburg, H., and de Jong; W.A., J. Catal., 28, 391 (1973).

53. Saletore, D.A., and Thomson, W.J., Ind. Eng. Chem., Process Des. Dev., Vol. 16, No. 1, 70 (1977).

54. Randhava, S.S., Camara, E.H., and Rehmat, A., Ind. Eng. Chem. Prod. Res. Develop., 8, 347 (1969).

55. Randhava, S.S., Rehmat, A., and Camara, E.H., Ind. Eng. Chem. Process Design Develop., 8, 482 (1969).

56. Huang, C.P., and Richardon, J.T., J. Catal., 51, 1 (1978).

57. Ho, S.V., and Harriott, P., J. Catal., 64, 272 (1980).

58. Eischens, R.P., Francis, S.A., and Pliskin, W.A., J. Chem. Phys., 22, 1789 (1954).

59. Yates, J.T., and Garland, C.W., J. Phys. Chem., 65, 617 (1961).

60. Besten, I.E.D., Fox, P.G., and Shelwood, P.W., J. Phys. Chem., 66, 450 (1962).

61. Eischens, R.P., Francis, S.A., and Pliskin, W.A., J. Phys. Chem., 60, 194 (1956).

62. Primet, M., Dalmon, J.A., and Martin, G.A., J. Catal., 46, 25 (1977).

63. Eischens, R.P., The Surface Chemistry of Metals and Semiconductors (H.C. Gatos, ed.), Wiley, N.Y., 1960.

64. Klostermann, K., and Hobert, H., J. Catal., 63, 355 (1980).

65. Neff, L.D., Sturdivant, A.E., Wallace, J.L., J. Catal., 63, 324 (1980).

66. Wentrcek, P.W., McCarty, J.G., Ablow, C.M., and Wise, H., J. Catal., 61, 232 (1980).

67. Yates, J.T., Jr., and Garland, C.W., J. Phys. Chem., 65, 617 (1961).

68. Blyholder, G., J. Phys. Chem., 68, 2772 (1964).

69. van Hardeweil, R., and Hartog, F., "Advances in Catalysis", 22, 75 (1972).

70. Heal, M.J., Leisegang, E.C., and Torrington, R.G., J. Catal., 51, 314 (1978).

71. Heal, M.J., Leisegang, E.C., and Torrington, R.G., J. Catal., 42, 10 (1976).

72. Fujimoto, K., Kameyama, M., and Kunugi, T., J. Catal., 61, 7 (1980).

73. Martin, G.A., Primet, M., and Dalman, J.A., J. Catal., 53, 321 (1978).

74. Siddiqi, M.M., and Tompkins, F.C., Actes du Deuxieme Congress International de Catalyse, Paris, 1960, pt. 2, Article 86.

75. Selwood, P.W., J. Catal., 42, 148 (1976)

76. Blyholder, G., and Neff, L.D., J. Phys. Chem., 66, 1664 (1962).

77. Blyholder, G., and Neff, L.D., J. Catal., 2, 138 (1963).

78. Kölbel, H., and Tillmetz, K.D., J. Catal., 34, 307 (1974).

79. Erley, W., and Wagner, H., J. Catal., 53, 287 (1978).

80. Rostrup-Nielsen, J., and Pedersen, K., J. Catal., 59, 395 (1979).

81. Burton, J.J., and Pugel, T.M., J. Catal., 47, 280 (1977).

82. Pannell, R.B., Chung, K.S., and Bartholomew, C.H., J. Catal., 46, 340 (1977).

83. Harberts, J.C.M., Bourgonje, A.F., Stephan, J.J., and Ponec, V., J. Catal., 47, 99 (1977).

84. Sexton, B.A., and Somorjai, G.A., J. Catal., 46, 167 (1977).

85. Griffin, C.W., J. Amer. Chem. Soc., 59, 2431 (1937).

86. Ghosh, J.C., Sastri, M.V.C., and Kini, K.A., Ind. Eng. Chem., 44, 2463 (1952).

87. Sastri, M.V.C., et. al., J. Catal., 26, 212 (1972).

88. Wedler, G., Papp, H., and Schroll, G., J. Catal., 38, 153 (1975).

89. Bahr, H.A., Ges. Abhandl. Kenntnis Kohle, 8, 219 (1929).

90. Russell, W.W., and Miller, G.H., J. Amer. Chem. Soc., 72, 2446 (1950).

91. Gibson, E.J., and Hall, C.C., J. Appl. Chem., 4, 464 (1954).

92. Pichler, H., "Advances in Catalysis", 4, 271 (1952).

93. Medsford, S., J. Chem. Soc., 123, 1452 (1923).

94. Pichler, H., Brennst.-Chem., 24, 39 (1943).

95. Binder, G.G., and White, R.R., Chem. Eng. Prog., 46, 563 (1950).

96. Dew, J.N., White, R.R., and Sliepcevich, C.M., Ind. Eng. Chem., 47, 140 (1955).

97. Vlasenko, V.M., Rusov, M.T., and Yuzefovich, G.E., Kinetika Katalez, 2, 525 (1961).

98. Eischens, R.P., and Pliskin, W.A., "Advances in Catalysis", 9, 662 (1957).

99. Blyholder, G., and Neff, L.D., J. Phys. Chem., 66, 1464 (1962).

100. Hirota, K., Kobayashi Y., and Kiji, J., Bull. Chem. Soc. Japan, 34, 1213 (1961).

101. Quinn, C.M., and Roberts, M.W., Trans. Faraday Soc., 58, 569 (1962).

102. Brennan, D., and Hayward, D.O., Phil. Trans. Roy. Soc., London, A258, No. 1089, 375 (1965).

103. Maatman, R., and Hiemstra, S., J. Catal., 62, 349 (1980).

104. Zagli, E., and Falconer, J.L., J. Catal., 69, 1 (1981).

105. Falconer, J.L., and Zagli, A.E., J. Catal., 62, 280 (1980).

106. Gupta, N.M., Kamble, V.S., Rao, K.A., and Iyer, R.M., J. Catal., 60, 57 (1979).

107. Solymosi, F., Erdöhelyi, A., and Bánsági, T., J. Catal., 68, 371 (1981).

108. Dwyer, D.J., and Somorjai, G.A., J. Catal., 56, 249 (1979).

109. Smith, J.M., and Van Ness, H.C., "Introduction to Chemical Engineering Themodynamics", 3rd Edition, McGraw-Hill, N.Y., 1975.

110. Smith, J.M., "Chemical Engineering Kinetics", McGraw Hill, N.Y., p. 362, 1970.

111. Levenspiel, O., "Chemical Reaction Engineering", John Wiley, N.Y., 1972.

112. Thomas, J.M., and Thomas, W.J., "Introduction to the Principles of Heterogeneous Catalysis", Academic Press, London, p. 475, 1967.

113. Peterson, E.E., "Chemical Reaction Analysis", Prentice-Hall, N.Y. (1965).

114. Hougen, O.A., Ind. Eng. Chem., 53, 509 (1961).

115. Anderson, R.B., "An Annotated Outline of a Course in Heterogeneous Catalysis", McMaster U., 1970.

116. Olson, R.W., Schuler, R.W., and Smith, J.M., Chem. Eng. Progr., 42, 614 (1950).

117. Pauls, A.C., Comings, E.W., and Smith, J.M., AIChE J., 5, 453 (1959).

118. Maymo, J.A., and Smith, J.M., AIChE J., 12, 845 (1966).

119. Otani, S., and Smith, J.M., J. Catal., 5, 332 (1966).

120. Bartholomew, C.H., Pannell, R.B., and Butler, J.L., J. Catal., 65, 335 (1980).

121. Vannice, M.A., J. Catal., 37, 449 (1975).

122. Vannice, M.A., J. Catal., 40, 129 (1975).

123. Vannice, M.A., J. Catal., 44, 152 (1976).

124. Vannice, M.A., J. Catal., 50, 228 (1977).

125. Vannice, M.A., and Garten, R.L., J. Catal., 56, 236 (1979).

126. Weller, S., Adv. Chem. Series, No. 148, 1975.

127. Weller, S., AIChe J., 2, 59 (1956).

128. Reilly, P.M., Can. J. Chem. Eng., 48, 168 (1970).

129. Draper, N.R., Smith H., "Applied Regression Analysis", John Wiley and Son, New York (1966).

130. Box, G., Draper, N.R., Biometrika, 52, 355 (1965).

131. Carberry, J., "Chemical and Catalytic Reaction Engineering", McGraw-Hill, New York (1976).

132. Nicolau, I., Ph.D. Thesis, McMaster U, Hamilton, 1975.

133. Freel, J., Pieters, W.J.M., and Anderson, R.B., J. Catal., 14, 247 (1969).

134. Freel, J., Pieters, W.J.M., and Anderson, R.B., J. Catal., 16, 281 (1970).

135. Freel, J., Robertson, S.D., and Anderson, R.B., J. Catal., 18, 243 (1970).

136. Robertson, S.D., and Anderson, R.B., J. Catal., 23, 286 (1971).

137. Robertson, S.D., and Anderson, R.B., J. Catal., 41, 405 (1976).

138. Robertson, S.D., Freel, J., and Anderson, R.B., J. Catal., 24, 130 (1972).

139. MacNab, J.I., and Anderson, R.B., J. Catal., 29, 328 (1973).

140. MacNab, J.I., and Anderson, R.B., J. Catal., 29, 338 (1973).

141. Brunauer, S., Emmett, P.H., and Teller, E., J. Amer. Chem. Soc., 60, 309 (1938).

142. Lippens, B.C., and De Boer, J.H., J. Catal., 4, 319 (1965).

143. Lippens, B.C., Linsen, B.G., and De Boer, J.H., J. Catal., 3, 32 (1964).

144. Brockhoff, J.C.P., and De Boer, J.H., J. Catal., 9, 8 (1967).

145. Brockhoff, J.C.P., and De Boer, J.H., J. Catal., 9, 15 (1967).

146. Anderson, R.B., J. Catal., 3, 50 (1964).

147. Anderson, R.B., J. Catal., 3, 301 (1964).

148. Bartholomew, C.H., and Pannell, R.B., J. Catal., 65, 390 (1980).

149. Solymori, F., Erdöhelyi, A., and Kocsis, M., J. Catal., 65, 428 (1980).

150. McVicker, G.B., Baker, R.T.K., Garten, R.L., and Kugler, E.L., J. Catal., 65, 207 (1980).

151. Ross, J.R.H., Steel, M.C.F., and Zeini-Isfahani, A., J. Catal., 52, 280 (1978).

152. Keier, N.P., and Roginskii, S.Z., Izv. Akd. Nauk SSSR Otd. Khim. Nauk, 27 (1950).

153. Rostrup-Nielsen, J., and Trimm, D.L., J. Catal., 48, 155 (1977).

154. Chilton, T.C., and Colburn, A.P., Ind. Eng. Chem., 26, 1183 (1934).

155. De Acetis, J., and Thodos, G., Ind. Eng. Chem., 52, 1003 (1960).

156. Argo, W.B., and Smith, J.M., Chem. Eng. Progr., 49, 443 (1953).

157. Kempling, J.C., Ph.D. Thesis, McMaster U, Hamilton, 1971.

158. Satterfield, C.N., "Mass Transfer in Heterogeneous Catalysis", MIT, Cambridge, 1970.

159. Satterfield, C.N., and Sherwood, T.K., "The Role of Diffusions in Catalysis", Addison-Wesley Pub. Co., Mass., 1963.

160. Weisz, P.B., Z. Phys. Chem., 11, 1 (1957).

161. Fontaine, R.W., Ph.D. Thesis, Cornell University, 1973.

162. Uken, A.H., and Bartholomew, C.H., J. Catal., 65, 402 (1980).

163. Dalla Betta, R.A., Piken, A.G., and Shelef, M., J. Catal., 40, 173 (1975).

164. Okamoto, Y., Matsunaga, E., Imanaka, T., and Teranishi, S., J. Catal., 74, 183 (1982).

165. Vannice, M.A., J. Catal., 74, 190 (1982).

166. Sughrue, E.L., and Bartholomew, C.H., to be published in Appl. Catal., 1981.

167. Elliott, D.J., and Lunsford, J.H., J. Catal., 57, 11 (1979).

168. Gardner, D.C., and Bartholomew, C.H., Ind. Eng. Chem. Prod. Res. Dev., 20, 80 (1981).

169. Singh, K.J., and Grenga, H.E., J. Catal., 47, 328 (1977).

170. Ott, G.L., Fleisch, T., and Delgass, W.N., J. Catal., 60, 394 (1979).

171. Ott, G.L., Fleisch, T., and Delgass, W.N., J. Catal., 65, 253 (1980).

172. Palmer, R.L., and Vroom, D.A., J. Catal., 50, 244 (1977).

173. Gardner, D.C., and Bartholomew, C.H., Ind. Eng. Chem. Fund., 20, 229 (1981).

174. Figueiredo, J.L., and Trimm, D.L., 40, 154 (1975).

175. Low, G.G., and Bell, A.T., J. Catal., 57, 397 (1979).

176. Palmer, R.L., and Smith, J.N., J. Chem. Phys., 60, 1453 (1974).

177. Smith, J.N., and Palmer, R.L., J. Chem. Phys., 56, 13 (1972).

178. Bernasck, S.L., and Somorjai, G.A., J. Chem. Phys., 62, 3149 (1975).

179. Vlasenko, V.M., Kukhar, L.A., Rusov, M.T., and Samchenko, N.P., Kinet. Catal., USSR, 5, 301 (1964).

180. Farrauto, R.J., J. Catal., 41, 482 (1976).

181. Blyholder, G., Shihabi, D., Wyatt, W.V., and Bartlett, R., J. Catal., 43, 122 (1976).

182. Goodman, D.W., Kelley, R.D., Madey, T.E., and White, J.M., J. Catal., 64, 479 (9180).

183. Dalla Betta, R.A., and Shelef, M., J. Catal., 48, 111 (1977).

184. Mori, T., Masuda, H., Imai, H., Miyamoto, A., and Murakami, Y., Shokubai, 22, 7 (1980).

185. Sakharov, M.M., and Dokukina, E.S., Kinet. Katal., 2, 710 (1961).

186. McKee, D.W., J. Catal., 8, 240 (1967).

187. Wilson, T.P., J. Catal., 60, 167 (1979).

188. Kellner, C.S., and Bell, A.T., J. Catal., 67, 175 (1981).

189. Van Barneveld, W.A.A., and Ponec, V., J. Catal., 51, 426 (1978).

190. Schwarz, J.A., and Smith, R.P., J. Catal., 62, 176 (1980).

191. Renouprez, A.J., Fouilloux, P., and Candy, J.P., Sur. Sci., 83, 285 (1979).

192. Blyholder, G., and Sheets, R.W., J. Catal., 39, 152 (1975).

193. Solymori, F., Tombacz, I., and Kocsis, M., J. Catal., 75, 78 (1982).

194. Cant, N.W., and Bell, A.T., J. Catal., 73, 257 (1982).

195. Demuth, J.E., and Ibach, H., Sur. Sci., 78, L238 (1978).

196. McCarty, J., Falconer, J., and Madix, R.J., J. Catal., 30, 235 (1973).

197. Weatherbee, G.D., and Bartholomew, C.H., J. Catal., 68, 67 (1981).

198. Weller, S.W., and Friedel, R.A., J. Chem. Phys., 17, 801 (1949).

199. Anderson, R.B., Lee, C.B., and Machiels, J.C., Canad. J. Chem. Eng., 54, 590 (1976).

200. Pichler, H., and Schulz, H., Chem. Eng. Techn., 42, 1162 (1970).

201. Schulz, H., Erdöl Kohle, 30, 123 (1977).

202. Herington, E.F.G., Chem. Ind., 65, 346 (1946).

203. Friedel, R.A., and Anderson, R.B., J. Amer. Chem. Soc., 72, 1212, 2307 (1950).

204. Flory, P.J., J. Amer. Chem. Soc., 58, 1877 (1936).

205. Schulz, G.V., Z. Phys. Chem., B30, 379 (1935).

206. Olivé, S., Angew. Chem. Int. Ed. Engl., 15, 136 (1976).

207. Anderson, R.B., J. Catal., 55, 114 (1978).

208. Henrici-Olive, G., and Olivé, S., J. Catal., 60, 481 (1979).

209. Anderson, R.B., J. Catal., 60, 484 (1979).

210. Madon, R.J., J. Catal., 60, 485 (1979).

211. Madon, R.J., J. Catal., 57, 183 (1979).

212. Anderson, R.B., Friedel, R.A., and Storch, H.H., J. Chem. Phys., 19, 313 (1951).

213. Blaustein, B.D., Wender, I., and Anderson, R.B., Nature, 189, 224 (1961).

214. Schulz, H., Rao, B.R., and Elstner, M., Erdöl Kohle, 23, 651 (1970).

215. Pichler, H., Schulz, H., and Kühne, D., Brennst. Chem., 49, 1 (1968).

216. Anderson, R.B., and Chan, Y.C., Adv. Chem. Ser., 178, 114 (1979).

217. Fletcher, R., and Powell, M.J.D., Computer J., 6, 163 (1963).

218. Davidon, W.C., A.E.C. Res. Develop. Rept., ANL-5990, Dec. 1959.

219. Fletcher, R., and Reeves, C.M., Computer J., 7, 149 (1964).

220. Hestenes, M.R., and Stiefel, E., J. Res. Natl. Bur. Std., 49, 409 (1952).

221. Swann, W.H., "I.C.I. Ltd. Central Instr. Res. Lab., Res. Note 64/3", London, 1964.

222. Weber, Ulrich von, Angew. Chem., 52, 607 (1939).

223. Brady, R.C. III, and Pettit, R., J. Amer. Chem. Soc., 102, 6181 (1980).

224. Brady, R.C. III, and Pettit, R., J. Amer. Chem. Soc., 103, 1287 (1981).

225. Kummer, J.T., and Emmett, P.H., J. Amer. Chem. Soc., 75, 5177 (1953).

226. Hall, W.K., Kokes, R.J., and Emmett, P.H., J. Amer. Chem. Soc., 82, 1027 (1960).

227. Eidus, Y.T., Zelinskii, N.D., and Ershov, N.I., Dokl. Akad. Nauk. SSSR., 60, 599 (1948).

228. King, D.I., J. Catal., 51, 386 (1978).

229. Erkerdt, J.G., and Bell, A.T., J. Catal., 62, 19 (1980).

230. Kibby, C.L., and Kobylinski, T.P., Symposium on Advances in Synthetic Fuels, Petroleum Div ACS, Miami Beach, Sept. 1978.

231. Weitkamp, A.W., and Frye, C.G., Ind. Eng. Chem., 45, 363 (1953).

APPENDIX A

ANALYSIS BY GAS CHROMATOGRAPHY

To analyse the composition of the effluent stream from the reactor, a model 90-P Varian Aerograph chromatograph in conjunction with a 0.2 cm^3 gas-sampling valve was used. Helium (high purity, Matheson) was used as carrier gas, and the column consisted of 3 m of 0.64 cm OD copper tubing packed with Poropak Q (50 - 80 mesh, Waters Associates Inc.). The system was able to separate hydrogen, carbon monoxide, methane, carbon dioxide and ethane, in that order. Helium from the gas cylinder passed through the reference side of the thermal conductivity cell (TDC) of the chromatograph to the sample valve. From the sample valve it was led to the column and then to the detector side of the TDC. This single-helium-stream arrangement prevented possible problems due to imbalance in carrier gas flow rate. The operation was simple since no multicolumn arrangement was necessary. The signal in millivolt was processed by a Hewlett-Packard Integrator (model 3380-A). Table A-1 shows the conditions of the operation of the gas chromatograph; table A-2 shows the retention times of the various components.

The responses of the components in helium were linear except for hydrogen. The linear responses for methane and

carbon monoxide were established by analysing binary mixtures of $CO + CO_2$ and $CH_4 + CO_2$, assuming that CO_2 was linear in response. This latter assumption was then checked by analysing binary mixtures of $CH_4 + CO$. It was found that for all these mixtures, assumption of linear response in one component always resulted in linear response in the other component. Therefore it was concluded that the responses for these gases were linear under the gas chromatograph operating conditions.

By analysing mixtures of H_2 and CO, the response of H_2 was found to be nonlinear. Therefore it was necessary to calibrate the hydrogen curve over the whole range of compositions.

Table A-1

Operating Conditions of Gas Chromatograph

Gas Chromatograph	Varian 90-P
Column	3 m of Poropak Q
Column Temperature	Room Temperature
Detector Temperature	Room Temperature
Filament Current	220 mA
Carrier Gas	Helium
Carrier Gas Flow Rate	62 cm^3/min.

Table A-2

Retention Times for Components (min.)

Hydrogen	1.9
Carbon Monoxide	2.5
Methane	3.7
Carbon Dioxide	7.5
Ethane	23.0

A P P E N D I X B

CALCULATION PROCEDURES

B.1 Calculation of Conversion and Rate of Reaction

The composition of the effluent gas was used in the calculation of conversion and methanation rate. Other measured variables were reaction temperature and pressure. In calculating the partial pressures of the components, ideal gas behaviour was assumed. The fractional conversion X of the feed was defined as the ratio of moles feed reacted and the moles of feed supplied to the reactor.

For both CO and CO_2 methanations, no ethane was detected in the effluent. The conversion can be calculated from a knowledge of CH_4 mole fraction in the product gas as shown below:

With n_{H_2} and n_{CO} as the moles of hydrogen and carbon monxode fed to the reactor, and x and y moles of methane and carbon dioxide formed, the composition of the effluent, with the water removed, is given by:

$$f_{H_2} = (n_{H_2} - 3x + y)/n_{out}$$

$$f_{CO} = (n_{CO} - x - y)/n_{out}$$

$$f_{CO_2} = y/n_{out}$$

$$f_{CH_4} = x/n_{out}$$

where f = mole fraction of corresponding component;

n_{out} = moles of product minus water

The total conversion X is given by:

$$X = \frac{4x + y}{n_{in}} = \left(\frac{4x + y}{n_{out}}\right)\left(\frac{n_{out}}{n_{in}}\right)$$

The ratio n_{out}/n_{in} is related to the effluent composition by:

$$\frac{n_{out}}{n_{in}} = \frac{1}{1 + 3f_{CH_4} - f_{CO_2}}$$

Thus the total conversion is given by:

$$X = \frac{4f_{CH_4} + f_{CO_2}}{1 + 3f_{CH_4} - f_{CO_2}}$$

and the conversion due to methane formation only X_{CH_4} is given by:

$$X_{CH_4} = \frac{4f_{CH_4}}{1 + 3f_{CH_4} - f_{CO_2}}$$

The methanation rate is calculated as:

$$r = \frac{F\, X_{CH_4}}{W}$$

where F = feed rate (moles/second)

W = weight of catalyst (gram)

In expressing the methanation rate in terms of turnover numbers (TON), the following expression is used:

$$TON = \frac{r\ k}{4\ s}$$

where TON = molecule of methane per nickel site per second

k = Avogadro number = 6.0238×10^{23}

s = number of surface nickel atoms per gram of catalyst = 2.9025×10^{20}

For CO_2 methanation, similar considerations yield the following:

$$X = \frac{5f_{CH_4} + 2f_{CO}}{1 + 4f_{CH_4} + f_{CO}}$$

$$X_{CH_4} = \frac{5f_{CH_4}}{1 + 4f_{CH_4} + f_{CO}}$$

$$TON = \frac{r\ k}{5\ s}$$

B.2 Parameter Estimations

Parameters in the power rate law and the Langmuir-Hinshelwood type equations were estimated from the kinetic data. The best estimates of the parameters were taken to be those that minimized the sum of squares of the differences between the experimental and calculated values of rates. Nonlinear least square analysis was used in all these parameter estimations.

A general nonlinear equation can be represented by

$$\underline{y} = f(\underline{X}, \underline{\theta}) + \underline{e}$$

where $\underline{y}$ = vector of observations (dependent variables)

$\underline{X}$ = matrix of independent variables (temperature, partial pressures etc.)

$\underline{\theta}$ = vector of parameters

$\underline{e}$ = vector of errors

The errors includes

(1) measurement errors

(2) inadequacy of the model

(3) errors in the independent variables

In least square analysis, the following assumptions are made:

(1) the independent variables have fixed and known values

(2) the model is adequate

(3) the errors are independent and normally distributed with constant variance

If these assumptions are valid, the parameter values minimizing

the residual sum of squares are also the maximum likelihood estimate

$$RSS = \sum (\underline{Y} - f(\underline{X}, \underline{\theta}))^2$$

where RSS = residual sum of squares to be minimized.

The approximate individual 95% confidence intervals of the parameters, based on a linear approximation in the region of $\underline{\hat{\theta}}$, the best parameter estimates, is obtained by using the "Student's t" distribution corresponding the appropriate number of degrees of freedom:

$$\theta_i = \hat{\theta}_i + t_{0.95}^{n-p} (var(\theta_i))^{\frac{1}{2}}$$

There are several methods to minimize the residual sum of squares:

(1) a simple grid search

(2) minimization techniques such as Simplex or Rosenbrock methods

(3) Gauss linearization method by Taylor series expansion.

In the present work, an iterative method due to Marquardt was used, which combines the Gauss linearization method and the technique of steepest descent. The idea is that the steepest descent method works well on the initial iterations but the approach to the minimum grows progressively slower. On the other hand, the Gauss method works well when the minimum is approached, but often gives trouble on the initial iterations. The combination of these two methods gives a very

efficient technique of minimization. The subroutine GAUSHAUS based on the Marquardt's method was available from the McMaster University. A main program was written which supplied the rate data and the initial guessed values of the parameters, and called the subroutine GAUSHAUS and the subroutine for the model to be fitted. Criteria for convergence were relative changes in the residual sum of squares or the parameters between two iterations being less than 0.1%. The GAUSHAUS subroutine provided the estimated parameter values and their approximate individual 95% confidence intervals, the correlations between all the parameters, the final calculated function values, and their approximate confidence intervals. To ensure global minimum, different initial values of the parameters were tried.

A P P E N D I X C

DERIVATION OF RATE EQUATIONS

C.1 Derivation of Rate Equation 4-4 for CO Methanation

The methanation of carbon monoxide is perceived to proceed via the following steps:

$$H_2 + 2S \underset{k_{-1}}{\overset{k_1}{\rightleftharpoons}} 2H_s \quad (1)$$

$$CO + S \underset{k_{-2}}{\overset{k_2}{\rightleftharpoons}} CO_s \quad (2)$$

$$CO_s + S \underset{k_{-3}}{\overset{k_3}{\rightleftharpoons}} C_s + O_s \quad (3)$$

$$O_s + H_s \underset{k_{-4}}{\overset{k_4}{\rightleftharpoons}} (OH)_s \quad (4)$$

$$(OH)_s + H_s \underset{k_{-5}}{\overset{k_5}{\rightleftharpoons}} H_2O + 3S \quad (5)$$

$$C_s + H_s \underset{k_{-6}}{\overset{k_6}{\rightleftharpoons}} (CH)_s \quad (6)$$

$$(CH)_s + H_s \xrightarrow{k_7} (CH_2)_s + 2S \quad (7)$$

$$(CH_2)_s + H_s \underset{k_{-8}}{\overset{k_8}{\rightleftharpoons}} (CH_3)_s + S \quad (8)$$

$$(CH_3)_s + H_s \underset{k_{-9}}{\overset{k_9}{\rightleftharpoons}} CH_4 + 2S \quad (9)$$

The following assumptions are made:

(i) Dissociative adsorption of H_2 is rapid and in equilibrium with gaseous H_2

(ii) Chemisorption of CO is rapid and in equilibrium with gasesous CO

(iii) The dissociation of adsorbed CO is reversible

(iv) Surface carbon is hydrogenated stepwise to CH_x (x = 1-3) species

(v) Surface oxygen is hydrogenated stepwise to form water

(vi) The rate determining step is

$$(CH)_s + H_s \xrightarrow{k_7} (CH_2)_s + 2S \qquad (7)$$

Steps (2) and (3) can be simplified to

$$CO + 2S \underset{k_{-10}}{\overset{k_{10}}{\rightleftharpoons}} C_s + O_s \qquad (10)$$

Since the overall rate of methane formation is proportional to that of water formation, one has

$$r_{CH_4} = k_7 [CH_s][H_s]$$
$$= k'(k_5 [OH_s][H_s] - k_{-5} S^3 P_{H_2O})$$

where $k' \leqslant 1$ is a proportionality constant. Assuming that $k_{-5} \ll k_5$, one has

$$k_7 [CH_s][H_s] = k' k_5 [OH_s][H_s]$$

Using steps (4) and (6) above,

$$k_7 K_6 [C_s][H_s]^2 = k' k_5 K_4 [O_s][H_s]^2$$

from which the concentration of C_s is related to that of O_s via

$$[C_s] = k''[O_s]$$

where $k'' = k' k_5 K_4 / k_7 K_6$. Using step (10) we have

$$k_{10} P_{CO} S^2 = k_{-10} [C_s] [O_s]$$
$$= k_{-10} [C_s]^2 / k''$$
or $$C_s = \sqrt{K_{10} k''} \; P_{CO}^{\frac{1}{2}} \; S$$

The rate is given by

$$r_{CH_4} = k_7 [CH_s] [H_s]$$
$$= k_7 K_6 [H_s]^2 [C_s]$$
$$= K_1 k_7 K_6 \sqrt{K_{10} k''} \; P_{H_2} P_{CO}^{\frac{1}{2}} \; S^3$$

Assuming that the catalyst surface is mostly occupied by H_s and C_s, one has

$$\frac{S}{S_o} = \frac{1}{(1 + K_1^{\frac{1}{2}} P_{H_2}^{\frac{1}{2}} + (K_{10} k'')^{\frac{1}{2}} P_{CO}^{\frac{1}{2}})}$$

where S_o is the number of surface site per gram of catalyst. Thus the rate is given by

$$r_{CH_4} = \frac{S_0^3 k_7 K_1 K_6 (K_{10} k'')^{\frac{1}{2}} P_{H_2} P_{CO}^{\frac{1}{2}}}{(1 + K_1^{\frac{1}{2}} P_{H_2}^{\frac{1}{2}} + (K_{10} k'')^{\frac{1}{2}} P_{CO}^{\frac{1}{2}})^3}$$

which is the equivalent of equation 4-4.

C.2 Derivation of Rate Equation 5-2 for CO_2 Methanation

The following mechanism is proposed for CO_2 methanation:

$$H_2 + 2S \underset{k_{-1}}{\overset{k_1}{\rightleftharpoons}} 2H_s \quad (1)$$

$$CO_2 + S \underset{k_{-2}}{\overset{k_2}{\rightleftharpoons}} (CO_2)_s \quad (2)$$

$$(CO_2)_s + S \underset{k_{-3}}{\overset{k_3}{\rightleftharpoons}} CO_s + O_s \quad (3)$$

$$CO_s + S \underset{k_{-4}}{\overset{k_4}{\rightleftharpoons}} C_s + O_s \quad (4)$$

$$O_s + H_s \underset{k_{-5}}{\overset{k_5}{\rightleftharpoons}} (OH)_s \quad (5)$$

$$(OH)_s + H_s \underset{k_{-6}}{\overset{k_6}{\rightleftharpoons}} H_2O + 3S \quad (6)$$

$$C_s + H_s \underset{k_{-7}}{\overset{k_7}{\rightleftharpoons}} (CH)_s \quad (7)$$

$$(CH)_s + H_s \xrightarrow{k_8} (CH_2)_s + 2S \quad (8)$$

$$(CH_2)_s + H_s \underset{k_{-9}}{\overset{k_9}{\rightleftharpoons}} (CH_3)_s + S \quad (9)$$

$$(CH_3)_s + H_s \underset{k_{-10}}{\overset{k_{10}}{\rightleftharpoons}} CH_4 + 2S \quad (10)$$

The following assumptions are made:

(i) Dissociative adsorption of H_2 is rapid and in equilibrium with gaseous H_2

(ii) Adsorption and dissociation of CO_2 are reversible and in equilibrium, so that steps (2) to (4) can be simplified to

$$CO_2 + 3S \underset{k_{-11}}{\overset{k_{11}}{\rightleftharpoons}} C_s + 2O_s \qquad (11)$$

(iii) Surface carbon is hydrogenated stepwise to CH_x (x = 1-3) species

(iv) Surface oxygen is hydrogenated stepwise to form water

(v) The rate determining step is

$$(CH)_s + H_s \xrightarrow{k_8} (CH_2)_s + 2S \qquad (8)$$

Since the overall rate of methane formation is proportional to that of water formation, one has

$$r_{CH_4} = k_8 \left[CH_s\right] \left[H_s\right]$$
$$= \frac{k'}{2}\left(k_6 \left[OH_s\right] \left[H_s\right] - k_{-6} P_{H_2O} S^3\right)$$

where $k' \leqslant 1$ is a proportionality constant. Assuming that $k_{-6} \ll k_6$, one has

$$2k_8 \left[CH_s\right] \left[H_s\right] = k'k_6 \left[OH_s\right] \left[H_s\right]$$

Using steps (5) and (7) above,

$$2k_8K_7 \left[C_s\right] \left[H_s\right]^2 = k'k_6K_5 \left[O_s\right] \left[H_s\right]^2$$

from which the concentration of C_s is related to that of O_s via

$$\left[C_s\right] = k'' \left[O_s\right]$$

where $k'' = k'k_6K_5/2k_8K_7$. Using step (11), we have

$$k_{10} P_{CO_2} S^3 = k_{-11}[C_s]^3 / k''^2$$

or $$C_s = (K_{11}k''^2)^{1/3} P_{CO_2}^{1/3} S$$

The rate is given by

$$\begin{aligned} r_{CH_4} &= k_8 [CH_s][H_s] \\ &= k_8 K_7 [C_s][H_s]^2 \\ &= k_8 K_1 K_7 (K_{11}k''^2)^{1/3} P_{H_2} P_{CO_2}^{1/3} S^3 \end{aligned}$$

Assuming that the catalyst surface is mostly occupied by adsorbed H_s and CO_s, one has

$$S/S_o = 1 \Big/ \left(1 + K_1^{1/2} P_{H_2}^{1/2} + \frac{(K_{11}^2 k'')^{1/3}}{K_4} P_{CO_2}^{2/3}\right)$$

where S_o is the number of surface site per gram of catalyst. Thus the rate is given by

$$r_{CH_4} = \frac{S_o^3 k_8 K_1 K_7 (K_{11}k''^2)^{1/3} P_{H_2} P_{CO_2}^{1/3}}{\left(1 + K_1^{1/2} P_{H_2}^{1/2} + \frac{(K_{11}^2 k'')^{1/3}}{K_4} P_{CO_2}^{2/3}\right)^3}$$

which is the equivalent of equation 5-2.

A P P E N D I X D

TABLES OF EXPERIMENTAL DATA

TABLE D-1

Rate Data for the Effect of H_2 on CO Methanation Rate at 503.3 K

(Figure 4-1)

H_2 Partial Pressure (kPa)	CO Partial Pressure (kPa)	Turnover Number x 1000
8.6	14.3	0.97
8.4	14.4	1.01
17.9	14.4	2.05
18.6	14.3	1.96
33.6	14.5	3.74
33.0	14.5	3.80
75.8	14.2	7.87
75.2	14.2	7.90
138.1	14.4	16.71
134.7	14.3	16.68
136.4	1.9	30.22
136.5	2.1	30.63
76.7	2.1	23.16
76.8	2.0	22.61
40.6	2.0	13.72
40.4	2.1	13.21
17.0	1.8	6.19
16.6	1.9	6.15
7.9	2.2	2.46
7.8	2.1	2.38
4.3	2.1	1.21
4.1	2.1	1.53

TABLE D-2

Rate Data for the Effect of H_2 on CO Methanation Rate at 502.4 K

(Figure 4-2)

H_2 Partial Pressure (kPa)	CO Partial Pressure (kPa)	Turnover Number x 1000
128.7	25.0	4.30
155.3	24.3	5.39
155.1	24.6	5.35
181.2	24.4	5.99
181.3	24.3	5.84
91.2	25.7	3.27
91.2	25.7	3.32
39.6	84.4	0.97
39.7	84.3	0.84
81.8	83.2	1.78
25.0	85.6	0.57
25.0	85.0	0.58
51.4	86.4	1.20
51.5	86.3	1.21
109.0	83.7	2.47
67.3	83.8	1.55
66.7	84.4	1.46
95.2	83.7	1.88
94.7	84.1	1.77

TABLE D-3

Rate Data for the Effect of CO on Methanation Rate at 503.3 K

(Figure 4-3)

H_2 Partial Pressure (kPa)	CO Partial Pressure (kPa)	Turnover Number x 1000
75.4	12.9	6.82
75.5	12.9	7.12
76.0	7.4	9.71
76.2	7.5	9.99
75.2	4.0	12.94
74.7	4.0	13.27
77.0	2.1	21.01
76.9	2.1	20.68
75.2	1.2	19.62
75.2	1.2	19.37
75.2	0.8	17.10
75.7	0.8	17.14
68.9	38.8	3.43
70.3	39.0	3.24
70.2	77.5	1.98
70.2	77.8	2.06
10.4	2.7	2.42
10.3	2.7	2.44
10.7	8.5	1.10
10.2	8.4	1.02
10.5	1.4	3.71
10.8	1.4	3.72
10.8	1.4	3.77
9.9	16.3	0.79
10.1	16.3	0.72

TABLE D-4

Rate Data on the Effect of H_2/CO Ratio on Methanation Rate at 502.4 K

(Figure 4-4)

H_2 Partial Pressure (kPa)	CO Partial Pressure (kPa)	Turnover Number x 1000
169.1	23.2	6.05
71.5	121.2	1.12
147.3	45.4	3.50
128.6	64.4	2.53
100.7	92.5	1.64
178.7	13.9	8.63
133.6	59.1	2.79
69.7	123.1	1.01
84.1	108.6	1.21
58.3	134.4	0.80
154.4	38.3	3.93
119.3	73.5	2.17
29.9	162.9	0.36
96.3	96.8	1.51

TABLE D-5

Rate Data on the Effect of Total Pressure on CO Methanation

(Figure 4-5)

H_2 Partial Pressure (kPa)	CO Partial Pressure (kPa)	Turnover Number x 1000
	(At 480.7 K)	
91.9	29.0	0.97
91.9	29.0	0.97
105.1	33.1	0.99
104.9	33.1	1.00
136.7	43.2	1.04
136.8	43.2	1.06
117.1	37.0	1.01
117.3	37.0	1.00
117.2	37.0	0.99
105.1	32.8	0.98
104.4	33.0	0.98
104.5	33.0	1.00
136.2	43.1	1.03
136.0	43.0	1.05
136.7	42.9	1.04
50.6	15.9	0.88
50.5	16.0	0.86
37.4	11.9	0.85
37.4	11.9	0.85
37.6	11.9	0.85
23.4	7.2	0.78
23.4	7.2	0.78
23.4	7.2	0.77
	(At 505.4 K)	
92.1	29.2	5.64
134.7	42.7	5.92
135.3	42.7	6.00
134.7	42.7	6.02
134.6	42.7	5.94

TABLE D-5 (continued)

H_2 Partial Pressure (kPa)	CO Partial Pressure (kPa)	Turnover Number x 1000
104.1	32.9	5.62
103.9	33.0	5.66
103.9	33.0	5.63
36.3	12.5	4.53
39.4	12.5	4.58
39.4	12.5	4.57
49.0	15.5	4.79
48.9	15.5	4.73
49.0	15.5	4.77
23.4	7.3	4.13
23.4	7.3	4.07
23.4	7.3	4.11
30.4	9.7	4.29
30.5	9.7	4.26
30.5	9.7	4.24

TABLE D-6

Rate Data for the Effect of Temperature on CO Methanation Rate

(Figure 4-6)

H_2 Partial Pressure (kPa)	CO Partial Pressure (kPa)	Temperature (K)	Turnover Number x 1000
146.5	45.6	512.3	7.65
147.3	44.9	512.3	7.48
146.9	45.4	492.3	1.28
147.0	45.4	492.3	1.25
147.3	45.4	522.2	9.97
147.1	45.6	522.2	9.88
147.3	44.8	503.0	3.75
146.4	45.8	503.0	3.80
147.0	45.8	503.0	3.79
201.3	62.3	502.2	2.22
201.0	62.6	502.2	2.18
200.7	62.5	492.5	1.10
201.0	62.1	492.5	1.10
201.3	61.6	512.5	4.27
201.0	61.9	512.5	4.43
200.6	61.7	522.0	8.72
200.6	61.7	522.0	8.39
92.6	28.5	522.0	4.97
92.3	28.9	522.0	4.75
93.1	28.3	502.0	1.15
92.6	28.9	502.0	1.12
92.9	28.5	511.8	2.29
92.7	28.7	511.8	2.29
92.9	28.7	492.4	0.56
92.9	28.7	492.4	0.58

TABLE D-7

Rate Data for the Effect of Temperature on CO Methanation Rate

(Figure 4-7)

H_2 Partial Pressure (kPa)	CO Partial Pressure (kPa)	Temperature (K)	Turnover Number x 1000
92.4	29.0	503.7	4.50
91.7	29.0	503.7	4.48
91.1	28.8	495.0	2.43
91.0	28.8	495.0	2.41
90.6	28.5	475.8	0.58
90.5	28.5	475.8	0.59
90.4	28.5	475.8	0.60
90.6	28.7	484.2	1.18
90.7	28.6	484.2	1.16
90.6	28.6	484.2	1.18
90.0	28.7	484.2	1.12
92.5	29.2	515.0	11.34
91.8	29.2	515.0	11.30
91.7	29.0	503.7	4.48
91.6	29.0	503 7	4.48
91.3	28.8	495.0	2.49
91.1	28.8	495.0	2.43
30.2	9.5	493.3	1.76
30.2	9.6	493.3	1.77
30.3	9.7	493.3	1.80
30.6	9.5	504.4	3.75
30.5	9.5	504.4	3.77
29.4	9.3	474.0	0.41
29.6	9.3	474.0	0.46
29.4	9.3	474.0	0.45
29.7	9.4	483.7	0.96
29.9	9.4	483.7	0.95
30.1	9.4	494.1	1.87
30.0	9.4	494.1	1.86

TABLE D-8

Rate Data for the Effect of H_2 on CO Methanation Rate at 474.7 K

(Figure 4-8)

H_2 Partial Pressure (kPa)	CO Partial Pressure (kPa)	Turnover Number x 1000
124.2	17.5	1.57
150.0	17.4	2.00
167.4	16.9	2.13
136.8	17.2	1.77
136.5	17.0	1.79
167.7	17.5	2.21
168.4	17.4	2.12
150.8	17.1	1.97
124.4	17.0	1.61
123.4	17.1	1.64
100.2	17.9	1.24
69.4	17.9	0.83
69.3	17.9	0.84
84.6	17.8	1.10
85.1	17.9	1.07

TABLE D-9

Rate Data for the Effect of H_2 on CO Methanation Rate at 493.5 K

(Figure 4-9)

H_2 Partial Pressure (kPa)	CO Partial Pressure (kPa)	Turnover Number x 1000
50.6	13.2	2.79
50.7	13.2	2.75
29.1	13.1	1.92
29.0	13.1	1.92
106.4	13.3	4.80
106.7	13.2	4.72
61.7	13.2	3.25
61.9	13.2	3.28
39.2	13.1	2.40
39.2	13.0	2.33
69.3	13.2	3.48
69.1	13.2	3.46
18.7	13.2	1.39
18.6	13.2	1.38
10.2	13.0	0.95
143.8	13.4	6.16
144.1	13.4	6.17
124.0	32.8	2.97
124.7	32.8	3.10
104.2	32.5	2.67
105.2	32.5	2.70
57.6	32.5	1.65
57.6	32.5	1.62
27.0	32.5	0.93
27.0	32.6	0.92
48.2	32.4	1.41
48.3	32.5	1.44
146.8	32.7	3.50
147.1	32.7	3.54
87.4	32.3	2.27

TABLE D-9 (continued)

H_2 Partial Pressure (kPa)	CO Partial Pressure (kPa)	Turnover Number x 1000
87.4	32.3	2.29
54.8	32.5	1.61
54.5	32.5	1.61
33.8	32.5	1.10
33.9	32.5	1.09
62.9	32.6	1.77
62.9	32.6	1.74
40.5	32.4	1.28
40.7	32.4	1.24
113.4	7.0	6.49
113.3	7.0	6.47
64.6	7.1	4.35
64.5	7.1	4.47
31.2	7.0	2.61
31.2	7.0	2.64
9.9	7.0	1.15
9.9	7.0	1.13
86.3	7.1	5.45
86.4	7.1	5.45
41.6	7.1	3.21
42.4	7.1	3.24
53.9	7.1	3.89
54.1	7.1	3.90
76.5	7.0	4.94
76.0	7.0	4.96
20.5	7.1	2.03
20.6	7.1	1.94
113.4	7.1	6.83

TABLE D-10

Rate Data for the Effect of Hydrogen on CO Methanation Rate at 513.4 K

(Figure 4-10)

H_2 Partial Pressure (kPa)	CO Partial Pressure (kPa)	Turnover Number x 1000
24.3	63.4	1.09
24.4	63.4	1.09
33.6	63.4	1.45
33.6	63.4	1.45
17.4	63.4	0.77
55.3	63.6	2.41
55.2	63.6	2.31
89.9	63.4	3.17
90.0	63.4	3.15
24.5	63.4	0.84
24.5	63.4	0.87
33.9	63.6	1.17
34.0	63.6	1.16
34.1	63.7	1.20
17.5	63.4	0.65
55.0	63.6	1.97
55.7	63.6	1.94
90.5	63.6	2.75
90.0	63.6	2.72
39.4	26.4	1.60
39.4	26.4	1.64
39.6	26.5	1.71
17.2	26.6	0.85
17.3	26.6	0.82
92.3	26.5	3.31
92.6	26.5	3.30
55.0	26.6	2.14
55.2	26.6	2.15
22.5	26.5	1.03
22.3	26.5	1.05
28.6	26.6	1.33
28.6	26.6	1.32
92.0	26.6	3.47
91.5	26.6	3.45

TABLE D-11

Rate Data for the Effect of CO on Methanation Rate at 474.7 K

(Figure 4-11)

H_2 Partial Pressure (kPa)	CO Partial Pressure (kPa)	Turnover Number x 1000
161.2	8.8	2.88
160.6	8.8	2.86
161.1	12.5	2.22
160.9	12.5	2.21
162.2	6.9	3.25
161.8	6.8	3.25
161.5	6.3	3.40
161.2	5.7	3.67
161.0	1.9	6.55
161.1	1.8	6.43
161.2	3.5	4.53
161.0	3.5	4.62

TABLE D-12

Rate Data for the Effect of CO on Methanation Rate at 493.5 K

(Figure 4-12)

H_2 Partial Pressure (kPa)	CO Partial Pressure (kPa)	Turnover Number x 1000
87.4	32.7	2.31
87.2	32.8	2.29
87.0	5.9	6.36
87.2	5.9	6.30
86.6	14.3	3.68
86.9	14.3	3.74
86.7	14.3	3.65
86.9	25.4	2.60
86.7	25.4	2.62
87.2	10.1	4.67
87.8	10.1	4.66
86.8	14.3	3.80
87.6	54.9	1.60
86.8	54.9	1.55
87.0	54.9	1.54
87.2	18.3	3.31
87.1	18.3	3.21
42.6	76.8	0.70
42.7	76.8	0.68
42.5	39.9	1.06
42.4	39.9	1.08
42.6	13.0	2.23
42.9	13.0	2.21
42.5	8.4	2.87
42.4	8.5	2.97
42.6	48.6	0.94
42.5	48.5	0.94
42.5	48.5	0.95
42.6	22.0	1.60
42.7	21.9	1.62

TABLE D-12 (continued)

H_2 Partial Pressure (kPa)	CO Partial Pressure (kPa)	Turnover Number x 1000
42.6	6.0	3.45
42.5	5.9	3.49
137.9	13.6	5.10
138.2	13.6	5.13
136.6	23.8	3.56
136.7	23.8	3.64
136.8	23.8	3.58
136.9	44.9	2.37
136.5	45.0	2.39
136.9	6.5	8.10
136.2	6.5	8.31
136.2	34.1	2.85
136.2	34.2	2.79

TABLE D-13

Rate Data for the Effect of CO on Methanation Rate at 513.4 K

(Figure 4-13)

H_2 Partial Pressure (kPa)	CO Partial Pressure (kPa)	Turnover Number x 1000
69.6	48.7	1.78
69.4	48.7	1.85
70.3	9.9	4.34
70.1	9.9	4.23
70.2	17.7	3.15
70.5	17.7	3.25
70.1	13.3	3.73
69.7	13.3	3.69
69.8	22.8	2.69
69.6	22.8	2.75
70.1	34.5	2.17
70.4	34.5	2.19
69.5	29.2	2.40
69.8	29.2	2.37
35.6	11.6	2.39
35.6	11.7	2.40
35.5	11.7	2.36
35.6	21.2	1.66
35.4	21.2	1.73
35.7	8.1	2.93
35.7	8.0	2.89
35.4	32.8	1.25
35.5	32.8	1.23
35.6	15.2	2.11
35.6	15.3	2.04
35.7	44.2	1.01
35.7	44.2	0.95

TABLE D-14

Rate Data for the Effect of Methane on CO Methanation Rate

(Figure 4-14)

H_2 Partial Pressure (kPa)	CO Partial Pressure (kPa)	CH_4 Partial Pressure (kPa)	Turnover Number x 1000
	(At 486 K)		
60.1	7.1	0.0	6.10
60.2	7.1	38.3	5.95
60.3	7.1	12.6	5.48
59.8	7.1	5.8	5.85
60.1	7.1	20.2	6.13
59.5	7.1	51.5	6.94
60.1	7.1	25.7	6.04
59.6	7.1	32.2	6.32
59.6	7.1	44.9	6.56
	(At 493 K)		
63.8	3.6	0.0	12.04
63.4	3.6	45.7	12.60
63.2	3.6	32.4	10.68
64.0	3.6	13.1	11.93
63.3	3.7	19.4	9.72
63.9	3.7	6.1	10.00
63.7	3.6	39.5	13.33
63.6	3.6	26.4	13.27
62.2	3.6	52.1	12.65
55.0	12.4	0.0	4.73
54.5	12.4	31.0	4.89
55.0	12.4	37.6	4.84
54.5	12.4	18.5	4.90
54.5	12.4	50.3	5.26
54.4	12.4	43.3	5.30
54.7	12.4	12.1	4.49
55.0	12.4	25.0	4.69

TABLE D-15

Rate Data for the Effect of Water on CO Methanation Rate at 493.5 K

(Figures 4-15 and 4-16)

H_2 Partial Pressure (kPa)	CO Partial Pressure (kPa)	H_2O Partial Pressure (kPa)	Turnover Number x 1000
89.7	29.2	0.0	2.77
90.2	29.2	0.0	2.78
89.8	29.0	20.7	2.38
89.8	29.0	20.7	2.38
90.2	28.5	13.9	2.45
90.2	28.6	13.9	2.44
90.1	28.6	13.9	2.45
89.8	28.5	13.9	2.45
89.4	29.3	7.0	2.57
89.4	29.4	7.0	2.57
89.2	29.1	9.3	2.51
89.4	29.1	9.3	2.50
89.1	29.1	3.4	2.68
89.4	29.1	3.4	2.69
89.5	28.4	27.7	2.34
89.6	28.4	27.7	2.34
89.0	28.8	41.4	2.29
89.8	28.8	41.4	2.26
83.2	27.1	8.2	2.05
83.2	27.0	8.2	2.05
120.5	38.4	7.1	2.32
120.6	38.5	7.1	2.31
122.2	39.9	4.7	2.34
122.5	39.8	4.7	2.35
79.7	26.1	15.7	1.90
79.8	25.9	15.7	1.92
80.2	34.9	16.8	2.06
79.6	34.9	16.8	2.05

TABLE D-15 (continued)

H_2 Partial Pressure (kPa)	CO Partial Pressure (kPa)	H_2O Partial Pressure (kPa)	Turnover Number x 1000
82.9	27.0	8.2	2.07
83.2	27.0	8.2	2.03
113.8	37.0	11.2	2.14
113.6	37.1	11.2	2.11
113.9	37.1	11.2	2.10
73.8	23.5	22.6	1.82
73.8	23.5	22.6	1.86
73.8	23.6	22.6	1.88
107.6	35.2	21.1	1.96
107.4	35.2	21.1	1.97
102.5	32.9	31.5	1.95
102.9	32.9	31.5	1.95
102.7	32.9	31.5	1.95
81.4	26.1	12.5	1.94
87.4	28.5	3.3	2.26
87.1	28.4	3.3	2.29
87.6	28.5	3.3	2.30
87.5	28.5	3.3	2.32
85.8	27.6	5.0	2.16
86.3	27.6	5.0	2.13
86.1	27.5	5.0	2.15
85.7	27.5	5.0	2.14
97.7	31.9	37.8	1.95
98.1	31.8	37.8	1.96
97.9	31.8	37.8	1.93
69.6	22.7	26.8	1.81
69.8	22.7	26.8	1.78
69.8	22.7	26.8	1.80
69.7	22.7	26.8	1.77
62.7	19.9	37.0	1.72
62.9	20.0	37.0	1.72
62.7	20.0	37.0	1.72
62.7	20.0	37.0	1.73
50.3	16.1	3.0	1.99
50.5	16.1	3.0	1.99
50.1	16.1	3.0	2.07
50.2	16.1	3.0	2.06
47.4	14.4	4.7	1.94

TABLE D-15 (continued)

H_2 Partial Pressure (kPa)	CO Partial Pressure (kPa)	H_2O Partial Pressure (kPa)	Turnover Number x 1000
47.2	14.4	4.7	1.96
47.3	14.4	4.7	1.92
47.2	14.4	4.7	1.93
44.7	13.7	11.2	1.81
44.6	13.7	11.2	1.81
44.7	13.7	11.2	1.84
41.1	12.5	20.4	1.63
40.9	12.5	20.4	1.65
41.0	12.5	20.4	1.65
40.7	12.5	20.4	1.66

TABLE D-16

Rate Data for the Effect of Carbon Dioxide on CO Methanation

(Figure 4-17)

H_2 Partial Pressure (kPa)	CO Partial Pressure (kPa)	CO_2 Partial Pressure (kPa)	Turnover Number x 1000
106.1	33.4	27.2	2.31
105.9	33.4	27.4	2.33
106.2	33.3	27.6	2.36
105.3	33.1	5.0	2.26
105.6	33.0	5.0	2.21
107.4	33.2	40.4	2.32
106.9	33.4	40.3	2.32
106.5	33.4	40.8	2.33
106.0	33.4	41.0	2.28
105.6	33.0	0.0	2.24
104.9	33.1	0.0	2.22
104.9	33.0	0.0	2.19
105.6	33.2	1.4	2.23
105.6	33.2	1.5	2.24
105.2	33.2	1.5	2.20
52.8	16.7	51.3	2.22
52.9	16.6	51.2	2.23
52.7	16.7	6.6	2.04
52.8	16.7	6.6	2.04
51.9	16.5	0.0	2.02
52.6	16.5	0.0	2.02
53.0	16.8	2.1	2.01
52.8	16.8	2.1	2.02
52.3	16.5	0.0	2.03
52.3	16.5	0.0	2.01
52.9	16.7	9.9	2.09
52.7	16.7	9.9	2.09
53.0	16.5	31.6	2.16
52.6	16.6	31.6	2.12
52.5	16.6	16.7	2.09
52.7	16.6	16.7	2.07
52.3	16.6	4.3	2.02
52.4	16.6	4.4	2.05

TABLE D-17

Rate Data for the Preliminary Study of CO_2 Methanation at 503 K

(Figure 5-1)

H_2 Partial Pressure (kPa)	CO_2 Partial Pressure (kPa)	Turnover Number x 1000
128.1	25.9	4.77
145.7	26.3	5.00
99.5	26.0	4.58
62.7	25.5	4.20
91.0	26.1	4.54
39.1	25.9	3.67
20.1	26.1	2.99
65.6	17.2	3.96
65.6	9.2	3.42
65.7	36.2	4.33
66.9	70.6	4.65
65.1	112.9	4.59

TABLE D-18

Rate Data for the Effect of Total Pressure on CO_2 Methanation Rate at 504 K

(Figure 5-2)

H_2 Partial Pressure (kPa)	CO_2 Partial Pressure (kPa)	Turnover Number x 1000
36.1	9.1	2.43
53.5	13.8	2.91
76.1	20.3	3.33
24.1	6.0	2.07
47.4	12.1	3.38
85.0	22.7	3.38
93.2	24.8	3.43
141.0	37.6	3.86
81.9	21.2	3.35

TABLE D-19

Rate Data for the Effect of Temperature on CO_2 Methanation Rate

(Figure 5-3)

H_2 Partial Pressure (kPa)	CO_2 Partial Pressure (kPa)	Temperature (K)	Turnover Number x 1000
95.4	25.0	523.2	8.45
95.5	25.0	523.2	8.40
96.5	25.2	493.8	2.21
96.5	25.2	493.8	2.21
95.8	25.1	481.8	1.14
95.8	25.1	481.8	1.12
95.4	25.0	503.2	3.40
95.2	25.0	503.2	3.48
95.5	25.0	514.0	5.71
95.6	25.0	514.0	5.67
141.9	37.0	503.7	3.99
141.8	36.9	503.7	3.92
141.8	37.2	481.9	1.40
141.7	37.2	481.9	1.40
141.5	37.2	493.7	2.48
141.5	37.1	493.7	2.44
142.2	37.1	523.1	9.05
142.2	37.1	523.1	9.00
141.9	37.0	513.1	5.74
141.9	37.0	513.1	5.98
58.2	15.2	511.9	4.07
58.1	15.2	511.9	4.11
58.2	15.2	511.9	4.10
57.6	15.2	491.4	1.58
57.9	15.2	491.4	1.57
58.5	15.2	502.6	2.68
58.4	15.2	502.6	2.66
57.6	15.1	523.5	6.65
57.8	15.2	523.5	6.82
57.8	15.1	481.8	0.90
57.9	15.2	481.8	0.94

TABLE D-19 (continued)

H_2 Partial Pressure (kPa)	CO_2 Partial Pressure (kPa)	Temperature (K)	Turnover Number x 1000
33.0	8.8	484.2	0.89
33.0	8.8	484.2	0.83
33.4	8.9	511.1	3.04
33.4	8.9	511.1	3.07
33.2	8.8	491.8	1.25
33.3	8.8	491.8	1.25
33.7	9.0	523.3	5.11
33.8	9.0	523.3	5.18
33.3	8.8	501.6	1.94
33.4	8.9	501.6	2.03

TABLE D-20

Rate Data for the Effect of Hydrogen on CO_2 Methanation Rate at 483.9 K

(Figure 5-4)

H_2 Partial Pressure (kPa)	CO_2 Partial Pressure (kPa)	Turnover Number x 1000
35.9	13.7	5.15
35.8	13.8	5.15
106.5	13.7	5.97
106.5	13.8	5.99
8.2	13.9	3.57
8.4	13.8	3.51
21.2	13.8	4.77
21.2	13.9	4.77
89.2	13.8	5.97
125.0	13.8	6.13
197.1	13.7	6.09
28.5	13.8	4.98
42.9	13.7	5.35
160.5	13.8	6.15
183.5	13.7	6.14
17.4	13.9	4.43
17.4	13.9	4.50
52.5	13.8	5.50
53.3	13.9	5.50
61.6	13.9	5.73
106.2	13.8	5.99
95.1	27.4	6.97
95.4	27.4	6.99
176.6	27.6	7.16
140.9	27.6	7.16
28.3	27.6	5.63
20.5	27.6	5.26
13.7	27.5	4.49
6.6	27.5	3.39
42.3	27.6	6.23

TABLE D-20 (continued)

H_2 Partial Pressure (kPa)	CO_2 Partial Pressure (kPa)	Turnover Number x 1000
35.2	27.1	6.03
52.3	27.5	6.59
71.3	27.6	6.89
122.4	27.4	7.12
104.7	27.4	7.04
108.9	68.7	8.25
109.1	68.6	8.32
65.6	69.7	7.85
65.7	69.6	7.83
6.1	68.9	3.24
6.1	69.0	3.21
12.3	69.0	4.55
12.3	68.9	4.67
18.6	68.7	5.53
18.6	68.7	5.50
45.2	69.2	7.19
45.4	69.2	7.19
25.2	68.9	6.10
25.2	68.9	6.00
38.2	68.7	6.91
31.3	68.1	6.60
95.0	69.0	8.27
123.0	68.4	3.42
122.6	68.6	3.45
73.9	69.0	8.03
73.7	69.0	8.10
6.5	137.8	2.95
12.8	137.9	4.43
56.5	137.2	7.88
34.5	138.2	6.80

TABLE D-20 (continued)

H_2 Partial Pressure (kPa)	CO_2 Partial Pressure (kPa)	Turnover Number x 1000
19.9	138.1	5.39
49.5	137.5	7.52
28.1	137.8	6.13
64.4	138.2	8.02
41.9	137.6	6.97
34.6	137.4	6.70
41.8	137.6	7.00
19.8	137.6	5.34
19.9	137.8	5.30

TABLE D-21

Rate Data for the Effect of Hydrogen on CO_2 Methanation Rate at 483.9 K

(Figure 5-5)

H_2 Partial Pressure (kPa)	CO_2 Partial Pressure (kPa)	Turnover Number x 1000
71.6	9.2	5.53
50.8	9.2	5.28
32.3	9.1	4.84
84.3	9.1	5.53
14.6	9.2	4.20
91.8	9.1	5.54
106.7	8.8	5.54
107.9	9.1	5.59
172.0	9.2	5.53
107.8	9.0	5.48
172.6	9.2	5.52

TABLE D-22

Rate Data for the Effect of Hydrogen on CO_2 Methanation at 504.4 K

(Figure 5-6)

H_2 Partial Pressure (kPa)	CO_2 Partial Pressure (kPa)	Turnover Number x 1000
86.3	27.9	24.52
69.3	27.5	23.97
102.5	27.4	24.56
126.4	27.1	24.46
142.9	27.1	24.91
176.4	27.0	24.68
41.2	27.6	21.61
31.9	27.6	20.28
22.3	27.8	18.05
12.3	27.8	14.52
7.7	27.9	11.40
17.2	27.9	16.38
141.8	27.1	24.86
124.7	27.0	24.54
100.9	27.3	24.30
69.2	27.5	24.09
73.8	27.5	24.04
67.8	27.9	24.31
55.5	27.6	23.47
55.6	27.6	22.81
87.2	27.7	24.56
55.8	15.2	20.11
50.0	15.2	19.61
42.1	15.3	19.02
162.9	14.2	21.48
116.5	14.4	21.42
90.0	15.2	21.48
56.1	15.2	20.26
59.6	15.2	20.55
75.2	15.4	20.83

TABLE D-22 (continued)

H_2 Partial Pressure (kPa)	CO_2 Partial Pressure (kPa)	Turnover Number x 1000
17.5	15.4	15.43
9.0	15.4	12.11
99.1	14.3	21.37
132.5	14.4	21.41
163.8	14.5	21.65
83.8	15.4	21.33
75.4	15.3	21.24
42.0	15.1	18.80
13.1	15.4	13.81
50.3	15.2	19.77
34.2	15.2	18.04
26.1	15.4	17.05
74.3	15.2	20.81
59.7	15.2	20.53
59.8	15.2	20.36
150.6	14.3	21.43
150.4	14.6	21.26

TABLE D-23

Rate Data for the Effect of Hydrogen on CO_2 Methanation at 504.4 K

(Figure 5-7)

H_2 Partial Pressure (kPa)	CO_2 Partial Pressure (kPa)	Turnover Number x 1000
31.2	68.5	15.56
26.1	68.3	14.50
5.5	72.9	6.67
52.5	68.9	18.94
63.2	69.2	19.70
20.8	68.6	13.31
15.4	68.5	11.69
10.3	68.1	9.36
113.6	68.9	21.18
139.8	69.1	21.69
74.4	69.1	20.38
85.2	68.9	20.67
41.0	68.5	17.54
35.9	68.4	16.72
50.7	68.5	19.19
45.9	68.5	18.31
35.3	138.0	16.51
13.9	137.6	10.31
42.7	137.6	17.97
72.9	136.0	21.84
57.2	137.8	19.98
7.2	138.4	6.85
29.1	138.0	15.08
50.0	138.0	18.99
64.0	137.8	21.07
20.8	137.9	12.83

TABLE D-24

Rate Data for the Effect of Hydrogen on CO_2 Methanation Rate at 513.4 K

(Figure 5-8)

H_2 Partial Pressure (kPa)	CO_2 Partial Pressure (kPa)	Turnover Number x 1000
28.3	14.0	2.96
28.2	14.0	2.95
63.4	13.9	3.59
134.2	13.7	3.85
134.2	13.7	3.90
15.7	13.9	2.33
15.7	13.9	2.44
8.9	14.1	1.85
69.1	68.9	4.50
69.0	68.7	4.55
68.9	68.7	4.59
7.3	68.9	1.64
7.3	69.0	1.57
7.4	68.9	1.60
23.0	69.2	3.10
23.1	69.1	3.09
110.4	69.4	5.12
110.3	69.2	5.17
39.8	69.1	3.89
39.8	69.0	3.81

TABLE D-25

Rate Data for the Effect of Hydrogen on CO_2 Methanation Rate at 523.2 K

(Figure 5-9)

H_2 Partial Pressure (kPa)	CO_2 Partial Pressure (kPa)	Turnover Number x 1000
29.4	136.0	5.35
29.2	136.2	5.38
7.6	137.8	2.14
7.7	137.6	2.12
41.9	136.8	6.63
41.8	137.1	6.51
11.0	137.6	2.76
11.0	137.6	2.84
34.9	137.4	5.95
34.7	137.4	5.90
14.1	138.2	3.42
13.9	138.2	3.45
21.5	136.9	4.61
21.9	136.6	4.57
28.7	137.3	5.09
28.5	137.4	5.06
105.1	13.9	6.77
105.0	13.9	6.90
48.5	13.9	6.12
48.5	13.9	6.23
13.7	14.3	3.90
13.9	14.3	3.89
26.0	14.0	5.04
25.9	14.1	5.01
107.1	14.1	7.00
105.1	14.0	7.01
165.5	13.9	7.44
165.0	14.0	7.39
42.5	14.0	5.91
42.8	14.1	5.85

TABLE D-25 (continued)

H_2 Partial Pressure (kPa)	CO_2 Partial Pressure (kPa)	Turnover Number x 1000
10.6	14.1	3.44
10.6	14.1	3.42
17.9	14.0	4.33
17.9	13.9	4.42
35.5	13.9	5.42
35.6	13.9	5.47
6.1	14.2	2.52
6.0	14.1	2.46
63.3	14.2	6.28
62.9	14.4	6.14
137.1	14.2	7.23
136.6	14.2	7.04
78.7	7.2	6.31
78.9	7.2	6.18
131.3	6.6	6.40
130.7	6.6	6.37
131.1	6.7	6.46
26.1	7.0	4.48
26.1	7.0	4.44
55.2	7.2	5.40
55.0	7.2	5.51
55.2	7.1	5.46
55.0	7.1	5.44
39.4	7.0	5.03
39.3	7.0	5.16
8.8	7.0	2.85
8.8	7.0	2.94
5.2	7.0	2.04
5.2	7.0	2.08
112.7	6.8	6.47

TABLE D-25 (continued)

H_2 Partial Pressure (kPa)	CO_2 Partial Pressure (kPa)	Turnover Number x 1000
112.8	6.8	6.44
113.5	6.8	6.46
19.2	7.1	3.96
65.9	7.1	5.99
65.4	7.1	6.00
113.2	7.1	6.53
113.3	7.2	6.48
172.2	6.8	6.47
171.7	6.8	6.40
14.1	7.0	3.85
14.0	7.0	3.80
89.5	7.1	6.31
89.3	7.1	6.34
14.1	69.2	3.97
14.1	69.2	3.93
68.7	69.0	8.60
68.6	69.1	8.52
34.1	68.5	6.35
34.3	68.4	6.27
51.9	68.2	7.50
51.8	68.3	7.60
51.5	68.2	7.54
26.0	68.0	5.55
25.9	68.1	5.48
43.4	68.3	6.97
43.4	68.4	7.02
18.6	69.3	4.63
18.5	69.5	4.61
10.7	69.6	3.39
10.7	70.0	3.37
112.0	66.9	9.48
111.5	67.1	9.40
4.6	69.6	1.82
4.6	69.6	1.81
7.0	68.3	2.43
6.9	68.3	2.44

TABLE D-25 (continued)

H_2 Partial Pressure (kPa)	CO_2 Partial Pressure (kPa)	Turnover Number x 1000
93.1	27.4	8.50
93.4	27.4	8.45
111.6	26.9	8.47
111.1	27.0	8.50
31.6	27.4	6.04
31.6	27.2	5.94
51.6	27.7	7.11
51.6	27.7	7.07
10.7	27.4	3.59
10.6	27.2	3.59
19.7	27.6	4.97
19.7	27.6	4.88
26.0	28.2	5.50
25.9	28.3	5.59
5.0	27.8	2.20
5.1	27.6	2.19
6.8	27.7	2.72
6.9	27.7	2.72
6.8	27.8	2.76
27.1	27.6	5.51
27.2	27.6	5.43
40.7	28.0	6.71
40.7	28.1	6.59
15.0	27.9	4.31
14.8	27.7	4.33
150.8	27.8	8.99
150.2	27.8	8.94
129.6	27.4	8.62
129.8	27.5	8.62
75.2	27.4	7.97
75.2	27.4	7.88

TABLE D-26

Rate Data for the Effect of Carbon Dioxide on Methanation Rate at 483.9 K

(Figure 5-10)

H_2 Partial Pressure (kPa)	CO_2 Partial Pressure (kPa)	Turnover Number x 1000
27.9	95.2	6.18
27.9	95.6	6.16
27.3	125.2	6.01
27.6	125.5	6.12
27.6	150.2	6.00
27.0	165.7	5.79
27.2	166.0	5.80
28.1	96.1	6.07
28.4	116.7	6.01
28.3	116.8	6.04
27.6	44.8	5.87
27.7	44.7	5.81
27.5	59.4	6.04
27.7	59.6	5.97
27.4	29.3	5.59
27.5	29.4	5.55
27.5	75.1	5.97
27.4	75.2	6.04
27.5	87.0	6.11
27.4	87.1	6.16
27.4	21.7	5.52
27.4	21.7	5.43
27.6	10.4	4.98
27.6	10.5	4.99
28.0	3.0	3.96
27.9	3.0	3.97
28.4	142.0	6.10
28.2	141.5	6.07
27.5	14.2	5.24
27.5	14.1	5.24

TABLE D-26 (continued)

H_2 Partial Pressure (kPa)	CO_2 Partial Pressure (kPa)	Turnover Number x 1000
27.6	37.4	5.81
27.8	37.2	5.82
27.7	6.6	4.78
27.8	6.6	4.72
27.6	176.9	5.87
27.5	176.9	5.79
28.5	142.7	6.07
27.6	151.9	6.03
27.7	167.0	5.93
28.3	116.5	6.01
27.9	177.8	5.92
27.5	165.6	5.94
27.6	165.8	5.92
27.7	172.8	5.87
27.9	176.9	5.87
66.5	70.2	7.74
66.5	70.3	7.76
69.3	110.3	8.03
68.7	95.1	7.92
68.7	50.6	7.52
69.0	50.7	7.46
68.4	6.8	5.37
68.7	6.8	5.33
68.3	14.5	6.14
69.1	45.6	7.31
68.7	2.8	4.38
68.6	14.6	6.19
69.3	38.3	7.18
66.8	70.6	7.70
69.5	96.0	7.96

TABLE D-26 (continued)

H_2 Partial Pressure (kPa)	CO_2 Partial Pressure (kPa)	Turnover Number x 1000
70.4	84.6	7.89
66.8	70.5	7.71
69.5	132.7	8.17
68.7	57.7	7.51
68.6	6.6	5.30
69.1	119.9	7.99
69.2	120.2	7.87
69.4	132.5	8.02
68.7	30.1	6.91
68.6	30.1	6.81
68.9	110.0	7.99
68.9	109.7	7.86
68.5	132.0	7.81
68.4	119.3	7.94
68.5	63.5	7.66
136.7	20.0	6.81
138.5	7.4	5.55
138.3	12.3	6.12
136.2	26.3	7.07
137.2	38.4	7.63
137.5	38.8	7.56
138.2	56.5	7.99
138.9	63.5	8.19
136.8	29.5	7.24
137.9	67.5	8.23
137.6	15.2	6.26
136.2	4.0	4.73
137.3	45.7	7.81
14.0	47.6	4.86
13.7	33.5	4.70

TABLE D-26 (continued)

H_2 Partial Pressure (kPa)	CO_2 Partial Pressure (kPa)	Turnover Number x 1000
13.7	19.4	4.55
13.8	61.6	4.83
13.7	12.3	4.38
13.4	103.3	4.74
13.6	103.6	4.69
13.8	88.3	4.84
13.7	9.0	4.31
14.0	137.6	4.46
13.8	101.9	4.79
13.9	7.1	4.18
13.8	120.1	4.65
14.0	74.7	4.84
13.8	120.2	4.60
13.9	128.1	4.55
13.9	75.4	4.79
13.6	102.9	4.72
13.9	47.4	4.79
13.8	101.8	4.74
14.0	113.8	4.64
13.7	137.7	4.37
13.8	120.7	4.37
13.7	75.6	4.89

TABLE D-27

Rate Data for the Effect of Carbon Dioxide on Methanation Rate at 504.4 K

(Figure 5-11)

H_2 Partial Pressure (kPa)	CO_2 Partial Pressure (kPa)	Turnover Number x 1000
69.1	22.7	18.50
68.8	30.5	19.40
69.2	45.7	21.39
69.0	96.0	24.24
69.1	133.3	26.31
68.8	14.6	16.77
69.3	7.0	14.30
69.2	3.0	11.97
66.7	70.5	23.17
63.5	57.4	22.23
69.4	50.8	21.60
68.8	38.1	20.66
68.4	110.2	24.69
68.3	110.2	24.65
68.8	115.8	24.89
69.6	121.6	25.63
69.4	84.3	23.78
69.7	70.7	22.84
137.8	35.1	21.84
138.0	14.0	17.84
138.3	9.4	16.46
137.8	21.6	19.87
138.4	60.7	24.32
137.6	67.8	25.27
137.9	29.7	20.94
138.8	47.8	23.23
138.4	41.4	22.44
137.0	60.5	24.24
27.8	176.7	16.96
27.6	168.2	16.81

TABLE D-27 (continued)

H_2 Partial Pressure (kPa)	CO_2 Partial Pressure (kPa)	Turnover Number x 1000
27.6	46.3	15.25
27.8	46.4	15.06
27.7	41.4	14.63
27.7	36.3	14.48
27.5	31.2	14.02
27.8	64.2	16.09
27.4	69.4	16.49
27.6	69.3	16.26
27.8	74.6	16.81
27.6	74.5	16.74
27.4	79.8	16.79
27.7	80.0	17.02
27.6	115.1	17.19
27.4	91.4	17.24
27.4	91.6	17.23
28.1	60.2	15.65
27.5	11.5	12.38
26.8	7.8	11.88
27.8	129.6	16.99
27.8	102.2	17.17
27.6	59.0	15.85
27.6	50.7	15.37
27.6	102.1	17.03
27.6	102.1	17.15
27.8	26.5	13.87
27.8	21.4	13.61
27.6	15.9	12.99
27.2	91.2	16.09
27.3	91.5	17.35
27.4	139.1	17.05
27.9	149.8	16.83
27.9	139.5	17.04

TABLE D-28

Rate Data for the Effect of Partial Pressures on CO_2 Methanation Rate at 504.4 K
(Figure 5-12)

H_2 Partial Pressure (kPa)	CO_2 Partial Pressure (kPa)	Turnover Number x 1000
13.9	51.2	11.27
13.9	62.3	11.33
14.0	45.6	11.28
13.9	51.1	11.12
13.9	56.7	11.26
13.8	23.0	10.70
13.9	17.4	10.48
13.8	11.9	10.26
13.9	6.6	9.78
13.9	34.1	10.82
13.8	28.5	10.81
13.7	101.8	10.70
13.8	101.9	10.73
13.8	90.4	11.05
14.0	96.1	10.91
13.9	39.9	11.04
13.8	34.3	10.88
13.7	28.6	10.64
13.9	67.9	11.29
14.0	73.4	11.24
13.9	79.1	11.10
13.9	84.6	11.06
13.9	116.9	10.59
13.9	116.7	10.61
14.1	133.0	10.24
13.8	123.3	10.43
41.2	68.9	19.99
36.1	68.7	18.50
31.2	68.7	17.12
52.4	68.8	22.96

TABLE D-28 (continued)

H_2 Partial Pressure (kPa)	CO_2 Partial Pressure (kPa)	Turnover Number x 1000
73.9	68.8	25.24
137.1	68.5	27.61
5.5	68.0	5.99
15.5	68.7	11.75
20.9	68.7	13.80
26.2	68.6	15.33
113.5	68.8	26.88
45.6	68.4	20.65
51.8	68.3	22.29
10.5	67.9	9.41
10.5	67.9	9.40
62.7	69.0	24.83
85.4	69.4	26.22

TABLE D-29

Rate Data for the Effect of Carbon Dioxide on Methanation Rate at 513.4 K

(Figure 5-13)

H_2 Partial Pressure (kPa)	CO_2 Partial Pressure (kPa)	Turnover Number x 1000
28.2	58.7	3.27
28.1	58.7	3.24
28.2	109.6	3.30
28.4	109.6	3.21
27.9	11.9	2.81
27.6	11.9	2.87
28.3	150.9	3.36
28.2	150.9	3.22
28.2	40.5	3.38
28.2	40.7	3.42
27.9	23.3	3.22
27.8	23.3	3.21
28.2	6.1	2.48
28.1	6.1	2.56
28.2	17.9	2.92
28.3	17.7	3.04
137.9	41.2	5.03
138.0	41.5	5.04
137.5	21.2	4.74
136.9	21.2	4.74
138.0	14.5	4.20
138.4	14.5	4.22
137.2	7.3	3.62
137.3	7.2	3.62
137.1	14.5	4.27
137.2	14.5	4.23
138.2	27.9	4.73
138.3	27.9	4.79
137.5	10.7	4.07
137.3	10.7	4.05

TABLE D-29 (continued)

H_2 Partial Pressure (kPa)	CO_2 Partial Pressure (kPa)	Turnover Number x 1000
69.2	50.3	4.40
69.1	50.3	4.30
69.5	30.0	4.15
69.7	29.9	4.15
69.0	68.3	4.52
68.8	68.3	4.52
69.3	7.2	3.24
69.2	7.2	3.23
69.6	19.9	3.83
69.6	19.9	3.81
69.2	109.6	4.67
69.0	109.7	4.67
69.8	16.0	3.67
69.7	15.9	3.58
69.4	22.5	3.92
69.4	22.5	3.93

TABLE D-30

Rate Data for the Effect of Carbon Dioxide on Methanation Rate at 523.2 K

(Figure 5-14)

H_2 Partial Pressure (kPa)	CO_2 Partial Pressure (kPa)	Turnover Number x 1000
70.0	19.1	5.76
70.1	19.2	5.79
69.4	13.7	5.74
69.5	13.7	5.65
69.6	68.4	7.12
68.5	67.2	7.10
69.6	51.0	6.96
69.6	51.0	6.98
69.9	9.7	5.18
69.5	28.1	6.45
69.9	28.1	6.48
69.2	107.2	7.26
69.4	107.1	7.18
137.5	42.3	8.30
137.1	42.5	8.52
138.0	21.1	7.39
137.9	21.1	7.44
138.4	28.7	7.73
138.5	28.6	7.89
138.2	6.8	5.77
138.2	6.8	5.77
138.2	10.5	6.47
138.6	10.5	6.47
138.3	14.1	6.84
138.6	14.1	6.86
28.1	68.3	5.57
28.1	68.4	5.52
28.4	20.0	4.99
28.3	20.0	5.01
27.9	17.0	4.99

TABLE D-30 (continued)

H_2 Partial Pressure (kPa)	CO_2 Partial Pressure (kPa)	Turnover Number x 1000
27.9	7.0	4.93
28.6	150.0	5.21
28.8	150.0	5.14
28.4	50.0	5.32
28.4	50.3	5.29
28.5	5.3	4.23
28.5	5.2	4.24
28.3	1.6	3.38
28.4	1.6	3.37
28.5	4.2	4.13
28.5	4.3	4.11
28.5	30.1	5.17
28.4	30.3	5.33
28.3	37.4	5.41
28.2	37.6	5.39
28.2	109.0	5.28
28.3	109.1	5.25
27.4	151.3	5.28
27.2	151.1	5.20
28.1	9.7	4.56
28.1	9.7	4.74
28.1	76.7	5.45
28.1	76.8	5.51
28.1	109.3	5.56
27.8	109.4	5.51
14.2	104.9	3.90
14.3	104.8	3.79
14.3	43.5	4.13
14.3	43.4	4.08
14.2	30.7	4.12

TABLE D-30 (continued)

H_2 Partial Pressure (kPa)	CO_2 Partial Pressure (kPa)	Turnover Number x 1000
14.2	30.5	4.02
14.5	12.1	3.96
14.5	12.1	4.04
14.4	78.2	3.93
14.4	78.3	3.93
14.8	164.0	3.54
14.8	164.1	3.43
14.3	5.0	3.69
14.4	5.0	3.56
14.2	2.1	3.20
14.2	2.1	3.07
14.5	8.1	3.40
14.4	8.0	3.60
14.1	20.8	4.05
14.2	20.8	4.00
14.1	54.1	4.01
14.3	54.1	3.94

TABLE D-31

Rate Data for the Effect of Water on CO_2 Methanation Rate

(Figure 5-17)

H_2 Partial Pressure (kPa)	CO_2 Partial Pressure (kPa)	H_2O Partial Pressure (kPa)	Turnover Number x 1000
	(At 493.5 K)		
96.6	23.4	0.0	9.31
96.6	23.4	0.0	9.36
96.3	23.5	13.8	6.62
96.7	23.5	13.8	6.63
95.8	23.6	13.8	6.66
96.4	23.6	6.9	7.11
96.3	23.5	6.9	7.11
96.5	23.3	9.3	6.90
96.0	23.3	9.3	6.91
96.3	23.3	9.3	6.92
96.0	23.4	3.4	7.61
96.5	23.4	3.4	7.57
96.3	23.2	20.7	6.37
96.1	23.2	20.7	6.34
96.2	23.1	4.8	7.46
96.9	23.1	4.8	7.45
96.9	23.1	4.8	7.44
50.4	11.8	0.0	6.73
50.8	11.8	0.0	6.73
50.2	12.0	13.7	4.40
50.3	12.0	13.7	4.40
50.5	12.2	13.7	4.39
50.7	12.1	13.7	4.39
50.5	12.0	13.7	4.41
50.3	12.0	6.9	4.80
50.6	12.0	6.9	4.74
50.7	11.8	9.3	4.63
50.8	11.9	9.3	4.58
50.8	11.8	9.3	4.63
50.7	11.9	3.4	5.18
51.0	11.9	3.4	5.21
50.8	11.9	3.4	5.20
51.2	11.9	20.7	4.13
51.0	11.9	20.7	4.20

TABLE D-31 (continued).

H_2 Partial Pressure (kPa)	CO_2 Partial Pressure (kPa)	H_2O Partial Pressure (kPa)	Turnover Number x 1000
	(At 483 K)		
95.7	23.2	0.0	3.80
95.6	23.2	0.0	3.82
96.0	23.2	0.0	3.78
95.6	23.0	20.7	2.56
95.7	23.0	20.7	2.54
95.6	23.0	20.7	2.54
94.9	23.3	7.0	2.73
94.7	23.3	7.0	2.73
94.7	23.1	3.4	2.86
94.7	23.2	3.4	2.89
94.5	23.1	9.4	2.68
94.6	23.1	9.4	2.67
94.9	23.3	13.9	2.60
94.9	23.3	13.9	2.61
94.7	23.3	13.9	2.61

TABLE D-32

Additional Data for the Effect of Water on CO_2 Methanation Rate at 493.5 K

(Figure 5-18)

H_2 Partial Pressure (kPa)	CO_2 Partial Pressure (kPa)	H_2O Partial Pressure (kPa)	Turnover Number x 1000
89.5	21.6	7.8	6.04
89.6	21.6	7.8	6.12
89.4	21.6	7.8	6.06
87.1	20.8	10.8	5.10
87.7	20.8	10.8	5.10
91.8	21.9	4.6	6.35
92.2	22.0	4.6	6.33
92.6	22.0	4.6	6.35
92.5	22.0	4.6	6.35
80.0	19.1	19.8	5.07
80.5	19.1	19.8	5.11
80.2	19.1	19.8	5.09
86.0	20.9	12.5	5.23
85.8	20.9	12.5	5.24
86.0	20.9	12.5	5.51
93.3	22.8	2.7	6.58
93.5	22.8	2.7	6.56
94.2	22.8	2.7	6.53
134.0	32.5	9.8	7.23
133.8	32.5	9.8	7.23
133.8	32.5	9.8	7.19
127.1	30.9	18.5	6.29
127.0	30.8	18.5	6.24
127.0	30.9	18.5	6.28
138.1	33.6	4.0	7.95
138.5	33.6	4.0	7.92
138.4	33.6	4.0	7.92
117.6	28.1	29.2	5.70
117.3	28.1	29.2	5.70
117.9	28.1	29.2	5.70

TABLE D-32 (continued)

H_2 Partial Pressure (kPa)	CO_2 Partial Pressure (kPa)	H_2O Partial Pressure (kPa)	Turnover Number x 1000
135.3	32.3	6.7	7.37
135.8	32.3	6.7	7.36
135.4	32.3	6.7	7.37
128.1	30.7	16.0	6.16
128.3	30.6	16.0	6.17
128.7	30.6	16.0	6.16
46.1	10.6	10.4	4.34
46.3	10.6	10.4	4.32
46.2	10.6	10.4	4.33
48.8	11.2	4.3	4.88
48.6	11.2	4.3	4.86
48.8	11.2	4.3	4.89
42.7	9.8	19.2	3.80
42.8	9.8	19.2	3.76

TABLE D-33

Rate Data for the Effect of Methane on CO_2 Methanation

(Figure 5-19)

H_2 Partial Pressure (kPa)	CO_2 Partial Pressure (kPa)	CH_4 Partial Pressure (kPa)	Turnover Number x 1000
	(At 486 K)		
69.0	9.1	0.0	8.71
69.3	9.0	41.4	8.70
68.9	9.0	20.7	8.76
68.7	9.0	31.5	8.67
68.7	9.0	12.5	8.58
68.3	9.0	23.71	8.68
68.3	9.0	35.2	8.42
	(At 493 K)		
51.0	12.4	0.0	11.57
50.8	12.4	28.2	11.74
51.1	12.4	14.0	11.49
50.8	12.4	19.5	11.72
51.0	12.4	5.3	11.49
50.8	12.4	44.8	11.71
51.0	12.4	36.4	11.38

TABLE D-34

Rate Data for the Effect of Carbon Monoxide on CO_2 Methanation at 523.2 K

(Figure 5-20)

H_2 Partial Pressure (kPa)	CO_2 Partial Pressure (kPa)	CO Partial Pressure (kPa)	Turnover Number x 1000
109.8	28.5	0.2	9.51
109.6	28.5	0.2	9.35
109.1	29.0	3.7	13.49
109.2	29.0	3.7	13.33
110.0	28.6	0.2	9.77
109.9	28.6	0.2	9.69
109.0	29.0	6.9	10.33
108.9	29.0	7.0	10.20
109.0	29.0	10.4	8.39
109.0	29.0	10.4	8.29
109.6	29.2	41.5	3.92
109.5	29.2	41.4	3.91
108.5	28.9	20.8	5.71
108.5	29.0	20.8	5.61
109.0	29.0	14.1	6.95
109.0	29.0	14.0	7.03
108.9	28.9	1.6	13.31
108.9	29.0	1.6	13.20
108.8	29.1	27.5	4.92
108.7	29.0	27.5	4.84
55.5	14.6	0.1	7.65
55.5	14.6	0.1	7.63
55.6	14.8	27.4	2.14
55.8	14.8	27.4	2.19
55.4	15.1	19.0	2.58

TABLE D-34 (continued)

H_2 Partial Pressure (kPa)	CO_2 Partial Pressure (kPa)	CO Partial Pressure (kPa)	Turnover Number x 1000
55.3	14.7	19.0	2.61
55.3	14.7	7.3	4.15
55.2	14.7	7.3	4.16
55.4	14.8	1.2	8.63
55.6	14.8	1.2	8.55
54.9	14.7	3.2	5.95
55.0	14.7	3.1	5.98
55.3	14.7	10.3	3.62
55.3	14.8	10.2	3.51
55.4	14.8	5.9	4.44
55.6	14.8	5.9	4.60
55.1	14.7	14.5	3.03
55.4	14.7	14.5	2.92